Author:
Williams, Steven Mark

Title:
The run-up and overtopping of shallow water waves

The Run-up and Overtopping of Shallow Water Waves

Steven Mark Williams

School of Mathematics

University of Bristol

A Thesis submitted to The University of Bristol

for the degree of Doctor of Philosophy

in the Faculty of Science

November 2003

Abstract

To be able to estimate the amount of water that may overtop a coastal structure, is of great importance, especially in the protection of mankind and objects of value.

Shallow water theory is used to model the run-up of bores over planar beaches. The solution of Shen & Meyer (1963) for the run-up of a single swash event is extended analytically to include the effects of overtopping over a truncated plane beach. This solution is used to provide an expression for the amount of water that may overtop the edge.

Multiple swash events are modelled numerically and the effects of the interactions between swash events are discussed. The effects of overtopping on these swash events is also discussed, with volumes of overtopping being found.

When violent water waves interact with a wall, a thin jet of fluid is seen to project upwards. A mathematical model is set-up to model this situation. When the wave is on its way back down, some water is found to overtop the wall. It is this volume of overtopping that we wish to find.

The motion of the jet along the wall is modelled using a modified form of a solution from Longuet-Higgins (1976). This solution is then extended using shallow water theory to model how the jet evolves as it passes the top of the wall. The motion of the jet interacting with the top of the wall on its way down is modelled using a free surface flow technique. From this an analytical expression is found for the evolution of the jet and the amount of water that overtops the wall.

ALL MISSING
PAGES ARE
BLANK
IN
ORIGINAL

Acknowledgements

I would like to thank my supervisor Prof. Howell Peregrine for his advice, suggestions, help and support throughout the preparation of this thesis.

I would also like to thank Richard Kerswell, Andrew Hogg, Diki Porter and David Pritchard for all their help and support.

I would like to thank my parents for all their support and belief in me over the years. Thanks also goes out to Ben, Anne and Al, without whom I would never have got this far. I would also like to thank the rest of my family and friends for all their support.

Last but not least I would like to thank Katherine, your love and support got me through it.

During the period of my study for this work I was in receipt of a grant from the UK Engineering Physical Sciences Research Council to whom I am indebted.

This PhD thesis is dedicated to all my family and those who are no longer with us.

Author's Declaration

I declare that the work in this dissertation was carried out in accordance with the Regulations of the University of Bristol. The work is original except where indicated by special reference in the text and no part of the dissertation has been submitted for any other degree.

Any views expressed in the dissertation are those of the author and in no way represent those of the University of Bristol.

The dissertation has not been presented to any other University for examination either in the United Kingdom or overseas.

Steven M. Williams

26/11/03.

Contents

1 Introduction 1

1.1 Run-up 6

1.1.1 Theoretical analyses 6

1.1.2 Laboratory experiments 10

1.1.3 Numerical simulations 11

1.2 Overtopping 14

1.2.1 Theoretical analyses 14

1.2.2 Laboratory experiments 15

1.2.3 Numerical simulations 20

1.3 Overview of thesis 23

2 Equations of motion 25

2.1 Introduction 25

2.2 Shallow water theory 25

2.2.1 Introduction 25

2.2.2 Equations of motion 27

2.2.3 Gas dynamics analogy 28

2.2.4 Bore conditions 29

2.2.5 Dam-break problem 31

2.3 Work of Shen, Ho & Meyer 31

2.3.1 Introduction 31

2.3.2 Run-up of a bore on a beach 32
2.4 Dam-break transformation 35
2.5 Conclusion 37

3 A single swash event overtopping a truncated plane beach 39
3.1 Introduction 39
3.2 Formulation of problem 40
3.3 Overtopping solution 42
3.3.1 The swash solution 42
3.3.2 Overtopping solution 45
3.3.3 Volume of overtopping 48
3.4 Conclusion 51

4 Numerical method 53
4.1 Introduction 53
4.2 Nessyahu & Tadmor scheme 54
4.2.1 Method of solution 54
4.2.2 Source terms 58
4.2.3 RUSH scheme 59
4.2.4 RUSH-OVER scheme 59
4.3 Stability 59
4.4 Boundary conditions 60
4.4.1 Introduction 60
4.4.2 Seaward boundary condition 61
4.4.3 Shoreline boundary condition 62
4.4.4 Overtopping boundary condition 63
4.5 Comparison of RUSH to analytic and numerical results 65
4.5.1 Dam-break problem 65
4.5.2 Carrier & Greenspan solution 68

4.5.3 Shen & Meyer solution 70
4.5.4 Peregrine & Williams solution 76
4.5.5 Testing RUSH for bores 77
4.6 Conclusion 82

5 The run-up of multiple swash events **83**
5.1 Introduction 83
5.2 Setup of problems 84
5.2.1 Boundary conditions for multiple swash 84
5.2.2 The Iribarren Number 93
5.3 Results - Periodic bores of equal amplitudes 93
5.3.1 Quadratic variation in α_0 106
5.4 Results - Random, periodic bores 108
5.5 Results - Random, non-periodic bores 118
5.6 Conclusion 120

6 The overtopping of multiple swash events **123**
6.1 Introduction 123
6.2 Results - Periodic bores 125
6.2.1 Flux comparison 131
6.2.2 Volumes of overtopping 136
6.3 Results - Random, periodic bores 138
6.3.1 Flux comparison 143
6.3.2 Volumes of overtopping 147
6.4 Random, non-periodic bores 152
6.5 Conclusion 152

7 The overtopping of a vertical wall by a thin jet **155**
7.1 Introduction 155
7.2 General wall flow 159

7.2.1 Jet flow above the wall 160
7.2.2 Downward motion 162
7.3 Parabolic free surface: Longuet-Higgins (1976) solution 163
7.4 Parabolic free surface moving under gravity 167
7.5 Thin jets along a wall 168
7.5.1 The wall flow 168
7.5.2 The jet flow 170
7.5.3 Downward motion 174
7.6 Jet flow hitting the top of a wall 176
7.7 Conclusion 190

8 Conclusions **191**
8.1 Review of thesis 191
8.2 Remarks 193
8.3 Further work 194

References **197**

List of Figures

1.1 Nearshore zones 3

1.2 Criteria for critical overtopping discharges. 22

2.1 Definition sketch taken from Shen & Meyer (1963). 33

3.1 Definition sketch for the overtopping of a single swash event 41

3.2 Characteristics for the swash solution 45

3.3 General (x,t)-diagram showing different regions of flow. 47

3.4 Overtopping volume per unit width $V(E)$. 49

3.5 $V(E)$ with a logarithmic scale. 50

4.1 Height of dambreak flow. 66

4.2 Velocity of dambreak flow. 66

4.3 Mass flux for dambreak flow. 67

4.4 Surface elevation of Carrier & Greenspan wave. 69

4.5 Shoreline position of Carrier & Greenspan wave. 70

4.6 'Real life' setup for Shen & Meyer 71

4.7 Shen & Meyer shoreline comparison. 72

4.8 Shen & Meyer height comparison. 72

4.9 Shen & Meyer velocity comparison. 73

4.10 Shen & Meyer flux comparison. 73

4.11 Shen & Meyer volume comparison. 74

4.12 Shen & Meyer momentum comparison. 74

4.13 Shen & Meyer energy comparison 75

4.14 Peregrine & Williams flux comparison. 76

4.15 Peregrine & Williams overtopping volume comparison. 77

4.16 Height profile for a uniform bore travelling into still water. 78

4.17 Velocity profile for a uniform bore travelling into still water. 78

4.18 Surface elevation at $t = 0.4$ to 3.2 in intervals of 0.4. 79

4.19 Water velocity at $t = 0.4$ to 3.2 in intervals of 0.4. 80

4.20 Surface elevation at $t = 3.6$ to 6.8 in intervals of 0.4. 80

4.21 Water velocity at $t = 3.6$ to 6.8 in intervals of 0.4. 81

4.22 Shoreline position of a uniform bore travelling over a plane beach. . 81

5.1 Timestack from DELILAH 85

5.2 Uniform bore approaching a beach 86

5.3 α_0 as a function of time. Case of time periodic bores of equal amplitudes. 89

5.4 Height profile at the seaward boundary against time. Case of time periodic bores of equal amplitudes. 89

5.5 α_0 as a function of time. Case of time periodic bores of random amplitudes. 90

5.6 Height profile at seaward boundary against time. Case of time periodic bores of random amplitudes. 91

5.7 α_0 as a function of time. Case of bores of random amplitude and period. 91

5.8 Summary of breaking and swash of regular waves. 92

5.9 Shoreline position of swash with forcing period 1.3. 95

5.10 Height and velocity profiles at the seaward boundary as a function of time. Forcing is 1.3. Swash from bores of equal amplitudes. 95

5.11 Shoreline position of swash with forcing period 3.0. 97

5.12 Height and velocity profiles at the seaward boundary as a function of time. Forcing is 3.0. Swash from bores of equal amplitudes. 97

5.13 Height and velocity profiles between times $t = 4.6$ and $t = 5.6$ in intervals of 0.2. 98

5.14 Height and velocity profiles as a function of time, at position $x = -0.425$ on the beach. 99

5.15 Shoreline position of swash with forcing period 2.2. 101

5.16 Height and velocity profiles at the seaward boundary as a function of time. Forcing is 2.2. Swash from bores of equal amplitudes. 101

5.17 Relative wave height as a function of the Iribarren number. 102

5.18 The period of response t_r against Iribarren number ξ. 104

5.19 Relative wave height as a function of the period of response, t_r. . . . 104

5.20 Ratio of incident waves to response waves as a function of ξ. Swash is from bores of equal amplitudes. 105

5.21 Quadratic variation in α_0 106

5.22 Shoreline position of swash with forcing period 3.0. Quadratic variation in α_0. $\alpha_i = 3.3$. 107

5.23 Height and velocity profiles at seaward boundary. Quadratic variation in α_0 with forcing period 3.0. 108

5.24 Shoreline position of random swash with forcing period 1.0. 109

5.25 Height and velocity profiles at the seaward boundary as a function of time. Forcing period is 1.0. Swash from bores of random amplitudes. 110

5.26 Shoreline position of random swash with forcing period 2.0. 112

5.27 Height and velocity profiles at the seaward boundary as a function of time. Forcing period is 1.0. Swash from bores of random amplitudes. 113

5.28 Shoreline position of random swash with forcing period 4.0. 113

5.29 Relative wave height as a function of the Iribarren number for random, periodic bores. 114

5.30 Period of response as a function of the Iribarren number for random, periodic bores. 116

5.31 Relative wave height as a function of the period of response for random, periodic bores. 116

5.32 Ratio of incident waves to response waves as a function of ξ. 117

5.33 Shoreline position of swash with random period. Period is between $t = 1.0$ and $t = 1.5$. 119

5.34 Shoreline position of swash with random period. Period is between $t = 1.0$ and $t = 2.0$. 119

5.35 Shoreline position of swash with random period. Period is between $t = 1.0$ and $t = 4.0$. 120

6.1 Overtopping of swash with forcing period 1.3. Swash from bores of equal amplitudes. 126

6.2 Height and velocity profiles at the seaward boundary as a function of time. Forcing is 1.3. Overtopping case of swash from bores of equal amplitudes. 127

6.3 Overtopping of swash with forcing period 3.0. Swash from bores of equal amplitudes. 128

6.4 Height and velocity profiles at the seaward boundary as a function of time. Forcing is 3.0 and $\alpha_i = 3.3$. Overtopping case of swash from bores of equal amplitudes. 129

6.5 Overtopping of swash with forcing period 2.2. Swash from bores of equal amplitudes. 130

6.6 Height and velocity profiles at the seaward boundary as a function of time. Forcing is 2.2. Overtopping case of swash from bores of equal amplitudes. 131

6.7 Flux comparison at various cut-off points between overtopping and non-overtopping data. Forcing period 1.3. Swash from bores of equal amplitudes. 132

6.8 Flux comparison at various cut-off points between overtopping and non-overtopping data. Forcing period 2.2. Swash from bores of equal amplitudes. 134

6.9 Flux comparison at various cut-off points between overtopping and non-overtopping data. Forcing period 3.0. Swash from bores of equal amplitudes. 135

6.10 Volume of overtopping against cut-off position $x = E$. Swash from bores of equal amplitudes. 137

6.11 Volume of overtopping against the cut-off position on a logarithmic scale. Swash is from bores of equal amplitudes. 137

6.12 Overtopping of random swash with forcing period 1.0. Swash from bores of random amplitudes. 139

6.13 Height and velocity profiles at the seaward boundary as a function of time. Forcing is 1.0. Overtopping case of swash from bores of random amplitudes. 140

6.14 Overtopping of random swash with forcing period 2.0. Swash from bores of random amplitudes. 141

6.15 Height and velocity profiles at the seaward boundary as a function of time. Forcing is 1.0. Overtopping case of swash from bores of random amplitudes. 141

6.16 Overtopping of random swash with forcing period 2.0. Swash from bores of random amplitudes. 142

6.17 Height and velocity profiles at the seaward boundary as a function of time. Forcing is 4.0 and $\alpha_i = 3.3$. Overtopping case of swash from bores of random amplitudes. 142

6.18 Flux comparison at various cut-off points between overtopping and non-overtopping data. Forcing period 1.0. Swash from bores of equal amplitudes. 144

6.19 Flux comparison at various cut-off points between overtopping and non-overtopping data. Forcing period 2.0. Swash from bores of equal amplitudes. 145

6.20 Flux comparison at various cut-off points between overtopping and non-overtopping data. Forcing period 4.0. Swash from bores of equal amplitudes. 146

6.21 Volume of overtopping against cut-off position $x = E$. Swash from bores of random amplitudes. 147

6.22 Volume of overtopping against the cut-off position on a logarithmic scale. Swash is from bores of random amplitudes. 148

6.23 Volume of overtopping against forcing period for swash from bores of random amplitudes. Cut-off is at $x = 1.1$. 149

6.24 Volume of overtopping against forcing period for swash from bores of random amplitudes. Cut-off is at $x = 1.4$. 150

6.25 Volume of overtopping against forcing period for swash from bores of random amplitudes. Cut-off is at $x = 1.8$. 151

6.26 Volume of overtopping against forcing period for swash from bores of random amplitudes. Cut-off is at $x = 2.2$. 151

7.1 Violent wave impact against a wall. 158

7.2 Setup of initial wall flow 159

7.3 A cross-section of the parabolic free surface given by Longuet-Higgins (1976). 165

7.4 Free surface of the modified Longuet-Higgins solution. 165

7.5 Jet width at top of wall as a function of τ 170

7.6 Vertical velocity at top of wall as a function of τ 171

7.7 Vertical position of a jet element as a function of time. 172

7.8 Vertical velocity above wall against time, t 173

7.9 Jet width above wall against time, t 174

7.10 Horizontal displacement as a function of the impact time, t_i. The wall height is $H = 0.3$ and $\epsilon = 0.0001$. 175

7.11 Jet of water on its way down. 177

7.12 Overtopping of water from jet on its way down. 178

7.13 Flow setup for jet hitting the corner of the wall. 179

7.14 $w = u - iv = e^{-i\theta}$ plane. 181

7.15 t-plane. 181

7.16 Angle of deflection β against impact time t_i 185

7.17 x_d as a function of β 185

7.18 Overtopping volume as a function of wall height. 187

7.19 Impact of a jet element with top of wall of height 0.3. Plots are for $t_i = 0.8, 0.9$ and 1.0 188

7.20 Impact of a jet element with top of wall of height 0.3. Plots are for $t_i = 1.1, 1.2$ and 1.3 189

List of Tables

1.1 Models for average overtopping discharge formulae. Table is taken from Kofoed (2002). 16

1.2 Models for average overtopping discharge formulae, continued. Table is taken from Kofoed (2002). 17

1.3 Models for average overtopping discharge formulae, continued. Table is taken from Kofoed (2002). 18

4.1 Calculating the errors involved in numerical scheme 68

5.1 Comparison of ξ for equal and random bore amplitudes. 111

5.2 Comparison of number of waves per swash event for equal and random bore amplitudes. 115

7.1 Volumes of overtopping for different wall heights 186

7.2 Properties of a jet element for varying t_i, with $H = 0.3$ 187

Chapter 1

Introduction

In coastal protection, whether against flooding or to prevent wave disturbance in harbours, it is often valuable to be able to estimate the flow of water over the top of a structure, or natural feature. When the mean water level is below the crest of such a feature any overtopping is due to the run-up from incident waves.

The motivation for predicting the overtopping of structures is linked to the design of structures protecting mankind and objects of value against the violent force of the surrounding sea. Typically, rubble mounds or vertical breakwaters have been used for the protection of harbours, whereas dikes and offshore breakwaters have been used for the protection of beaches and land. All these structures are designed to avoid overtopping or at least reduce it to a minimum, as overtopping can lead either to functional or structural failure of structures. Here functional failure refers to cases where for example large wave overtopping discharges might damage persons, ships, the structure itself or equipment on it, or generate waves behind the structure (in the case when water is present there), which again is hazardous to the manoeuvring or mooring of ships. Structural failure refers to cases where the overtopping discharge is heavy enough to damage the lee side of the breakwater or dike, which can ultimately lead to the collapse of the structure.

The information gathered from research on overtopping has practical application to coastal defence. Japan is vulnerable to attack by tsunami waves, which are usually generated by earthquake activity under the ocean, and which may cause run-up of

up to 30m. The Netherlands is low-lying and used to be a regular victim of flooding by sea water, although a large area has now been reclaimed for farmland and is protected by a series of dikes and river sluices. These two countries have carried out extensive work on run-up and overtopping. In the planning stages of coastal defence projects it is necessary to consider whether or not any over-run or damage to a seawall can be tolerated, depending upon the population density and land-use at the site. Whatever is decided, there must be an estimate of the expected wave activity during a storm and of the maximum wave run-up height during the worst possible conditions.

As a water wave travels from deep water towards the shoreline its form is modified considerably by the changing water depth. The forward slope of the wave increases and the distance between successive wave crests shortens. On approaching a beach the wave refracts, reflects and breaks to form a turbulent wave-front. When the wave ultimately reaches the shoreline it transforms into a thin sheet of water, which runs up the beach. As the water flows back down the beach it exerts a modifying effect on the following wave. Energy in the nearshore region is dissipated in a number of ways: through the generation of turbulence; formation of reflected waves and possibly the appearence of further waves and currents. Residual energy is involved in excavation and deposition of seabed material.

The nearshore region can be divided into a number of zones. A different approach to modelling is commonly used within each zone, and different equations of motion: Shallow water theory is commonly used in the swash zone, the Boussinesq equations are used in the surf zone and linear wave theory is used in deep water. Each approach attempts to account for the dominant aspects of the varied physical processes taking place. Away from the shoreline waves usually originate from deep water, that is, water whose depth is large compared to the wavelength of any waves. Waves experience the shoaling effect caused by the decreasing water depth, and change both their phase velocity and angle of incidence. Wave crests are deflected towards the coastline, according to a modified form of Snell's law in the absence of any currents, or by a more elaborate description (Longuet-Higgins 1972*b*,

Longuet-Higgins 1970*a*, Longuet-Higgins 1970*b*) in the presence of currents.

Where incoming waves are initially influenced by the decreasing water depth defines the seaward boundary of the refraction zone. This zone extends landward to the shoreline. The major effect of the refraction process is the tendency to align wave crests parallel to the shoreline, reducing the three-dimensional character of oblique incident waves on a straight shoreline. Decreasing water depth causes the front face of the wave slope to steepen and ultimately break, the wave then dissipating energy in turbulent motions as it travels shorewards.

The breaker line is defined as the position where the waves start to dissipate energy through surface turbulence. This may vary in relation to the shoreline from a few metres on a steep beach to several hundred metres on a gently sloping beach. The region between the breaker line and the shoreline is known as the surf zone and is the area within which waves dissipate energy by surface turbulence. Between the final breaker and the dry beach is called the swash zone. A depiction of these zones is represented in figure 1.1.

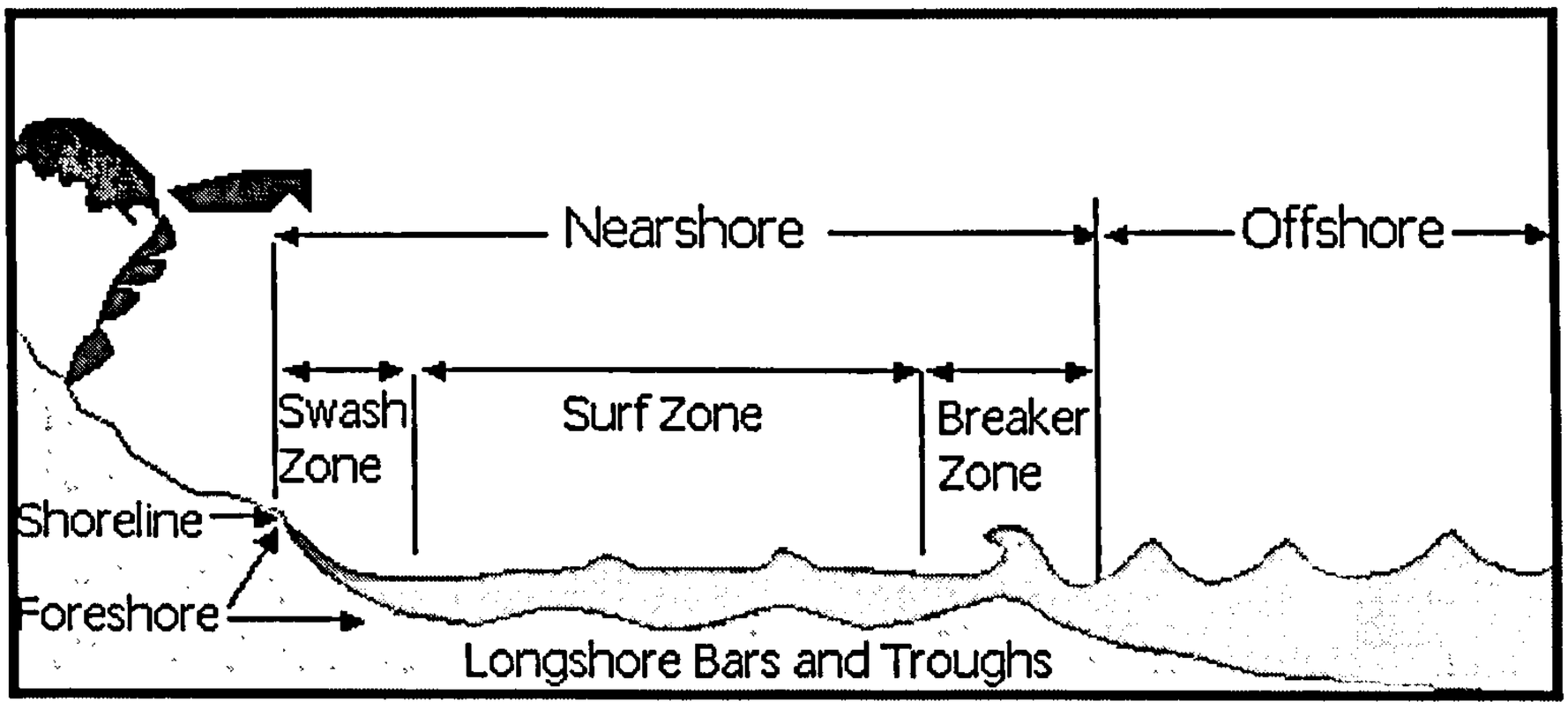

Figure 1.1: Nearshore zones

Waves approaching a beach break in various ways according to beach slope and incident wave characteristics; consequently the exact point of breaking is often difficult to determine. Galvin (1968) and Galvin (1972) classifies four possible forms of breaking waves: spilling, plunging, collapsing and surging breakers. More than one

type may be seen on a single beach. Various nearshore wave parameters have been suggested as indepedent parameters in a quantitative classification for the breaker type. The most widely used variables for classification are the wave height, wave period and beach slope.

Spilling breakers are predominantly found on gently sloping beaches; these waves break at their crests with the formation of bubbles and foam, which flow down the front face eventually to cover the wave front as it propagates shoreward. The wave form changes only slowly as spilling breakers propagate through the surf zone. In its final stages of travel the turbulent front face is often narrow and has the appearance of a bore or undulatory bore.

Plunging and collapsing breakers change their shape more dramatically. The wave front falls into the preceding water resulting in an amorphous motion. In a plunging breaker the wave crest curls over the front face, often accompanied by a sheet of spray, while in a collapsing breaker the upper part of the front drops to the base of the wave.

Surging breakers are found mostly on steep beaches and have a close physical resemblance to standing waves, with the front remaining relatively smooth and only minor surface turbulence.

After a wave has broken it may undergo much transformation with the wave shape changing continually, although not always continuously. In the case of the plunging or collapsing breaker the whole wave front reforms after the wave crest curls forward into the wave. The transition state while the wave reforms is highly turbulent and, due to the presence of foam, indeterminate in shape. Before reaching the shoreline waves usually evolve into a form with a relatively smooth back slope but headed by a turbulent region. The resulting wave shape is asymmetric about a vertical line passing through the wave crest. This applies to most real waves.

Our attention is confined in the main to bore or surf wave motion and run-up, thinking mostly of motion of gently sloping beaches, where these regions are most prevalent. But, as discussed in the description of equations of chapter 2, the method is not confined to beaches of small slope.

For analytic treatment of breaking water waves, simplifications must be made. The first relies on the observation that a wave once broken and reformed often has a front face consisting of a highly turbulent zone, whose width is typically of the order of the water depth. Across this zone both wave height above mean water level and wave velocity change rapidly. Mathematically this transition region may be replaced by an abrupt change of water height and velocity, the discontinuity moving with the phase velocity of the wave. The resulting configuration, once mass and momentum are specified as conserved quantities across the wave front, is described as a bore, see Stoker (1957). Stationary bores within a flow, known as a hydraulic jump, have been well investigated, see Binnie & Orkney (1955). Other major simplifying assumptions are that the flow may be considered two-dimensional and the incident waves will be restricted to being long-waves.

Most beaches are much longer than the width of the surf zone and the main features of the flow, provided the waves are incident normal to the shore, are in the onshore/offshore direction. So any longshore variation is ignored although three dimensional behaviour is common on real beaches. The waves are restricted to being long waves in order to make certain simplifications to the equations of motion. The long wave assumption is that the amplitude of the wave is very much less than the wavelength. On shallow beaches this is commonly the case. The foaming fronts of water are separated by distances that are many times the height of the wave itself, so this restriction presents no problem. On steeper beaches however the region of the surf zone over which this is true is reduced and on very steep beaches only in the swash zone, where the water depth is always small compared to the wavelength, can waves be said to be long waves. So although the method developed here can be used for steep beach flows this restriction has to be considered.

The shoreline motion created when a single bore runs up and down the beach determines the run-up elevation until such time as it, in turn, is overtaken by a succeeding bore. The maximum run-up produced by a wave gives a good idea of its potential for damage. It is this level which determines whether or not inundation will occur.

In contrast to regular waves, a random sea does not give the same number of run-up cycles as waves, due to overtaking of and interactions between neighbouring waves. Furthermore, a large wave does not necessarily lead to high run-up if it encounters strong backwash from the previous wave, and it is not always apparent which wave has caused which shoreline oscillation. For both regular and irregular waves, the mean run-up height is higher than the still water level in the absence of waves due to the unbalanced momentum flux directed shorewards by the broken waves. This tends to pile water up onto the beach. This pile-up is known as wave set-up. When waves break on a beach, they produce a set-up, a rise in the mean water level above the still-water elevation of the sea. Accompanying the set-up, is a region called the set-down where the mean elevation of the sea is depressed, as one would expect from continuity. Estimates of both set-up and set-down were made by Longuet-Higgins & Stewart (1962) using an energy balance method.

1.1 Run-up

The study of wave propagation, breaking and run-up has been the subject of numerous analytical, numerical and experimental studies in recent years. Various simplified models have been used to describe the wave run-up process, which is a strongly non-linear and dispersive wave phenomenon e.g., the Boussinesq equations and the non-linear shallow water wave equations.

1.1.1 Theoretical analyses

In theory, the non-linear effects and the dispersive effects can be estimated by two parameters

$$a = \frac{H}{h}, \qquad \epsilon = \frac{h}{l}, \tag{1.1.1}$$

where H is the offshore height, h is the depth and l is the characteristic horizontal length. For the propagation of long waves such as tsunamis, the Ursell number, U_r (Ursell 1953) is defined as

$$U_r = \frac{a}{\epsilon^2}, \tag{1.1.2}$$

it is important in this process to measure the relative importance of non-linear effects and frequency dispersion. When $a = H/h << 1$ and $\epsilon = h/l << 1$, both non-linear effects and frequency dispersion can be neglected and the linearised shallow water wave equations can adequately describe wave propagation (Mei 1983). As these long waves approach the coast the wave height increases and at some point the effects of non-linearity cannot be neglected. In that case, the fully non-linear shallow water wave equations are the suitable model, assuming one can neglect the effects of frequency dispersion.

Carrier & Greenspan (1958) studied the non-linear shallow water equations and proposed a method to transform these equations into a set of linear equations that can be solved analytically. It is still one of the few analytical solutions available for non-linear wave dynamics. Using this they investigated the run-up on a plane slope of periodic waves with several different initial shapes. Tuck & Hwang (1972) and Spielvogel (1976) extended the Carrier & Greenspan (1958) transformation and used it to solve long wave run-up also under prescribed initial water surface configurations. Tuck & Hwang (1972) investigated the problem of the generation of waves on a slope due to a bottom disturbance. Spielvogel (1976) extended the Carrier & Greenspan (1958) transformation and used it inversely to determine initial wave conditions offshore from the long wave run-up assuming a logarithmic initial surface profile on the slope at the instant of the maximum run-up.

Synolakis (1987) simplified the Carrier & Greenspan (1958) transformation, and applied it to the problem of a solitary wave propagating in a constant depth and running up a plane beach. His analytical results agreed well with laboratory experiments for non-breaking waves on the slope. Based on this simplification, Synolakis (1986) drew the conclusion that the maximum run-up predicted by the linear shallow-water equations was the same as that predicted by the non-linear shallow water equations, although the behaviour of the wave on the slope such as the wave amplitude and the water particle velocities were quite different. Kanoglu & Synolakis (1998) studied long wave evolution and run-up on piecewise linear two and three dimensional bathymetries using the linear shallow water wave equations. In addition, they de-

fined the amplification factors of different ocean bathymetry to study the evolution of solitary waves over variuos bathymetries.

Tsunami run-up and backwash on a plane beach is considered by Carrier, Wu & Yeh (2003). This work extends the work of Carrier & Greenspan (1958) to include more initial-value problems.

Pritchard & Hogg (2003) consider the introduction of fine sediment transport into the solution of Carrier & Greenspan (1958).

All of the simplified models above deal with non-breaking wave run-up. If the wave breaks during the run-up or run-down process, the basic physics of the run-up is complicated and far from being completely understood. Most of the previous work on breaking wave run-up consists of experimental studies or numerical simulations. It has been found from field and laboratory studies that after a wave breaks, the form of the propagating wave is similiar to a propagating bore in terms of appearance. Thus, the study of bore propagation and bore run-up may provide valuable information about breaking wave run-up. Ho & Meyer (1962) and Shen & Meyer (1963) proposed an analytical theory (see chapter 2 for details) for bore run-up using the non-linear shallow water wave equations. From this derivation, they found that when the bore arrived at the initial shoreline, the height of the bore became zero and, thus the bore collapses at the shoreline. After that, the fluid motion entered another stage in the form of a thin sheet of water propagating up the slope. The maximum run-up predicted by Shen & Meyer (1963) was:

$$R = \frac{u_0^2}{2g}, \tag{1.1.3}$$

which is independent of the beach slope. u_0 is the horizontal velocity of the bore at the instant it reaches the initial shoreline. Miller (1968) experimentally measured the maximum run-up of a bore on four beaches with different angles and compared those results with the prediction, given by equation (1.1.3). He found that the beach angle and the bottom roughness of the slope were important factors in determining the run-up of a bore, and the experimental results differed significantly from the theoretical predictions. Yeh (1991) also investigated the bore-like tsunami run-up in the laboratory and reported that bore collapse did not occur in his experiments.

The transition process that took place when the bore approached the initial shoreline was more of a 'momentum exchange' (Yeh 1991) between the incident bore and the small wedge-shaped water that was initially still ahead of the bore along the shore. The maximum run-up, however, seemed to be predicted from the initial offshore condition given by equation (1.1.3) by reducing the value of u_0. Thus, it appears that the bore run-up theory can give qualitative information about the physical process, and it is one of few analytical solutions available to describe the process of wave propagation after wave breaking.

The numerical solution of Keller, Levine & Whitham (1960) was studied analytically by Sachdev & Seshadri (1976), using an extension of Whitham's (1958) approach. This solution gives the entire flow behind the bore and is shown to be equivalent to the theory of modulated simple waves of Varley, Ventakaraman & Cumberbatch (1971). Another analytic solution for the motion of a bore over a sloping beach is given by Gupta (1993). In this case the initial bore is considered to be supercritical.

Analytical solutions for forced long waves on a sloping beach have been considered by Liu, Lynett & Synolakis (2003). The forced linear shallow water equation is considered. This equation has been used to describe landslide generated tsunamis (Tuck & Hwang 1972) and also long waves induced by moving atmospheric pressure distributions.

Svendsen & Madsen (1984) develop a theoretical model of turbulence effects in the modelling of a bore travelling through the surf zone. This work gives a moderately detailed description of the flow in a turbulent bore, the velocity profiles, the shear stresses and the energy dissipation. An analysis of the flow conditions at the toe of the turbulent front indicates significant differences from the usual description based on the finite-amplitude shallow water equations.

1.1.2 Laboratory experiments

Battjes (1974) used dimensional analysis to analyse the characteristics of periodic wave breaking and run-up on plane slopes. He showed that breaking criterion, breaker type, breaker height-to-depth ratio and the maximum run-up are approximately governed by only one parameter referred to as the surf similarity parameter:

$$\xi = \frac{\tan\beta}{(H/L_0)^{1/2}}, \tag{1.1.4}$$

where L_0 is the deep water wavelength of the incident periodic wave. Battjes (1974) summarised published experimental data to present empirical formulae of several wave characteristics as a function of the surf similarity parameter, ξ. For example, the maximum run-up normalised by the incident wave height was written by Hunt (1959) as:

$$\frac{R}{H} = \xi \qquad \text{for} \qquad 0.1 < \xi < 2.3. \tag{1.1.5}$$

This formula is known as Hunt's formula.

Stansby, Chegini & Barnes (1998) investigated the flow induced by 'dam-breaking' with different ratios of the upstream depth to the downstream depth. An interesting observation was the generation of a 'mushroom like' jet similar to the plunging jet of a breaking wave. While the structure and the evolution of the jet and the splash-up were complex and difficult to define, the overall surface profiles at different times agreed remarkably well with exact solutions of the non-linear shallow water equations. These results suggest that the same non-linear shallow water equations may also be applicable to breaking wave run-up if the details of plunging jets are not included in the analysis.

Jensen, Pedersen & Wood (2003) compare their experimental measurements for moderately non-linear wave run-up on steep beaches to existing long wave theories. These include a Boussinesq model and the dam-break solution from shallow water theory.

A review of experimental work on the study of turbulence in the surf and swash zone is given by Longo, Petti & Losada (2002). A review of the study of sediment tranport in the swash zone is given by Elfrink & Baldock (2002). Also cross-shore

sediment transport in the swash zone of natural beaches is considered by Butt & Russell (2000).

Experimental and numerical analyses were made by Archetti & Brocchini (2002) to assess the validity and potentialities of the integral swash zone model by Brocchini & Peregrine (1995). The numerical work also included the effects of seabed friction, which were previously neglected. Applications of the model to experimental data showed that it is a simple and useful tool for modelling swash zone flows.

An experimental study of the hydrodynamics in the swash zone was made by Petti & Longo (2001*a*). An impermeable concrete beach in a laboratory flume was considered. From the measurements it was seen that fluid velocity is almost uniform along the vertical, especially during run-up.

Turbulence and water surface elevation measurements in the swash zone were carried out by Petti & Longo (2001*b*). The swash motion was induced by plunging and collapsing breakers in a wave flume.

The shoreline motion given by Shen & Meyer (1963) was extended to include the effects of friction on a sandy beach by Puleo & Holland (2001). This was then compared to experimental results taken from field data.

An experimental study of tsunami run-up on coastlines was considered by Chanson, Aoki & Maruyama (2003). The study found that for tsunami run-up the wave front travels faster than a 'classical' dam break wave, because of the higher momentum of the wave. But further downstream the bore propagates at a similar speed to that predicted by the analytical solutions, discussed earlier.

1.1.3 Numerical simulations

There have been a number of numerical solutions relating to the run-up of non-breaking waves and breaking waves using different simplified models. For example, an early study by Brennen & Whitney (1970) used the inviscid dynamical equations of motion in Lagrangian co-ordinates to investigate run-up of waves, their calculation was reasonable for non-breaking waves, but computation stopped when the wave was breaking.

The non-linear shallow water wave equations have been widely employed to model long wave propagation and the run-up process. If provision is made in the numerical model to account for the energy dissipation associated with wave breaking, they may also be used to simulate the breaking wave run-up.

Two basic types of numerical methods have been used to solve the shallow water equations: (i) the method of characteristics and (ii) finite difference methods. The characteristics method has the advantage that the line of characteristics has clear physical meaning, and the path of the shoreline is always a characteristic line (except for still water), thus, the position of the shoreline can be obtained directly from the computation. Freeman & Mehaute (1964) used this method to study wave breaking and surging on a dry bed. Finite difference methods have been used more successfully to compute the shallow water wave equations. Keller et al. (1960) solved these equations to calculate the motion of a bore over a sloping beach. The results found compared well to the formula given by Whitham (1958) for the variation in the strength and height of a bore.

Hibberd & Peregrine (1979) solved the shallow water equations in conservative form using the Lax-Wendroff scheme, and applied the scheme to calculate the evolution and run-up of a uniform bore on a plane slope. The moving shoreline was treated by adding new grid points during the run-up, and, if necessary, subtracting the points that were not covered by water during the backwash. A predictor-corrector-smoothing procedure was presented to predict whether or not the grid-points are needed to be adjusted.

Titov & Synolakis (1995) solved the characteristic form of the shallow water equations using the finite difference methods and used it to model the propogation and run-up of solitary waves. The characteristic equations were solved using a Godunov scheme to avoid the numerical instabilities problem associated with wave breaking.

Non-breaking and breaking solitary wave run-up was considered both experimentally and numerically by Li & Raichlen (2002). The nonlinear shallow water equations were solved using the weighted essentially non-oscillatory (WENO) shock

capturing scheme.

Numerical simulations of swash oscillations on a steep beach are considered by Baldock & Holmes (1999). Simulations of the shoreline displacements based on bore run-up theory are compared with experimental data for regular waves, wave groups and random waves. The theory is used to derive parameters that predict the onset of swash saturation and the spectral characteristics of the saturated shoreline motion. Simulation of irregular wave run-up using a series of overlapping monochromatic swash events is found to reproduce the typical features of swash oscillations in the swash zone.

Swash oscillations on gentle and steep slopes are considered by Kobayashi, De-Silva & Watson (1988). A numerical model is developed, based on the solver of Kobayashi, Otta & Roy (1987) to predict the wave transformation in the surf and swash zones on gentle slopes as well as the wave reflection and swash oscillations on relatively steep beaches. The numerical results are compared with small-scale test data from monochromatic waves spilling on gentle slopes and for waves plunging and surging on steep slopes.

Swash on a gently sloping beach is considered by Raubenheimer, Guza, Elgar & Kobayashi (1995). Waves observed in the inner surf and swash zones of a fine grained gently sloping beach are modelled with the non-linear shallow water equations. The model is compared to field data.

A statistical model for the distribution of swash maxima on natural beaches is considered by Holland & Holman (1993). A method from Cartwright & Longuet-Higgins (1956) is used as a comparison to run-up field data. The model is found to be satisfactory for describing the distribution of average swash maxima.

Packwood (1983) modelled the influence of a porous bed on the run-up of a bore on a gently sloping sandy beach. It was shown that fine-medium grade sands have very little effect in the run-up phase. Significant differences were found between impermeable and porous bed solutions in the backwash mode. These differences could possibly explain certain sand erosion and deposition phenomena.

1.2 Overtopping

Research into wave overtopping of coastal structures has been the subject of numerous investigations over the past 50 years. Since then the overtopping prediction tools for typical sea defense structures have continuously been refined. The term wave overtopping is used here to refer to the process where waves hit a sloping structure, run up the slope, and eventually, if the crest level of the slope is lower than the highest run-up level, overtop the structure.

1.2.1 Theoretical analyses

Very few analytical results exist for wave overtopping. Most of the results available for overtopping of various structures are based on laboratory and numerical experiments. Theoretical work is done based on the results of the experiments and formulae are provided for overtopping rates. Details of these types of studies are given below in the proceeding subsections.

Kikkawa, Shi-Igai & Kono (1968) presented an overtopping expression based on a weir analogy. The expression was verified by model tests with regular waves. Based on this model Oezhan & Yalciner (1991) introduced an analytic model for solitary wave overtopping of a sea dike.

Another method based on wave energy considerations is used by Umeyama (1993) to formulate the wave overtopping discharge on a vertical barrier, and the model is compared well with model tests.

A set of equations are derived by Mizuguchi (1993) for the wave overtopping rate over a vertical wall. An expression is derived for the resultant reflection coefficient based on a wave energy concept with the assumption that overtopping yields partially standing waves. The energy loss due to wave overtopping is evaluated using an ideal fluid model over a sharp-edge weir.

A theoretical and numerical model of overtopping over a vertical wall was considered by Jervis & Peregrine (1996). This work is dicussed in more depth in chapter 7.

A solution for the overtopping of swash over a truncated beach is given by Peregrine & Williams (2001) based on the solution of Shen & Meyer (1963). In this work an analytic solution of the non-linear shallow water waves equations is found for the behaviour of the wave height and velocity at the beach truncation point. An expression is also presented for the amount of water that may overtop the beach for varying truncation points. This work is also presented in chapter 3 of this thesis.

1.2.2 Laboratory experiments

When investigating wave overtopping of structures it is evident that the discharge depends not only on environmental conditions such as wave height, wave period and water level, but also on the geometrical layout and material properties of the structure. Thus, there are almost infinite possible combinations. Therefore, although a lot of investigations related to wave overtopping have been conducted, none of these cover all situations. Each of the investigations typically covers one or a few specific cases, which are then conducted by means of physical model tests in the laboratories (typically small scale). Such investigations usually lead to an empirical relationship between the environmental conditions, geometrical layout and material properties of the structure and the overtopping discharge.

Tables 1.1, 1.2 and 1.3 present overtopping investigations based on model tests of various coastal structures exposed to irregular waves, along with the resulting overtopping discharge predictions formulae. The tables are taken from Kofoed (2002).

In these tables Q is the dimensionless discharge, R_c is the freeboard, H_s is the significant wave height and q is the average discharge per unit length of the structure. $R = R_c/H_s$ is called the relative freeboard. The freeboard is defined as the distance from the top of a structure to the still water line. For still water of depth d, over a structure of height l, the freeboard is given as $R_c = d - l$.

The overtopping discharge is, as can be seen in tables 1.1-1.3, completely dependent on the wave climate as given by the significant wave height, the water level (through the crest freeboard) and also in many cases, the wave peak or mean period. However, various studies have also shown dependency on other parameters related

Authors	Structures	Overtopping model	Dimensionless overtopping discharge Q	Dimensionless freeboard R
Owen (1980), Owen (1982)	Impermeable smooth, rough straight and bermed slopes	$Q = ae^{-bR}$	$\frac{q}{gH_sT_{m0}}$	$\frac{R_c}{H_s}\sqrt{\frac{s_{m0}}{2\pi}}\frac{1}{\gamma}$
Bradbury & Allsop (1988)	Rock armoured impermeable slopes with crown walls	$Q = aR^{-b}$	$\frac{q}{gH_sT_{m0}}$	$\left(\frac{R_c}{H_s}\right)^2\sqrt{\frac{s_{m0}}{2\pi}}$
Aminti & Franco (1988)	Rock, cube and Tetrapod double layer armour on rather impermeable slopes with crown walls	$Q = aR^{-b}$	$\frac{q}{gH_sT_{m0}}$	$\left(\frac{R_c}{H_s}\right)^2\sqrt{\frac{s_{m0}}{2\pi}}$
Ward & Ahrens (1992)	7 different seawall/revetment designs	$Q = ae^{-bR}$	$\frac{q}{\sqrt{gH_s^3}}$	$\frac{R_c}{(H_s^2L_{p0})^{1/3}}$
Pedersen & Burcharth (1992)	Rock armoured rather impereable slopes with crown walls	$Q = aR$	$\frac{qT_{m0}}{L_{m0}^2}$	$\frac{H_s}{R_c}$

Table 1.1: Models for average overtopping discharge formulae. Table is taken from Kofoed (2002).

Authors	Structures	Overtopping model	Dimensionless overtopping discharge Q	Dimensionless freeboard R
van der Meer & Janssen (1994)	Impermeable, smooth, rough straight and bermed slopes	$Q = a\mathrm{e}^{-bR}$	$\frac{q}{\sqrt{gH_s^3}}\sqrt{\frac{s_{p0}}{\tan\alpha}}$ for $\xi_{p0} < 2$ $\frac{q}{\sqrt{gH_s^3}}$ for $\xi_{p0} \geq 2$	$\frac{R_c}{H_s}\frac{\sqrt{s_{p0}}}{\tan\alpha}\frac{1}{\gamma}$ for $\xi_{p0} < 2$ $\frac{R_c}{H_s}\frac{1}{\gamma}$ for $\xi_{p0} \geq 2$
Franco, De Gerloni & van der Meer (1994), Franco & Franco (1999)	Vertical wall breakwater with and without perforated front	$Q = a\mathrm{e}^{-bR}$	$\frac{q}{\sqrt{gH_s^3}}$	$\frac{R_c}{H_s}\frac{1}{\gamma}$
Pedersen (1996)	Rock armoured permeable slopes with crown walls	$Q = R$	$\frac{qT_{m0}}{L_{m0}^2}$	$3.2 \times 10^{-5} \times \frac{H_s^5 \tan\alpha}{R_c^3 A_c B}$
Hedges & Reis (1998)	Impermeable smooth, rough, straight and bermed slopes (Data from Owen (1982))	$Q = a(1-R)^b$ for $0 \leq R < 1$ $Q = 0$ for $R \geq 1$	$\frac{q}{\sqrt{gR_{u_{\max}}^3}}$	$\frac{R_c}{R_{u_{\max}}}$

Table 1.2: Models for average overtopping discharge formulae, continued. Table is taken from Kofoed (2002).

Authors	Structures	Overtopping model	Dimensionless overtopping discharge Q	Dimensionless freeboard R
Hebsgaard, Sloth & Juhl (1998)	Rubblemound structures with and without super structure, armour layer of rounded stones, quarry rocks, Antifer, Accropode and Dolos units	$Q = ae^{-bR}$	$\frac{q}{\ln(s_{p0})\sqrt{gH_s^3}}$	$\frac{R_c^*}{R_s}\frac{1}{\gamma}$
Schüttrumpf, Möller, Oumeraci, Grüne & Weissmann (2001)	Impermeable smooth 1 : 6 slope (for no freeboard, $R_c = 0$) and without overtopping ($R_c > R_{\max}$)	$Q = ae^{-bR}$ (a dependent on ξ_{m0})	$\frac{q}{\sqrt{2gH_s^3}}$	$\frac{R_c}{1.5\xi_{m0}H_s}$

Table 1.3: Models for average overtopping discharge formulae, continued. Table is taken from Kofoed (2002).

to the wave climate.

Several investigations have shown that the overtopping discharge decreases when the angle of attack increases, except for small angles of incidence. The effect of oblique wave attack is included in the overtopping expressions by van der Meer & Janssen (1994) through the reduction factor γ_β for sloping structures.

Franco et al. (1994) comment on the effect of directional spreading on overtopping discharge on both slopes and vertical walls. For slopes, the effect of directional spreading is minimal for head-on waves but results in faster decay for increasing angle of attack compared with long crested waves. For vertical wall structures the directional spreading reduces the overtopping discharge significantly even for head-on waves. The reduction in overtopping discharge for multi-directional and oblique waves is also reported by Sakakiyama & Kajima (1998)

Typically, the model tests performed in overtopping investigations utilise standard wave spectra such as TMA or JONSWAP. These spectra apply to offshore conditions or conditions with simple foreshores.

In order to take more complicated situations into account, van der Meer & Janssen (1994) incorporate double-peaked spectra in their overtopping formulae by splitting the spectra into two, identifying the peak periods for each of the two parts and combining these into an equivalent peak period.

Hawkes (1999) comments on swell and bimodal seas, and states that they possibly represent worst case (here worst case refers to most overtopping) sea states with regard to mean overtopping discharge. The prediction methods by Owen (1980) and Hedges & Reis (1998) work well for wind sea overtopping, while the results of van der Meer & Janssen (1994) are realistic, but less consistent. Owen's (1980) method overpredicts swell overtopping by a factor of 5, as the predicted overtopping discharge increases indefinitely for increasing wave periods. Hedges and Reis' (1998) and van der Meer and Janssen's (1994) methods incorporate separate formulae for plunging waves, where overtopping is strongly dependent on wave period, and for surging waves, where it is much less dependent. According to Hawkes (1999), Hedges and Reis' (1998) method seems the most promising.

Schüttrumpf et al. (2001) performed large scale model tests with natural spectra from field measurements which are multi peaked due to the influence of the foreshore. They concluded that the peak period is of no use when describing run-up and overtopping, and have proposed to use the mean period instead, as it appears in table 1.3.

Shankar & Jayaratne (2003) consider wave run-up and overtopping on smooth and rough slopes of coastal structures. A series of hydraulic tests were carried out in a glass flume to investigate the influences of wave height, wave period, wave steepness, surf similarity parameter, roughness, layer thickness and porosity on wave run-up and overtopping of 1:2 sloped impermeable and permeable breakwaters fronted by a 1:10 gentle, smooth beach slope. The results are compared with the data given in the Shore Protection Manual (1984).

1.2.3 Numerical simulations

Monochromatic wave overtopping over the crest of an impermeable coastal structure on a sloping beach is considered numerically by Kobayashi & Wurjanto (1989). The numerical model is an extension of the model of Kobayashi et al. (1987) for run-up on such a structure. The model of Kobayashi et al. (1987) is basically the same model used by Packwood (1980) and Packwood & Peregrine (1980).

Hu & McCauley (1997) consider a model of applying a monchromatic wave overtopping equation to irregular waves. This method improves other methods based only on regular wave run-up. The overtopping formula of Weggel (1976) for regular waves is extended to include the consideration of irregular waves.

Dodd (1998) investigated wave run-up, overtopping and regeneration by solving the non-linear shallow water wave equations using a Roe-type Riemann solver, which was developed in gas dynamics to track shock waves. An energy dissipative term representing bottom friction was included in the model. Dodd (1998) conducted simulations of wave propagation and overtopping including random waves and compared them with experimental results, good agreements were found from his investigation.

Hiraishi & Maruyama (1998) presented a numerical model for calculation of overtopping discharges for a vertical breakwater in multi directional waves. The basic assumption is that the overtopping discharge can be described by a weir expression as suggested by Kikkawa et al. (1968).

Hu, Mingham & Causon (2000) presented a one-dimensional numerical model for calculation of overtopping using the non-linear shallow water equations. The model solutions were compared with analytical solutions and laboratory data for wave overtopping at sloping and vertical seawalls and good agreement was found. The only downfall is that the model was only compared with regular wave data with irregular waves not being considered.

Prototype measurements, physical model tests and numerical model computations of wave run-up and overtopping on dikes with shallow foreshores is considered by van Gent (2001). The numerical model used was a time-domain model that simulates wave motion on coastal structures. Details of this model can be found in van Gent (1994) and van Gent (1995).

A two-dimensional numerical model of wave run-up and overtopping is considered by Hubbard & Dodd (2002). The model is based on the two-dimensional non-linear shallow water water equations on a sloping bed. The model is an extension of the one-dimensional model of Dodd (1998). The two-dimensional nature of the model means it can be used to simulate wave transformation, run-up, overtopping and regeneration by obliquely incident and multi-directional waves over alongshore-inhomogeneous sea walls and complex, submerged or surface piercing features.

The overtopping of a plane slope by multiple swash events is considered by Williams & Peregrine (2003). This work is also described in chapter 6 of this thesis. Water waves overtopping a truncated plane slope are considered. The single swash case considered by Peregrine & Williams (2001) is extended numerically to consider multiple swash events. Wave sets of random amplitudes with different periods are considered.

With all these studies on overtopping, one might ask what levels of overtopping are deemed to be safe. Goda (1971) and Goda (1985) developed guidelines given in

figure 1.2 based on prototype investigations consisting of wave climate measurements and expert impressions of the impact of overtopping volumes on different objects situated on top of breakwaters. These guidelines are discussed in Franco et al. (1994), where experimental results are compared with figure 1.2. In figure 1.2 critical overtopping discharges are shown for typical structure types when considering sea defence structures.

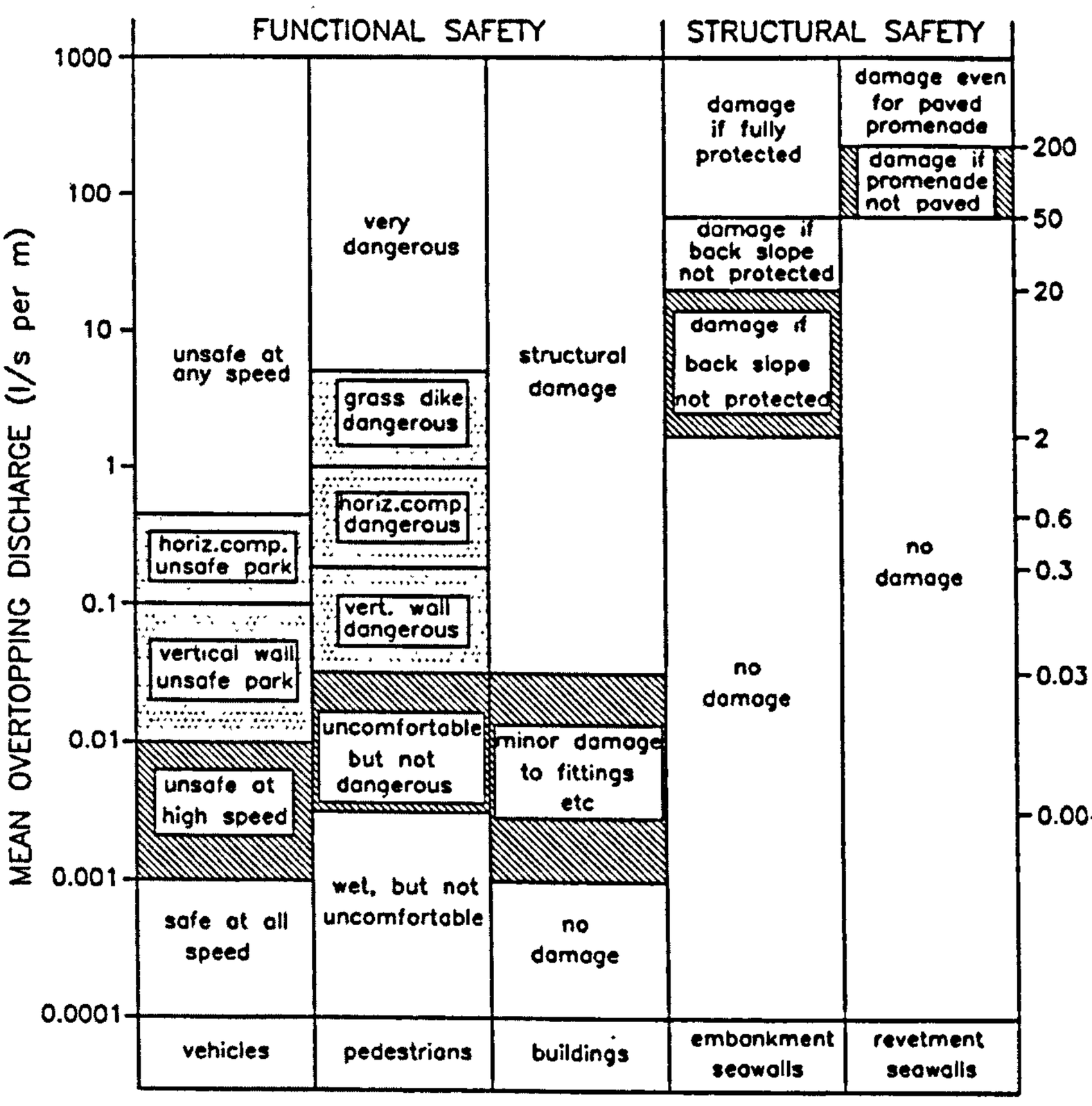

Figure 1.2: Criteria for critical overtopping discharges. Taken from Franco et al. (1994).

1.3 Overview of thesis

A literature review on run-up in the swash zone and overtopping has been given in the preceding sections.

In chapter 2, the equations of motion for this work are presented. These equations are the non-linear shallow water wave equations. An introduction to shallow water theory is presented in section 2.2. In section 2.3, the work of Ho & Meyer (1962) and Shen & Meyer (1963) is discussed, with the solution of Shen & Meyer (1963) being presented.

Chapter 3 considers the run-up and overtopping of a single swash event over a truncated plane beach. The solution of Shen & Meyer (1963) for swash on a beach is extended to include the effects of overtopping. Solutions for the height and velocity in the neighbourhood of the truncation point are presented. An analytic expression for the amount of water that may overtop the beach is also given.

In chapter 4 the numerical scheme used in chapters 5 and 6 is introduced. The scheme is described and tested against existing analytical and numerical results.

In chapter 5 the analytical results for run-up presented in chapter 3 are extended numerically to consider the run-up and interactions of multiple swash events on plane beaches. Waves of varying amplitudes and periods are considered.

Chapter 6 takes the waves presented in chapter 5 and includes the effects of overtopping. Numerical results are presented for the amount of water that may overtop beaches of varying lengths.

In chapter 7, analytical solutions are derived for the motion of a jet up a vertical wall. With these solutions, expressions are found for how the jet behaves as it passes up and over the top of the wall. An expression is found for the amount of water that may overtop a wall of varying height.

Finally, in chapter 8, this work is brought to a conclusion with a discussion of what has been considered and what could be considered next.

Chapter 1. Introduction

Chapter 2

Equations of motion

2.1 Introduction

The run-up of waves on a planar slope is of great importance. Various studies have been made by Carrier & Greenspan (1958), Keller et al. (1960), Ho & Meyer (1962), Shen & Meyer (1963), Meyer & Taylor (1972) and Synolakis (1987). In this thesis the work of Ho & Meyer (1962), Shen & Meyer (1963) and Meyer & Taylor (1972) is used. An introduction and discussion on their work is presented in section 2.3.

Another problem of great interest is the dam-break problem which has been considered by many including Stoker (1957). A brief description of the dam-break problem is discussed in section 2.2.5. The reason for considering this problem is that there is a connection between the dam-break problem and the solution due to Shen & Meyer (1963). This connection is discussed later in this work.

2.2 Shallow water theory

2.2.1 Introduction

The surf and swash zone is the area closest to the shoreline where waves break due to the effect of bottom topography. The wave motion is modelled here using the nonlinear shallow water equations. The nonlinear shallow water equations do not directly include the effects of turbulence or other small scale effects, instead they

model the flow field at a larger scale, the length scale of interest being the wavelength of the waves propagating shoreward.

The nonlinear shallow water equations are applicable at scales where gradients in water surface and bed topography are gentle and where the horizontal length scale is significantly greater than the vertical. The equations are also applicable over steep slopes. This is discussed further in chapter 3. The equations describe the motion of a thin layer of fluid of constant density in which the depth and velocity are functions of horizontal coordinates and time only. The pressure is taken as hydrostatic and the velocity fields are considered to be depth-averaged quantities. The nonlinear shallow water equations can be a good model for the surf and swash zone on beaches and are the simplest dynamic model of wave breaking on a beach of gentle slope. If details of the breaking and the associated turbulent motions are on shorter length and time scales than that are of interest, the breaking event can be modelled as the development of a surface and current discontinuity in the shallow water equations. Such discontinuities are bores and are dynamically consistent if mass and momentum are conserved.

The nonlinear character of the equations means that analytical techniques can only be used to solve them in very special circumstances (see chapter 3, where a special case of truncating a beach slope is considered). The equations admit multi-valued solutions which fall outside their realm of validity since shallow water dynamics is a long wave approximation. This multi-valuedness is avoided by introducing discontinuities at points and by requiring mass and momentum conservation across these discontinuities, where energy is now lost. Moving discontinuities represent bores. When discontinuities are involved in numerical simulations, the equations need to be considered in flux conservative form and should be written as hyperbolic conservation laws (see chapter 4).

In hyperbolic conservation form the nonlinear shallow water equations are similar to the well known Euler equations for compressible gas flow. The connection between these two sets of equations is discussed in section 2.2.3.

2.2.2 Equations of motion

Breaking waves generate a swash that is very thin compared with its extent along the slope. The nonlinear shallow water equations are thus a fair approximation to wave motion in the surf and swash zone (Barnes 1996; Raubenheimer et al. 1995; Kobayashi et al. 1988). The nonlinear shallow water equations for one-dimensional flow over the general surface $d^*(x^*)$ are given by

$$\frac{\partial h^*}{\partial t^*} + \frac{\partial (u^* h^*)}{\partial x^*} = 0, \tag{2.2.1}$$

$$\frac{\partial u^*}{\partial t^*} + u^* \frac{\partial u^*}{\partial x^*} + g \frac{\partial h^*}{\partial x^*} - g \frac{dd^*}{dx^*} = -f_c \frac{u^* |u^*|}{h^*}, \tag{2.2.2}$$

where x^* is measured horizontally, t^* is the time, $h^*(x^*, t^*)$ is the water depth above the sea bed and $u^*(x^*, t^*)$ is the water velocity in the x^* direction. The * denotes dimensional variables and g is the acceleration due to gravity. The term on the right hand side is a friction term, f_c is called the Chézy friction coefficient. In this work we deal only with shallow water flow over plane beaches without the effects of friction being considered. In this case $f_c = 0$ and $d(x) = -\gamma x$, where γ is the angle of the beach slope to the horizontal. In this case the dimensional shallow water wave equations are written as

$$\frac{\partial h^*}{\partial t^*} + \frac{\partial (u^* h^*)}{\partial x^*} = 0, \tag{2.2.3}$$

$$\frac{\partial u^*}{\partial t^*} + u^* \frac{\partial u^*}{\partial x^*} + g \frac{\partial h^*}{\partial x^*} + g\gamma = 0. \tag{2.2.4}$$

Non-dimensionalising with respect to some chosen water depth H_0 using the variables

$$x = \frac{\gamma x^*}{H_0}, \quad h = \frac{h^*}{H_0}, \quad d = \frac{d^*}{H_0}, \quad t = \gamma t^* \sqrt{\frac{g}{H_0}} \quad u = \frac{u^*}{\sqrt{g H_0}}, \tag{2.2.5}$$

our equations in dimensionless form are

$$\frac{\partial h}{\partial t} + \frac{\partial (uh)}{\partial x} = 0, \tag{2.2.6}$$

$$\frac{\partial u}{\partial t} + u \frac{\partial u}{\partial x} + \frac{\partial h}{\partial x} + 1 = 0. \tag{2.2.7}$$

When considering equations (2.2.6) and (2.2.7) for shallow water waves over a planar slope, it is often useful to write them in characteristic form, thus emphasising

their hyperbolic nature. If we introduce the local long wave velocity c, defined by $c^2 = h$, equations (2.2.6) and (2.2.7) may be written in the form

$$\left(\frac{\partial}{\partial t} + (u+c)\frac{\partial}{\partial x}\right)\alpha = 0, \tag{2.2.8}$$

$$\left(\frac{\partial}{\partial t} + (u-c)\frac{\partial}{\partial x}\right)\beta = 0, \tag{2.2.9}$$

where we define α and β to be the characteristic variables (Riemann invariants) given by

$$\alpha(x,t) = u + 2c + t, \qquad \beta(x,t) = u - 2c + t. \tag{2.2.10}$$

Equations (2.2.8) and (2.2.9) imply that α and β are constant along the characteristics C_+, C_-, in (x,t) given by

$$\frac{\mathrm{d}x}{\mathrm{d}t} = u + c, \quad \text{and} \quad \frac{\mathrm{d}x}{\mathrm{d}t} = u - c \tag{2.2.11}$$

respectively. The trajectories C_+ and C_- are called the advancing and receding characteristics and correspond physically to paths of infinitesimal wave disturbances on the flow.

2.2.3 Gas dynamics analogy

It is possible to introduce a set of dependent variables in such a way that the equations given by shallow water theory become analogous to the fundamental differential equations of gas dynamics, for the case of a compressible flow involving only one space variable x^*. According to Stoker (1957), this analogy was first realised by Riabouchinsky (1932).

If we introduce the mass per unit area or density as

$$\overline{\rho}^*(x^*,t^*) = \rho[\eta^*(x^*,t^*) + d^*(x^*)], \tag{2.2.12}$$

where $\eta^*(x^*,t^*) = h^*(x^*,t^*) - d^*(x^*)$ is the surface elevation. Since d^* depends only on x^* we have

$$\frac{\partial \overline{\rho}^*}{\partial t^*} = \rho\frac{\partial \eta^*}{\partial t^*}. \tag{2.2.13}$$

We define a corresponding pressure $\overline{p}^*$ as

$$\overline{p}^*(x^*,t^*) = \frac{g}{2\rho}[\overline{\rho}^*(x^*,t^*)]^2. \tag{2.2.14}$$

From the above we can see that this corresponds to a polytropic relation between the pressure $\overline{p}^*$ and the density $\overline{\rho}^*$ of power 2.

The momentum equation from the inviscid shallow water equations given by (2.2.2) with $f_c = 0$, can now be written as

$$\rho(\eta^* + d^*)\left(\frac{\partial u^*}{\partial t^*} + u^*\frac{\partial u^*}{\partial x^*}\right) = -g\rho(\eta^* + d^*)\frac{\partial \eta^*}{\partial x^*}, \tag{2.2.15}$$

using (2.2.12) and (2.2.14), we find

$$\overline{\rho}^*\left(\frac{\partial u^*}{\partial t^*} + u^*\frac{\partial u^*}{\partial x^*}\right) = -\frac{\partial \overline{p}^*}{\partial x^*} + g\overline{\eta}^*\frac{\partial h^*}{\partial x^*}. \tag{2.2.16}$$

The mass equation is written as

$$\frac{\partial(\overline{\rho}^* u^*)}{\partial x^*} = -\frac{\partial \overline{\rho}^*}{\partial t^*}. \tag{2.2.17}$$

The differential equations given by (2.2.16) and (2.2.17) together with the polytropic law (2.2.14) are identical in form to the equations of a polytropic compressible gas for a one-dimensional flow, except for the $g\overline{\rho}^* d_x^*$ term on the right hand side of (2.2.16). This term vanishes if the original undisturbed depth d^* of the water is constant. From (2.2.16) and (2.2.17) it can be seen that the analogy to the sound of speed, c^* in gas dynamics is given by $c^* = \sqrt{g(\eta^* + d^*)}$ and is called the local long-wave velocity.

2.2.4 Bore conditions

Relations governing the motion of bores are given by Stoker (1957), supplementing the equations of motion in the form of internal boundary conditions. The shallow water equations are valid where wave motion is continuous, but across the discontinuity of height and water velocity at the bore, separate conditions are required. For a bore of height h_2 travelling through water of height h_1 and velocity u_1, the water velocity u_2 is given by

$$u_2 = u_1 + \frac{h_2 - h_1}{h_2}\sqrt{\frac{gh_2(h_1 + h_2)}{2h_1}}, \qquad \text{for} \qquad h_2 > h_1. \tag{2.2.18}$$

Shortly after a wave has broken the surface slopes become sufficiently reduced, making it feasible to use the shallow water equations coupled with the bore relations

to describe the ensuing motion of the water. In this theory the bores are represented as a discontinuity at a point whereas in practice bores have finite width. This width is typically twice the greater water depth for a fully developed bore. Thus if the beach angle is small the waves are of sufficient length that not only shallow water theory is valid but also the width of any bores becomes unimportant.

There are however, three types of bores, depending on the strength of the bore, with only one type valid in this analysis which is given in point three below. Binnie & Orkney (1955) classify the types of bores as follows:

1. When the change in water levels is slight, the transition is formed by a smooth fronted wave carrying a train of waves behind. This is known as a smooth undular bore.

2. When the change in water level is more marked a wave train is again formed but the first one at least is breaking.

3. For the more acute change in water levels a turbulent bore is formed and the change in levels appear over a short region of intense turbulence.

If a long wave of elevation travels in shallow water it steepens and forms a bore. This bore was found undular in laboratory experiments performed by Favre (1935) and in numerical calculations of Peregrine (1966) if the ratio of the change in level to the initial depth of water is less than 0.28. If this ratio is greater than 0.28 but less than 0.75 there are still undulations, but the first one is breaking; the maximum amplitude of the undulations is limited by breaking. More accurate computations were made by Teles da Silva & Peregrine (1990). For greater differences in depth there are no undulations, and experiments by Miller (1968) confirm that the relation (2.2.18) gives an adequate description of the bore dynamics.

Undular bores do not suffer full energy loss. Some energy may be lost at the bore (e.g. type 2) but the rest is radiated rearwards forming the associated train of waves. Thus undular bores may extend for some hundred times the water depth in width and treating this region as a point discontinuity would not work.

2.2.5 Dam-break problem

Consider a height of water h_0 to be held behind a dam. If the dam were to instantaneously collapse, how would the flow be described? This problem is known as the dam-break problem. There exists an analytical solution to this problem. This solution is found by using the method of characteristics (Stoker 1957). The dimensionless solution is

$$h(x,t) = \frac{1}{9}\left(2\sqrt{h_0} - \frac{x}{t}\right)^2, \qquad u(x,t) = \frac{2}{3}\left(\sqrt{h_0} + \frac{x}{t}\right) \tag{2.2.19}$$

for $-\sqrt{h_0} \leq x/t \leq 2\sqrt{h_0}$. We introduce the dam-break problem here since direct correspondence is made in chapter 3, between this problem and the work of Shen & Meyer (1963). We also consider this problem further in chapter 4 as a test for our numerical scheme.

2.3 Work of Shen, Ho & Meyer

2.3.1 Introduction

Motion of a single bore incident on a beach was treated analytically by Ho & Meyer (1962) and the following run-up by Shen & Meyer (1963). These authors give an asymptotic description near the shoreline of the bore moving close to the initially undisturbed shoreline. Initial motion of the shoreline was found to have a singularity in the acceleration, derived from a singularity at the corresponding point in the characteristic formulation of the equations of motion. Major predictions of Meyer and his co-workers were:

1. Bore height approaches zero as it moves close to the shoreline.

2. Bore and water velocities approach a finite value as the bore nears the shoreline.

3. In the ensuing motion the position of the shoreline depends only on gravity and is thus characterised by a single parameter - the initial shoreline velocity at the instant the bore arrives at the shoreline.

4. A further bore forms in the backwash if there exists no following wave, and is landward facing.

Seaward input thus influences the value of the initial shoreline velocity only up to a certain time after which no further influence can be transmitted to the shoreline unless it meets a bore.

2.3.2 Run-up of a bore on a beach

Analytic work of Meyer and his collaborators concentrated on evaluating limiting properties as the bore approaches the shoreline and initial behaviour at the start of the run-up mode. Their approach was to consider limits taken along specified characteristics defined in the space-time plane. A boundary characteristic, C, was defined as the first receding characteristic emanating from the seaward boundary position x_0 at the initial time t_0. This 'mathematical' boundary replaced the more physically realistic boundary $x = x_0$ in the calculation. Input data was thus restricted to specifying the initial bore height (giving the values β_C on the characteristic C) and the distribution of the Riemann variable α along C, denoted by $\alpha_C(t)$. A limiting characteristic, L, was defined as the first advancing characteristic to meet the shoreline from behind the bore. Calculation of limits as the bore approached the shoreline arose from the area included by the bore path and the two characteristics L and C (see figure 2.1). The value of the constant of integration u_0 was taken such that the bore approached the space origin at time zero.

In the paper of Ho & Meyer (1962) the following assumptions were made, which led to the description of a bore up to the shoreline being described. Shen & Meyer (1963) used the analysis given by Ho & Meyer (1962) to calculate the run-up which emanates in the proceeding flow. The work of Shen & Meyer (1963) extends the limit approach in an attempt to derive the initial velocity of any reflected bore and the initial velocity of the shoreline. They considered various modes of approach to $\alpha = 0, \beta = 0$ in the characteristic plane (i.e. at the point in the characteristic plane corresponding to the space origin at the time of arrival of the bore), to derive their

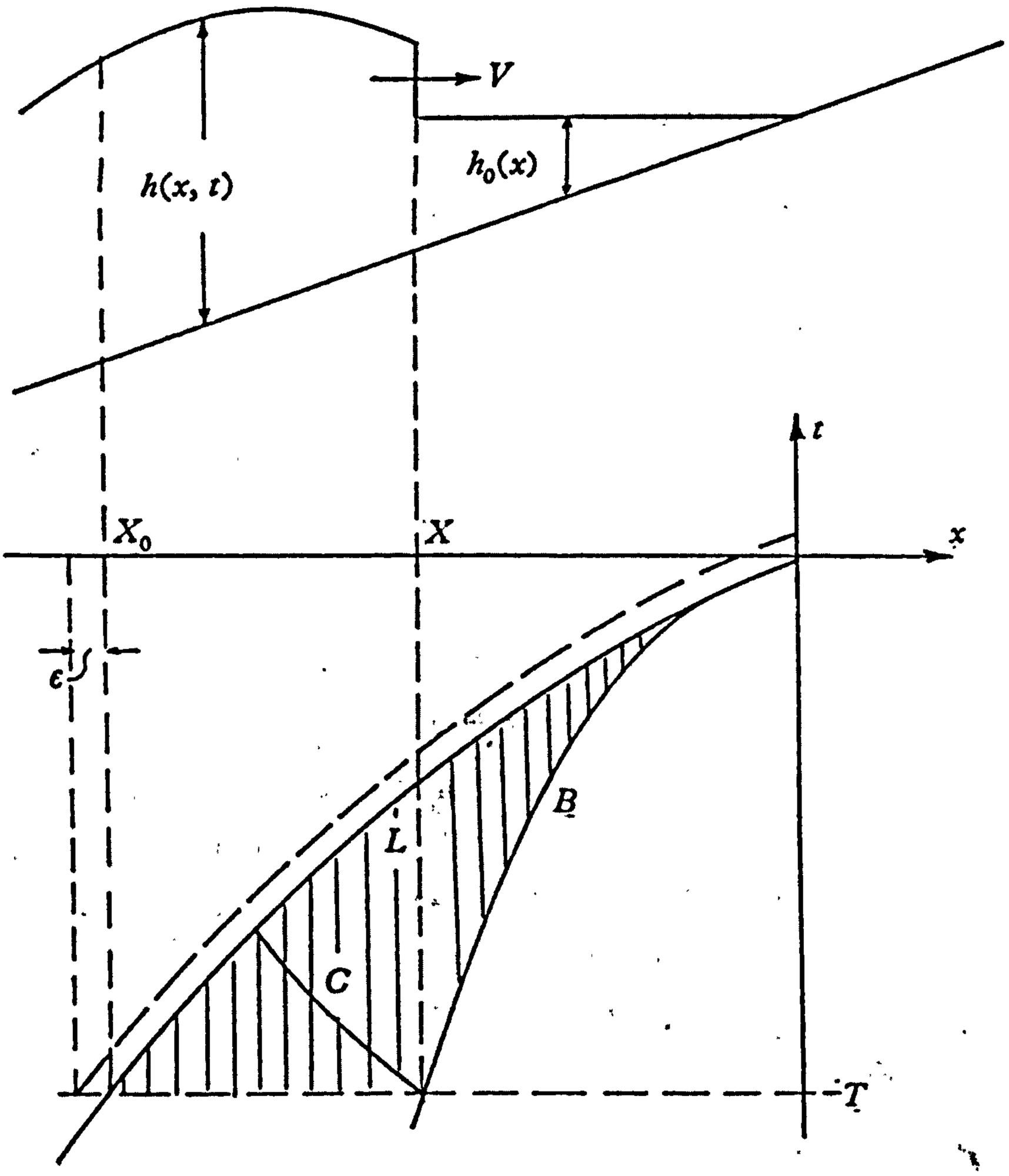

Figure 2.1: Definition sketch and (x,t)-diagram showing locus B of succesive bore positions, limiting characteristic L and seaward boundary characteristic C. A greatly contracted horizontal scale is implied. Figure taken from Shen & Meyer (1963).

predictions. The shoreline position was found to be of the form

$$x_s = u_0 - \frac{1}{2}t^2 + x_0, \tag{2.3.1}$$

where u_0 is the initial instantaneous shoreline velocity and x_0 is the initial position. The shoreline velocity is then given by

$$u_s = u_0 - t \tag{2.3.2}$$

and the shoreline acceleration

$$\frac{du_s}{dt} = -1 \quad \text{for} \quad t > 0. \tag{2.3.3}$$

Further, the water depth, h, local to the shoreline was given by

$$h(x,t) = \frac{(x_s - x)^2}{9t^2}, \tag{2.3.4}$$

and the water velocity, u, can be found as

$$u(x,t) = \frac{1}{3t}(u_0 t - 2t^2 + 2x). \tag{2.3.5}$$

At the shoreline

$$\alpha = u_s - u_0 + t = \beta$$

and thus the shoreline corresponds to $\alpha = 0, \beta = 0$ for all time $t > 0$. The shoreline is a coincidence of advancing and receding characteristics. No other characteristic line can meet the shoreline otherwise multi-valuedness must result. The shoreline is thus insensitive to wave motion behind the bore; the shoreline is specified completely by the initial shoreline velocity u_0 and from the position x_0, where it starts.

The possibility of a different mode of approach to the point $\alpha = 0, \beta = 0$ in the characteristic plane leads to a restriction on the time for which the above is valid. A different family of paths of approach to the extraordinary point $\alpha = 0, \beta = 0$ corresponds to limit lines (i.e. lines along which the inverse transformation from characteristic variables fails). Thus the solutions already obtained are only admissable until the time appearance of the first limit line. This is realised physically as the formation of a secondary bore, which forms from within the flow and eventually meets the shoreline. The shoreline is thus restricted from receding to large negative

values as predicted by (2.3.1) for times long after the initial shoreline motion. Precise details of the genesis and movement of the secondary bore is not available from the analysis of Shen & Meyer (1963). Their work does predict that the water level must rise from the landward to the seaward side and that the course of the newly formed bore is eventually seaward.

2.4 Dam-break transformation

The method of solution given by Shen & Meyer (1963) for the run-up of a bore on a plane beach is very complicated. A simpler but not as informative way to derive their solutions exist and shall now be presented.

The Shen & Meyer (1963) problem is equivalent to considering a dam-break problem on a plane beach. We wish to solve the dimensionless non-linear shallow water wave equations,

$$h_t + (uh)_x = 0, \tag{2.4.1}$$

$$u_t + uu_x + h_x + 1 = 0, \tag{2.4.2}$$

with respect to the initial conditions

$$h(x,0) = h_0, \quad u(x,0) = 0, \quad \text{for} \quad 0 \leq x \leq 1 \tag{2.4.3}$$

$$h(x,0) = 0, \quad u(x,0) = 0, \quad \text{for} \quad x > 1, \tag{2.4.4}$$

where x is measured up the slope, t is the time, h is the water thickness and u is the velocity measured parallel to the slope.

Using the change of variables $(\xi, \tau, U, C, H) = (x + \frac{1}{2}t^2, t, u + t, c, h)$. We find that our problem reduces to one of solving

$$H_\tau + (UH)_\xi = 0, \tag{2.4.5}$$

$$U_\tau + UU_\xi + H_\tau = 0, \tag{2.4.6}$$

with respect to the initial conditions

$$H(\xi,0) = H_0, \quad U(\xi,0) = 0, \quad \text{for} \quad 0 \leq \xi \leq 1 \tag{2.4.7}$$

$$H(\xi,0)=0, \quad U(\xi,0)=0, \quad \text{for} \quad \xi>1, \tag{2.4.8}$$

where ξ is measured along the horizontal, τ is the new time, H is the new water thickness and U is the new velocity measured parallel to the horizontal.

The equations of motion in the transformed variables are simply the shallow water wave equations on a horizontal bed, with dam-break initial conditions. From section 2.2.5 we can write the solution to this problem as

$$H(\xi,\tau)=\frac{1}{9}\left(2\sqrt{H_0}-\frac{\xi}{\tau}\right)^2, \tag{2.4.9}$$

$$U(\xi,\tau)=\frac{2}{3}\left(\sqrt{H_0}+\frac{\xi}{\tau}\right), \tag{2.4.10}$$

with shoreline position given by

$$\xi_s=2\tau\sqrt{H_0}. \tag{2.4.11}$$

By changing back to the original variables, we find the solution for the shoreline position, height and velocity for a dam-break on a slope is

$$x_s(t)=2\sqrt{h_0}t-\frac{1}{2}t^2, \tag{2.4.12}$$

$$h(x,t)=\frac{1}{9t^2}\left(2t\sqrt{h_0}-\frac{1}{2}t^2-x\right)^2=\frac{1}{9t^2}(x_s-x)^2, \tag{2.4.13}$$

$$u(x,t)=\frac{2}{3t}(t\sqrt{h_0}-t^2+x) \tag{2.4.14}$$

We notice that these solutions are the same as those given by Shen & Meyer (1963) with $u_0=2\sqrt{h_0}$.

The problem with this solution is that no information on the backwash is available. In the case of the Shen & Meyer (1963) solution, it was found that a landward facing bore was created in the backwash motion. The Shen & Meyer (1963) solution is much more informative, but the set-up described here is what is used when considering the Shen & Meyer (1963) solution numerically in chapter 4. Numerically the initial set-up is a dam-break on a plane slope.

2.5 Conclusion

Shallow water theory has been introduced. This is used throughout the rest of this work. We have introduced the work of Ho & Meyer (1962) and Shen & Meyer (1963), which is used in chapter 3. We have also seen the bore relations, which are used in chapters 4 and 5. The work of Shen & Meyer (1963) is used in chapter 3 to consider the overtopping of swash over a truncated plane beach. A modified solution is found to describe how the flow changes when a truncation is introduced.

Chapter 3

A single swash event overtopping a truncated plane beach

3.1 Introduction

Water wave motion at a shoreline on a sloping structure takes two different forms. If there is no breaking of the waves the motion is smooth as the incident waves are reflected and the wave motion can be described well either by linear theory for slopes of $O(1)$, see Whitham (1979) for a full account, or by Carrier & Greenspan's (1958) solutions for the nonlinear shallow-water equations.

On the other hand, if waves break near the shoreline, which is almost always the case for beaches of gentle slope and often occurs on steeper slopes, then flow in the swash zone, is quite different. Meyer & Taylor (1972) discuss the boundary between these two types of flow in the context of shallow-water theory. In the breaking case, for each wave crest reaching the shoreline there is a new 'swash event' generated. This runs up the slope until overtaken by another such event, or until it drains back under gravity.

The only theoretical description of such an event is in the context of shallow-water theory, where waves have broken and formed a bore which then meets the

shoreline. The swash from a 'uniform bore' on a plane beach, travelling over still water before meeting the shoreline is described by Shen & Meyer (1963). In shallow-water theory bores are represented by a moving discontinuity in water depth and velocity. Ho & Meyer (1962) show that as the bore meets the shoreline its height 'collapses' to zero. In the context of shallow-water theory this singularity emits a swash event, singular at the instant of creation, but characterized by an initial velocity which we replace with an equivalent parameter, the height of run-up above the initiation point of the swash event.

In this chapter we shall be considering the effects of overtopping, on the solution of Shen & Meyer (1963). We decide to truncate the beach at a given point and then proceed to find the new solution due to this modification. A full analytical solution is found for the form of the height and velocity near the truncation point, also an expression is found for the volume of water that may overtop such a structure.

In section 3.2 we formulate the problem, in section 3.3 we find and discuss the solution to the problem introduced.

3.2 Formulation of problem

We have already stated in chapter 2 that the nonlinear shallow-water equations are a good approximation to wave motion in the surf and swash zone. Normally they are used for beaches of gentle slope. However, since we are only considering the swash zone, where even for steep slopes a breaking wave generates a thin sheet of swash, we write the equations for one-dimensional flow over a beach sloping at an angle γ to the horizontal:

$$\frac{\partial h^*}{\partial t^*} + \frac{\partial (h^* u^*)}{\partial x^*} = 0, \tag{3.2.1}$$

$$\frac{\partial u^*}{\partial t^*} + u^* \frac{\partial u^*}{\partial x^*} + g \cos\gamma \frac{\partial h^*}{\partial x^*} = -g \sin\gamma, \tag{3.2.2}$$

where x^* is measured up the slope, t^* is time, $h^*(x^*, t^*)$ is the water thickness and $u^*(x^*, t^*)$ is the water velocity parallel to the beach. The * denotes dimensional variables and g the acceleration due to gravity. These equations may be derived by assuming that water accelerations perpendicular to the slope and the shear in the

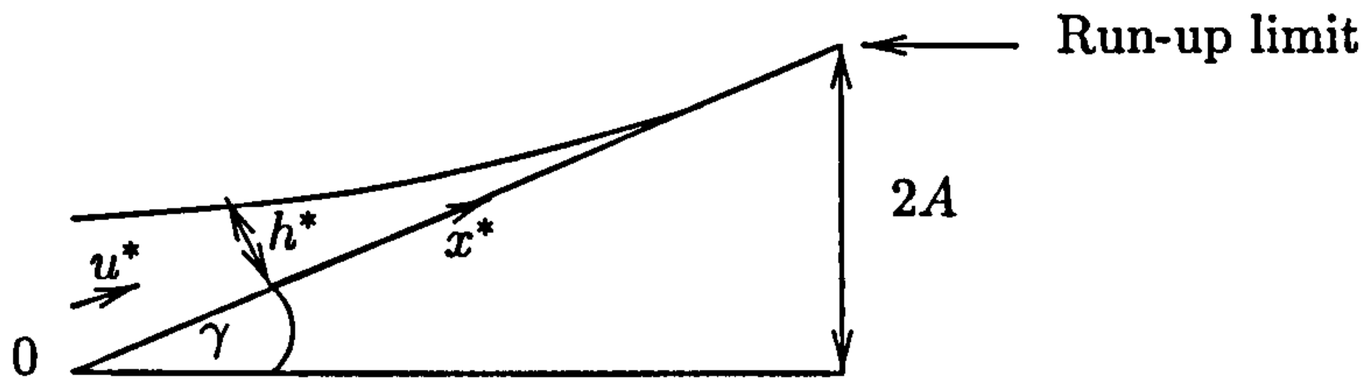

Figure 3.1: Definition sketch.

water are negligible (Peregrine 1972). This last assumption may fail in the backwash, see Peregrine (1974) for a description of the waves that may then arise.

Equations (3.2.1) and (3.2.2) can be made dimensionless and free of both the parameters g and γ. We relate lengths to the vertical excursion of the undisturbed swash, $2A$, see figure 3.1. That is, the swash event has a maximum height of run-up on an unbroken plane beach of $2A$ above its point of initiation, which is the lower boundary of the swash. We place the origin of x^* at this lower boundary, and measure it upslope so that the swash runs up to $x^* = 2A/\sin\gamma$ at the run-up limit. Thus we choose to make x^* dimensionless with $A/\sin\gamma$. The thickness of water h^* is measured perpendicular to the slope, so it is made dimensionless with $A/\cos\gamma$. We use $g\cos\gamma$ and $A/\cos\gamma$ to make t^* and u^* dimensionless.

In order that the scaling for t matches that for x, it needs an extra factor of $\tan\gamma$; then our new scaled dimensionless variables are

$$x = \frac{(\sin\gamma)x^*}{A}, \quad t = (\sin\gamma)t^*\sqrt{\frac{g}{A}}, \quad h = \frac{(\cos\gamma)h^*}{A}, \quad u = \frac{u^*}{\sqrt{gA}}. \tag{3.2.3}$$

This gives the equations

$$h_t + (hu)_x = 0, \tag{3.2.4}$$

$$u_t + uu_x + h_x + 1 = 0, \tag{3.2.5}$$

which are free from any parameters (cf. equations (2.2.6) and (2.2.7)).

To understand the overtopping solution, we need to consider the nonlinear shallow water equations in characteristic form. From (2.2.8) and (2.2.9) we have:

$$\left(\frac{\partial}{\partial t} + (u+c)\frac{\partial}{\partial x}\right)\alpha = 0, \tag{3.2.6}$$

and

$$\left(\frac{\partial}{\partial t}+(u-c)\frac{\partial}{\partial x}\right)\beta=0, \tag{3.2.7}$$

where the Riemann invariants are

$$\alpha(x,t)=u+2c+t, \tag{3.2.8}$$

and

$$\beta(x,t)=u-2c+t. \tag{3.2.9}$$

It is this form of the shallow water equations that will be used in the proceeding sections to consider the effects of overtopping.

3.3 Overtopping solution

3.3.1 The swash solution

The effectively discontinuous nature of the swash event generated by bores and breakers is readily seen on most beaches. Shen & Meyer (1963) set out to develop Ho & Meyer's (1962) results for a bore reaching the shoreline. The expectation was that a solution might be found for some further small time interval. Remarkably the paper describes the way in which the whole swash event has much of its flow determined by the initial motion. This is particularly so for the flow close to the instantaneous shoreline which moves up and down the beach under gravity just like a freely moving particle. Another remarkable feature is that the tip of the run-up is very thin, and not just thin because that is necessary for the shallow-water approximation to hold. Waves which do not break, such as Carrier & Greenspan's (1958) solutions, have a moving shoreline with a finite gradient, h_x, for the water depth. However, a swash event caused by a bore is such that $h_x=0$ at the shoreline and the analytic solution is tangential to the bed. This implies that the actual tip of the solution is invalid in practice because of bed roughness, surface tension or viscosity. Even so, comparisons with numerical solutions for water depths near the tip are remarkably good for water depths greater than 2 mm (Packwood 1980; Titov & Synolakis 1995; Barnes 1996). A numerical version of this type of flow is described in detail in Hibberd & Peregrine (1979) and is also given in chapter 4.

The swash solution from Shen & Meyer (1963) has a single free parameter, the initial velocity of the shoreline. Here, the scaling with $2A$ effectively fixes that parameter so we need only consider the unique solution with shoreline motion

$$x_s(t) = 2t - \tfrac{1}{2}t^2. \tag{3.3.1}$$

The depth of water local to the shoreline is

$$h(x,t) = \frac{1}{9t^2}[x_s(t) - x]^2 = \frac{1}{36t^2}(4t - t^2 - 2x)^2. \tag{3.3.2}$$

Using this form of $h(x,t)$, we find the long-wave velocity, $c(x,t)$, as

$$c(x,t) = \frac{1}{3t}(x_s - x) = \frac{1}{6t}(4t - t^2 - 2x), \tag{3.3.3}$$

and from (3.2.4) and (3.2.5)

$$u(x,t) = \frac{2}{3t}(t - t^2 + x). \tag{3.3.4}$$

With both $u(x,t)$ and $c(x,t)$ known, the characteristics are found. The advancing characteristics C_+ are

$$x = 2t - \tfrac{1}{2}t^2 - at^{\frac{1}{3}}, \tag{3.3.5}$$

on which $\alpha = 2$. The receding characteristics C_- are

$$x = 2t - \tfrac{1}{2}t^2 - bt, \tag{3.3.6}$$

on which $\beta = 2 - \frac{4}{3}b$. The constants a and b are parameters for the family of C_+ and C_- characteristics. The shoreline is common to both families, with $a = b = 0$. Increasing a or b from zero gives the other characteristics. The solution is not useful close to its singularity at the origin of (x,t).

Note that this solution is related to the well-known dam break problem on a horizontal bed, by changing variables to $(\xi, \tau, U, C, H) = (x + \frac{1}{2}t^2, t, u + t, c, h)$, giving the solution

$$U = \frac{2}{3}\left(1 + \frac{\xi}{\tau}\right), \qquad C = \frac{1}{3}\left(2 - \frac{\xi}{\tau}\right). \tag{3.3.7}$$

At $t = \tau = 0$ this is singular, but is usually interpreted as being derived from the initial conditions $H = 1$, $U = 0$ in $\xi < 0$. However strictly all that is needed is that

$$U + 2C = 2 \quad \text{in} \quad \xi < 0. \tag{3.3.8}$$

Hence other distributions of U and C, or equivalently u and h, satisfying this condition also make sensible initial conditions for this same swash event.

Figure 3.2 shows both families of characteristics for this solution. Note that strictly only a strip close to the shoreline is fully determined from the initial time and α could be varying with each incoming characteristic. However, in the absence of any other explicit solutions we work with this solution.

In dimensional units the expressions for x_s^*, h^* and u^* are

$$x_s^*(t^*) = 2t^*\sqrt{gA} - \tfrac{1}{2}gt^{*2}\sin\gamma, \tag{3.3.9}$$

$$h^*(x^*,t^*) = \frac{1}{36gt^{*2}\cos\gamma}(4t^*\sqrt{gA} - gt^{*2}\sin\gamma - 2x^*)^2, \tag{3.3.10}$$

and

$$u^*(x^*,t^*) = \frac{2}{3t^*}(t^*\sqrt{gA} - gt^{*2}\sin\gamma + x^*). \tag{3.3.11}$$

For reference in the next section, figure 3.2 also includes the line in (x,t) where the flow is critical, that is $u = c$. This line is $x = \frac{1}{2}t^2$. To the left of this critical line i.e. $x > \frac{1}{2}t^2$, we have supercritical flow with $u > c$. To the right of the critical line i.e. $x < \frac{1}{2}t^2$, we have subcritical flow with $u < c$.

We note the solution (3.3.10), (3.3.11), has a singularity at $t^* = 0$. We can check the consistency of the swash solution with the shallow-water approximation by evaluating the acceleration of water particles perpendicular to the beach. This is more appropriate than simply requiring $h^* << A$. For the dimensionless solution a particle on the surface has position $x = x(t)$, $y = h(x,t)$, and since $\mathrm{d}x/\mathrm{d}t = u$, we have

$$\frac{\mathrm{d}^2y}{\mathrm{d}t^2} = \left(\frac{\partial}{\partial t} + u\frac{\partial}{\partial x}\right)^2 h = h_{tt} + 2uh_{xt} + u^2h_{xx} + (u_t + uu_x)h_x. \tag{3.3.12}$$

This acceleration has been evaluated and in figure 3.3 the lines $\frac{\mathrm{d}^2y}{\mathrm{d}t^2} = 0.1$ and 0.2 are shown. These lines give an indication of where the solution may not be a good representation of the swash, since vertical accelerations must be negligible for the pressure to be approximately hydrostatic; the region where $\frac{\mathrm{d}^2y}{\mathrm{d}t^2} > 0.1$ is shaded.

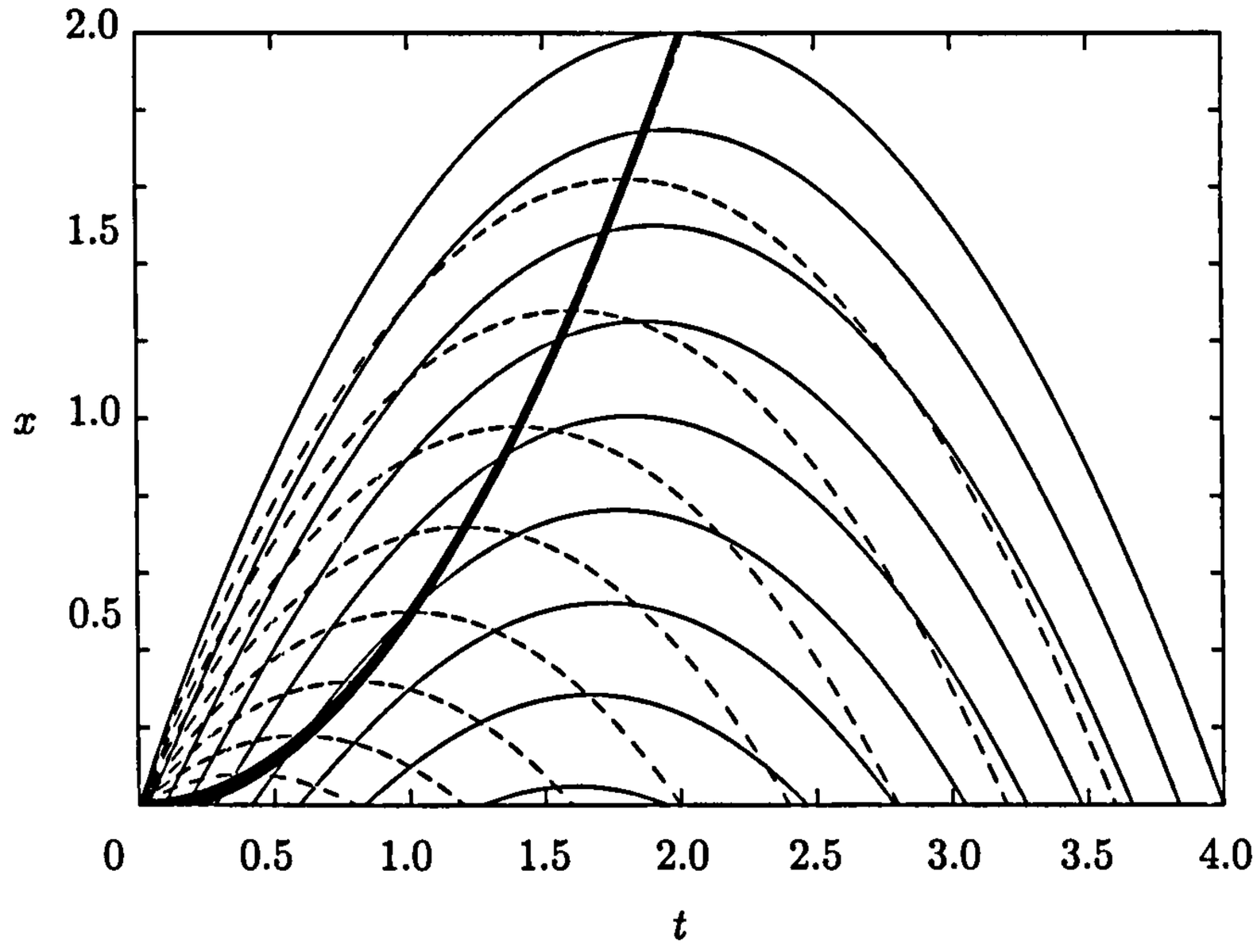

Figure 3.2: Characteristics C_+ (solid line) and C_- (dashed line) and the critical line (heavy line) for the swash solution. The parameters a and b for the characteristics are increased from 0 at the shoreline in steps of 0.2.

3.3.2 Overtopping solution

We consider a plane beach cut-off at a point below the maximum run-up, say at $x = E$, $E < 2$. At $x = E$ the flow is initially supercritical, with $u > c$, which implies that there is no influence from the overtopping edge on the flow. The flow does not sense the edge ahead, hence the water shoots over the edge like a jet as if the edge were not there. When $u \leq c$ the flow is assumed to fall freely over the edge of the beach. The swash solution is unaffected until the flow at the edge slows down and becomes critical at time $t = T_2 = \sqrt{2E}$.

Once the flow velocity drops to critical with Froude number of unity, that is $u = c$, the crest of the beach acts like a weir. The essence of shallow-water theory is that the water depth is negligibly small compared with its horizontal variations, and this also implies that shallow-water time scales are long compared with those related to the depth. Therefore close to the crest the flow may be taken to be almost steady and, as in steady-flow hydraulics, the beach crest 'weir' acts as a 'control point' at

which the flow remains critical unless it is submerged. Alternatively, we simply note that once water passes over the crest it is in free fall and can no longer influence flow on the beach: hence the C_- characteristics at the crest of the beach cannot propagate in the $-x$ direction.

The combination of supercritical flow, which needs no boundary condition, and a critical flow boundary condition are sufficient to determine the modification to the swash flow described above by the truncation of the beach. To aid discussion figure 3.3 shows the relevant portion of the (x,t) plane divided into four regions.

Region I is the initially dry beach, and is bounded by the moving shoreline (3.3.1) of the undisturbed swash solution, which reaches $x = E$ at $t = T_1 = 2 - \sqrt{4-2E}$.

Region II is the undisturbed swash solution of section 3.3.1, whose C_+ and C_- characteristics all originate from the initial singularity. This solution is undisturbed until the flow slows sufficiently for a C_- characteristic to travel down the beach from immediately below $x = E$. This characteristic can start, when $u = c$, at time $t = T_2 = \sqrt{2E}$. From equation (3.3.6) we see that this C_- characteristic bounding region II is

$$x = \sqrt{2E}\,t - \tfrac{1}{2}t^2, \tag{3.3.13}$$

on which $\beta = \frac{4}{3}\sqrt{2E} - \frac{2}{3}$.

Region III is where the swash is reduced by overtopping, and is discussed further below.

Region IV is where the water has drained away and as indicated in figure 3.3 starts earlier, at time $t = T_3$, than for the undisturbed swash solution, because water is lost over the edge.

The flow affected by overtopping, region III, can be determined since in that flow all the C_+ characteristics enter from the undisturbed swash flow and hence give

$$\alpha = u + 2c + t = 2. \tag{3.3.14}$$

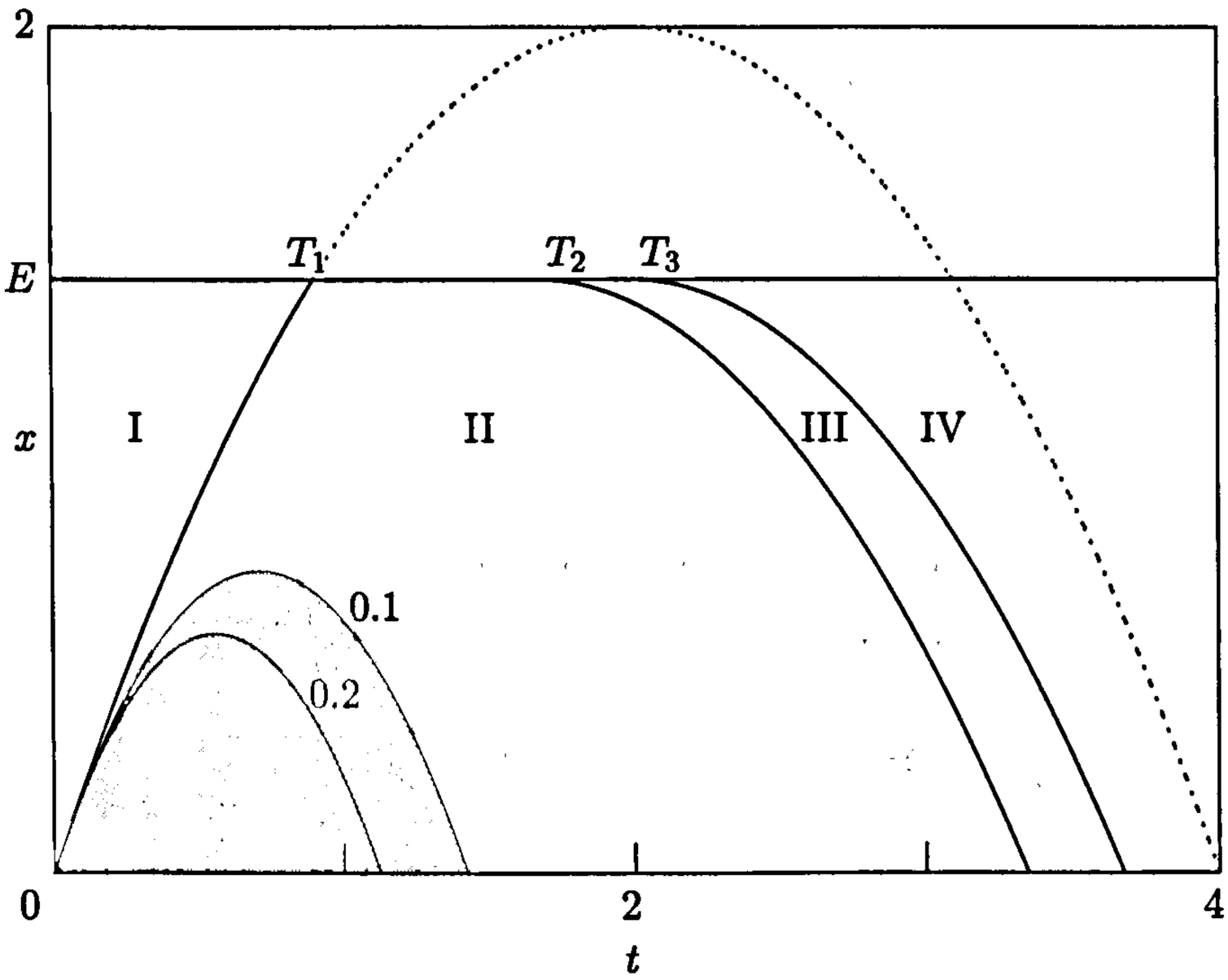

Figure 3.3: General (x,t)-diagram showing different regions of flow. The shaded region is where shallow-water theory is likely to be invalid.

If we use this equation to eliminate u from equation (3.2.7) governing β we find

$$c_t + (2 - 3c - t)c_x = 0. \tag{3.3.15}$$

At the edge, for $T_2 < t < T_3$, we have both equation (3.3.14) and $u = c$. Thus we know u, c and β:

$$u = c = \tfrac{1}{3}(2 - T), \quad \beta = \tfrac{2}{3}(2T - 1), \tag{3.3.16}$$

where we write $t = T$ on $x = E$ since it now is a parameter determining the C_- characteristics. From (3.3.15) or (2.2.11) these are

$$x = E - \tfrac{1}{2}(t - T)^2, \tag{3.3.17}$$

carrying constant values of c and β.

An explicit solution is found by solving (3.3.17) for

$$T = t - \sqrt{2(E - x)}. \tag{3.3.18}$$

Then substituting in the expression (3.3.16) for c, and (3.3.14) for u, gives

$$c(x,t) = \tfrac{1}{3}[2 - t + \sqrt{2(E-x)}], \tag{3.3.19}$$

$$u(x,t) = \tfrac{1}{3}[2 - t - 2\sqrt{2(E-x)}], \tag{3.3.20}$$

and $h = c^2$. The shoreline position is found from $c = 0$ as

$$x_s = E - \tfrac{1}{2}(t-2)^2 \tag{3.3.21}$$

and thus is similar to the initial swash solution, in falling freely under gravity. The dimensional form of this solution is

$$h^*(x^*,t^*) = \frac{1}{9\cos\gamma}[2\sqrt{A} - \sqrt{g}t^*\sin\gamma + \sqrt{2(EA - x^*\sin\gamma)}]^2, \tag{3.3.22}$$

$$u^*(x^*,t^*) = \tfrac{1}{3}[2\sqrt{gA} - gt^*\sin\gamma - 2\sqrt{2g(EA - x^*\sin\gamma)}]. \tag{3.3.23}$$

3.3.3 Volume of overtopping

The above explicit solution to the nonlinear shallow-water equations was found directly, using the result of Shen & Meyer (1963) for the run-up height near the shoreline to describe a swash event. With the assumption that after a finite time $T_2 = \sqrt{2E}$, the flow becomes critical at the cut-off point $x = E$ we have found the overtopping solution (3.3.19) and (3.3.20). It is useful as a test solution for numerical schemes and as a reference solution for studies of wave overtopping. For this latter application we give a few more results and discuss its relevance to practical application.

For overtopping, the greatest interest lies in the flow at $x = E$. At that point the flow is initially supercritical and the swash solution gives

$$u = \frac{2}{3T}(T - T^2 + E), \quad h = \frac{1}{36T^2}(4T - T^2 - 2E)^2, \tag{3.3.24}$$

giving a flow rate

$$q = uh = \frac{1}{54T^3}(T - T^2 + E)(4T - T^2 - 2E)^2, \tag{3.3.25}$$

for the time interval $T_1 = 2 - \sqrt{4-2E} < T < \sqrt{2E} = T_2$.

Following this, the subcritical flow is

$$u = \tfrac{1}{3}(2 - T), \quad h = \tfrac{1}{9}(2 - T)^2, \tag{3.3.26}$$

with

$$q = uh = \tfrac{1}{27}(2 - T)^3, \tag{3.3.27}$$

for the interval $T_2 = \sqrt{2E} < T < 2 = T_3$. It is interesting to note that regardless of the height at which the beach is truncated the overtopping stops at the same time.

From the expressions (3.3.25) and (3.3.27) for the volume flux q overtopping the beach, we can find the total volume of overtopping water:

$$\begin{aligned} V(E) = \int_{T_1}^{T_3} q \, \mathrm{d}T &= \tfrac{4}{27}(2\sqrt{2E} - 6E + 3E\sqrt{2E} - E^2) + \tfrac{1}{27}(\sqrt{2} - \sqrt{E})^4 \\ &= \tfrac{1}{27}(4 - 12E + 8E\sqrt{2E} - 3E^2). \end{aligned} \tag{3.3.28}$$

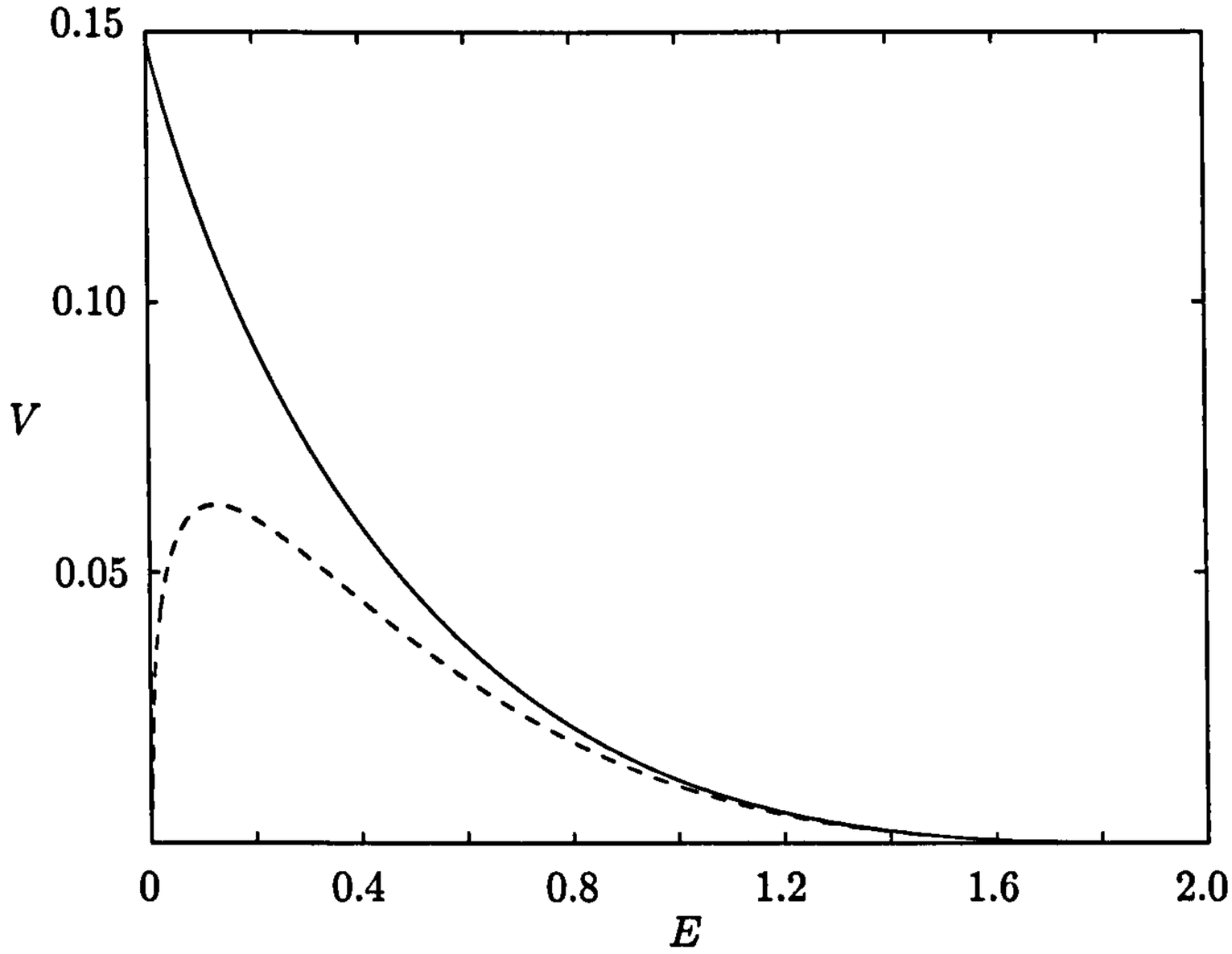

Figure 3.4: Overtopping volume per unit width $V(E)$. Solid line indicates total overtopping. Dashed line indicates overtopping for the supercritical flow only.

The function $V(E)$ is plotted in figure 3.4, distinguishing between the flow during the supercritical and critical stages of overtopping. Since even a small amount of overtopping may be of importance in some circumstances, we also show these quantities on a logarithmic scale in figure 3.5.

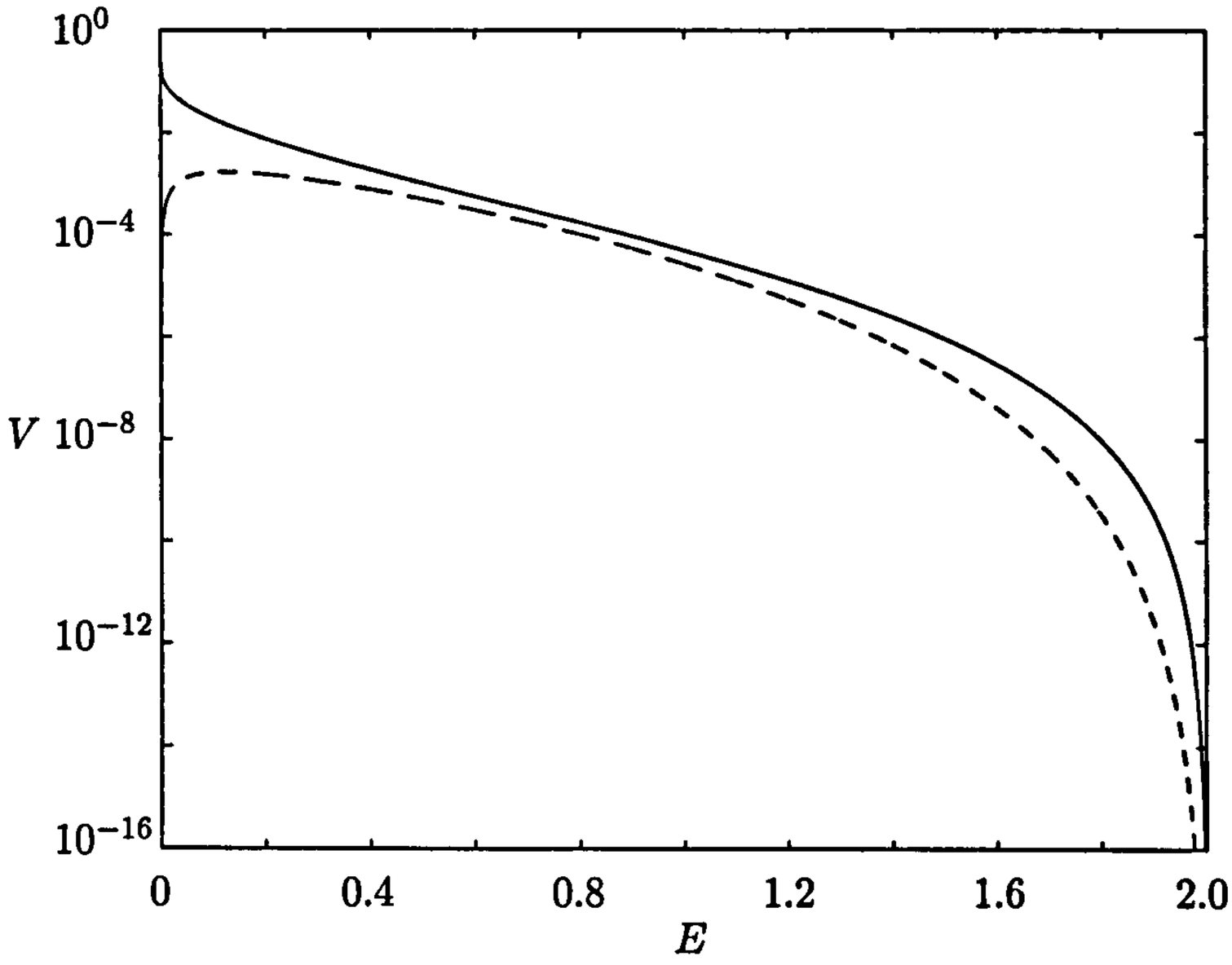

Figure 3.5: $V(E)$ with a logarithmic scale. Solid line is for the total volume per unit width. Dashed line is for the supercritical flow only.

For E near its upper limit, $E = 2 - \delta$, and

$$V \approx \frac{1}{108}\delta^3 + \frac{1}{576}\delta^4 + O(\delta^5). \tag{3.3.29}$$

In dimensional terms $V^*(E) = 2A^2V(E)/\sin 2\gamma$, per unit width of beach. The variation with beach slope γ is remarkable: for given E, maximum overtopping occurs as the two, inapplicable, limit values $\gamma = 0$ and $\pi/2$ are approached. It appears that for given vertical range of swash, a slope of $\pi/4$ minimizes the overtopping. The limit of $\gamma = 0$ is easy to model since this corresponds to a dam break near the edge of a horizontal bed. The dam break solution (2.2.19) then applies, since the flow is supercritical at the edge. The flow then continues for all time, unless the initial volume of water is bounded, which is true in the case of a single swash event.

3.4 Conclusion

Unfortunately real life waves are not as simple as the above analysis. For a start, we have chosen a special solution for the swash. It is clear that the value of α on the C_+ characteristics 'feeding' the swash on $x = 0$ would in general deviate from the initial value of 2. Also real fluid effects such as friction with the bed influence the flow, though indications from comparisons between computations with the shallow-water equations and laboratory experiments (Packwood 1980; Barnes 1996) indicate that frictional effects in the uprush are small, unless γ is as small as 0.02 or water depth less is than 2 mm.

Regardless of the special nature of this overtopping solution it can provide a useful reference against which computational and experimental results for overtopping may be compared. A note is made that the swash solution of section 3.3.1 is only relevant when the shoreline is moved impulsively due to arrival of a bore or breaking wave. On steep slopes non-breaking waves are also a frequent cause of swash.

Chapter 4

Numerical method

4.1 Introduction

We consider solving the nonlinear shallow water equations numerically, so that we can advance the studies which were made using analytical techniques in chapter 3. We implement a staggered scheme based on the non-oscillatory scheme of Nessyahu & Tadmor (1990) for a system of hyperbolic equations.

In section 2 the method of Nessyahu & Tadmor (1990) will be introduced, along with a description of how it's implemented in this thesis. The stability of this scheme is discussed in section 4.3. The boundary conditions which are considered in this work are discussed in section 4.4, these are the seaward, shoreline and overtopping boundary conditions. In section 4.5 a comparison is made between the results of our scheme RUSH (**Run-Up** of **SH**allow water) to exisiting analytical results for the nonlinear shallow water equations.

The rest of this section is dedicated to introducing a way of writing the nonlinear shallow water equations in a form suitable for numerical study. In non-dimensional form the nonlinear shallow water equations are (see chapter 2 for more details)

$$\frac{\partial h}{\partial t} + \frac{\partial (hu)}{\partial x} = 0, \tag{4.1.1}$$

$$\frac{\partial u}{\partial t} + u\frac{\partial u}{\partial x} + \frac{\partial h}{\partial x} - \frac{\partial d}{\partial x} = -f_c \frac{u|u|}{h}, \tag{4.1.2}$$

where h is the total height, d is the shape of the beach surface and $h = \eta + d$, where

η is the surface elevation above the mean sea level. The term on the right hand side of (4.1.2) is a friction source term, known as the Chézy friction. The main use of the Chézy friction is for uniform flow in rivers, canals and channels and thus may not be a good representation of friction on a beach. Numerical experiments have been made by Puleo & Holland (2001), Kobayashi et al. (1987), Packwood (1980), in which they compare their results to laboratory and field experiments. These results are enough to show that the Chézy friction is a good enough representation of friction on a beach.

To consider the shallow water equations numerically we must write equations (4.1.1) and (4.1.2) in flux-conservative form as

$$\frac{\partial \mathbf{w}}{\partial t} + \frac{\partial \mathbf{F(w)}}{\partial x} = \mathbf{S}, \tag{4.1.3}$$

where $\mathbf{w} = (h, q)^T$, $\mathbf{F(w)} = (q, q^2/h + h^2/2)^T$ and $\mathbf{S} = (0, h\frac{\partial d}{\partial x} - f_c|\frac{q}{h}|\frac{q}{h^2})^T$ and $q = uh$ is the flow rate. In this work we ignore the effects of friction so we shall take the friction as zero and thus $f_c = 0$, so we have $\mathbf{S} = (0, h)^T$. The only beach surface we are interested in, in this work is the case of a plane beach. In this case the form of d is given as $d = -x$. The form of d is non-dimensional, thus when re-dimesionalising we would find $d = -\gamma x$, where γ is the angle of the beach slope to the horizontal.

4.2 Nessyahu & Tadmor scheme

4.2.1 Method of solution

Several different methods exist for solving such a system as given by (4.1.3). There are the methods of finite differences, finite-element, finite-volume and up-wind schemes. There are advantages and disadvantages in choosing each different method. There isn't one method that stands out over any of the others. It comes down to a matter of preference and ease of computation.

In RUSH(**R**un-**U**p of **SH**allow water), a scheme is employed from the class of methods developed by Nessyahu & Tadmor (1990), which was extended to 2-D by Jiang & Tadmor (1998). This method has previously been used successfully, but

without bores, by Pritchard (2001), where the scheme is used to model shallow flow over mudflats. Patterson (2002) used the scheme to model shallow water flow over porous beds and McCabe (2003), used the scheme to model the influence of air in violent water wave impact.

The scheme is both simple to compute and numerically simple. The scheme uses a finite difference scheme based on the first order Lax-Wendroff scheme (Lax & Wendroff 1960), thus avoiding the complications involved with computing the upwind differencing schemes and Riemann-solver methods, which are powerful methods, but can be more difficult to implement.

For the rest of this work, a vector of dependent variables $\mathbf{w}$ is represented on our grid by quantities $v_{j,k}^t$, where $v_{j,k}^t$ is the approximation to $w_k(j\Delta x, t)$, the k'th component of $\mathbf{w}(x,t)$. In general we shall suppress the superscript t, so v_j represents the numerical variable at time t. The quantity v_j' denotes the numerical approximation to the quantity $\Delta x \partial w/\partial x$ evaluated at the point $(j\Delta x, t)$.

The method which was first used by Hibberd & Peregrine (1979) to model the NLSWE numerically was the Lax-Wendroff scheme, on a staggered grid. It has the form

$$v_{j+\frac{1}{2}}^{t+\Delta t} = \frac{1}{2}[v_j + v_{j+1}] - \lambda[f(v_{j+1}) - f(v_j)], \tag{4.2.1}$$

where $\lambda = \frac{\Delta t}{\Delta x}$.

The scheme is simple to compute and is robust, but this method suffers from excessive numerical viscosity, the result is therefore less accurate than alternative available first-order schemes (Press, Teukolsky, Vetterling & Flannery 1992). The method used here is that of Nessyahu & Tadmor (1990), which is an extension of the Lax-Wendroff scheme to second order accuracy in space. A third order accurate scheme is available which was developed by Liu & Tadmor (1998). In this paper comparisons are made between this third order method and the second order method, the difference is minimal, the third order scheme is also more difficult to implement. For this reason we proceed with the second order accurate method.

This scheme is thought of as a predictor-corrector operation. A prediction is

made

$$v_j^{t+\frac{1}{2}\Delta} = v_j - \frac{1}{2}\lambda f'_j, \tag{4.2.2}$$

where f'_j stands for an approximate numerical derivative of the flux f at the point $x = j\Delta x$,

$$f'_j = \Delta x \frac{\partial f}{\partial x} + O(\Delta x^2), \tag{4.2.3}$$

at $x = j\Delta x$. The solution at the subsequent time-step at a staggered x-grid point is then given by

$$v_{j+\frac{1}{2}}^{t+\Delta t} = \frac{1}{2}[v_j + v_{j+1}] + \frac{1}{8}[v'_j - v'_{j+1}] - \lambda[f(v_{j+1}^{t+\frac{1}{2}\Delta t}) - f(v_j^{t+\frac{1}{2}\Delta t})], \tag{4.2.4}$$

where v'_j is the vector derivative at the point $x = j\Delta x$, given by

$$v'_j = \Delta x \frac{\partial v}{\partial x} + O(\Delta x^2). \tag{4.2.5}$$

The difference between the scheme of Nessyahu & Tadmor (1990) and Lax & Wendroff (1960), is that Nessyahu & Tadmor (1990) use a piecewise-linear approximation to the dependent variable at time t, whereas Lax & Wendroff (1960) use a piecewise-constant approximation. In the third order scheme of Liu & Tadmor (1998) a piecewise-quadratic approximation is made. The method of Nessyahu & Tadmor (1990) is accurate to second order, in both space and time, provided f'_j and v'_j are accurate to $O(\Delta x^3)$ at all grid points.

Applied to a single scalar dependent variable, Nessyahu & Tadmor (1990) established that their scheme converges to the unique physically relevant solution of the flux-conservative system. This result does not necessarily extend to a system of dependent variables, but personal results (given in section 4.5), as well as those given by Nessyahu & Tadmor (1990) and also Pritchard (2001) are enough to suggest that the method represents the mathematical system accurately and that the scheme is a definite improvement on the Lax-Wendroff scheme. Patterson (2002) found problems with the scheme of Nessyahu & Tadmor (1990) when considering the two-dimensional shallow water equations. Since we are only concerned with the one-dimensional shallow water equations, we don't worry about these problems.

The scheme of Nessyahu and Tadmor is rewritten in the form

$$v_{j+\frac{1}{2}}^{t+\Delta t} = \frac{1}{2}[v_j + v_{j+1}] - \lambda[g_{j+1} - g_j], \tag{4.2.6}$$

where g_j is the modified numerical flux given by

$$g_j = f(v_j^{t+\frac{1}{2}\Delta t}) + \frac{1}{8\lambda} v'_j. \tag{4.2.7}$$

It can be seen that the above is now written in the same form as the Lax-Wendroff scheme.

To complete this method, we require numerical estimates of the spatial derivatives, v'_j and f'_j. Nessyahu & Tadmor (1990) describe a number of different estimates that can be used and compare each different estimate. We shall employ their most successful method, where the numerical estimates of the derivatives of the vector of conserved quantities is

$$v'_j = MM\{\delta\Delta v_{j+\frac{1}{2}}, \frac{1}{2}(v_{j+1} - v_{j-1}), \delta\Delta v_{j-\frac{1}{2}}\}, \tag{4.2.8}$$

where $\Delta v_{j+\frac{1}{2}} = v_{j+1} - v_j$ and $\Delta v_{j-\frac{1}{2}} = v_j - v_{j-1}$ and $MM(x, y, z)$ is the min-mod function, defined as

$$MM(x, y, z) = \frac{1}{3}(\mathrm{sgn}(x) + \mathrm{sgn}(y) + \mathrm{sgn}(z))\min(|x|, |y|, |z|). \tag{4.2.9}$$

The parameter $\delta > 1$ is chosen heuristically, and allows the derivative to be limited in the locality of a strong discontinuity. In the work reported here, we choose $\delta = 2$. This value is chosen, since experimentation shows it gives rise to the smoothest solutions. Typically as long as the local gradient is not too large, the centered estimate $\frac{1}{2}(v_{j+1} - v_{j-1})$ is used, but if this becomes very large, then the scheme chooses a compromise one-sided estimate. This estimate helps to prevent spurious oscillations from developing near such a discontinuity.

To find the estimates of the numerical flux derivatives, we could use the same method as described for the conserved quantities using the min-mod function. An easier way to estimate the derivatives is given by

$$f'_j = A(v_j)v'_j, \tag{4.2.10}$$

where A is the Jacobian matrix, defined as $A(v_j) = \frac{\partial f}{\partial w}$. For the nonlinear shallow water equations, given by (4.1.1) and (4.1.2), with $f_c = 0$, the Jacobian matrix A has the form

$$A = \begin{pmatrix} 0 & 1 \\ h - \frac{q^2}{h^2} & \frac{2q}{h} \end{pmatrix}.$$

It is this form of A that we use in the remainder of this work.

A series of premliminary programs were written to implement this scheme in a simple domain (a horizontal bed with periodic boundary conditions), with simple initial conditions which were intended to test the general performance of the numerical method. The results were found to be insensitive to the timestep Δt, as long as the ratio λ remained sufficiently small (see equation (4.3.3) in section 5.3 for an upper bound on λ). Numerical integration also confirmed that the fluxes q and $q^2/h + h^2/2$ were conserved to a relative accuracy of about 10^{-4}. Accuracy was maintained in the case of a set-up with an initial discontinuity, provided that care was taken with the choice of δ and Δt. The sharpness of profiles was reduced by decreasing Δt, or by decreasing δ. However, if the timestep Δt was too large then the scheme became unstable, and if the limiting parameter δ was too large then spurious oscillations could be observed near to discontinuities.

4.2.2 Source terms

To include a source term in our scheme, we would have to modify the scheme to take account of the source term. Adding the source term to the scheme is done by evaluating it as a function of the half-time step 'predictor' variables $v_j(t + \frac{1}{2}\Delta t)$, and then adding it in to the final stage of the update. The solution given by (4.2.6) now becomes

$$v_{j+\frac{1}{2}}^{t+\Delta t} = \frac{1}{2}[v_j + v_{j+1}] - \lambda[g_{j+1} - g_j] - S(v_j^{t+\frac{1}{2}\Delta t}), \qquad (4.2.11)$$

where in the case of shallow water theory on a plane beach

$$S(v_j) = h_j - \frac{f_c u_j |u_j|}{h_j}, \qquad (4.2.12)$$

where $u_j = \frac{q_j}{h_j}$. If we include the effects of friction, a lower bound must be placed on $h_j^{t+\frac{1}{2}\Delta t}$. This quantity should be set to be larger than a small cut-off depth $h_{\min}$. This limitation acts to stop a 'blow-up' effect at the shoreline in the value of the source term.

4.2.3 RUSH scheme

In RUSH, the nonlinear shallow water equations are numerically solved using the scheme of Nessyahu & Tadmor (1990), described above.

We use RUSH to model the interactions of swash events, caused by bores breaking on a beach slope. Bores are modelled mathematically by discontinuities in height and velocity. Using the bore conditions it is possible to send bores in from one end of our computational domain, called the seaward boundary, which is discussed later. The bores proceed to move along the mean still water level towards the still shoreline.

The mean water level is where the water is initially motionless. The shoreline is defined to be the last wet point before the dry land. Water waves usually break before the shoreline.

When a wave breaks it forms a bore which proceeds to move towards the still shoreline. The bore then proceeds to break as is reaches the still shoreline. Once the bore has broken a thin sheet of water runs up the face of the beach, this thin sheet of water is called swash. Each bore that approaches the beach, breaks and creates a thin run-up. Not every bore affects the shoreline motion, since they might not be travelling fast enough or they could be taken with the backwash from another bore.

4.2.4 RUSH-OVER scheme

In RUSH-OVER(**Run-Up** of **SH**allow water with **OVER**topping), the effects of overtopping are implemented into the RUSH scheme. To do this an extra boundary condition is implemented into the scheme, details of this boundary condition are given in section 4.4.4.

4.3 Stability

A method is defined numerically stable if small errors in the initial data do not lead to unbounded errors in the approximate solution. Predictions on stability are usually obtained by a linear analysis of the equations, assuming the changes of local

quantities are not significant enough to disturb the stability criterion obtained. Any exceptions are likely to be at the linear stability boundary. Stability of the Nessyahu and Tadmor scheme is similar to that for the Lax-Wendroff scheme, it is ensured for (Nessyahu & Tadmor 1990)

$$\lambda = \frac{\Delta t}{\Delta x} \leq \frac{\omega}{|u_m| + c_m}, \tag{4.3.1}$$

where $|u_m|$ is the absolute value of the maximum water velocity and c_m^2 is the maximum water depth and ω is given as

$$\omega \leq \frac{1}{2\delta}(\sqrt{4 + 4\delta - \delta^2} - 2). \tag{4.3.2}$$

It was stated in section 4.2 that in this work we take $\delta = 2$, so our restriction on λ is now

$$\lambda \leq \frac{\sqrt{2} - 1}{2(|u_m| + c_m)}. \tag{4.3.3}$$

If we keep λ within this limit then we are guaranteed stability. The criterion above is based on the Courant-Friedrichs-Levy condition, for explicit hyperbolic difference schemes, which states that the characteristics at a point on the new time level must be in the domain of dependence of the points used at the previous time level. Numerical instability results if the difference scheme transmits data into the interior of the flow faster than the natural rate of transport of the information as dictated by the characteristics.

In all the numerical comparisons in section 5.5, the spatial discretisation parameter $\Delta x = 0.0125$ and the temporal discretisation parameter is $\Delta t = 0.00055$. Thus the value of the stability parameter λ defined above has the value $\lambda = 0.044$.

4.4 Boundary conditions

4.4.1 Introduction

The situation we are interested in is where we have two boundaries, one is the shoreline point and the other is where the fluid extends beyond the computational domain, which is called the seaward boundary. Each of these boundaries require

special treatment and shall now be discussed. In the case of overtopping we must invoke an different boundary condition, which is also discussed.

4.4.2 Seaward boundary condition

We take the seaward boundary to be at the leftmost side of the domain, herein taken to be at $x = -1$ unless otherwise stated. To impose the boundary conditions at the seaward boundary we need to use 'ghost' cells. These are cells outside the domain, which help to calculate u and h. The way we give information to the seaward boundary, is through using the Riemann invariants α and β. For the nonlinear shallow water equations, the Riemann invariants are

$$\alpha = u + 2c + St \tag{4.4.1}$$

and

$$\beta = u - 2c + St, \tag{4.4.2}$$

where $S = -\frac{\mathrm{d}d}{\mathrm{d}x}$ is the local beach slope. This representation is exact for a plane beach with $d(x) = -x$, and may be used as an approximation when the depth varies gradually in space. In this case we neglect all terms at higher order in S. For shallow water on a plane beach the Riemann invariants are

$$\alpha = u + 2c + t, \tag{4.4.3}$$

and

$$\beta = u - 2c + t, \tag{4.4.4}$$

where c is defined as the local long wave velocity given as $c = \sqrt{h}$.

We specify the incoming information by setting α at the seaward boundary to be 'transparent' to outgoing information by determining β at the boundary from inshore values of the variables. The physical values of h and u are then

$$h = \frac{(\alpha - \beta)^2}{16}, \qquad u = \frac{\alpha + \beta}{2} - t. \tag{4.4.5}$$

This method has been employed successfully in the past by Hibberd & Peregrine (1979), Packwood (1980) and Pritchard (2001) to name a few.

From the form of the chosen incoming wave, we can calculate $\alpha = u + 2c + t$ at the seaward boundary. To calculate the values of the other Riemann invariant $\beta = u - 2c + t$ at the seaward boundary at time t, we use the characteristic form of the equations of motion relating to β (cf. equation (3.2.7))

$$\frac{\partial \beta}{\partial t} + (u - c)\frac{\partial \beta}{\partial x} = 0. \tag{4.4.6}$$

To find the value of β in the ghost-cells, we use a one-sided differencing on the above for values of $\beta_{-\frac{1}{2}}$:

$$\beta_{-\frac{1}{2}} = \frac{3}{2}\beta_{\frac{1}{2}} - \frac{1}{2}\beta_{\frac{3}{2}} + \lambda\left(\frac{3}{2}(c_{\frac{1}{2}} - u_{\frac{1}{2}}) - \frac{1}{2}(c_{\frac{3}{2}} - u_{\frac{3}{2}})\right)(\beta_{\frac{3}{2}} - \beta_{\frac{1}{2}}). \tag{4.4.7}$$

With the values of α and β known in the ghost cells, we then use (4.4.5) to calculate h and u at the seaward boundary.

4.4.3 Shoreline boundary condition

The shoreline boundary is much harder to deal with than the seaward boundary, problems occur in the neighbourhood of the shoreline, since $h = 0$ there. A method used by Pritchard (2001) and Bokhove, Patterson & Peregrine (2000) will be used which calculates the hydrodynamic variables at the grid points closest to the shore. The shoremost 'wet' grid point at time t is denoted by $j = N$. We use a staggered numerical scheme to calculate all variables at points upto and including the point $N - \frac{3}{2}$. Due to the nature of the scheme, results at $N - \frac{1}{2}$ cannot be calculated using the Nessyahu and Tadmor method. Thus a different scheme is used for the final two near-shore points. Pritchard (2001) states that for a suitable choice of λ, the shoreline will not move more than $\frac{1}{2}\Delta x$ over one time step, so $j = N - \frac{1}{2}$ will be a 'wet' point at $t + \Delta t$.

Now we need to be able to calculate the numerical derivatives v'_N at the point $N - \frac{1}{2}$. The simplest way to achieve this is by using a one-sided second-order estimate

$$v'_N = \frac{3}{2}v_N - 2v_{N-1} + \frac{1}{2}v_{N-2}. \tag{4.4.8}$$

From this, estimates for $v_N^{t+\frac{1}{2}\Delta t}$ can be found and also for the modified fluxes g_N. We then obtain $v_{N-\frac{1}{2}}^{t+\Delta t}$ as before.

The problem is now one of finding the position of the moving shoreline boundary x_{sh}, and to be able to calculate $v_{N+\frac{1}{2}}$ if necessary. The best way to tackle this problem is to use a well-established predictor-corrector method, first implemented by Hibberd & Peregrine (1979). Variables are extrapolated from beyond the shoreline and either declared 'wet' or 'dry' depending on whether the estimated depth is greater or less than a cut-off depth h_{min}.

The shoreline scheme implemented in RUSH is based on the one used in CANUTE by Dr. David Pritchard (Pritchard 2001). The scheme tracks the position of the instantaneous shoreline, x_{sh}, by advecting it using an extrapolated velocity $u(x_{\text{sh}}(t))$, defined as

$$u_{\text{sh}} = u_N + \frac{(x_{\text{sh}} - x_N)}{\Delta x}\left[\frac{3}{2}u_N - 2u_{N-1} + \frac{1}{2}u_{N-2}\right], \tag{4.4.9}$$

$$x_{\text{sh}}(t + \Delta t) = x_{\text{sh}} + \Delta t u_{\text{sh}}. \tag{4.4.10}$$

The position of the shoreline is used to determine whether the point $j = N + \frac{1}{2}$ is 'wet' or 'dry'. For the case when the quantities $v_{N+\frac{1}{2}}^{t+\Delta t}$ are required, they are calculated using the one-sided flux scheme

$$v_{N+\frac{1}{2}}^{t+\Delta t} = (v_N + \frac{1}{2}v'_N) - \lambda f'_{N+\frac{1}{2}}, \tag{4.4.11}$$

where $f'_{N+\frac{1}{2}} = 2f_N - 3f_{N-1} + f_{N-2}$. We omit the contribution from the source term, because in small water depths it is likely to lead to instabilities.

The scheme described above is implemented on a staggered grid, which is updated at alternate timesteps.

4.4.4 Overtopping boundary condition

When we consider the effects of overtopping a new boundary condition must be imposed at the point where overtopping takes place. We shall assume that at some point $x = x_e$ (In chapter 3 we used $x = E$) the beach is truncated. Our new boundary condition must allow water to freely overshoot this point and be lost from the system. As the flow approaches the edge it may be supercritical or subcritical. If at the edge $u > c$, then the flow is supercritical and will not sense the edge ahead. This is because the receding characteristic does not propagate back into the flow.

Hence the water shoots over the edge as if it were not there. Some means is still needed to calculate the values of u and h at the boundary at the next time level. A first order accurate, one sided difference scheme is used on the equations of motion. The values of h and u at the next time step are given by

$$h_e^{t+\Delta t} = h_e - \lambda(u_e h_e - u_{e-1} h_{e-1}), \tag{4.4.12}$$

$$u_e^{t+\Delta t} = u_e - \frac{\lambda}{2}(u_e^2 + h_e - d_e - u_{e-1}^2 - h_{e-1} + d_{e-1}). \tag{4.4.13}$$

When the flow in the vicinity of the edge is subcritical, $u < c$, it must accelerate smoothly to supercritical flow as it passes over the edge and into free-fall. Hence at some point close to the edge the flow must be critical. We assume this transition point is at the edge. This flow is exactly what we dealt with analytically in chapter 3. The receding C_- characteristic curve (cf. equation (2.2.11)) at the edge has zero velocity, thus in the space-time plane the characteristic remains on the edge. On the advancing characteristic curve the invariant α at the edge has form

$$\alpha = 3u + t. \tag{4.4.14}$$

Once α is known at the edge, the overtopping boundary condition is solved. Using equation (3.2.6), for the C_+ characteristic invariant, the value of α at the edge at the next time level may be estimated. As at the seaward boundary a one-sided first order finite difference form is used for α, it is

$$\alpha_e^{t+\Delta t} = \alpha_e - \lambda(u_e - c_e)[\alpha_e - \alpha_{e-1}]. \tag{4.4.15}$$

The variables α_e and α_{e-1} are calculated from known values of u and h at time level t. Knowing $\alpha_e^{t+\Delta t}$ from (4.4.15), $u_e^{t+\Delta t}$ is calculated from (4.4.14) and is given by

$$u_e^{t+\Delta t} = u_e + 2c_e - \Delta t - \frac{1}{3}\lambda(u_e - c_e)[u_e + 2c_e - u_{e-1} - 2c_{e-1}]. \tag{4.4.16}$$

We know that $h_e^{t+\Delta t} = (u_e^{t+\Delta t})^2$ since the flow is critical. While the shoreline position x_N is less than x_e the shoreline calculation proceeds as described in section 4.4.3. When the run-up reaches the edge the boundary condition is switched to the overtopping mode. During run-up the flow is most often supercritical initially and

equations (4.4.12) and (4.4.13) are used. When the flow decelerates to critical flow the characteristic calculation (4.4.15) is used to estimate h and u at the edge. When h_e falls below the accepted tolerance level $h_{\min}$, which we take as 0.0001, the shoreline is cut back to just below the edge and the usual shoreline procedure picks up the calculation once more.

4.5 Comparison of RUSH to analytic and numerical results

The scheme used in RUSH is validated against four analytical solutions and a computational solution of the nonlinear shallow water equations. The four exact solutions used are the dambreak solution, see Stoker (1957), the Carrier & Greenspan (1958) solution for a reflected wave on a plane beach, the Shen & Meyer (1963) solution for run-up of swash and finally the overtopping solution due to Peregrine & Williams (2001). The computational solution is that of Hibberd and Peregrine (1979) for a uniform bore running up a beach.

4.5.1 Dam-break problem

The dambreak solution is a very simple non-trivial exact solution to the nonlinear shallow water equations, which was first considered by Ritter (1892). The solution describes what would happen if water of height h_0 contained behind a dam were to be released by an instantaneous and complete collapse of the dam. When there is no water in front of the dam, the analytical solution is based on the method of characteristics (Stoker 1957). The solution is given as

$$h(x,t) = \frac{1}{9}\left(2\sqrt{h_0} - \frac{x}{t}\right)^2, \qquad u(x,t) = \frac{2}{3}\left(\sqrt{h_0} + \frac{x}{t}\right),$$

for $-\sqrt{h_0} \leq x/t \leq 2\sqrt{h_0}$. Plots of h and u are given in figures 4.1 and 4.2.

The flow is not represented well for small times, since the discontinuity adjusts to a smooth parabolic profile. This is because during this phase of flow, the curvature of $h(x)$ near the front is high, and thus the extrapolation of variables required by the nose scheme is less accurate. The error induced correponds to a very small mass.

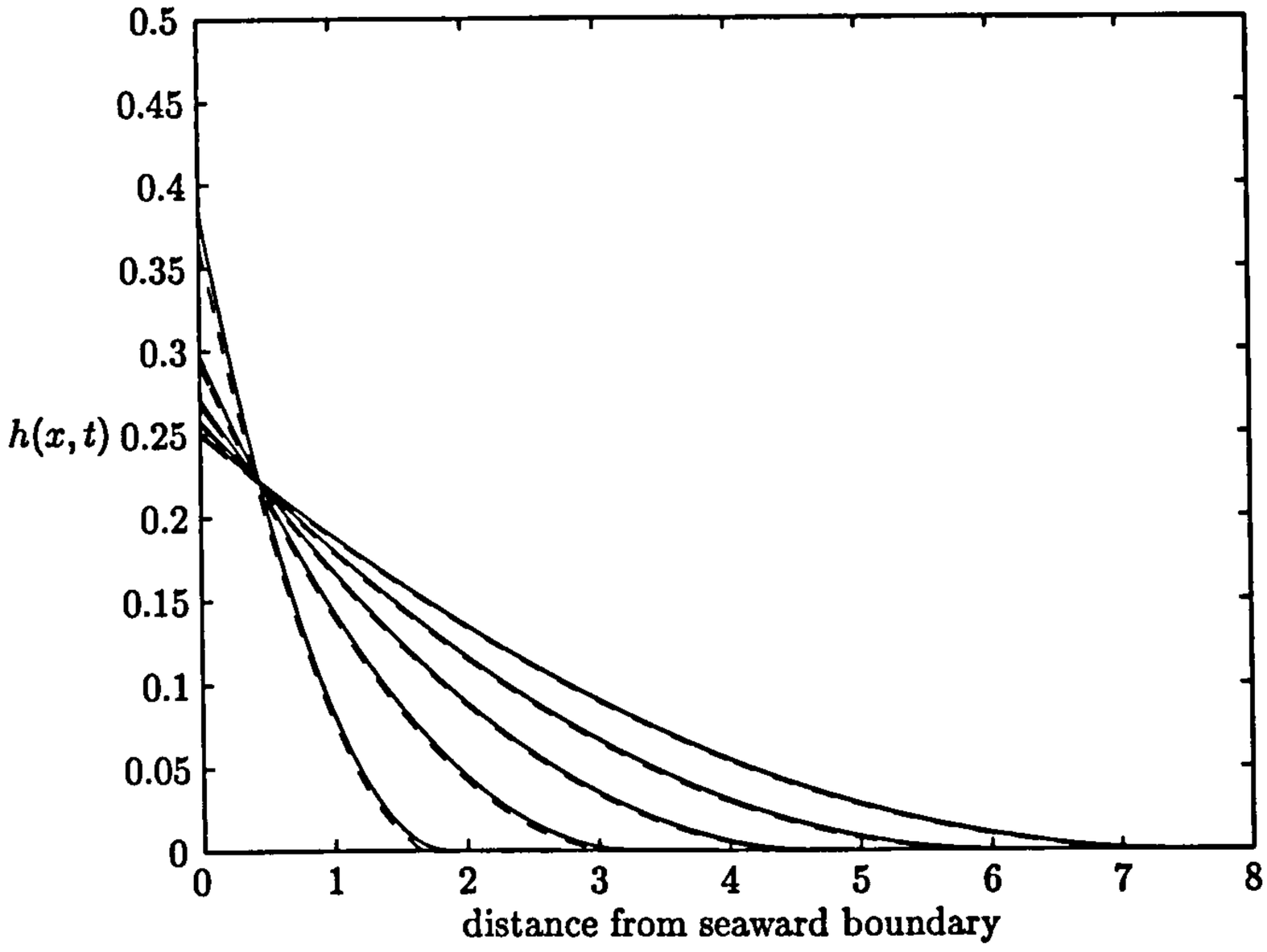

Figure 4.1: Height of dambreak flow with $h_0 = 0.5$ for $t = 1, 2, 3, 4, 5$. Numerical (- -) and analytical (–).

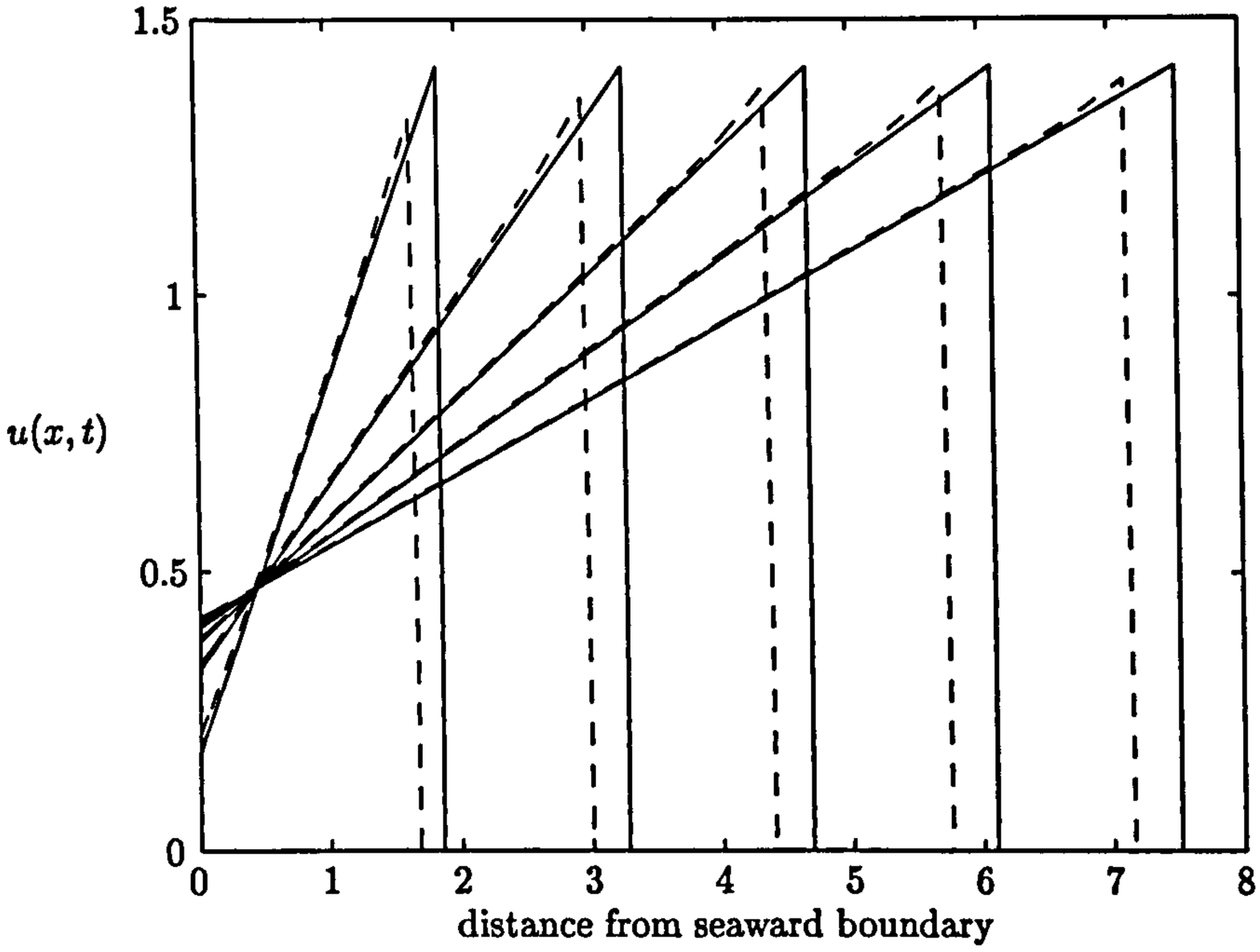

Figure 4.2: Velocity of dambreak flow with $h_0 = 0.5$ for $t = 1, 2, 3, 4, 5$. Numerical (- -) and analytical (–).

A plot of the mass flux $q = uh$ is shown in figure 4.3. An explicit form for $q(x,t)$ is given below

$$q(x,t) = \frac{2}{27}\left(4h_0\sqrt{h_0} - 3\sqrt{h_0}\frac{x^2}{t^2} + \frac{x^3}{t^3}\right). \tag{4.5.1}$$

In our example here we take $h_0 = \frac{1}{2}$, so q is

$$q(x,t) = \frac{1}{27}\left(2\sqrt{2} - 3\sqrt{2}\frac{x^2}{t^2} + 2\frac{x^3}{t^3}\right). \tag{4.5.2}$$

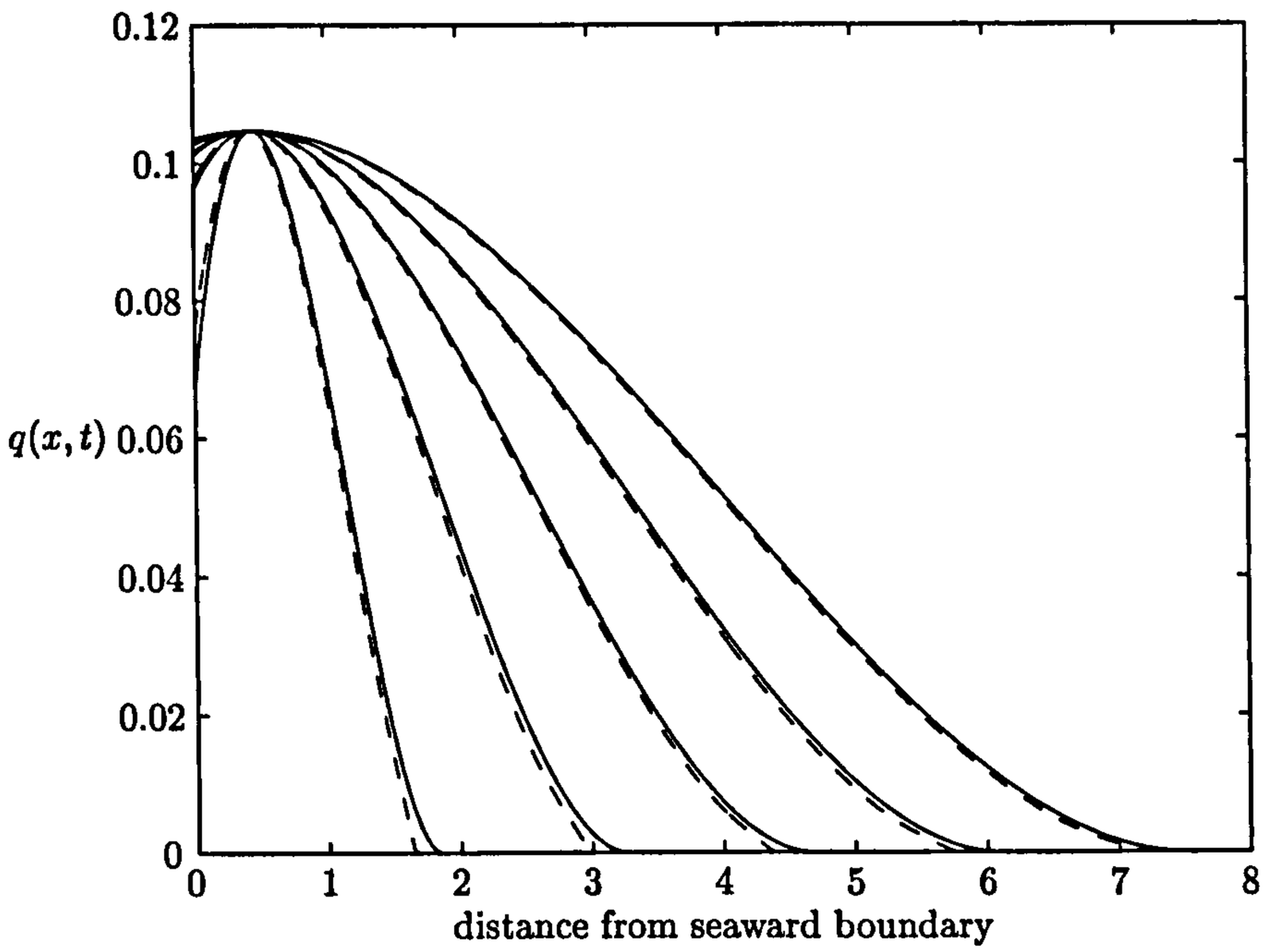

Figure 4.3: Mass flux for dambreak flow with $h_0 = 0.5$ for $t = 1, 2, 3, 4, 5$. Numerical (- -) and analytical (–).

To evaluate the mass of water which is lost due to the numerical scheme, we need to integrate $q(x,t)$ for each value of t considered, with respect to the seaward distance x, between the numerical shoreline position and the analytic shoreline position. We find:

$$Q = \int_{x_{\text{num}}}^{x_{\text{anal}}} q\,\mathrm{d}x = \frac{1}{27}\left(2\sqrt{2}x - \sqrt{2}\frac{x^3}{T^2} + \frac{x^4}{2T^3}\right)\Bigg|_{x_{\text{num}}}^{x_{\text{anal}}}, \tag{4.5.3}$$

where x_{num} and x_{anal} are respectively the numerical and analytical shoreline positions for a fixed T. To show how small the mass lost due to the numerical scheme is,

we calculate the percentage of water mass lost. The results are shown in table 4.1. From table 4.1 we see that for $t \geq 2$ the amount of water lost due to the numerical

t	x_{anal}	x_{num}	$Q_0 = \int_0^{x_{\text{anal}}} q\,\mathrm{d}x$	Q	$\frac{Q}{Q_0} \times 100\%$
1	$\sqrt{2} + \frac{4}{9} = 1.86$	1.68	0.0794	0.0043	5.42
2	$2\sqrt{2} + \frac{4}{9} = 3.27$	3.00	0.1494	0.0012	0.80
3	$3\sqrt{2} + \frac{4}{9} = 4.69$	4.40	0.2228	0.0008	0.36
4	$4\sqrt{2} + \frac{4}{9} = 6.10$	5.76	0.2966	0.0003	0.10
5	$5\sqrt{2} + \frac{4}{9} = 7.52$	7.16	0.3706	0.0002	0.05

Table 4.1: Calculating the errors involved in numerical scheme

scheme is less than 1% of the total amount. This shows us that the differences in the shoreline positions, shown best in figure 4.2 do not give rise to imprecise answers as one might first assume.

From figures 4.1 and 4.2 we can see that the implementation of the seaward boundary condition is working successfully. It seems like the receding characteristics propagate through the boundary without difficulty and also there is no sign of distortion in the region of solution.

4.5.2 Carrier & Greenspan solution

The Carrier and Greenspan reflected wave, see Carrier & Greenspan (1958) is an exact solution of the nonlinear shallow water equations on a plane beach. This solution is a good test for numerics as it is strongly nonlinear (if near its limiting amplitude) and involves a shoreline which advances and retreats. The surface elevation at intervals of half a period are shown in figure 4.4 and the shoreline position is shown in figure 4.5. From Carrier & Greenspan (1958) expressions can be found for the height and velocity of the wave far at sea. The expressions are given by

$$h(x,t) \sim -\frac{A}{4} J_0(4|x|^{\frac{1}{2}}) \sin 2t - x, \tag{4.5.4}$$

$$u(x,t) \sim -\frac{A}{4} \frac{J_1(4|x|^{\frac{1}{2}})}{|x|^{\frac{1}{2}}} \cos 2t, \tag{4.5.5}$$

where J_0 is the Bessel function of first kind, order zero and J_1 is the Bessel function of first kind, order one. An expression can also be found for the shoreline position

of the wave. This is given by

$$x_s(t) = -\frac{A}{4}\sin 2t - \frac{1}{8}(A\cos 2t)^2. \tag{4.5.6}$$

In the above three expressions, A is a constant which is introduced to stop the Jacobian vanishing. With expressions for the height and velocity known, an expression fro the Riemann invariant α is found as

$$\alpha \sim -\frac{AJ_1(4|x|^{\frac{1}{2}})}{4|x|^{\frac{1}{2}}}\cos 2t + 2\left(-\frac{A}{4}J_0(4|x|^{\frac{1}{2}})\sin 2t - x\right)^{\frac{1}{2}} + t \tag{4.5.7}$$

There are slight discrepancies in the comparison in figure 4.4, this is possibly down to the fact that the value of the Riemann invariant is represented approximately at the seaward boundary. This is down to the fact that the Bessel functions are approximated using the tables of Abramowitz & Stegun (1965).

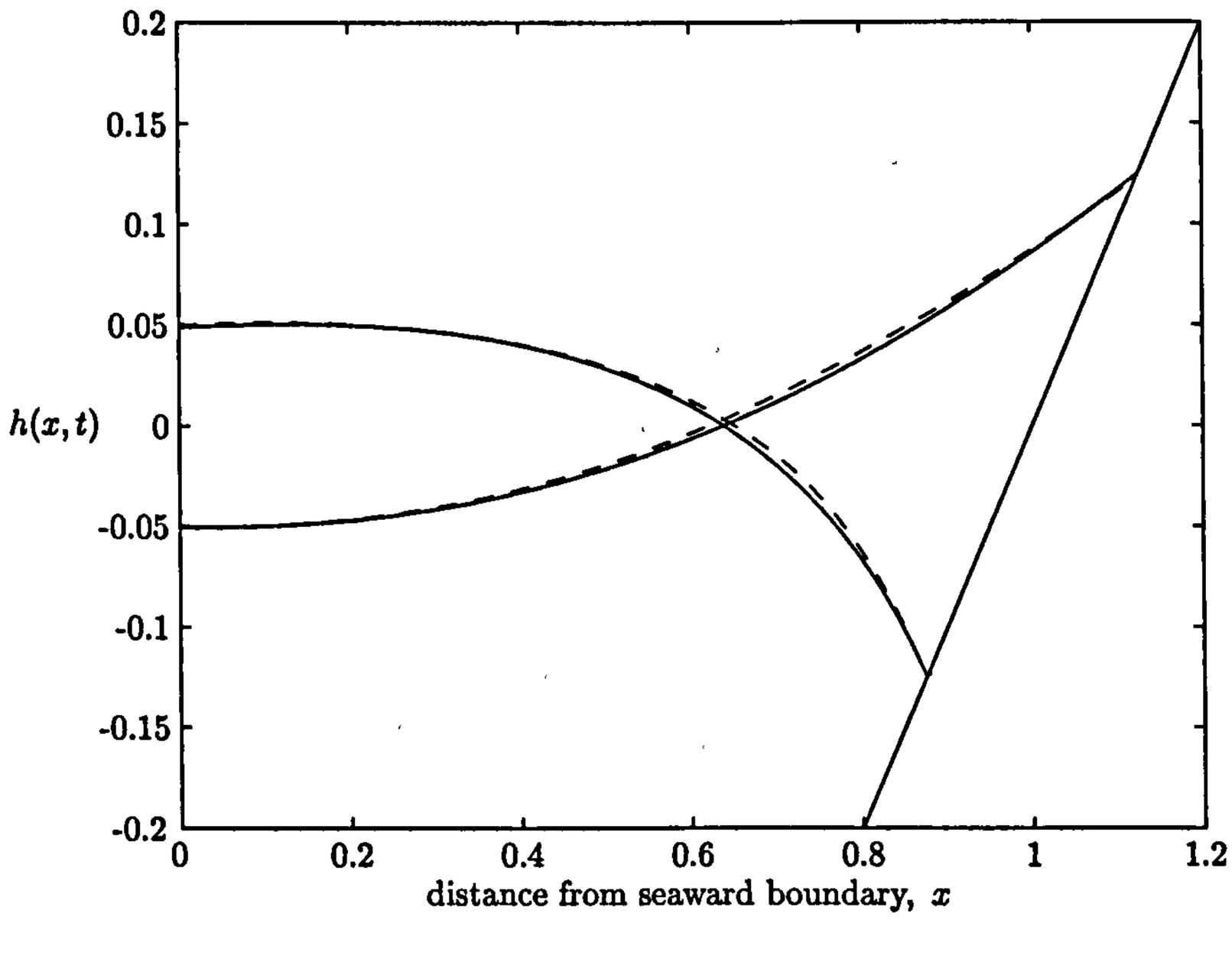

Figure 4.4: Surface elevation of Carrier and Greenspan (1958) wave with amplitude $A = 0.5$ at interval $\frac{1}{2}$ period. Numerical (- -) and analytical (–).

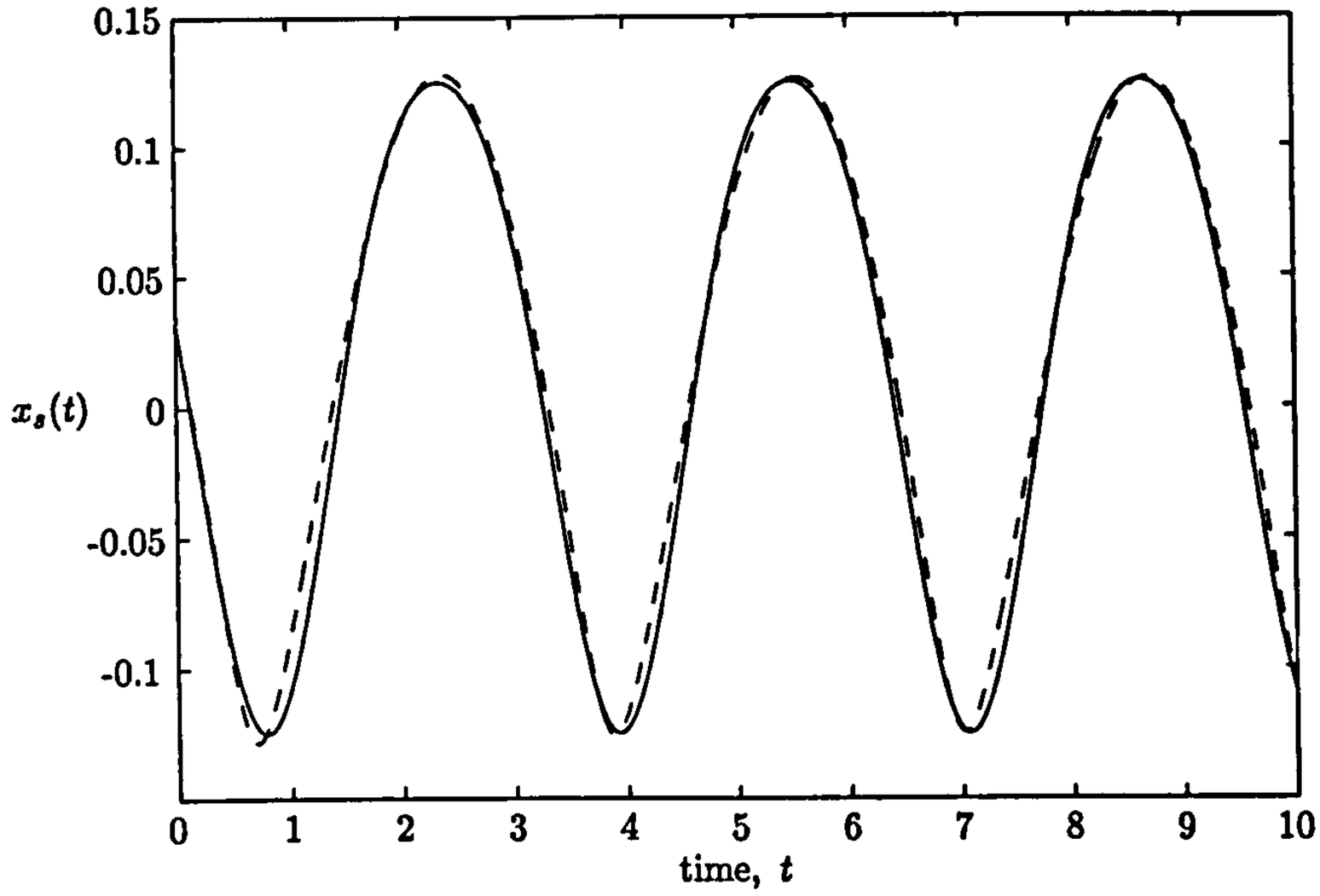

Figure 4.5: Shoreline position of Carrier and Greenspan (1958) wave with amplitude $A = 0.5$. Numerical (- -) and analytical (–).

4.5.3 Shen & Meyer solution

The solution due to Shen & Meyer (1963) for the run-up of a bore on a plane beach (cf. equations (3.3.1), (3.3.2) and (3.3.4)) is compared to numerical results using RUSH. The seaward boundary is taken to be at the point $x = -1$. The still water level is taken as zero and extends to $x = 0$. Thus the initial shoreline position is at $x = 0$.

To find the value of the positive Riemann invariant at the seaward boundary we use the expressions given by Shen & Meyer (1963) for the velocity and local long wave velocity. This gives $\alpha = u + 2c + t = 2$ at the seaward boundary.

Initially we choose a fixed bore of height 0.25 on the slope. In the scaling of the shallow water equations in chapter 2, the beach slope is actually scaled out. The beach is implicitly contained in the form of the shallow water equations. Thus the initial bore which we want to be on the beach slope, is just setup as if there were no slope. This bore is setup to run from the seaward boundary at $x = -1$ to the initially still shoreline at $x = 0$. To create the exact swash event described by Shen & Meyer (1963), we must satisfy the condition $\alpha = 2$. Using this fact, with the

choice that $h = 0.25$, we find that the bore must have initial velocity $u = 1$ (See figure 4.6 for 'real life' depiction of the setup. This figure does not show the actual initial condition used in RUSH, since the slope is actually considered as part of the scheme).

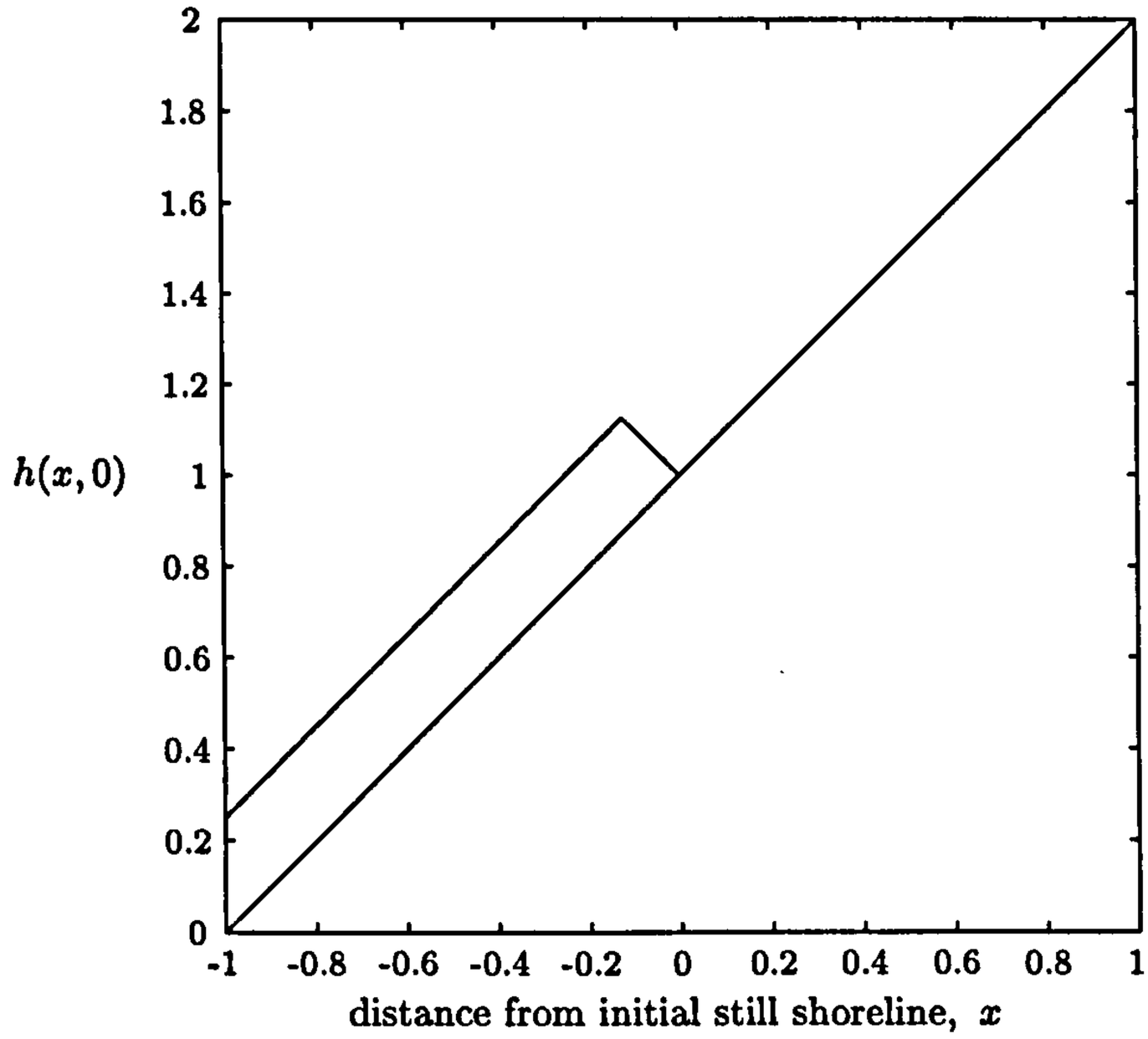

Figure 4.6: 'Real life' setup for Shen & Meyer

At a fixed point in space, taken here as $x = 0.4$, the height, velocity and flux are recorded over a time variation. Numerical comparisons are made to the analytical solutions provided by Shen & Meyer (1963) for these quantities and are given in figures 4.8 and 4.9. A comparison is also made with the shoreline position and is given in figure 4.7.

We can see from figure 4.7 that the numerical result for the shoreline position deviates slightly from the analytical result. This is because like in the dam-break case a linear extrapolation is used for the shoreline nose point and thus under estimates the parabolic nature of the analytical solution near the front. The difference in shoreline position up the beach is approximately 4%, which is not too bad for the thin parabolic profile.

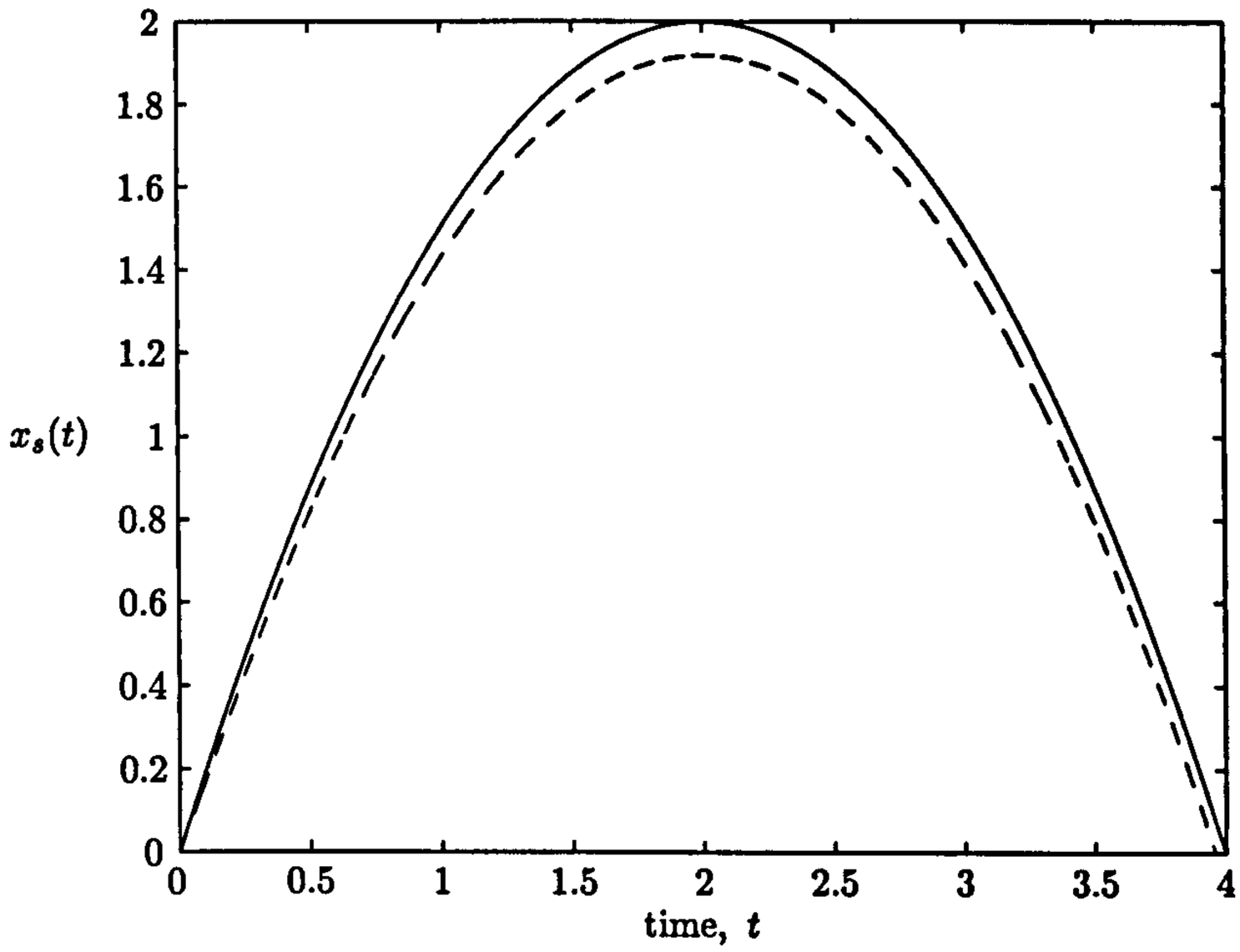

Figure 4.7: Shoreline position $x(t)$. Analytical (–), numerical (- -).

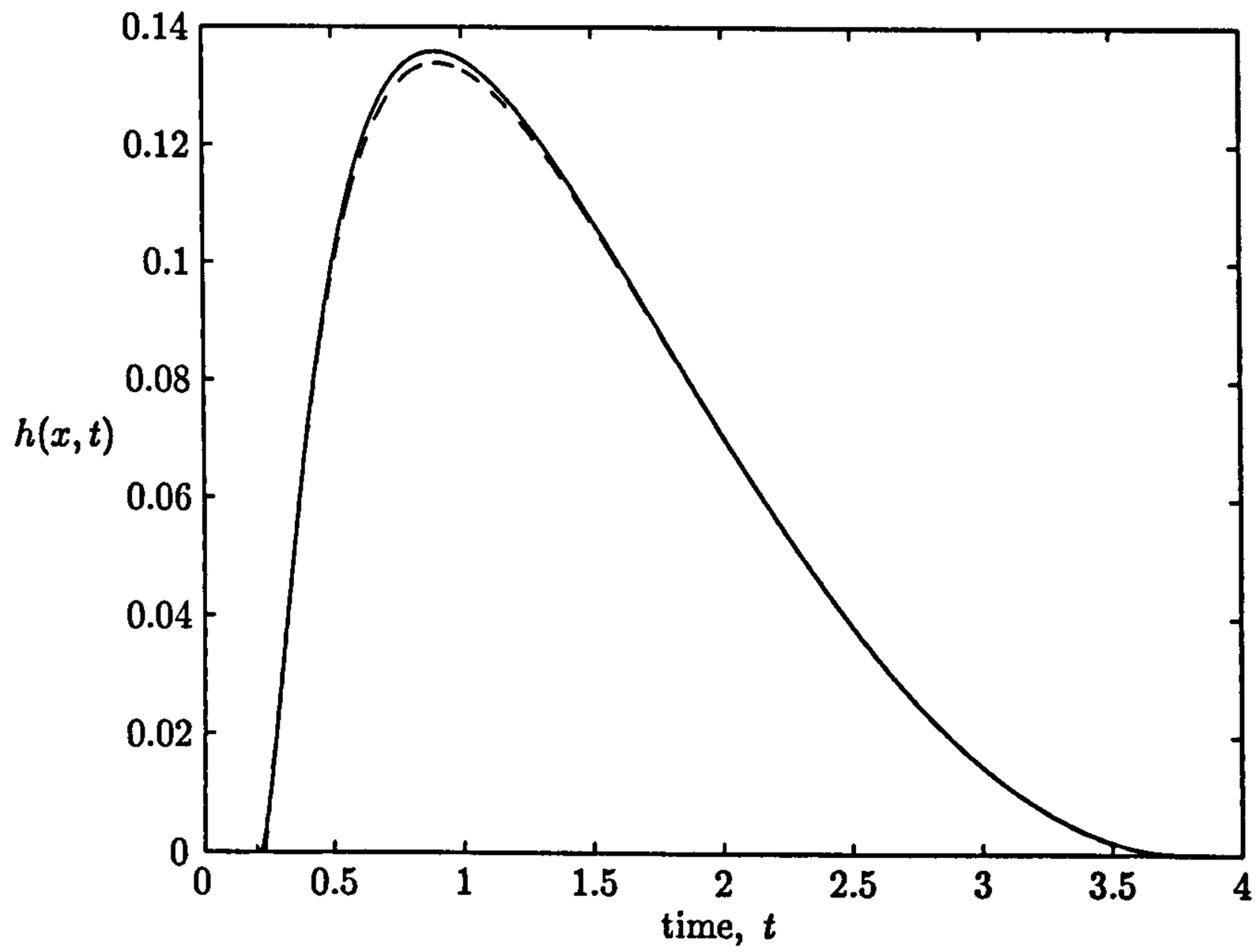

Figure 4.8: Height h against time, t at a fixed point $x = 0.4$. Analytical (–), numerical (- -).

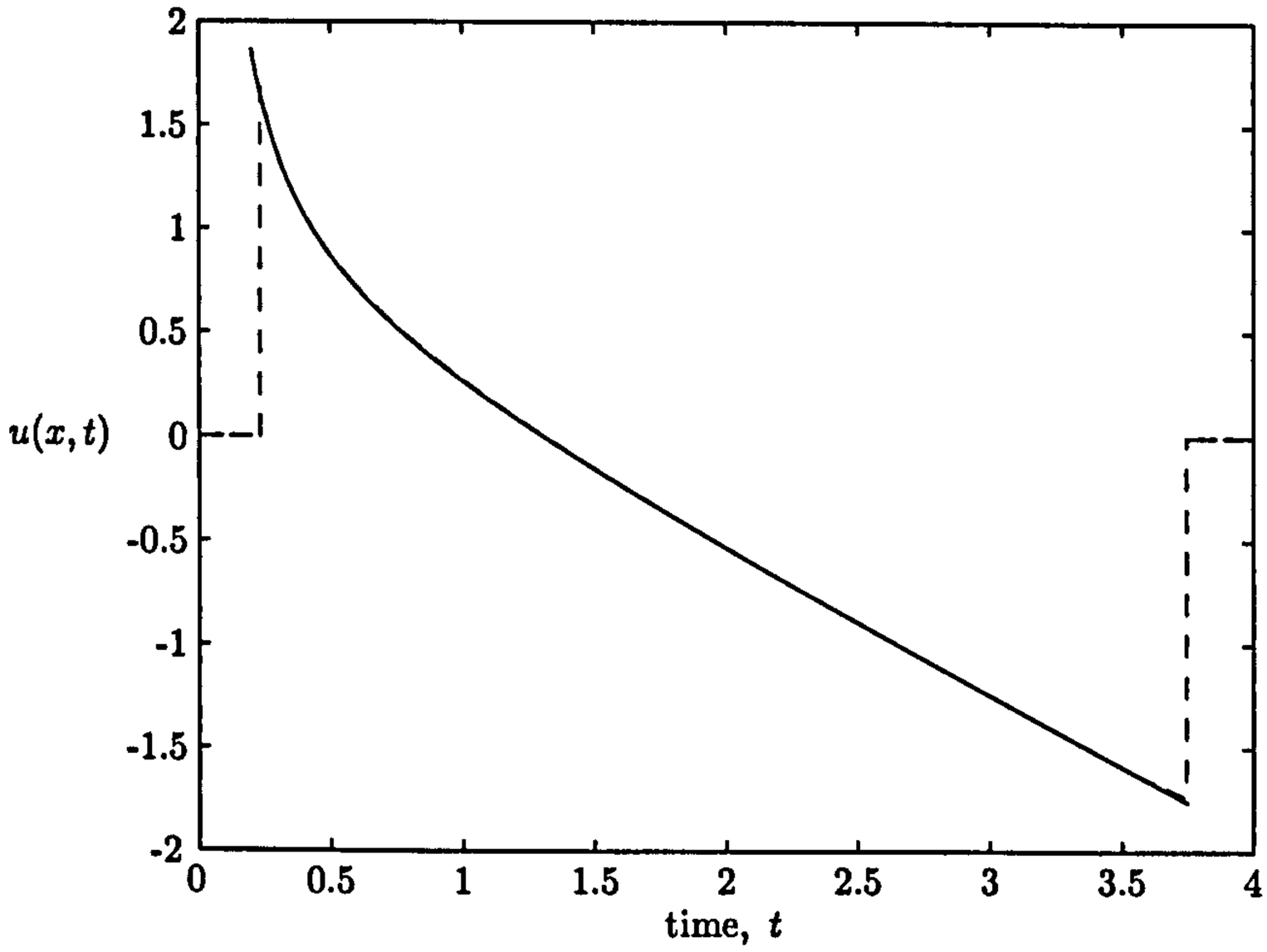

Figure 4.9: Velocity u against time, t at a fixed point $x = 0.4$. Analytical (–), numerical (- -).

Figure 4.10: Flux q against time, t at a fixed point $x = 0.4$. Analytical (–), numerical (- -).

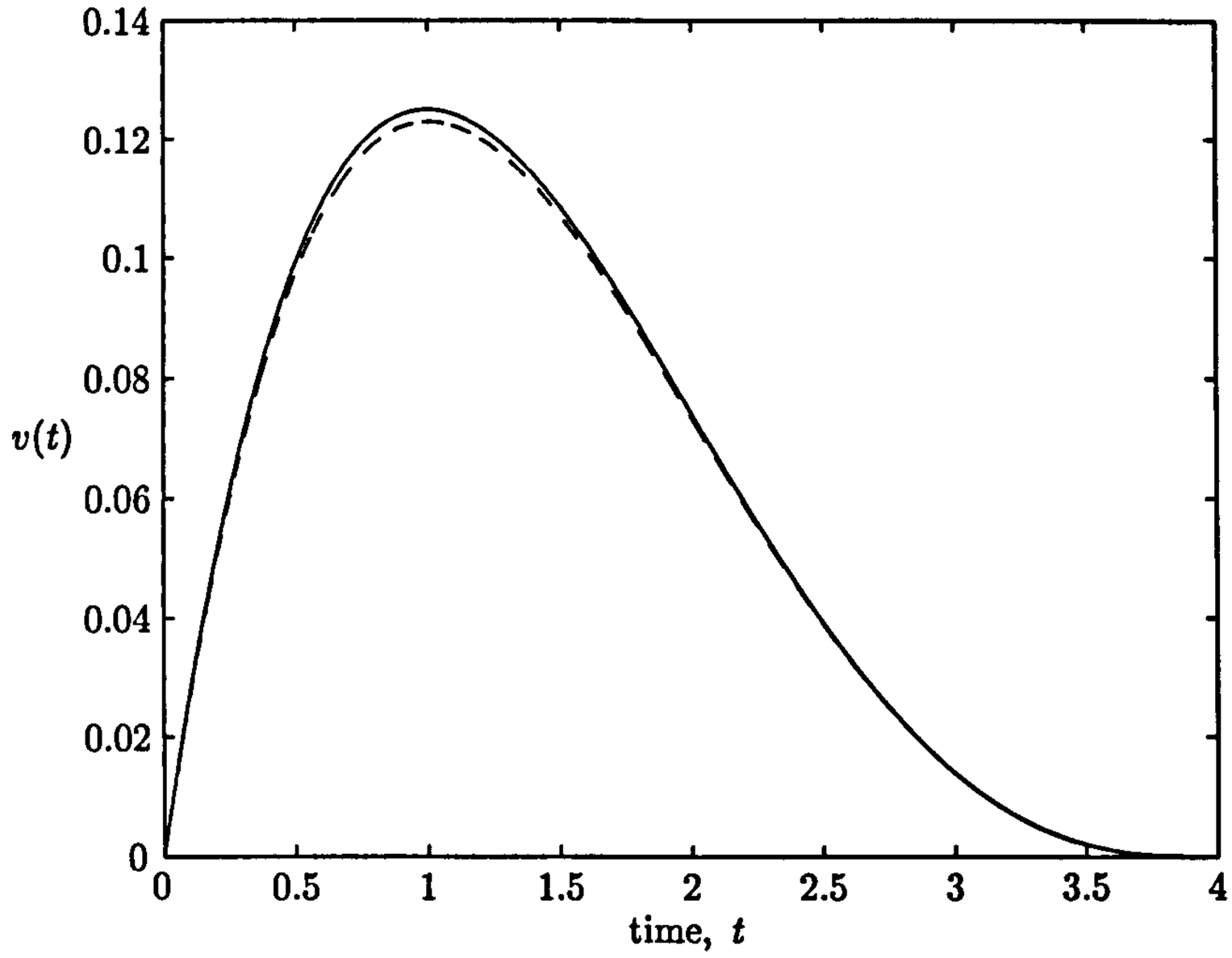

Figure 4.11: Volume v against time, t. Analytical (–), numerical (- -).

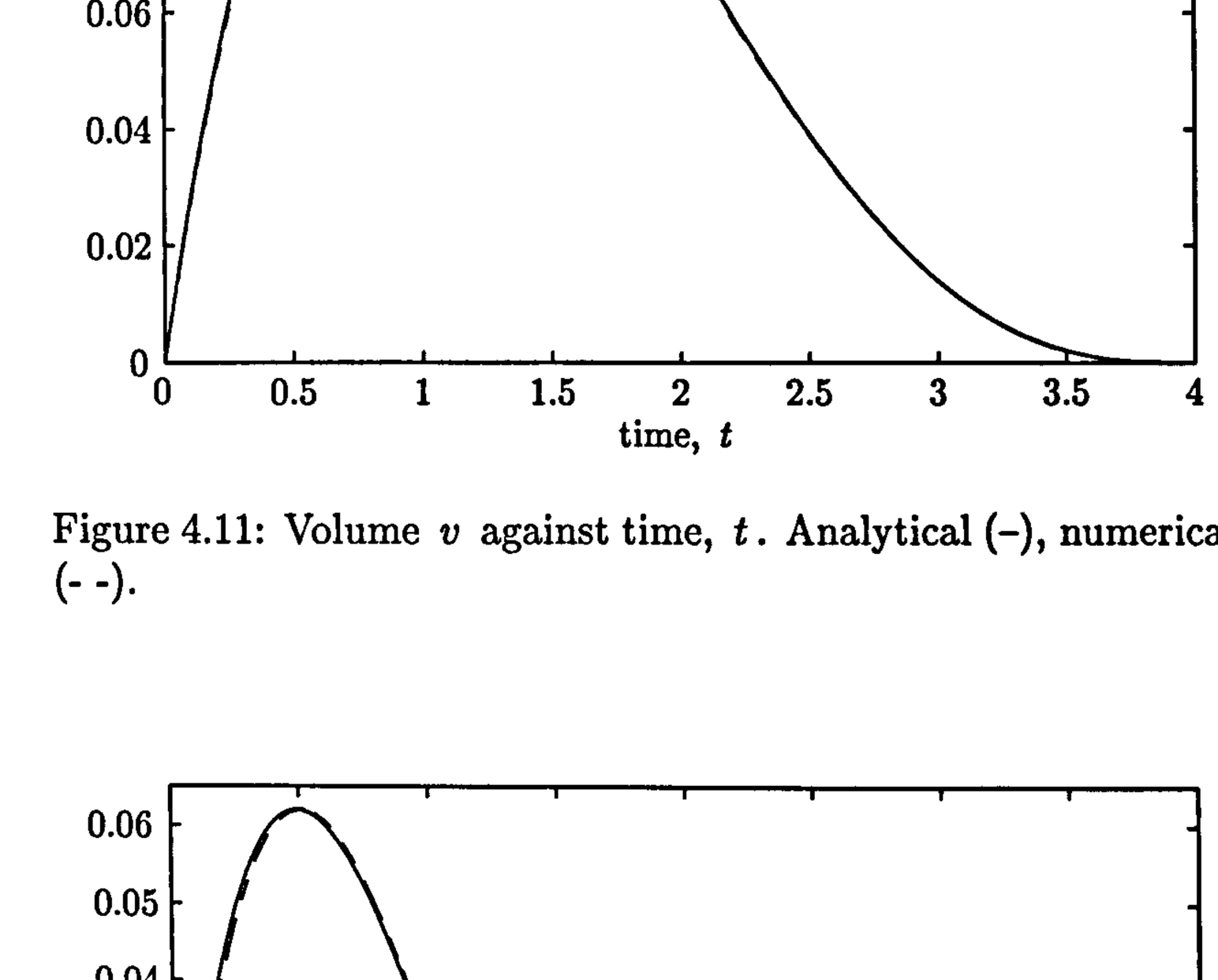

Figure 4.12: Momentum M against time, t. Analytical (–), numerical (- -).

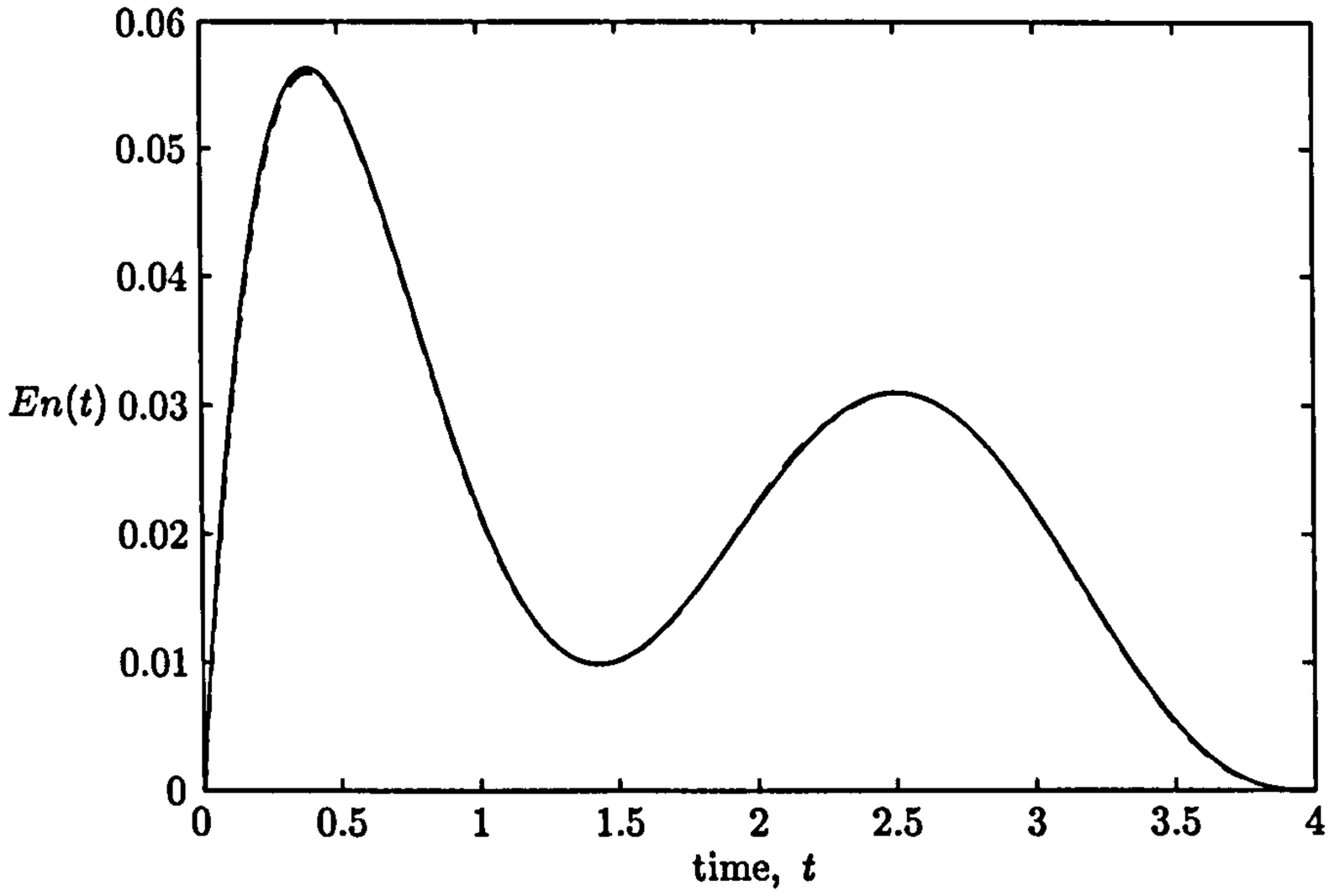

Figure 4.13: Energy En against time, t. Analytical (–), numerical (- -).

Figures 4.11, 4.12 and 4.13 show us how well volume, momentum and energy results from RUSH compare with analytical results. Here volume, momentum and energy are functions of time defined by

$$v(t) = \int_0^{x_s(t)} h \, \mathrm{d}x = \frac{t}{216}(4-t)^3, \tag{4.5.8}$$

$$M(t) = \int_0^{x_s(t)} uh \, \mathrm{d}x = \frac{t}{864}(t-4)^3(3t-4), \tag{4.5.9}$$

$$En(t) = \int_0^{x_s(t)} u^2 + \frac{h^2}{2} \, \mathrm{d}x = \frac{t}{8640}(4-t)^3(48-64t+23t^2). \tag{4.5.10}$$

Notice that we integrate from zero, thus we are considering only the flow in the initially dry region ($x \geq 0$).

Even though we don't have a perfect shoreline comparison we can see from figures figures 4.6 - 4.11 that the numerical results from RUSH fit the analytic solutions from Shen & Meyer (1963) very well. This shows that the RUSH scheme seems to work well.

4.5.4 Peregrine & Williams solution

A numerical comparison is made to the analytical overtopping solution given in chapter 3 and by Peregrine & Williams (2001). The seaward boundary is taken at $x = -1$, the value of the positive Riemann invariant here is $\alpha = 2$, as in the Shen & Meyer case. The initial setup is also the same as for the Shen & Meyer case described earlier. The difference here is that we truncate the plane beach at a point $x = E$. So all flow that passes this point does not affect the subsequent flow.

This comparison is a good test to see if the overtopping boundary condition is working successful. A comparison is made between the analytic and numerical flux at the truncation point E for different values of E, a comparison is also made of the overtopping volume. These are given in figures 4.14 and 4.15 respectively.

Figure 4.14 shows a slight discrepancy in the numerical result. But if we integrate over the total time we find that the numerical volume is a much better fit (see figure 4.15). From both these figures we see that the implementation of the overtopping boundary condition is working successfully.

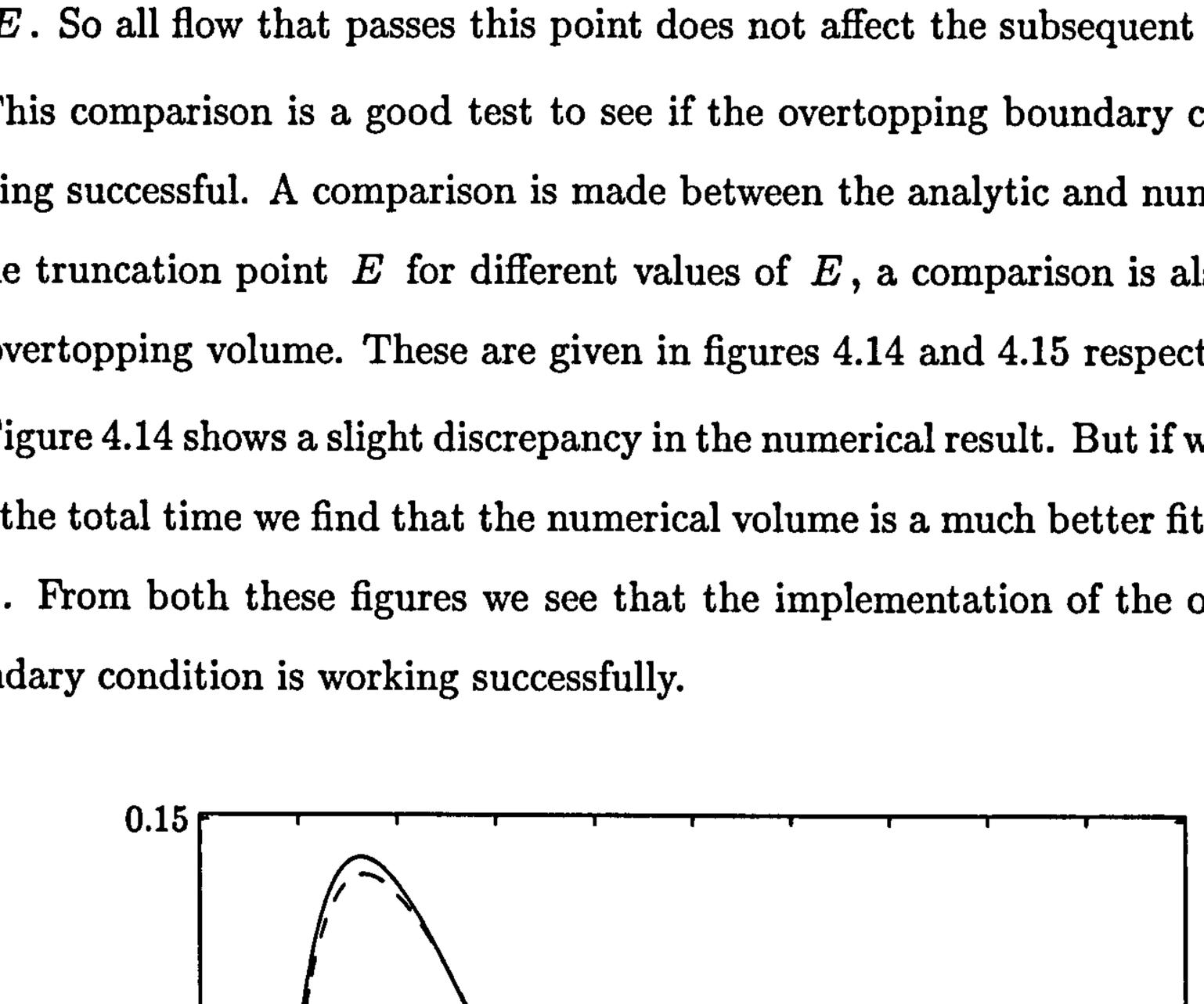

Figure 4.14: Flux q against time, t. Analytical (–), numerical (- -) E is increased from 0.2 to 1.4 in steps of 0.2.

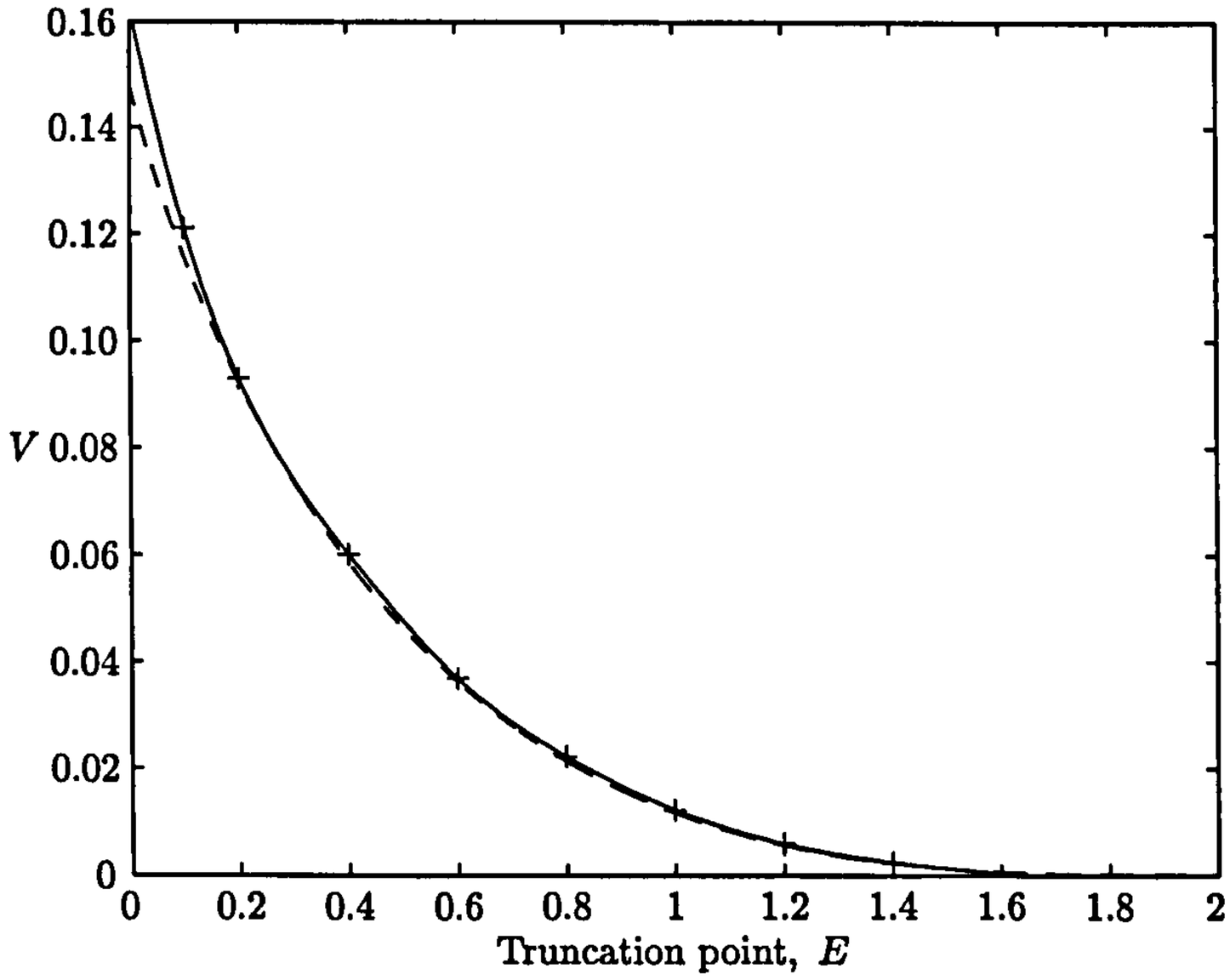

Figure 4.15: Overtopping volume per unit width $V(E)$. Analytical (- -), numerical (+). Line of best fit through numerical data (–)

4.5.5 Testing RUSH for bores

Testing RUSH with uniform bores has not yet been discussed. We shall do this here. Since in proceeding sections we are concerned with the interactions of swash events as a consequence of uniform bores breaking near the shoreline, we need to see if RUSH behaves with the introduction of a uniform bore. Uniform bores are modelled mathematically and numerically by discontinuities. To describe an incoming bore we invoke the bore relations (Lamb 1932,Whitham 1974).

The simplest problem to consider is that of a bore moving into still water of constant depth. We initially have a fixed height of water in the computational domain. We then setup a bore to travel through this medium. The bore should progress through the still water without losing it's form.

Figures 4.16 and 4.17 show the height and velocity profiles for a bore of height 1 travelling into still water of constant depth 0.5. We see from both these figures that the form of the bore is consistent as it travels through the still water. This

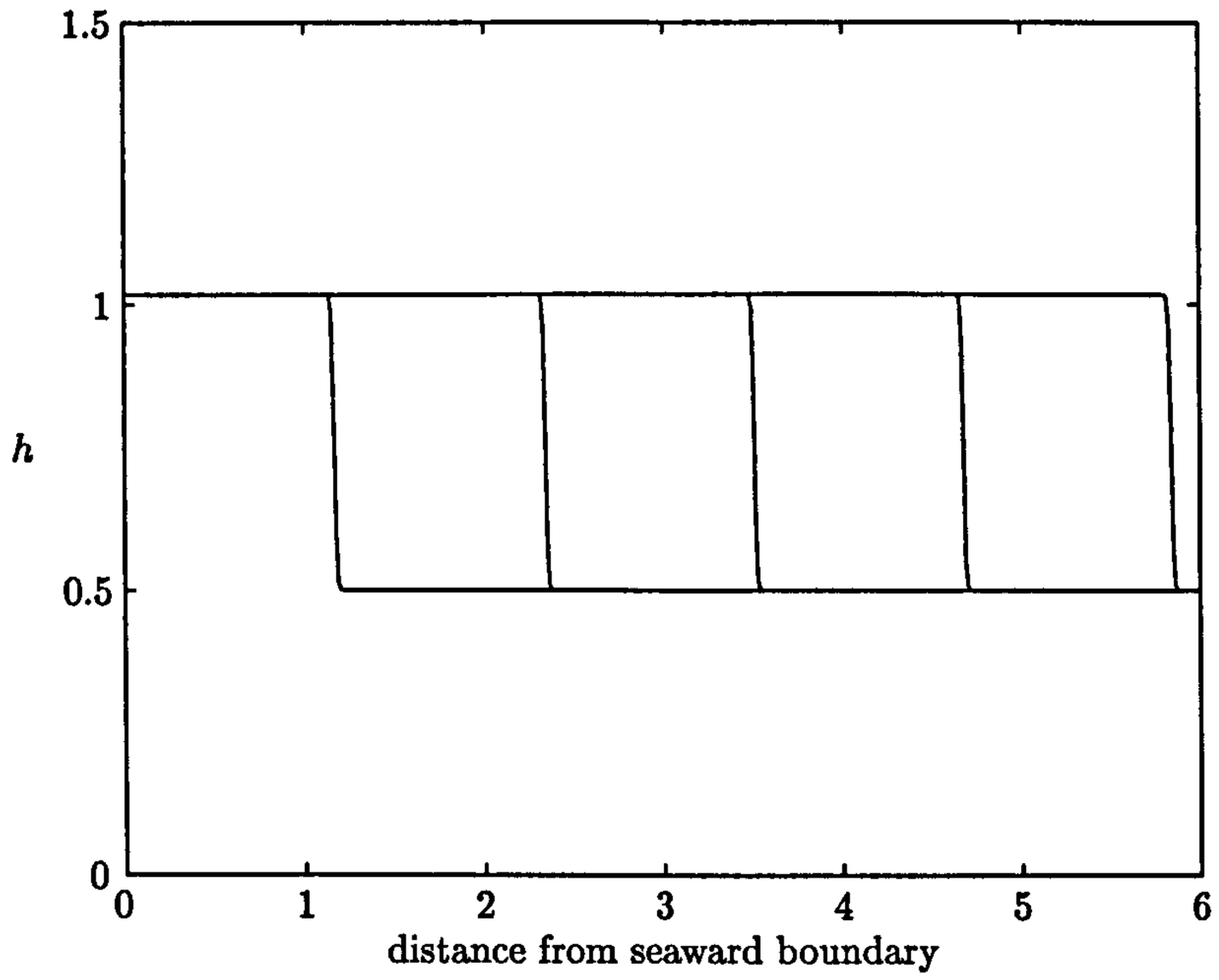

Figure 4.16: Height profile for a uniform bore of height 1 travelling into still water of constant depth 0.5. Profiles are at times $t = 1, 2, 3, 4, 5$.

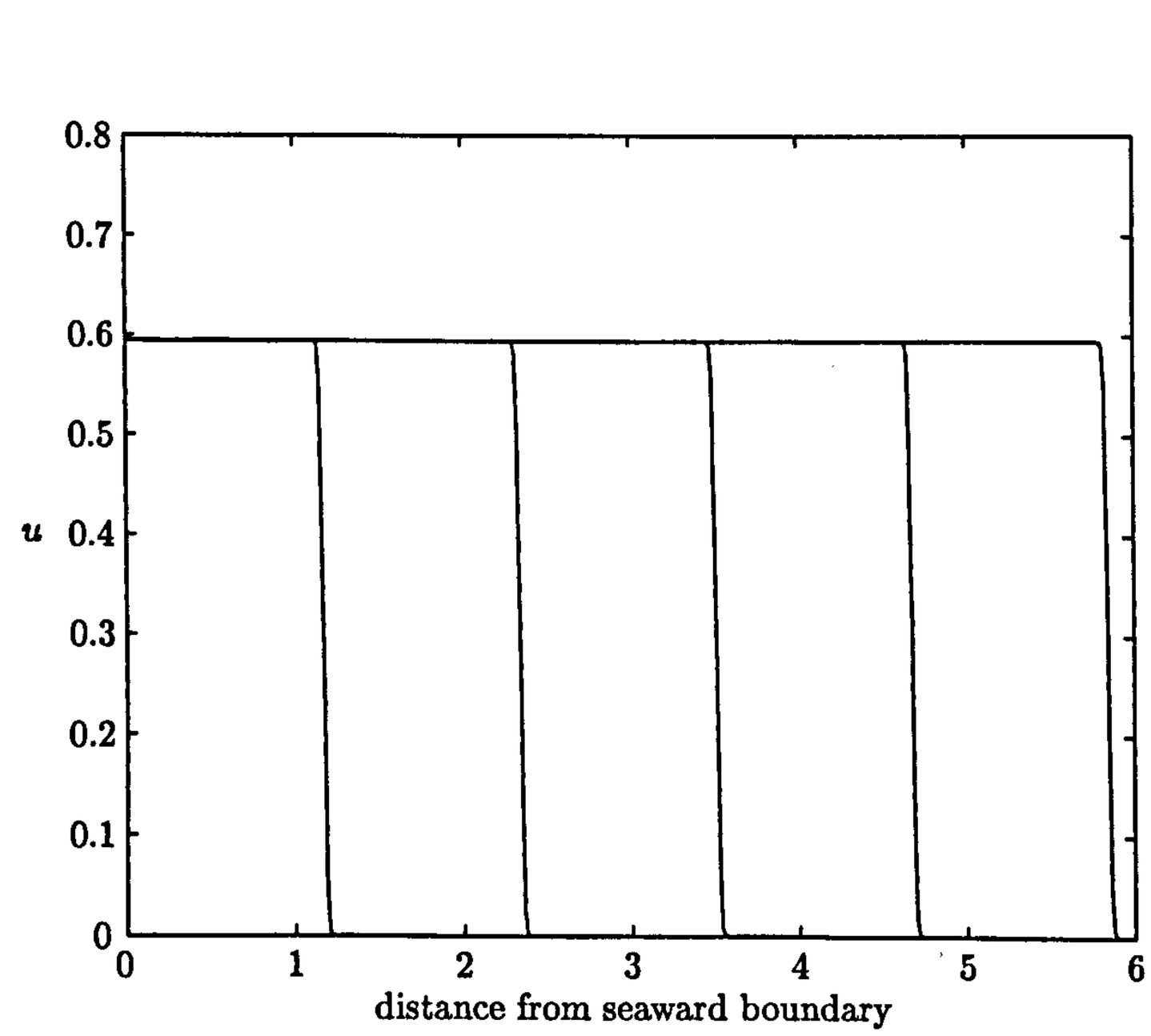

Figure 4.17: Velocity profile for a uniform bore of height 1 travelling into still water of constant depth 0.5. Profiles are at times $t = 1, 2, 3, 4, 5$.

shows us that RUSH seems to work fine with the introduction of a uniform bore.

Another test for bores is to consider the run-up of a uniform bore over a sloping beach. Hibberd & Peregrine (1979) obtained a numerical solution to describe the behaviour of a uniform bore over a sloping beach. The same problem is solved using RUSH. Whether the results of Hibberd & Peregrine (1979) are more accurate than the results produced by RUSH is hard to say, since they are both numerical results, and no analytic result exists. The computed heights and velocities for the run-up of a bore of initial height 1.6 are shown in figures 4.18 and 4.19. The initial shoreline position is at $x = 0$.

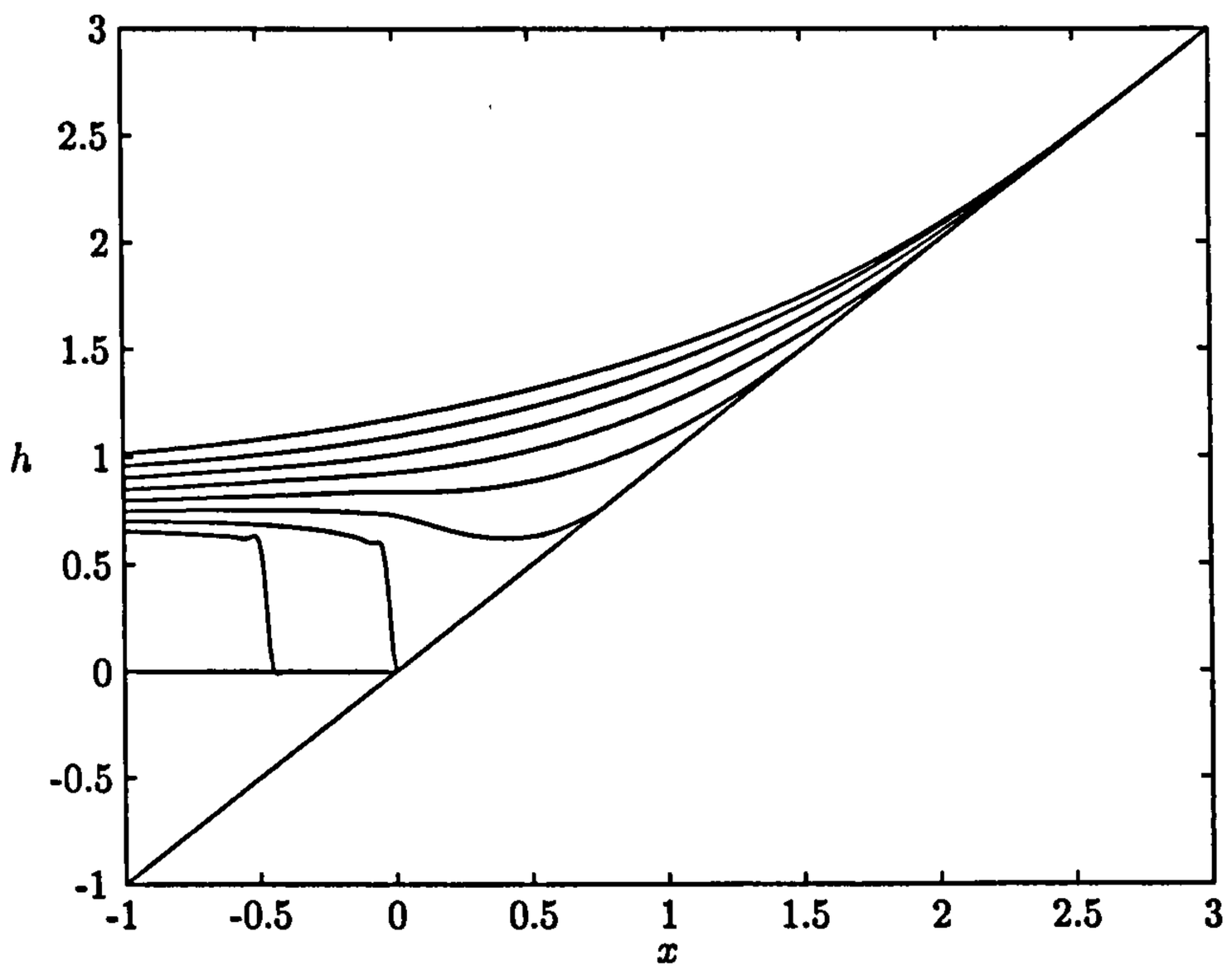

Figure 4.18: Surface elevation at $t = 0.4$ to 3.2 in intervals of 0.4.

The noticable differences between the results in figures 4.18 and 4.19 and figure 6 of Hibberd & Peregrine (1979), is that their shoreline seems to extend further at $t = 3.2$. Also their velocity profile at $t = 3.2$ goes negative whereas in figure 4.19, the velocity does not go negative at this time. This implies that the backwash in the Hibberd & Peregrine (1979) case starts at an earlier time than found here.

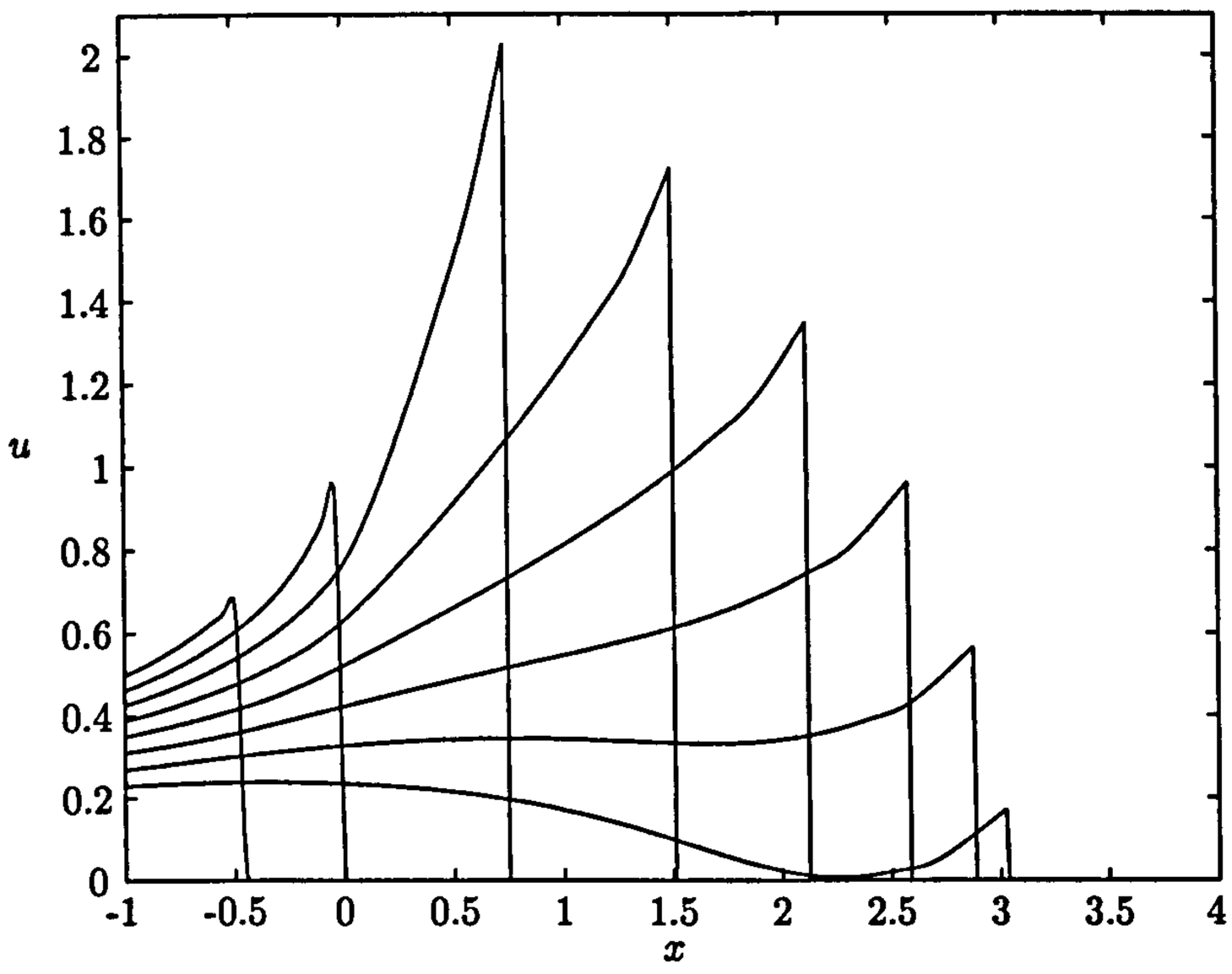

Figure 4.19: Water velocity at $t = 0.4$ to 3.2 in intervals of 0.4.

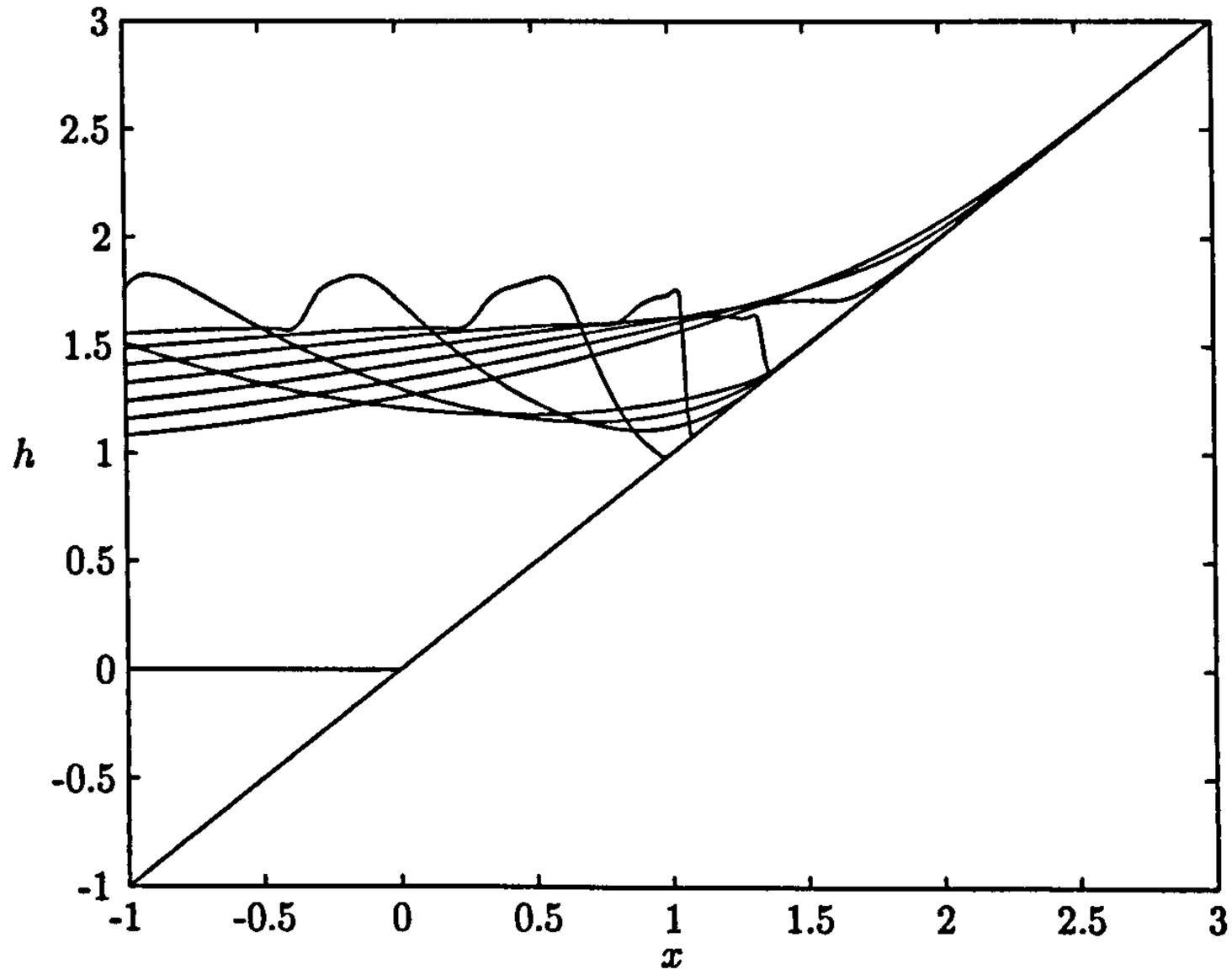

Figure 4.20: Surface elevation at $t = 3.6$ to 6.8 in intervals of 0.4.

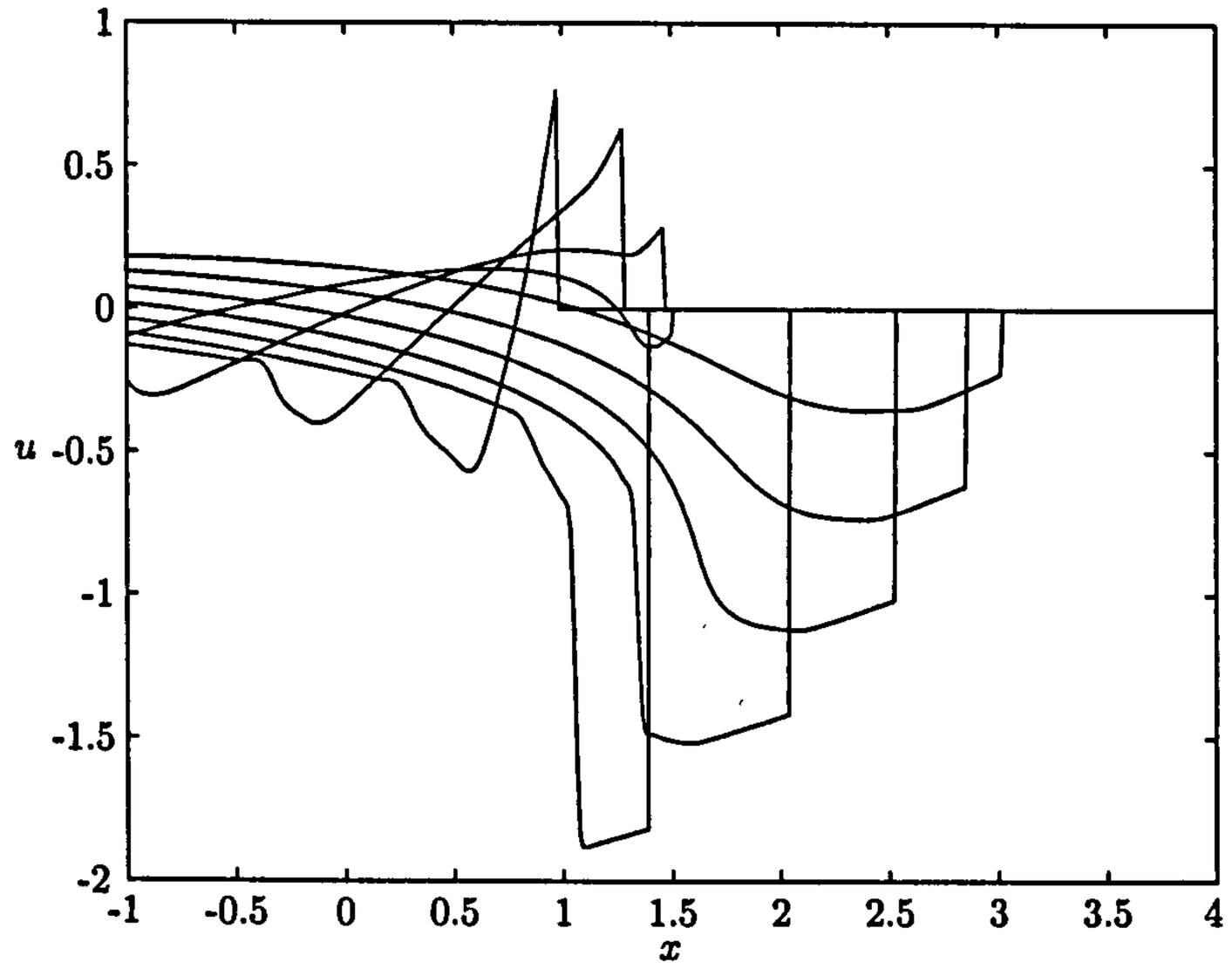

Figure 4.21: Water velocity at $t = 3.6$ to 6.8 in intervals of 0.4.

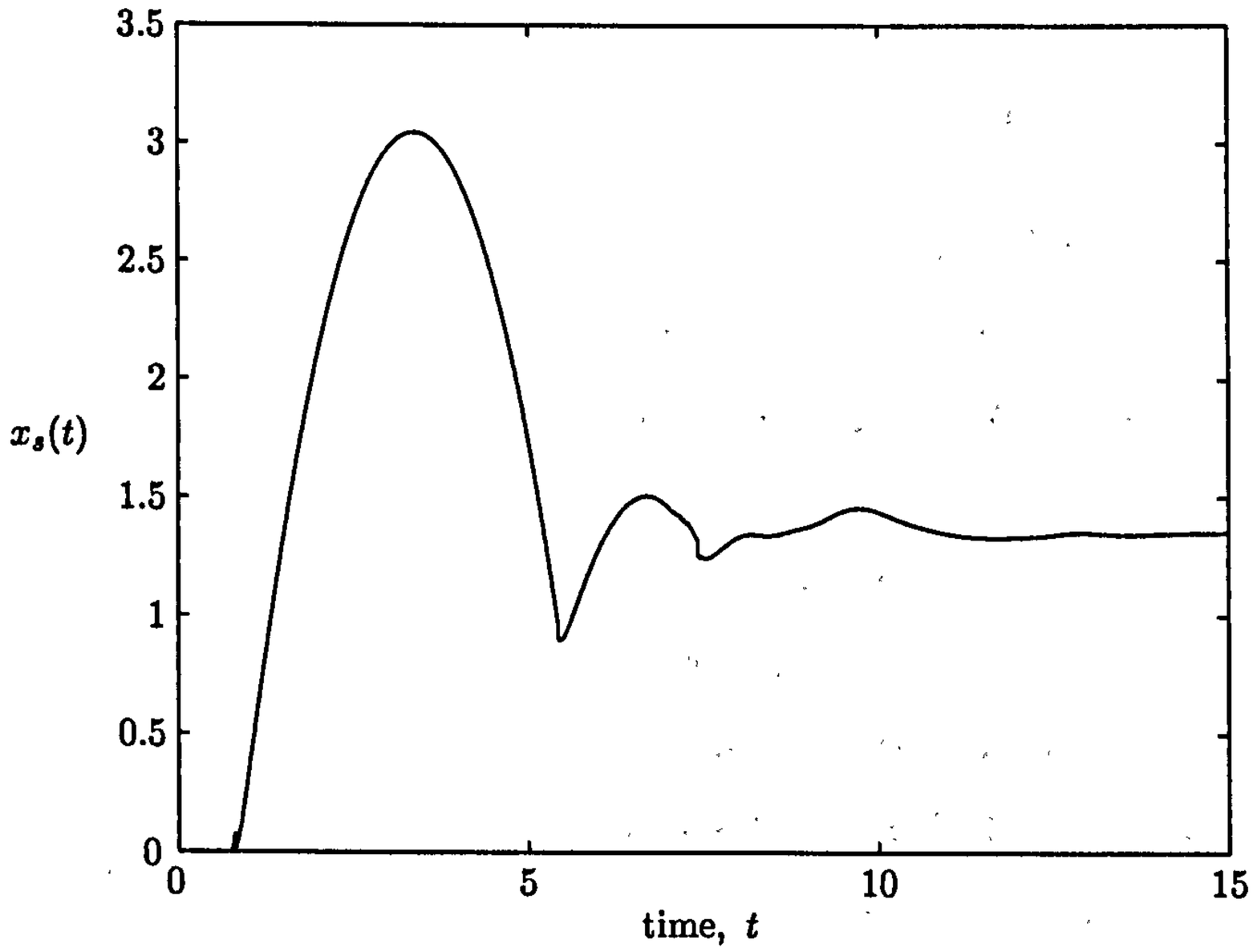

Figure 4.22: Shoreline position of a uniform bore travelling over a plane beach.

Figures 4.20 and 4.21 show what happens in the backwash mode. We can see from figure 4.20 that a landward facing bore appears in the backwash. This agrees with the findings of Shen & Meyer (1963). This is also seen in figure 4.22, which shows the shoreline position for the flow. We notice from these two figures that once the shoreline returns to its initial position, we have a depression below the new mean level. This comes from the interaction of the backwash with the bulk of water stopping its continued acceleration. The consequence of this is that a new swash event proceeds to run-up the beach. If the numerical experiment is run for a further time then eventually the water settles to a new height, which is seen in figure 4.22. This new height can be calculated from:

$$u_2 = \frac{h_3 - h_2}{h_3}\left[\frac{h_3(h_2+h_3)}{2h_2}\right]^{\frac{1}{2}}, \tag{4.5.11}$$

where h_2 is the incident bore height, u_2 is the incident water velocity and h_3 is the final water height. For the bore considered here the final height given by RUSH is $h_3 = 1.351$. Using the above expression, we find $h_3 = 1.346$. From this we see that RUSH is giving us accurate results for the case of uniform bores.

4.6 Conclusion

The numerical method used in this thesis has been introduced. The method is based on a scheme introduced by Nessyahu & Tadmor (1990). This scheme is used to solve the non-linear shallow water equations. The program RUSH has been introduced and discussed.

The main use of RUSH is to model the interactions of bores in the swash zone, this is considered in chapter 5. Results from RUSH have been compared to existing analytical solutions and the results compare well. The scheme is also tested against an existing numerical solution when the case of bores is considered. The success of these comparisons leads us to believe that the scheme and the boundary conditions are implemented correctly and thus can be used to consider more complicated examples. RUSH and RUSH-OVER are used in chapters 5 and 6 to model the run-up and overtopping of multiple swash events.

Chapter 5

The run-up of multiple swash events

5.1 Introduction

Real surface waves naturally occur in wave trains where they may interact not only with the beach, but also with neighbouring waves. There is a great deal of interest in periodic and irregular wave motion on beaches, the primary concern being the overtopping of shore structures such as seawalls and dykes (see chapter 6). Thus a natural extension to the work of Peregrine & Williams (2001) (work of chapter 3) is to consider the more realistic overtopping of multiple swash events, this is discussed in chapter 6. There exist no analytical models of multiple swash events, thus we use a numerical scheme to see how useful our solution may be (see chapter 4).

In this chapter, we introduce and discuss the numerical modelling of multiple swash events. Several different types of multiple swash are considered. Three cases are considered, the first is the case of periodic waves, where the input for each new wave event is the same i.e. bores with same amplitudes, this is given in section 5.3. Secondly periodic waves which have a random input for each new bore i.e. bores with random amplitudes are considered, this is given in section 5.4. Finally irregular waves are considered i.e. waves which are not time periodic with both random and equal input for each new wave event.

The wave inputs considered in each section are such that the nonlinearity parameter a, from equation (1.1.1) is not small. When this parameter $a << 1$, nonlinear effects are usually neglected. We also note that in all calculations the frequency dispersion parameter ϵ is small and thus shallow water theory is valid. If $a << 1$ and $\epsilon << 1$, then one would use the linearised shallow water wave equations, see Mei (1983) for further details.

The overtopping of the events considered in this chapter is then considered in chapter 6. The form of the wave inputs in this case are the same as presented here. Figure 5.1 shows a timestack taken from a real beach in Duck, North Carolina. The timestack is taken from the field experiment DELILAH (Duck Experiment on Low-frequency and Incident-band Longshore and Across-shore Hydrodynamics), the figure is taken from Holland & Holman (1993). For more information about DELILAH see Birkemeier, Hathaway, Smith, Baron & Leffler (1991). We show this timestack, so that we can see the types of waves we aim to produce in the subsequent sections. If the waves produced give similiar swash motions, then we may assume that our model included in RUSH is acceptable.

5.2 Setup of problems

In this section the way in which the boundary conditions are calculated for each different situation is discussed. These boundary conditions are implemented into RUSH and thus produce numerical simulations of the interaction of swash events.

5.2.1 Boundary conditions for multiple swash

The only boundary condition that we need to specify is the seaward boundary condition. The shoreline boundary as described in chapter 4 is the same for all inputs. The overtopping boundary condition is used in chapter 6 when we introduce the effects of overtopping.

In the work presented here we mainly consider swash generated from waves breaking near the shoreline which transform into bores. Each bore is sent in from

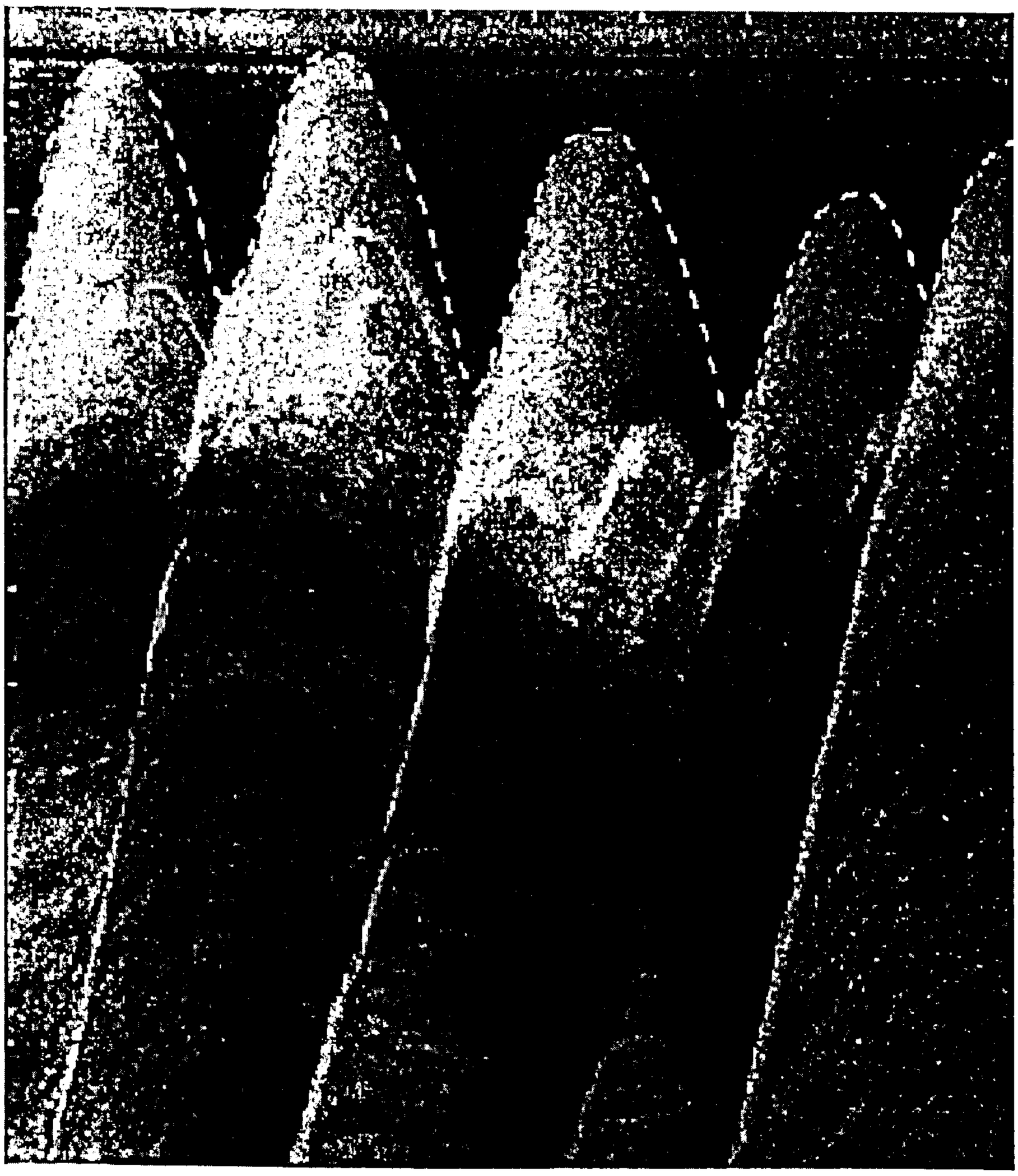

Figure 5.1: Timestack from DELILAH swash experiment, showing the cross-shore location of the run-up edge (dashed line) over time. Figure taken from Holland & Holman (1993). Time is along the horizontal axis and onshore distance is along the vertical axis.

the seaward boundary. Information is introduced at the seaward boundary through the incoming Riemann invariant $\alpha = u + 2c + t$. The form of the waves entering the computational domain is dependent on the form of α. When bores are required to be sent in from the seaward boundary, the bore conditions must be invoked to determine a value for $\alpha_0 = u + 2c$. For a given bore height h_2 travelling through water at rest of height h_1, the velocity of the bore is given by the bore conditions (Lamb (1932), Stoker (1957), Whitham (1974)). Referring back to chapter 2.2.4, the velocity behind the incoming bore is given as

$$u_2 = \frac{h_2 - h_1}{h_2} u_b, \tag{5.2.1}$$

where u_b is the velocity of the bore, given by

$$u_b = \sqrt{\frac{h_2(h_1 + h_2)}{2h_1}}. \tag{5.2.2}$$

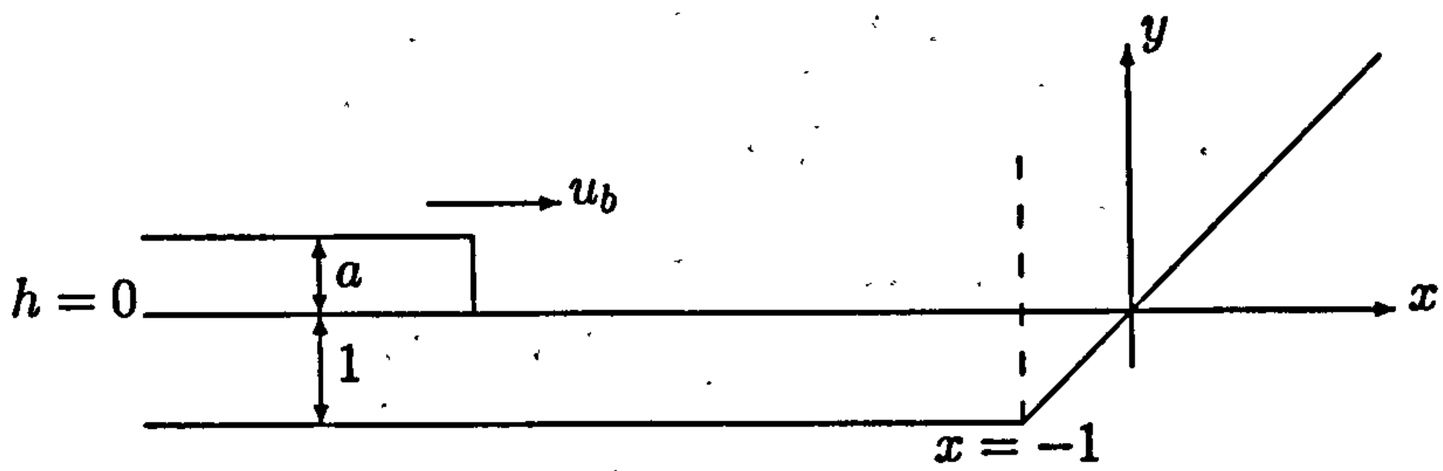

Figure 5.2: Uniform bore approaching a beach

For a bore of amplitude a travelling through still water of height 1, we find that α_0 is given by (see figure 5.2)

$$\alpha_0 = \frac{a}{a+1}\sqrt{\frac{(a+1)(a+2)}{2}} + 2\sqrt{a+1}. \tag{5.2.3}$$

At the seaward boundary, taken in the rest of this thesis to be at the point $x = -1$, we provide an expression for the form of the incoming and outgoing Riemann invariants α and β. Different approaches must be made depending on whether the flow at the boundary is subcritical (i.e. $u < c$) or supercritical (i.e. $u > c$). This results from analysing the behaviour of characteristics near the seaward boundary. As the slope of an incoming characteristic is given by $\frac{dx}{dt} = u + c$, only flows where

$u + c > 0$, are considered. Violation of this condition means the outgoing flow is supercritical and no boundary condition should be imposed. The slope of outgoing characteristics is given by $\frac{dx}{dt} = u - c$ and this changes sign according to whether the incoming flow is subcritical or supercritical.

When the flow is supercritical shorewards, both advancing and receding characteristics cross the boundary in a positive space direction. Values of both α and β need to be specified for a solution. Both characteristics arise from outside the region considered and enter the computational domain from the seaward boundary. This situation continues until a seaward facing bore is formed within the region of calculation or until a new bore enters the region. Flow through the seaward boundary then becomes subcritical and the seaward input is then determined from information selected from both the flow behind the seaward travelling bore and from within the region of calculation.

When the flow is subcritical, the slope of the outgoing characteristic is reversed, meeting the seaward boundary in the direction of decreasing x. Thus values of β on these characteristics are determined by the flow in the calculated region and only values on the incoming characteristics need be specified.

Supercritical bores rarely occur on natural beaches. In this case we must have $u > c$ which implies that at the seaward boundary

$$\frac{a}{a+1}\sqrt{\frac{(a+1)(a+2)}{2}} > \sqrt{a+1}. \tag{5.2.4}$$

Rearranging the above inequality we find

$$a^3 - 4a - 2 > 0. \tag{5.2.5}$$

The above inequality has only one real positive solution and that is $a = 2.215$. Thus a supercritical bore advancing through still water of height 1 must have an amplitude greater than 2.215. Bores with smaller amplitudes than this value are subcritical. Since the occurence of supercritical bores are rare we choose to only deal with subcritical bores here.

Since we are only dealing with subcritical waves, we model the incident waves by specifying $\alpha_0 = \alpha(-1,t) - t = u + 2c$ only. With α_0 given as a function of time

and β calculated from within the flow, expressions for u and h at the seaward boundary are found from

$$u = \frac{\alpha_0 + \beta - t}{2} \quad \text{and} \quad h = \left(\frac{\alpha_0 - \beta + t}{4}\right)^2 . \tag{5.2.6}$$

In our first case of periodic bores with equal amplitudes, results of which are in section 5.3, α_0 is given by a linear saw-tooth time profile at the seaward boundary (see figure 5.3). The maximum and minimum values of the saw-tooth are taken as 3.3 and 2.0 respectively. The first input corresponds to a bore of height 0.75 travelling through still water. We define the height of a bore here to be the height above the mean sea-level position, where the mean sea-level is at $h = 0$ (see figure 5.2). When the bore travels through the still water a new mean sea level is produced. Thus the height of the next bore entering the domain is not known, unless we know the height of the wake behind the first bore at the instant that the new bore enters the computational domain.

In this first case the time interval between each new bore is the same. Thus the bores are time periodic. A depiction of a typical height profile at the seaward boundary is given in figure 5.4. In this figure the amplitude of each new bore is calculated by measuring the length of each discontinuity in the profile. Measuring each discontinuity and taking the average, we find an estimate for the average bore height H_0 at the seaward boundary.

In the second case, we deal with time periodic bores of random amplitudes, the results of which are in section 5.4. This time the maximum and minimum values of the saw-tooth profile for α_0 are different at each time interval. The maximum and minimum values are taken from a uniform random distribution at periodic intervals. To produce this random distribution, the `rand` function of `Fortran` is used. The seed of the function is chosen as 0. This produces random numbers in the interval $[0,1]$. This interval is then extended to numbers in the interval $[a,b]$, for general a and b. This is done as follows: If we consider z_1, say, to be an element in the interval $[0,1]$ and z_2 an element in the interval $[a,b]$, then to transform elements z_1 into elements z_2, we use the transformation $z_2 = a + (b-a)z_1$.

The maximum value of α_0 is chosen to be between 2.9 and 3.7 and the min-

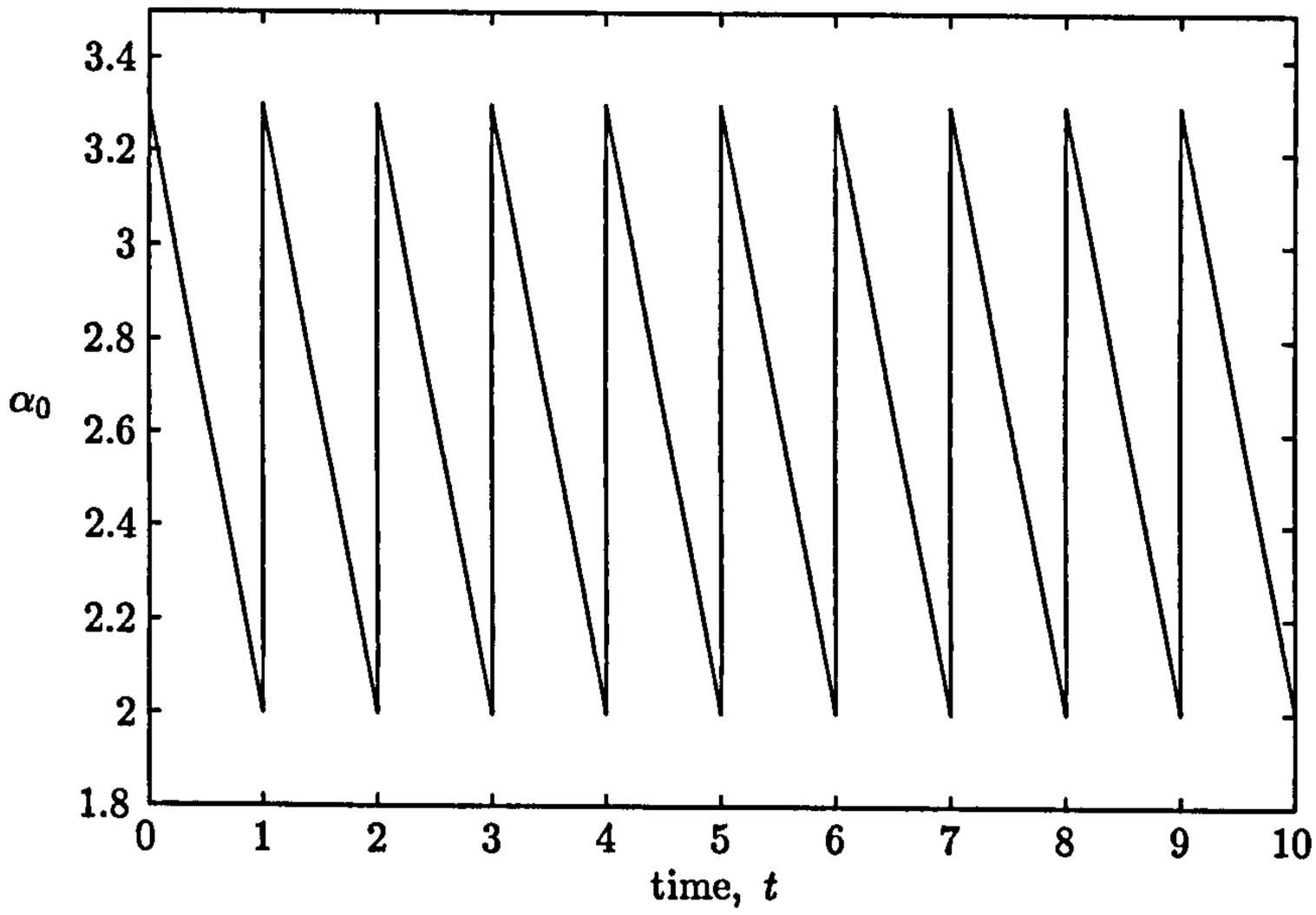

Figure 5.3: α_0 as a function of time. Case of time periodic bores of equal amplitudes.

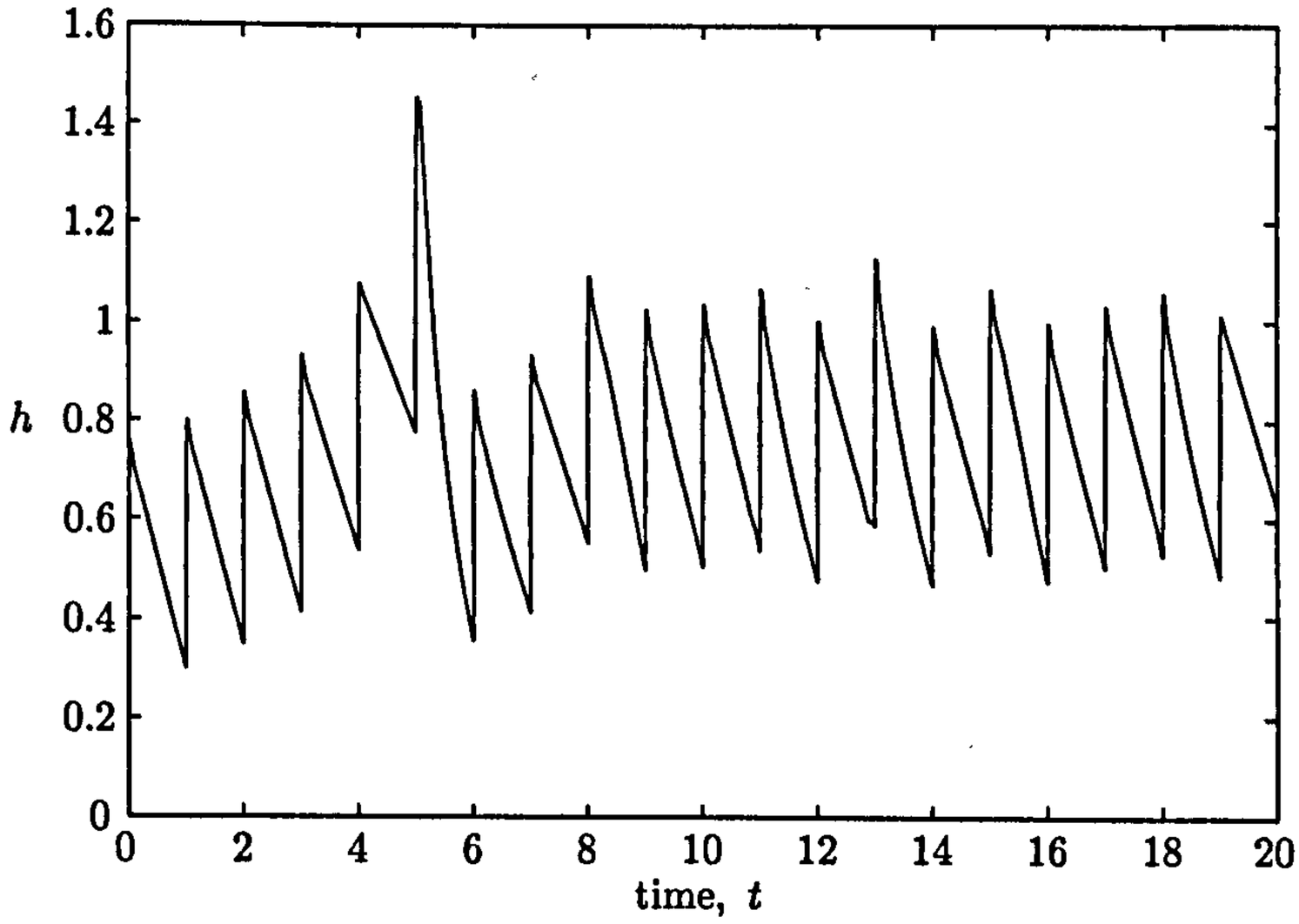

Figure 5.4: Height profile at the seaward boundary against time. Case of time periodic bores of equal amplitudes.

imum values between 1.9 and 2.1. If we were considering each bore entering still water of height 1 then these values of α_0 would correspond to bore amplitudes in the interval $[0.5, 1.0]$. Since the water level is continuously changing, the height of each new bore entering the computational domain is not known from the offset, we can only state the height of the first bore to enter the domain and calculate the height of each bore as it enters the numerical domain (as shown in figure 5.6). A typical form of α_0 in this case is given in figure 5.5. The subsequent height profile at the seaward boundary is shown in figure 5.6.

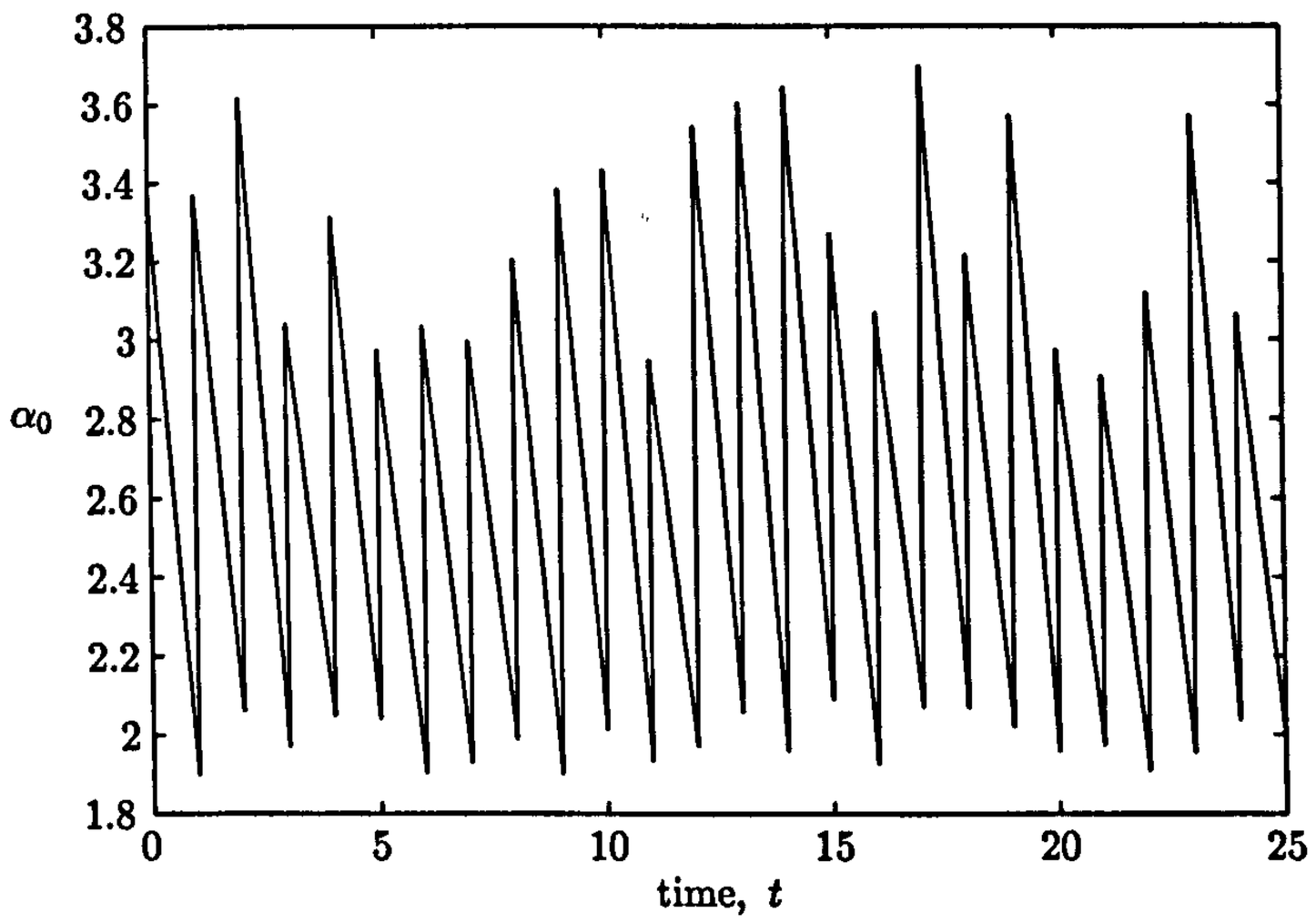

Figure 5.5: α_0 as a function of time. Case of time periodic bores of random amplitudes.

In the third case we also consider a random input for the time interval between each new bore. These times are produced in the same way as the maximum and minimum values of α_0 above i.e. they are based on a uniform random distribution. A typical form of α_0 in this case is shown in figure 5.7. Various different intervals of time are considered, details are given in section 5.5. In all the results presented the step size in space $\Delta x = 0.0125$ and the step size in time is $\Delta t = 0.00055$, this correponds to $\lambda = 0.044$.

When the time intervals between each new event become very long, a quadratic variation between crests in the saw-tooth may be more appropriate.

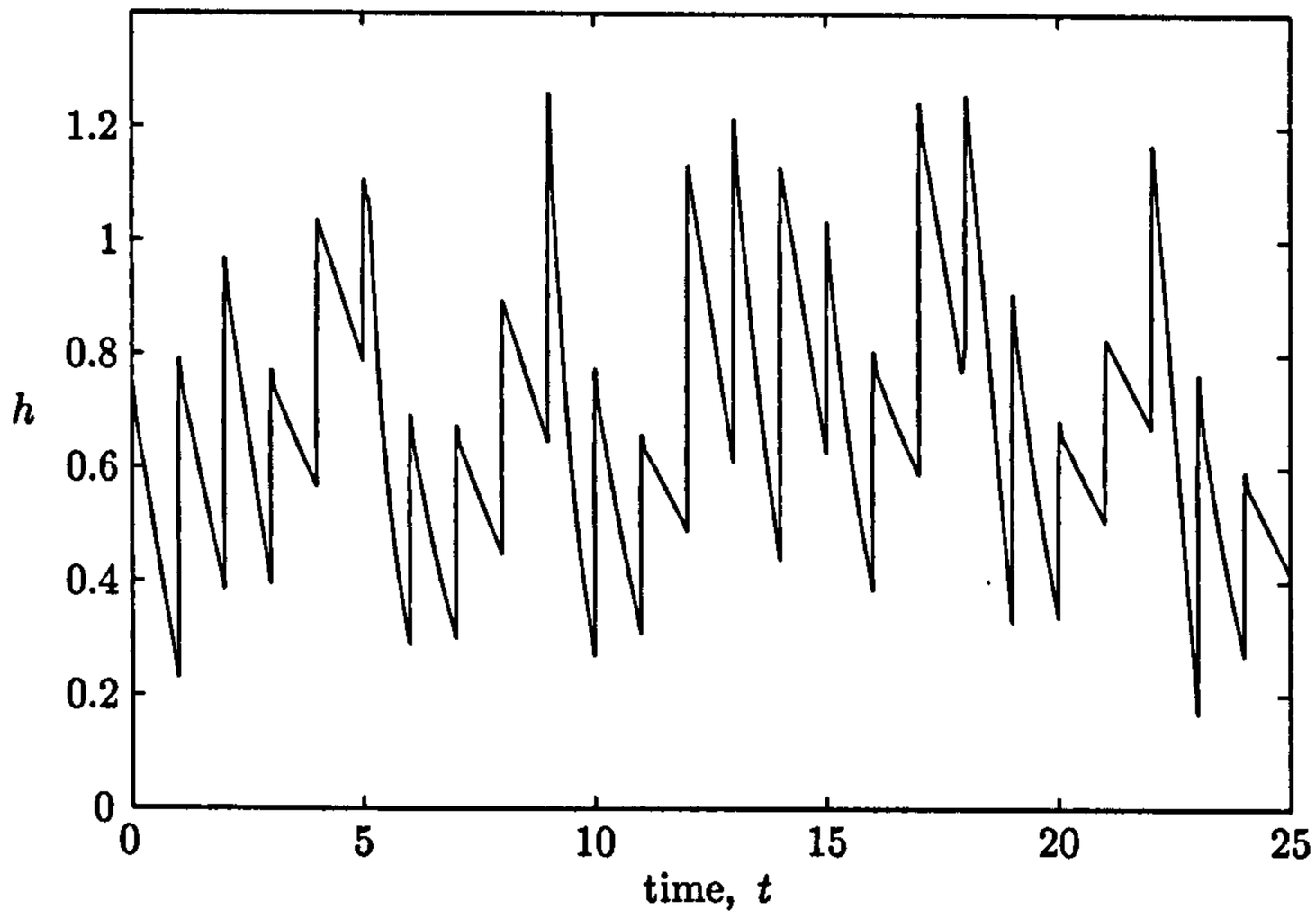

Figure 5.6: Height profile at seaward boundary against time. Case of time periodic bores of random amplitudes.

Figure 5.7: α_0 as a function of time. Case of bores of random amplitude and period.

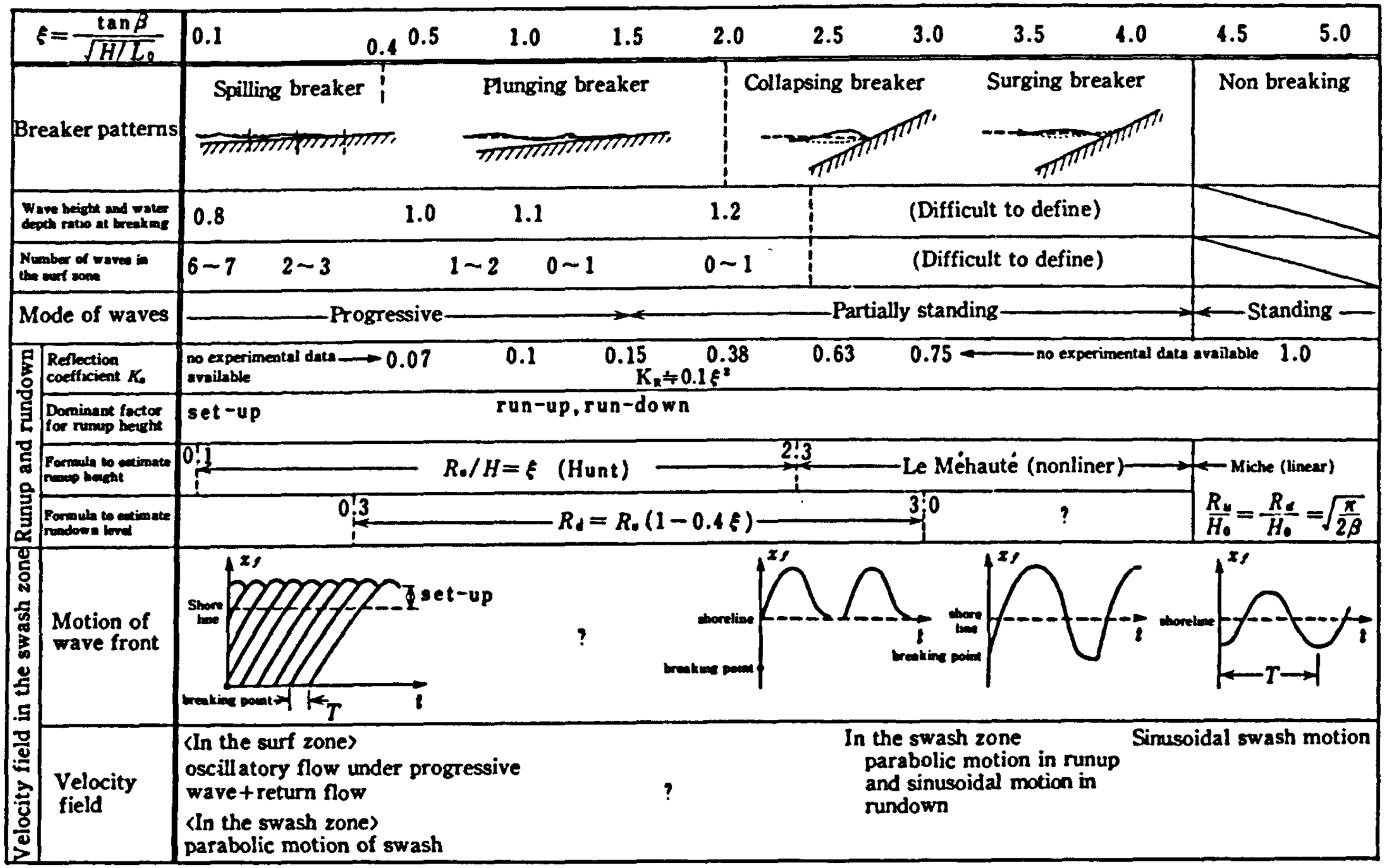

Figure 5.8: Summary of breaking and swash of regular waves. Figure taken from Horikawa(1988).

5.2.2 The Iribarren Number

The Iribarren number, or surf similarity parameter, is often used to describe wave behaviour in the surf and swash zone on a plane slope. It is defined as

$$\xi = \frac{\tan\gamma}{\sqrt{H_0/L_0}}, \tag{5.2.7}$$

where γ is the beach slope, H_0/L_0 is an offshore wave steepness. Small Iribarren numbers correspond either to swash on small beach slopes or very steep incident waves. On these slopes there is usually an appreciable interaction between successive waves. On the other hand for steep slopes or gentle waves with Iribarren number of O(1) there is little interaction between successive swashes. In sections 5.3-5.5, we highlight this by considering swash motion for various values of the Iribarren number. Figure 5.8 taken from Horikawa (1988) summarises studies on wave breaking, wave reflection, and swash motion in terms of the Iribarren number, ξ. The studies were made by Battjes (1974), Kemp & Plinston (1974), Brunn & Günbak (1976) and van Dorn (1976).

5.3 Results - Periodic bores of equal amplitudes

In this section time periodic bores are considered. Periodic bores are considered mainly as a test to see if the numerical scheme RUSH works well with the introduction of multiple bores. From the studies of Hibberd (1977) and Packwood (1980), we know how the form of the solution should look, therefore it acts as a good test. As the water is taken initially still, the solution is not wholly periodic until sufficient time has elapsed.

Input values were given by specifying a periodic form of the positive Riemann invariant α (see figure 5.3) for the advancing characteristics entering the beach through the seaward boundary. As described in section 5.2, a simple linear shape was taken at the seaward boundary, by specifying $\alpha = \alpha_0 + t$, where α_0 is altered at periodic intervals in the form of a saw-tooth, such that new incident bores of fixed prescribed height were always given. From the relation for α we cannot deduce the form of either the wave elevation or the water velocity between the occurrence

of any two successive bores a priori. In order to obtain these quantities, at the seaward boundary values of the Riemann invariant β are required; these however are determined only from within the calculation. The only bore that we know information about is the first bore to enter the computational domain. The value from the α_0 saw-tooth for the first bore is denoted by α_i. In all cases considered the value of α_i is stated.

Since we are more interested here in the interactions of multiple swash events from bores of random amplitudes, we show and discuss only three cases of periodic swash events from bores of equal amplitudes, to highlight that RUSH seems to be working well with the introduction of multiple events.

Results for three different computations are presented in this section, these computations are based on varying the forcing time period between each new bore arriving from the seaward boundary. The different cases considered are for non-dimensional periods of 1.3, 2.2 and 3.0. These examples are chosen, since they all correspond to a different range of Iribarren number. In all the cases considered, 500 waves were sent into the computational domain from the seaward boundary. The forcing time period is altered in each example. The results shown are between times $t = 0$ and $t = 25$. Computations proceed in time until a wholly periodic state evolves.

In figure 5.9 the shoreline position of the swash generated from bores with forcing period 1.3 is shown. The first incident bore travels shoreward into water at rest, setting the shoreline into motion as it reaches the dry bed. A time 1.3 later a second incident bore enters the region of computation moving landwards through the disturbance caused by the first wave. As the bore nears the shoreline it travels into the fast flowing backwash of the first wave. This backwash velocity is larger than the propagation velocity of the bore with the consequence that the bore moves seawards, although it is, of course, still landward facing. The effect of this bore is to substantially reduce the backwash velocity. A third incident bore then quickly meets the rearward travelling second bore and coalesces. The velocity of the backwash from the second bore is greater than the velocity of the third bore, thus just as the second

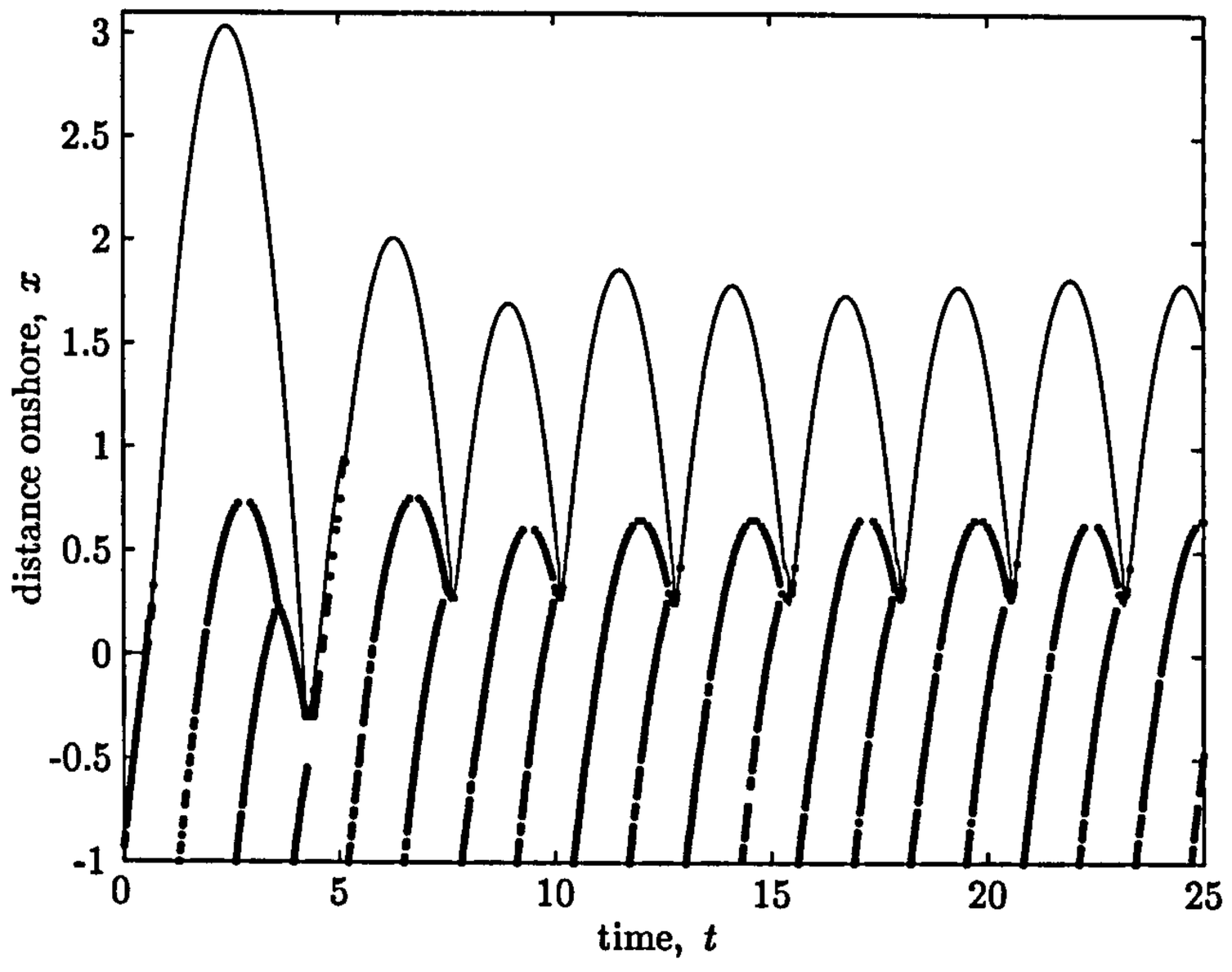

Figure 5.9: Shoreline position of swash with forcing period 1.3. Bold lines represent individual bore paths. $\alpha_i = 3.3$.

Figure 5.10: Height and velocity profiles at the seaward boundary as a function of time. Forcing is 1.3 and $\alpha_i = 3.3$. Swash from bores of equal amplitudes.

bore, the new bore moves seawards. By the time the fourth bore enters the region of computation the backwash from the first three waves is thinner, or is slowed down by the third bore, thus after coalescing the resulting combination is found to travel shorewards intersecting the shoreline and instigating a further swash event. From this point onwards every other new bore to enter the computational domain creates a new swash. Thus on average we can see from figure 5.9 that in this case, there are two waves per swash event. It is noticed that after an initial period the waves do settle down to a fully periodic solution, but at approximately the forcing period.

The form of the height and velocity at the seaward boundary is shown in figure 5.10 as a function of time. Each discontinuity in these profiles corresponds to a new bore entering the computational domain. The small peaks seen in the height profiles correspond to outgoing waves passing through the seaward boundary. We can see that these are indeed outgoing waves from the fact that the velocity at these times is negative. The outgoing waves are a consequence of the interactions between the retreating shorelines with the bores that create each new event.

To calculate the Iribarren number in this case, we need to find the average height H_0 of all waves passing into the computational domain through the seaward boundary. With this height calculated from the numerical data output, we find that in the case of forcing time period 1.3, the Iribarren number is 1.08.

We note that the run-up from the first wave is greater than the run-up from subsequent bores, which have to travel shorewards against backwash formed by previous waves. As the periodic forcing time interval between each new bore increases, the number of bores needed to create a new swash event decreases. This is due to the fact that when the period between each bore is large, the swash becomes thin and speeds up. Thus when a new bore intersects with the backwash the consequence is a new event.

To verify this, the case of forcing period 3.0 is now discussed. The shoreline position of swash generated by bores entering the computational domain at periodic intervals of 3.0 time units is given in figure 5.11.

In this case we now see that there is only one wave to each swash event as

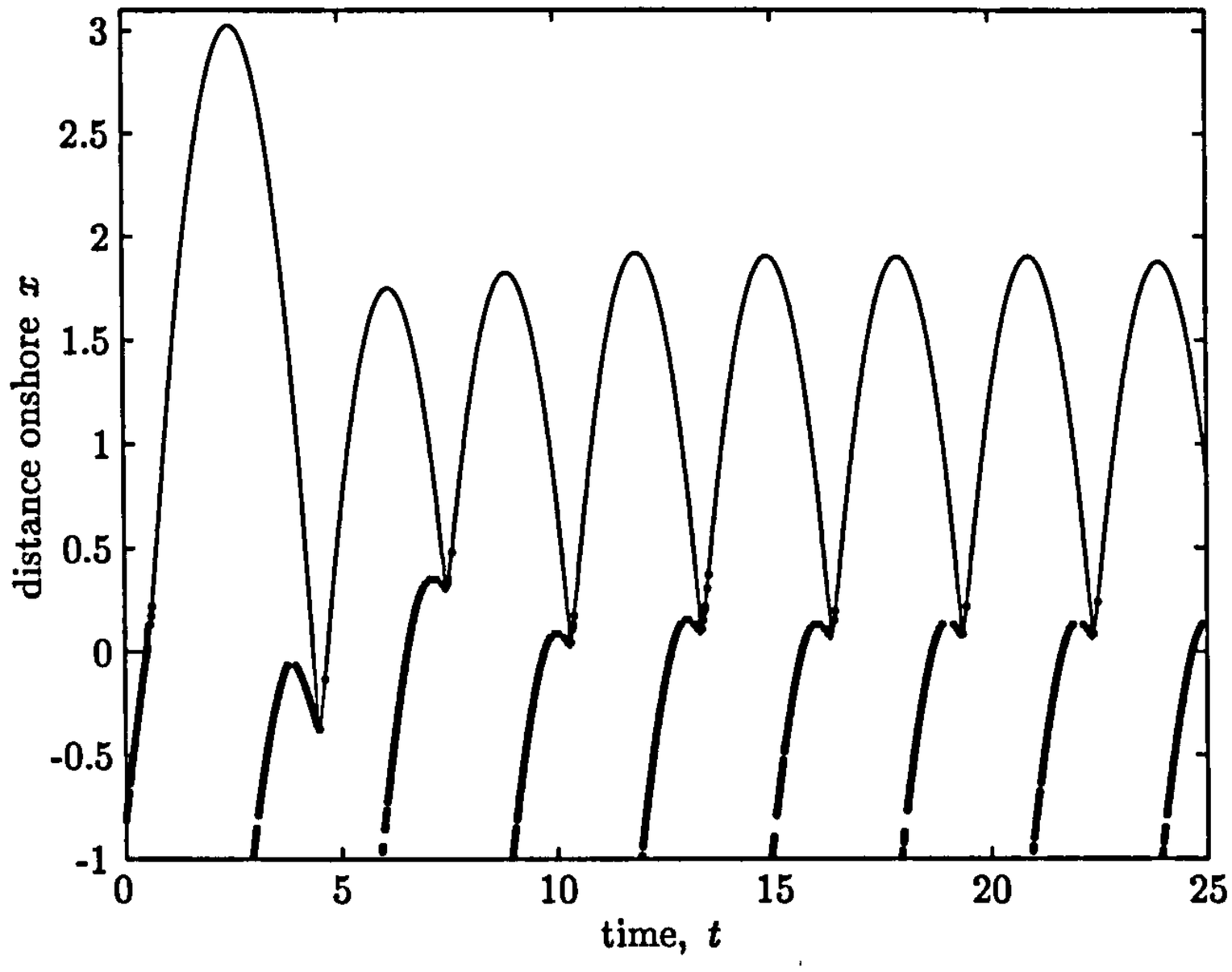

Figure 5.11: Shoreline position of swash with forcing period 3.0. $\alpha_i = 3.3$.

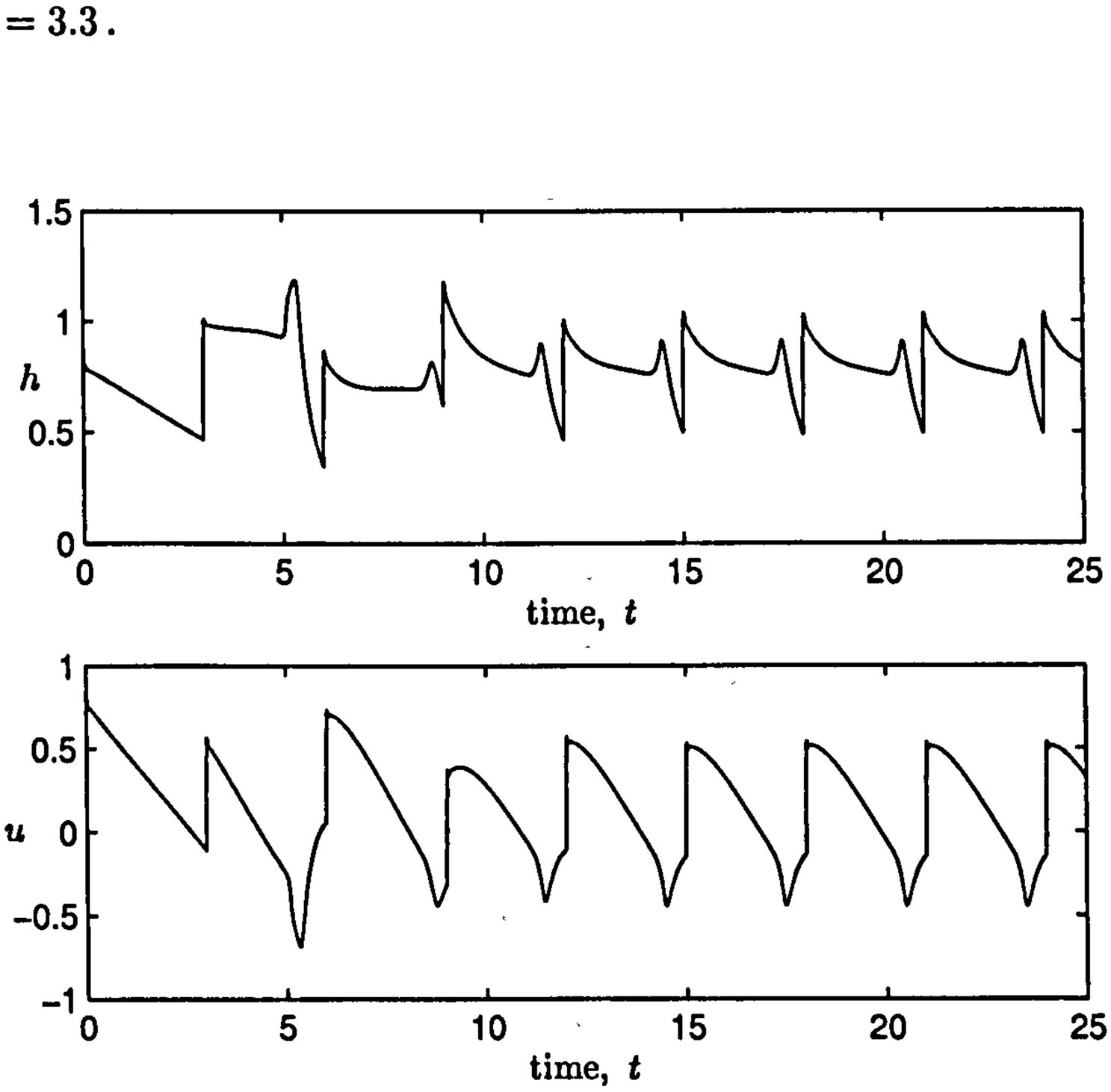

Figure 5.12: Height and velocity profiles at the seaward boundary as a function of time. Forcing is 3.0 and $\alpha_i = 3.3$. Swash from bores of equal amplitudes.

opposed to two waves per swash in the previous example. The reason that there is now only one wave per swash event is that the backwash has become thin and has speeded up, so that the incoming wave passes through it.

The height and velocity profiles of the flow at the seaward boundary are shown in figure 5.12. As in the first case, the discontinuities in the profiles correspond to new bores entering the computational domain. The small peaks again correspond to outgoing waves produced from the interactions between bore and shoreline. We see that these waves are indeed outgoing from the fact that at the time these peaks occur, the velocity is negative. Another way to see is to look at a height profile along the beach at relevant times. Height and velocity profiles at the times for which the first small peak in figure 5.12 occurs are shown in figure 5.13. We see from this figure that there is indeed an outgoing wave passing through the seaward boundary. This is highlighted by the waves given by a dashed line. One can see the presence of a left moving wave at the back of the height profile. The wave passes through the seaward boundary without interfering with the incoming flow.

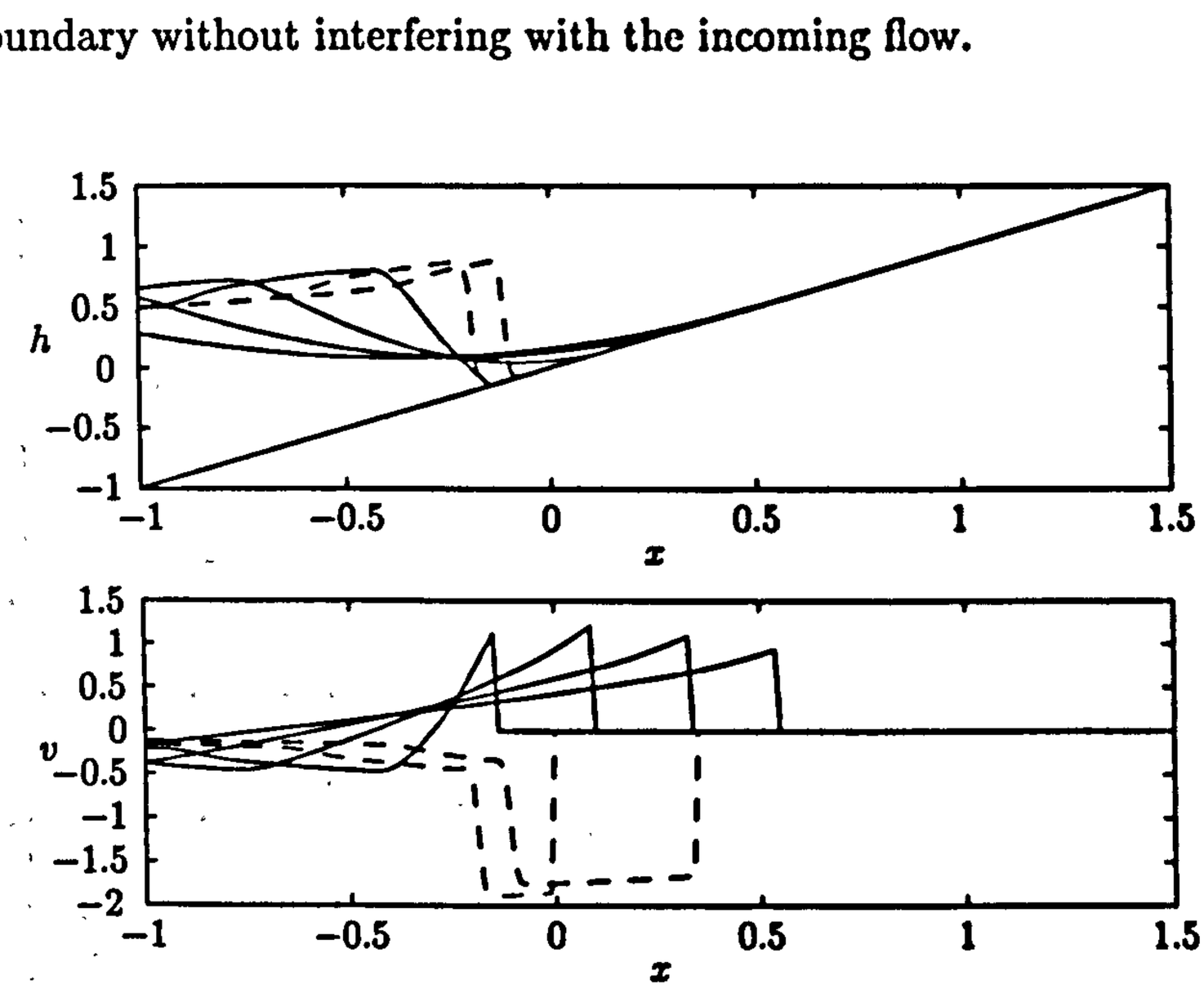

Figure 5.13: Height and velocity profiles between times $t = 4.6$ and $t = 5.6$ in intervals of 0.2. The dashed lines represent the backwash flow.

The formation of the second swash event in this case needs further investigation. We see from figure 5.11 that the second bore to enter the computational domain reaches a maximum position along the beach before the second swash is initiated. To investigate what is happening we look at the height and velocity profiles at the point where the second swash event starts. These profiles are shown in figure 5.14.

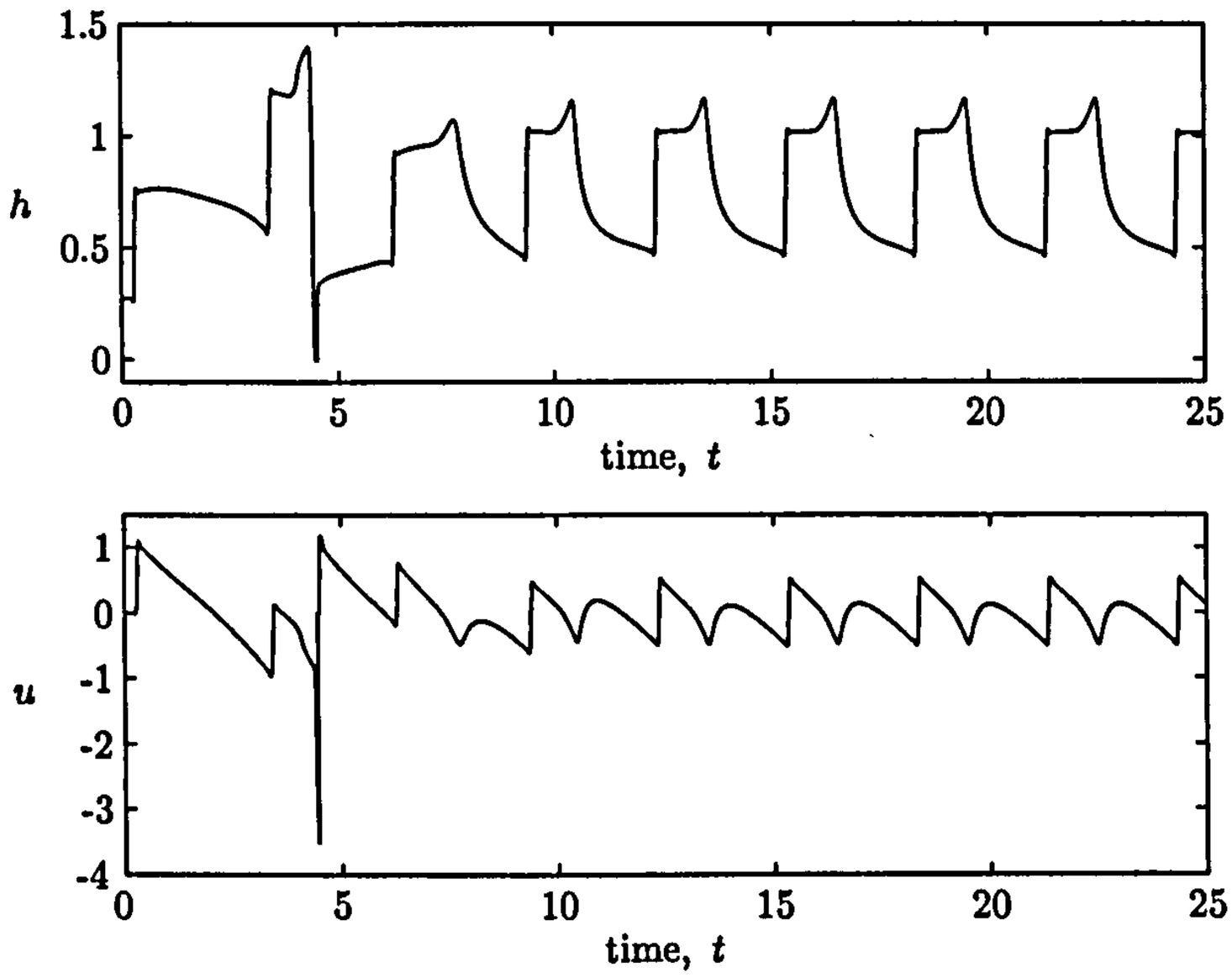

Figure 5.14: Height and velocity profiles as a function of time, at position $x = -0.425$ on the beach.

We see that at the time the second swash event is about to start, there is a very large negative velocity which instantaneously becomes positive. This velocity corresponds to the fast retreating shoreline. We know it's the shoreline since at the corresponding time in the height profile $h = 0$, which corresponds to the shoreline. The second wave to enter the domain does not pass through this backwash, it reaches its maximum then starts to travel rearward. At the same time the shoreline is moving rearward at a higher velocity, thus the shoreline catches up with the retreating second wave. The consequence of the interaction between these two is to create a new event travelling landwards. These types of bores occur frequently when the period between each new bore becomes larger. The formation of the backwash can

be seen in figure 5.13. The rightmost wave shown in 5.13 occurs when $t = 4.6$, this wave corresponds to the second bore retreating. At this point in time the shoreline is rapidly retreating, which can be seen from the velocity profiles. We see from the subsequent time profiles that this rearward travelling bore eventually starts to travel seawards without the introduction of another bore into the domain. This highlights the existence of the backwash bore. In fact we can see from figure 5.11 all subsequent swash events are created from backwash bores. As in the last case we calculate the Iribarren number for this flow. Measuring the mean height at the seaward boundary we find that the Iribarren number is $\xi = 2.496$.

Two cases have been considered. The first highlighted the effects of interactions in the swash zone, whereas the second example highlighted the effects of small interactions in the swash zone. In the first case we had on average 2 waves per swash event and in the second case one wave per swash event. We now look at a value of the forcing period inbetween the times already considered to see what the boundary is between one and two waves per swash. The case to be considered is for forcing period $t = 2.2$. The shoreline position in this case is shown in figure 5.15.

We see in this case that the run-up doesn't settle to a fixed level unlike the previous two cases. The first three swash events consist of two waves, then each new wave creates a new event. The period of response of the swash is of the same order as the forcing period. In fact it is nearly equal.

The height and velocity profiles at the seaward boundary as a function of time are shown in figure 5.16. We see from this figure that at the seaward boundary the height and velocity profiles do reach an approximately periodic state. The question now is why doesn't the shoreline motion settle to a fixed level. An obvious reason for this is not easy to find. Since we are dealing with non-linear waves there is obviously a possibility for solutions to become chaotic. There seems to be an interval on the periodic forcing time for which the run-up level doesn't settle to a fixed level. This interval is found here to be $[1.9, 2.4]$. For values outside this region all computations for run-up settled to a fixed value.

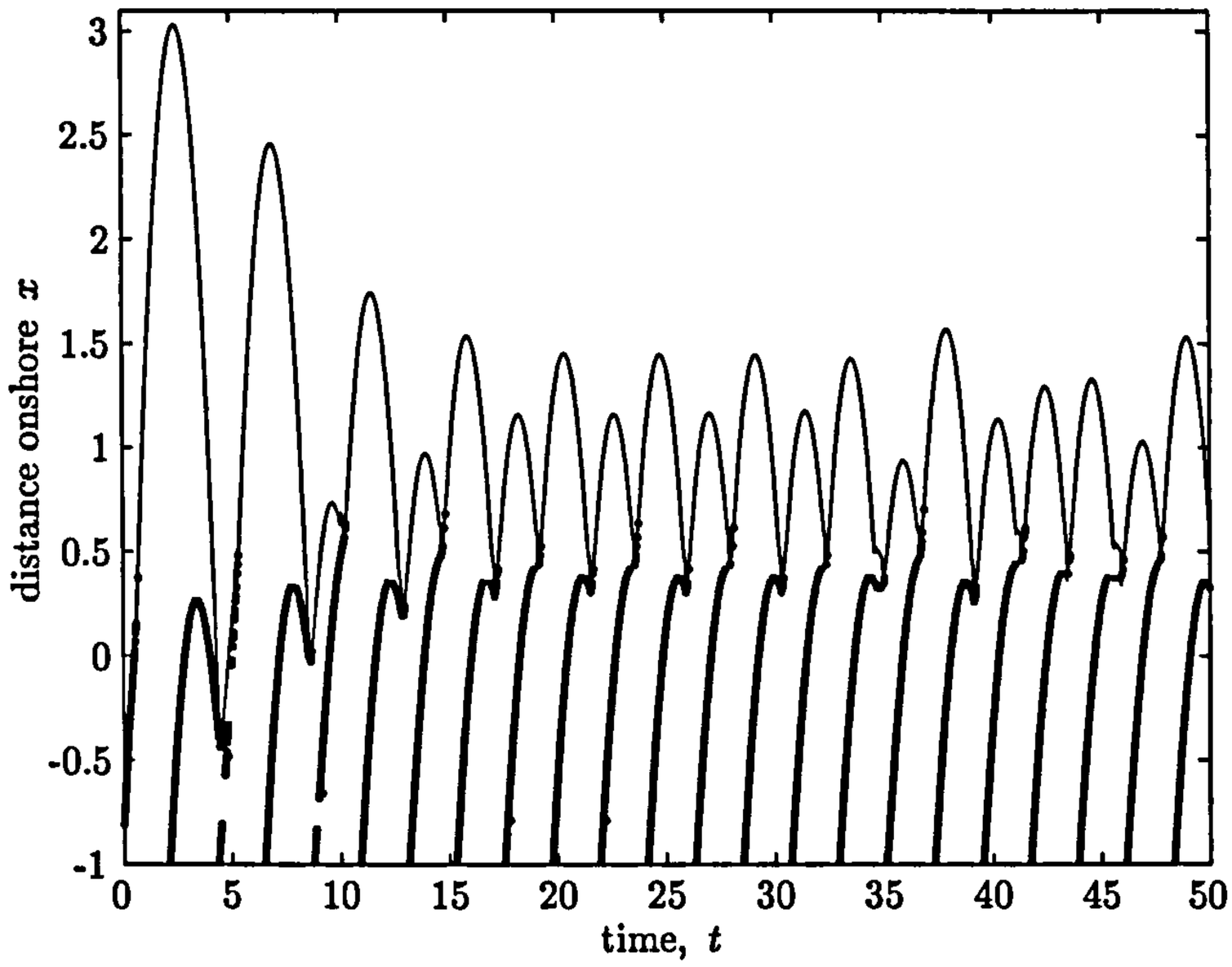

Figure 5.15: Shoreline position of swash with forcing period 2.2 . $\alpha_i = 3.3$.

Figure 5.16: Height and velocity profiles at the seaward boundary as a function of time. Forcing is 2.2 and $\alpha_i = 3.3$. Swash from bores of equal amplitudes.

The Iribarren number in this case is found to be 1.83. Computations were run for forcing period in the interval $[0.3, 4]$. The Iribarren number was calculated in each case and is presented in figure 5.17, plotted against the relative run-up height R/H_0, where R is the mean run-up position and H_0 is the mean wave height at the seaward boundary.

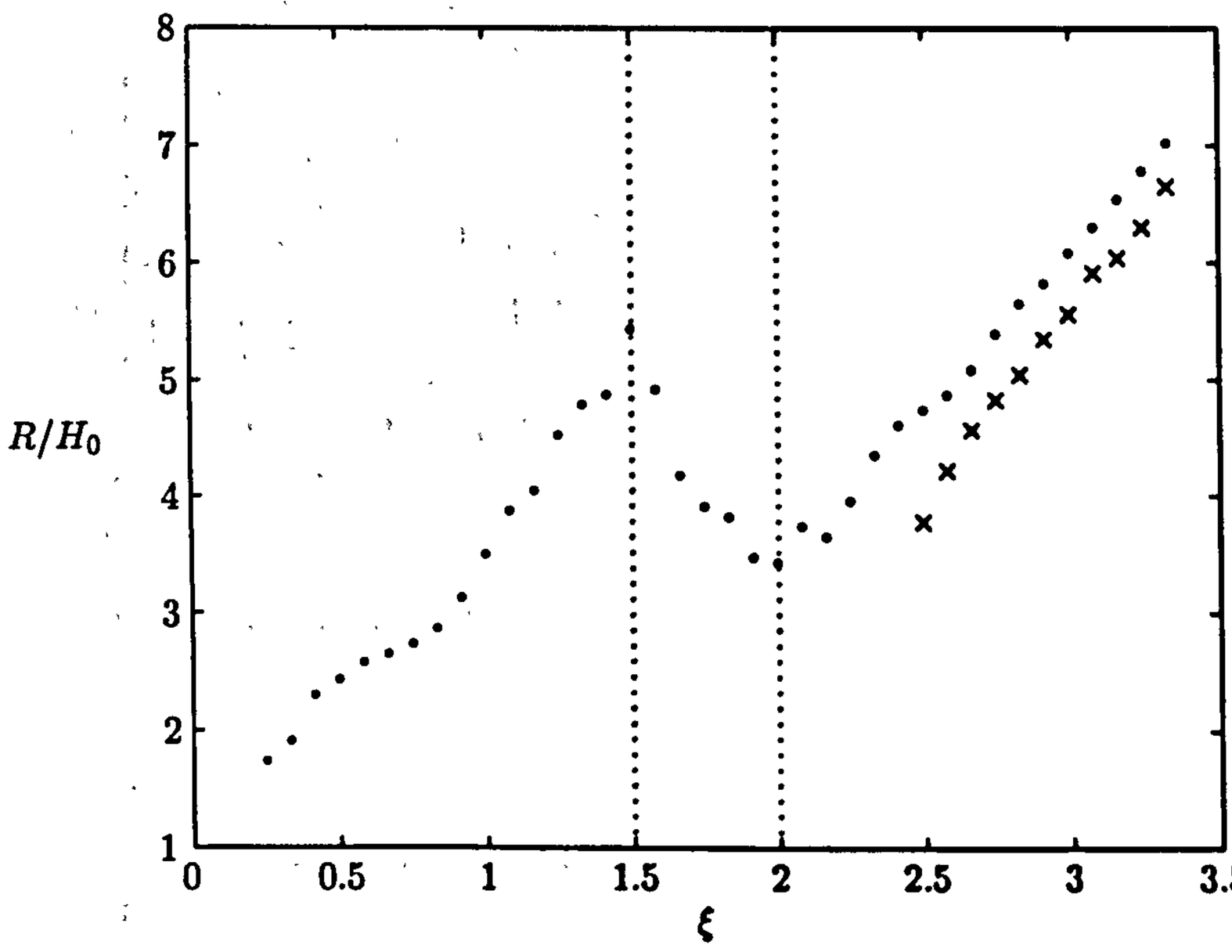

Figure 5.17: Relative wave height R/H_0 as a function of the Iribarren number ξ. Dots are for linear α_0 and crosses are for quadratic α_0

For breaking waves, Hunt (1959) empirically determined run-up as a function of beach slope, incident wave height and wave steepness on laboratory data. Hunt's formula, given in non-dimensional form (Battjes 1974), is

$$\xi = \frac{R}{H_0}, \quad \text{for} \quad 0.1 < \xi < 2.3 \tag{5.3.1}$$

for uniform smooth impermeable slopes. We see from figure 5.17, that this relationship in our case doesn't hold exactly. It can be seen that for $0.1 < \xi < 1.5$ there is a linear relationship between ξ and the relative wave run-up R/H_0. We also see that there is a linear relationship for $2 < \xi < 3.5$. Examining the computational data we find that the best line fit through both intervals of ξ have the same gradient.

The region where $1.5 < \xi < 2$ (between the dashed lines in figure 5.17) corresponds to the type of swash that we see in figure 5.15. In this region the waves do not settle to a fixed run-up height. From our data we find the relationship between ξ and R/H_0 as

$$\frac{R}{H_0} = \begin{cases} c_1 + m_1\xi & : \quad 0.1 < \xi < 1.5 \\ c_2 - m_2\xi & : \quad 1.5 < \xi < 2 \\ c_3 + m_1\xi & : \quad 2.0 < \xi < 3.5 \end{cases} \tag{5.3.2}$$

where m_1, m_2, c_1, c_2 and c_3 are determined from the computational data. Even though the results above are not exactly as those given by Hunt (1959), we see that a linear relationship can be found for both steep and gentle slopes with many or few interactions.

The average run-up period, which we shall now refer to as the period of response for a set of different computations is calculated and plotted against the Iribarren number, ξ in figure 5.18. This figure is very similar to that of figure 5.17 so we would expect to find a linear relationship between the relative wave height and the period of response. A figure of the relative wave height as a function of the period of response is given in figure 5.19. From this figure we see that there seems to be a linear relationship between the two sets of data.

As in figure 5.17 there seems to be a linear relationship between t_r and ξ for $0 < \xi < 1.5$ and for $\xi > 2$, which is seen in figure 5.18. As in figure 5.17 the region for $1.5 < \xi < 2$ seems to be a consequence of the boundary between one and two waves per swash event.

From figure 5.19 we see that the greater the relative wave height, the greater the period of response. Thus larger run-up heights correspond to swash events with longer periods.

For values of the forcing period t_f in the interval $[1, 1.9]$, there is on average two waves per swash. For values of t_f in the interval $[2.5, 4]$, there is on average one wave per swash event. Inbetween these two intervals i.e. in $(1.9, 2.5)$, there is on average 1.2 waves per swash event. It is in this last interval that the value of the relative wave height decreases as the Iribarren number increases. So one explanation for this would be that this interval is the boundary between one and two waves per

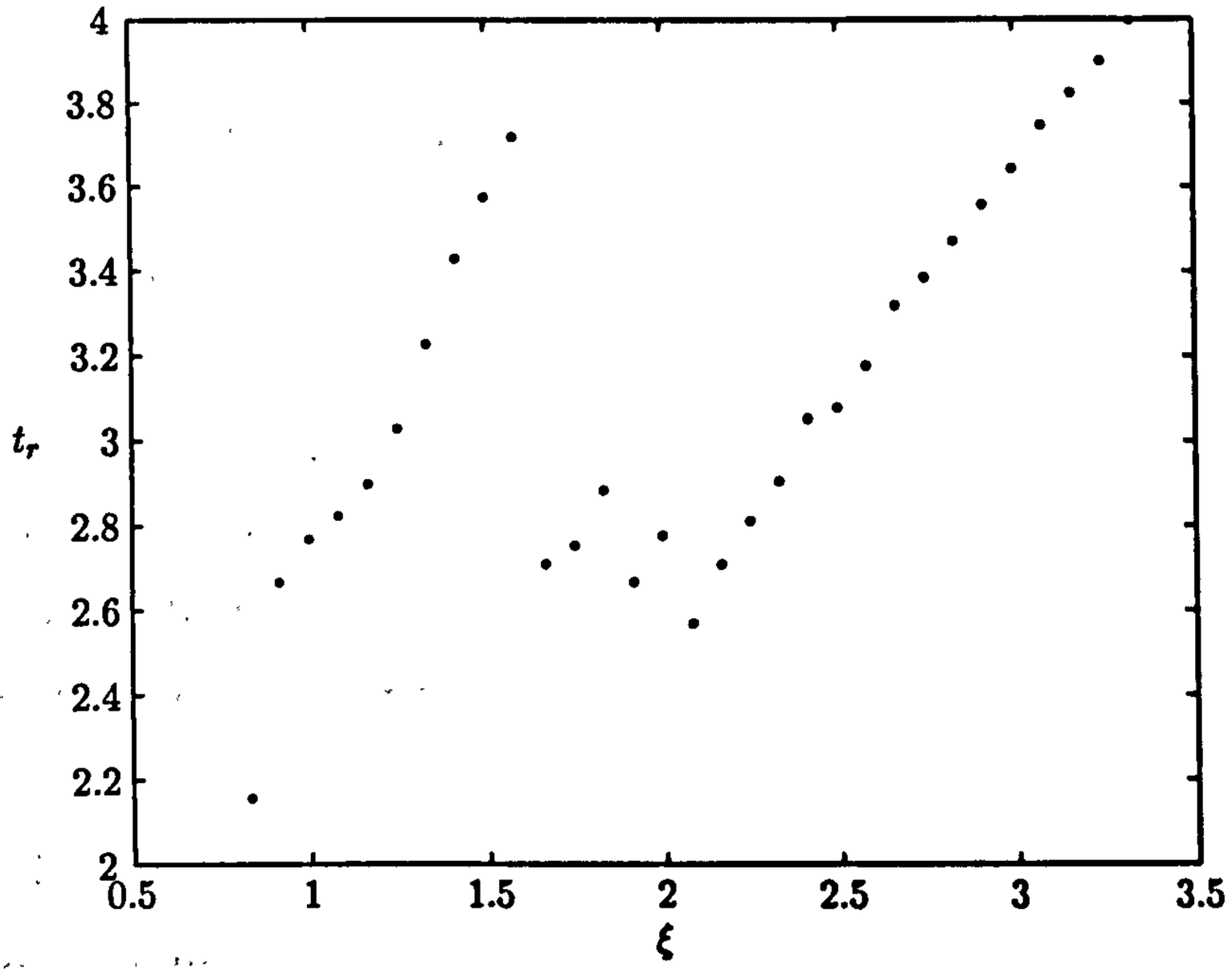

Figure 5.18: The period of response t_r against Iribarren number ξ.

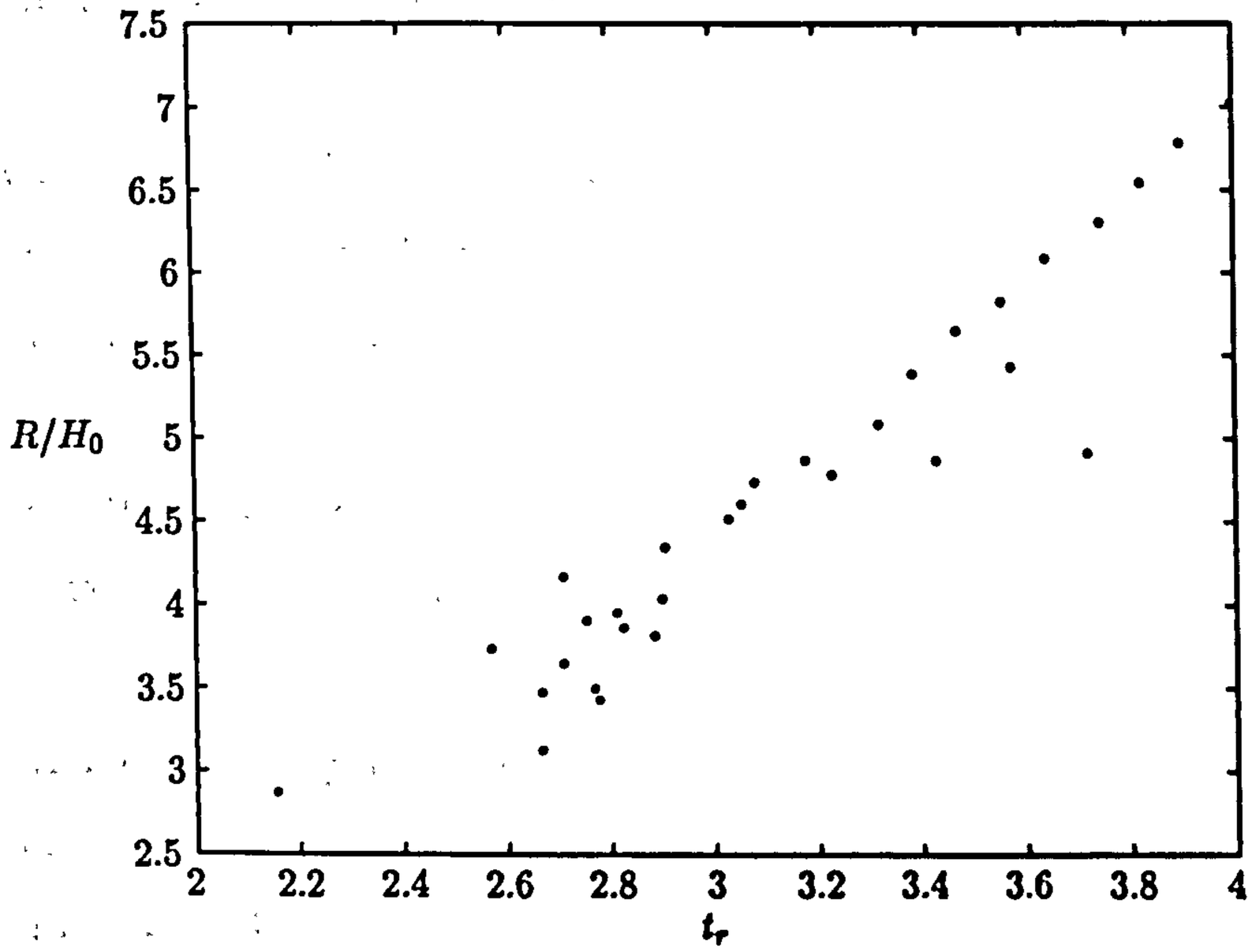

Figure 5.19: Relative wave height as a function of the period of response, t_r.

swash and so it is not surprising to find a solution of this type.

A study of the number of waves to each swash event for different wave inputs has been previously studied by Mase (1995). In this paper the frequency downshift of swash oscillations is compared to the incident waves. Different input signals are used to model the run-up of swash on beaches. Mase (1995) uses the data found by Mase (1989) for random wave run-up on gentle slopes to plot the ratio of incident waves to swash events as a function of the surf similarity parameter ξ. The same thing is done here, we plot for each considered earlier the ratio of incident waves to the number of swash events against ξ. The plot is given in figure 5.20.

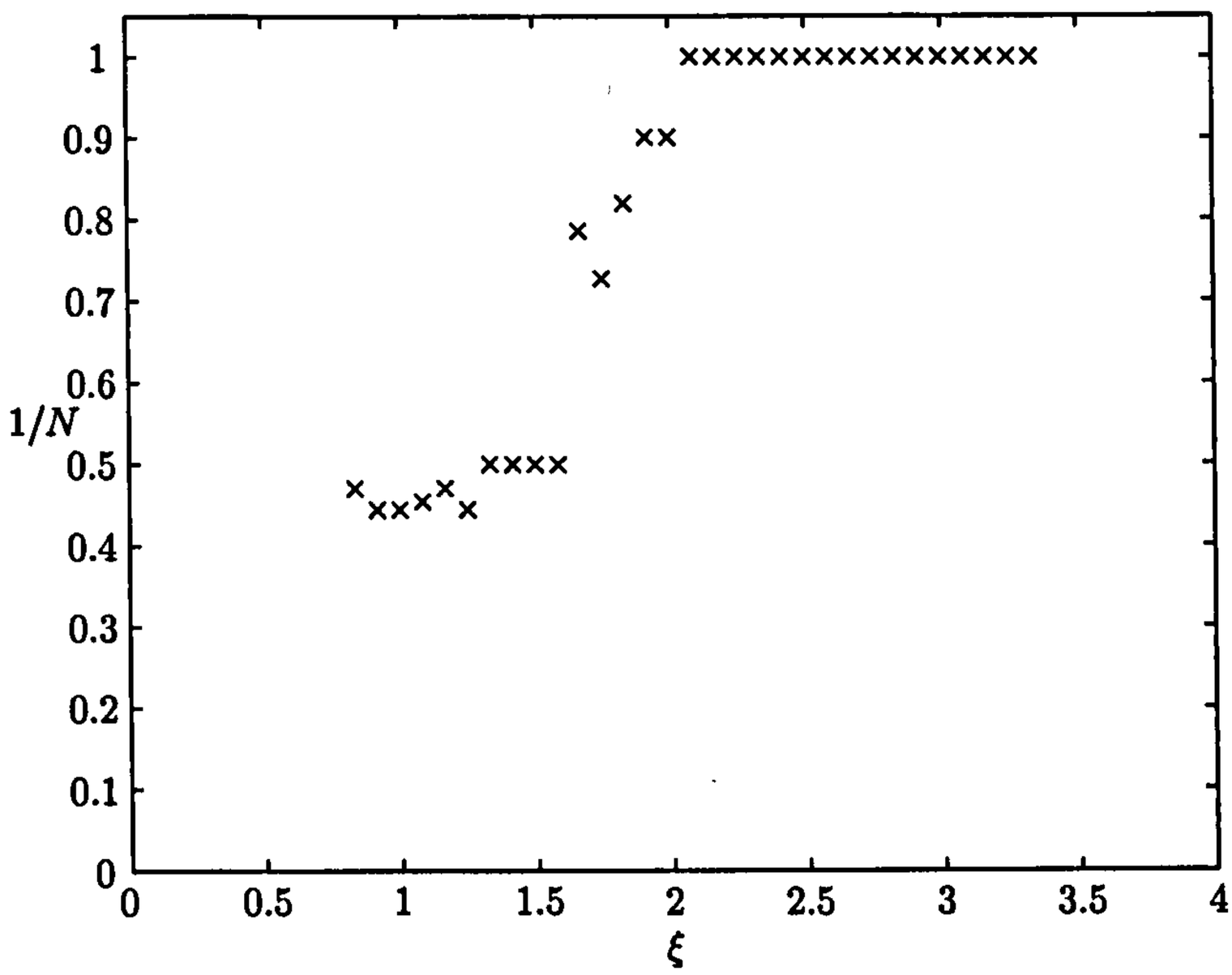

Figure 5.20: Ratio of incident waves to response waves as a function of ξ. N is defined to be the number of incident waves per swash event. Swash is from bores of equal amplitudes.

In the cases considered here we see that $\xi < 1.6$, the average number of waves per swash is two, whereas for $\xi > 2$, the average number of waves per swash is one. Figure 5.20 compares well with the results of Mase (1995), even though the results here are for periodic waves. The random case is considered in section 5.4.

5.3.1 Quadratic variation in α_0

In this section we change the form of α_0, the Riemann invariant used to describe what happens at the seaward boundary. In the previous section we used a linear saw-tooth form for α_0. Here we shall extend this to consider a quadratic form in the saw-tooth. A quadratic dependence on time after each peak is used for the waves of longer period. A figure of the type of α_0 considered is given in figure 5.21.

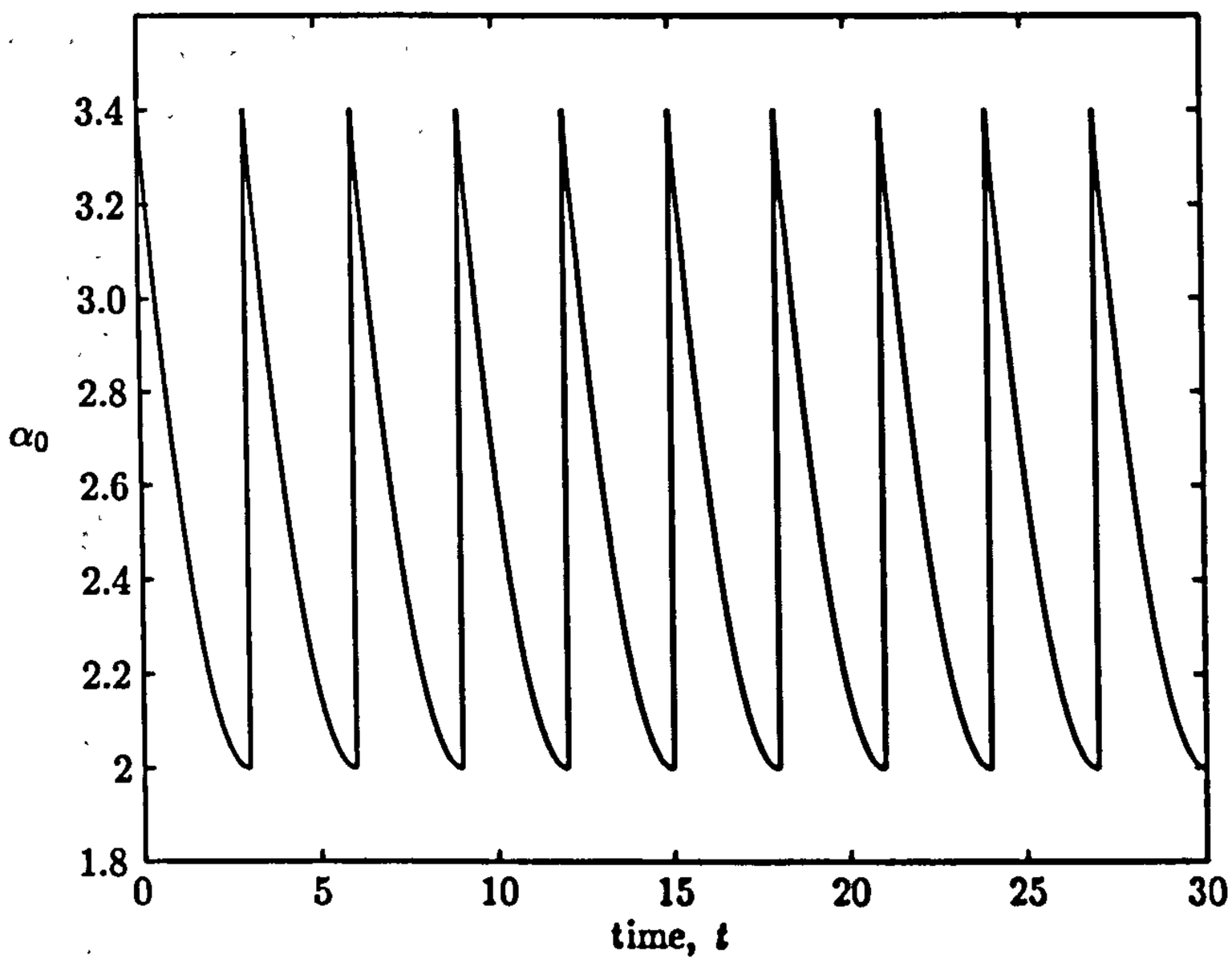

Figure 5.21: α_0 as a function of time. Quadratic variation between each new input. Case of time periodic bores of equal amplitudes.

Figure 5.22 shows the swash motion for waves of forcing period 3.0 with a quadratic variation in α_0. We see that in this case the swash events seem to be periodic, but the run-up heights of each event do not settle down to a fixed height as in the case of a linear α_0. In fact when the forcing period t_f is increased, the shoreline motion is very similar to that seen in figure 5.22.

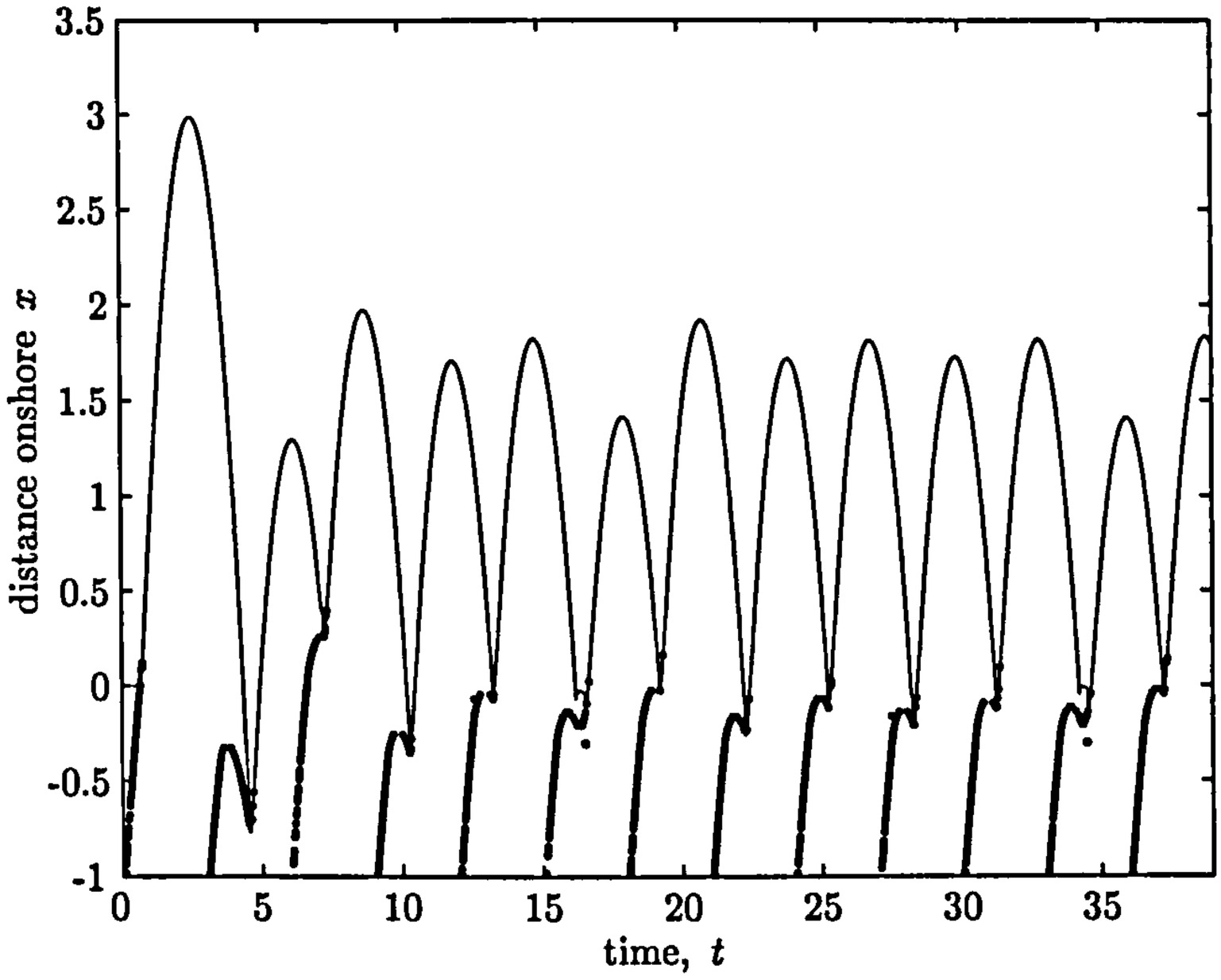

Figure 5.22: Shoreline position of swash with forcing period 3.0. Quadratic variation in α_0. $\alpha_i = 3.3$.

The Iribarren number is calculated for the forcing period t_f in the interval $[3, 4]$ and is plotted against the relative wave height in figure 5.17. We see in this case that we again have a linear relationship between the two quantities. The effect of the quadratic variation in α_0 is to decrease the relative wave height, which thus implies that the average run-up of the shoreline motion also decreases.

The height and velocity profiles of the flow at the seaward boundary are shown in figure 5.23. As in earlier cases, the discontinuities in the profiles correspond to new bores entering the computational domain. The profiles in this figure are very similar in appearance to those given in figure 5.11 with a linear saw-tooth variation in α_0. The only difference is the 'shape' of the velocity behind the shoreline.

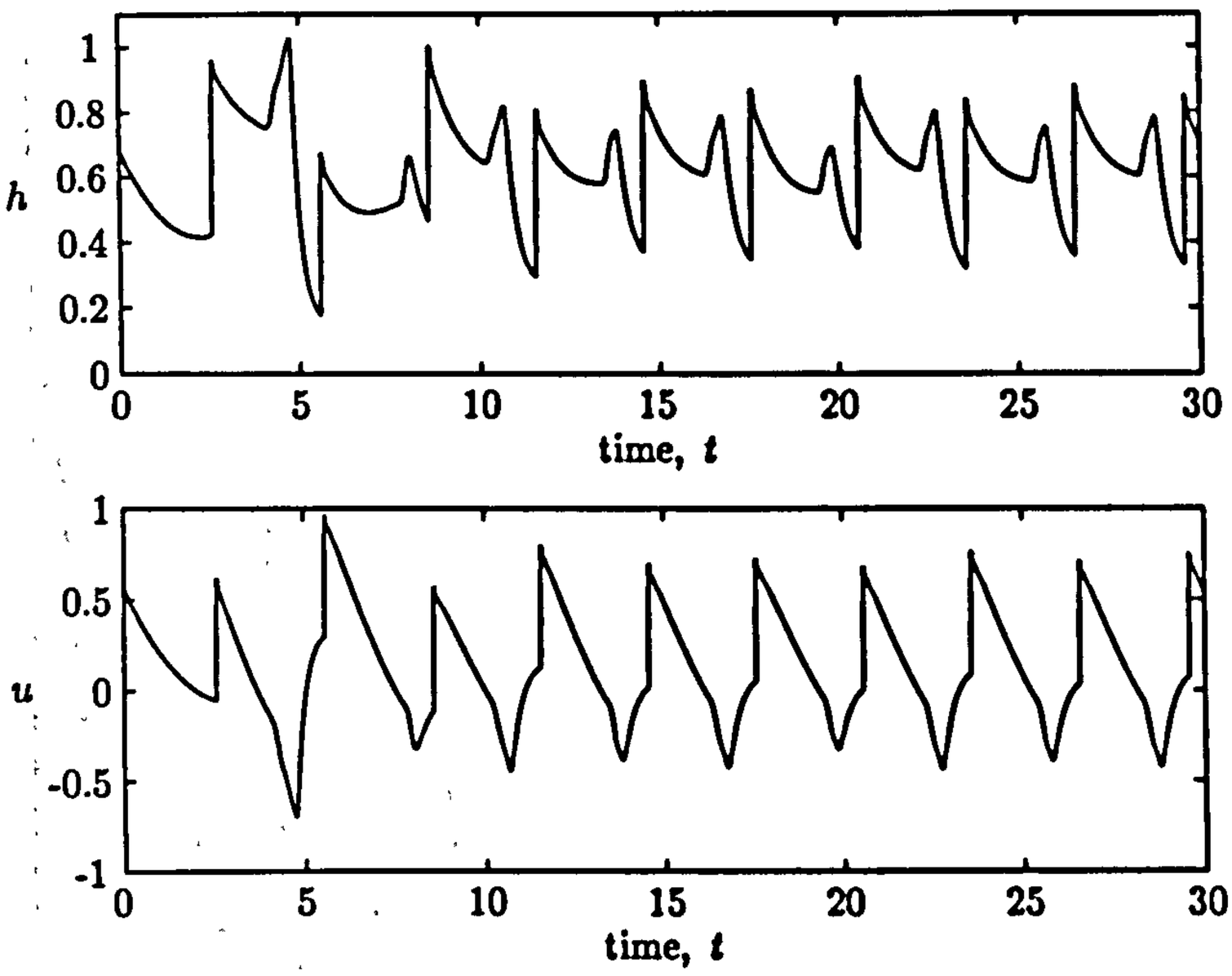

Figure 5.23: Height and velocity profiles at the seaward boundary as a function of time. Forcing period is 3.0 and $\alpha_i = 3.3$. Quadratic variation in α_0.

5.4 Results - Random, periodic bores

Periodic bores of equal amplitudes were considered and discussed section 5.3. We now consider the next natural case, which is periodic bores of random amplitudes. As in the periodic case we specify the form of the Riemann invariant α at the seaward boundary. The form of α_0 is that of a saw-tooth. In the previous section, the saw-tooth varied between a fixed maximum and minimum value. Here we set the maximum and minimum values that α_0 takes to lie in a certain interval. We choose maximum value of α_0 to lie between 2.9 and 3.7, whereas we choose the minimum value of α_0 to lie between 1.9 and 2.1. As discussed in section 5.2, the values which α_0 takes in these intervals is taken from a uniform random distribution on these intervals. A figure of the α_0 considered in this work is shown in figure 5.5.

If we were to consider each bore entering still water of height 1, then the considered values of α_0 would correspond to bore amplitudes in the interval $[0.5, 1]$.

Results for three different computations are presented in this section, these computations are based on fixing the forcing time period between each new bore arriving from the seaward boundary. The different cases considered here are for non-dimensional forcing periods of $t_f = 1.0, 2.0$ and $t_f = 4.0$. These examples are chosen, since they give a good indication of the swash motion for different time periods. Each example corresponds to a different value of the Iribarren number, for random waves it is difficult to calculate the Iribarren number, but we can say that for forcing period $t_f = 1.0$, we will have a small Iribarren number, and in the case when $t_f = 2.0$ the Iribarren will be nearing $O(1)$, and when $t_f = 4$, the Iribarren number is $O(1)$. The higher the value of the Iribarren number, the less interaction in the surf and swash zone. In the three cases considered here, the computational experiments were run until $t = 500$. The results are shown for the time interval $[0, 50]$.

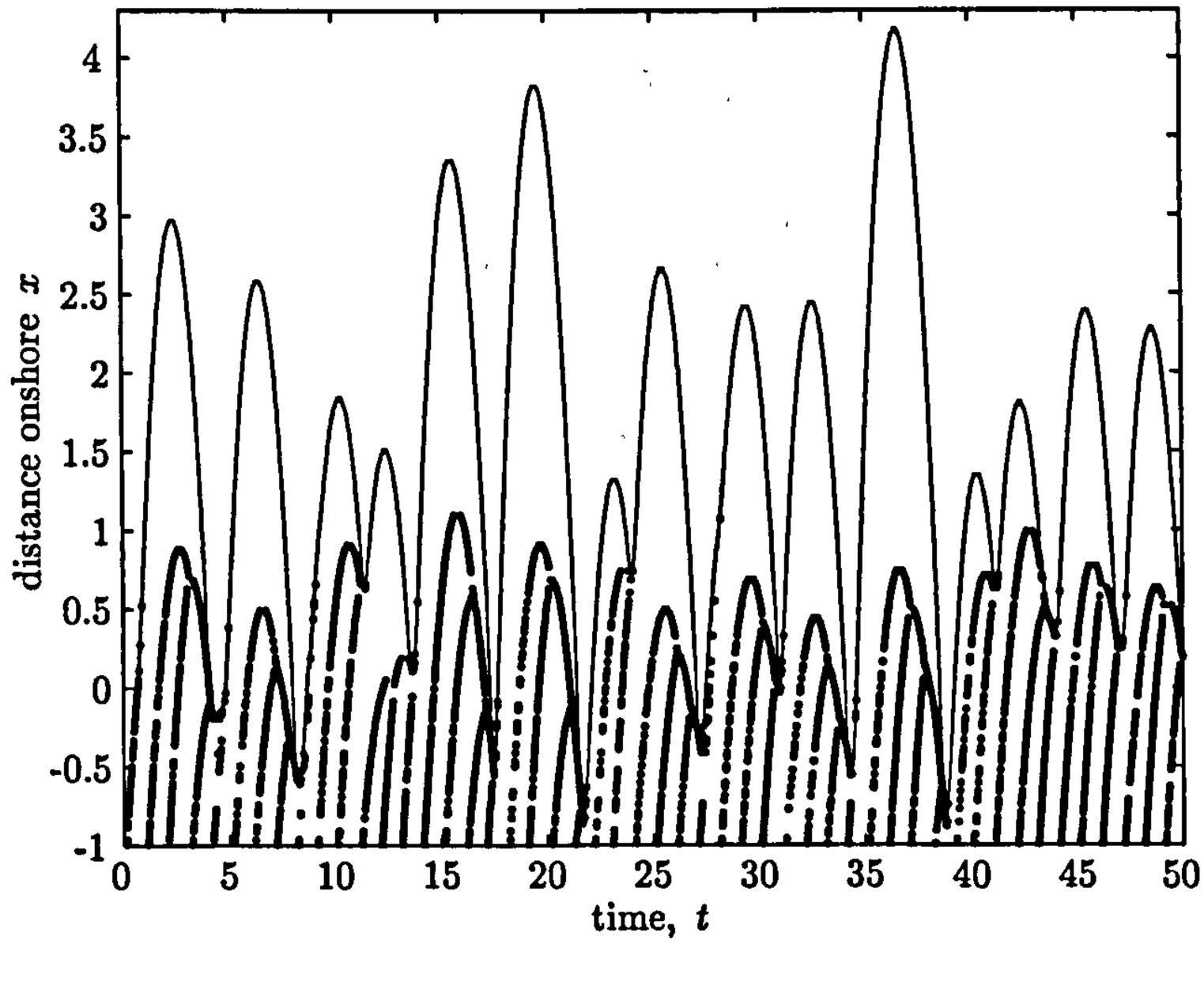

Figure 5.24: Shoreline position of random swash with forcing period 1.0. $\alpha_i = 3.3$.

In figure 5.24 the shoreline position of the swash generated by random bores with forcing period 1.0 is shown. In this case we notice that there seem to be many more waves per swash than in the cases considered earlier. This is down to the fact that since we are now considering bores with random amplitudes, we might have bores with small amplitudes being swept back by backwash from bores with large amplitudes. In the case of bores of equal amplitudes there were on average two waves per swash event. In this case the average is just over three waves per event.

Figure 5.25 shows the height and velocity profiles for the flow at the seaward boundary. As in the cases considered earlier the discontinuities in these profiles correspond to a new bore entering the computational domain through the seaward boundary. From figure 5.24 we see that for the time interval shown there is no occurence of any backwash bores. Backwash bores seem to only occur when there are less than two waves per swash event.

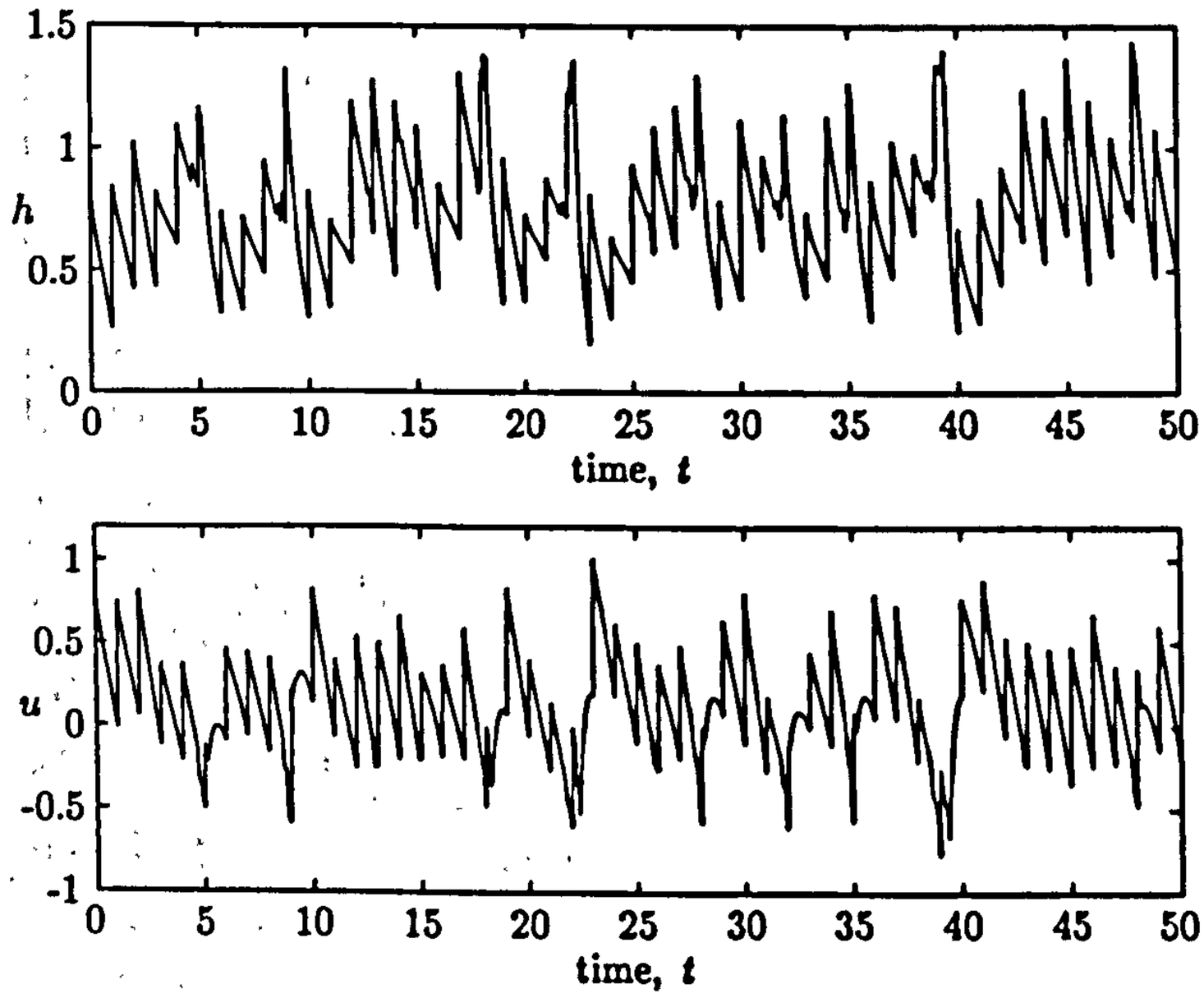

Figure 5.25: Height and velocity profiles at the seaward boundary as a function of time. Forcing period is 1.0 and $\alpha_i = 3.3$. Swash from bores of random amplitudes.

To calculate the Iribarren number in this case the average height of all the bores entering the computational domain through the seaward boundary was calculated and used. In this case the Iribarren number was found as $\xi = 0.67$. In the case of periodic waves from bores of equal amplitudes, the value of the Iribarren number for forcing period $t_f = 1.0$ was $\xi = 0.832$. The Iribarren number is smaller in the case considered here since we are now dealing with waves emanating from bores of random amplitudes. In all cases considered the average bore height calculated was found to be less than the bore heights considered earlier in section 5.3. A comparison of ξ in the case of equal and random bores is given in table 5.1. In this table, ξ_1 and ξ_2 correspond respectively to the cases of equal and random bore amplitudes.

t_f	ξ_1	ξ_2		t_f	ξ_1	ξ_2		t_f	ξ_1	ξ_2
1.0	0.832	0.670		2.0	1.664	1.349		3.0	2.496	2.023
1.1	0.915	0.742		2.1	1.747	1.416		3.1	2.579	2.090
1.2	0.998	0.809		2.2	1.830	1.484		3.2	2.662	2.158
1.3	1.081	0.877		2.3	1.913	1.551		3.3	2.745	2.225
1.4	1.165	0.944		2.4	1.996	1.618		3.4	2.828	2.293
1.5	1.248	1.010		2.5	2.080	1.686		3.5	2.911	2.360
1.6	1.331	1.079		2.6	2.163	1.753		3.6	2.995	2.430
1.7	1.414	1.146		2.7	2.246	1.821		3.7	3.078	2.495
1.8	1.497	1.214		2.8	2.329	1.890		3.8	3.161	2.563
1.9	1.581	1.280		2.9	2.412	1.956		3.9	3.244	2.630
								4.0	3.327	2.697

Table 5.1: Comparison of ξ for equal and random bore amplitudes.

We now examine the case when $t_f = 2.0$, shown in figure 5.26. For this case a new set of random data was produced, to see if any different effects would occur. In all the other cases considered so far, the first swash event is always bigger than the second, in this case that is not true. This example is shown to highlight the fact that the first event needn't always be the biggest event. In this case the second swash event is created by the third bore to enter the surf zone.

The form of the height and velocity at the seaward boundary is shown in figure 5.27. We notice from this figure and figure 5.25 that the length of the discontinuities is varying across the time interval. Each different discontinuity length corresponds

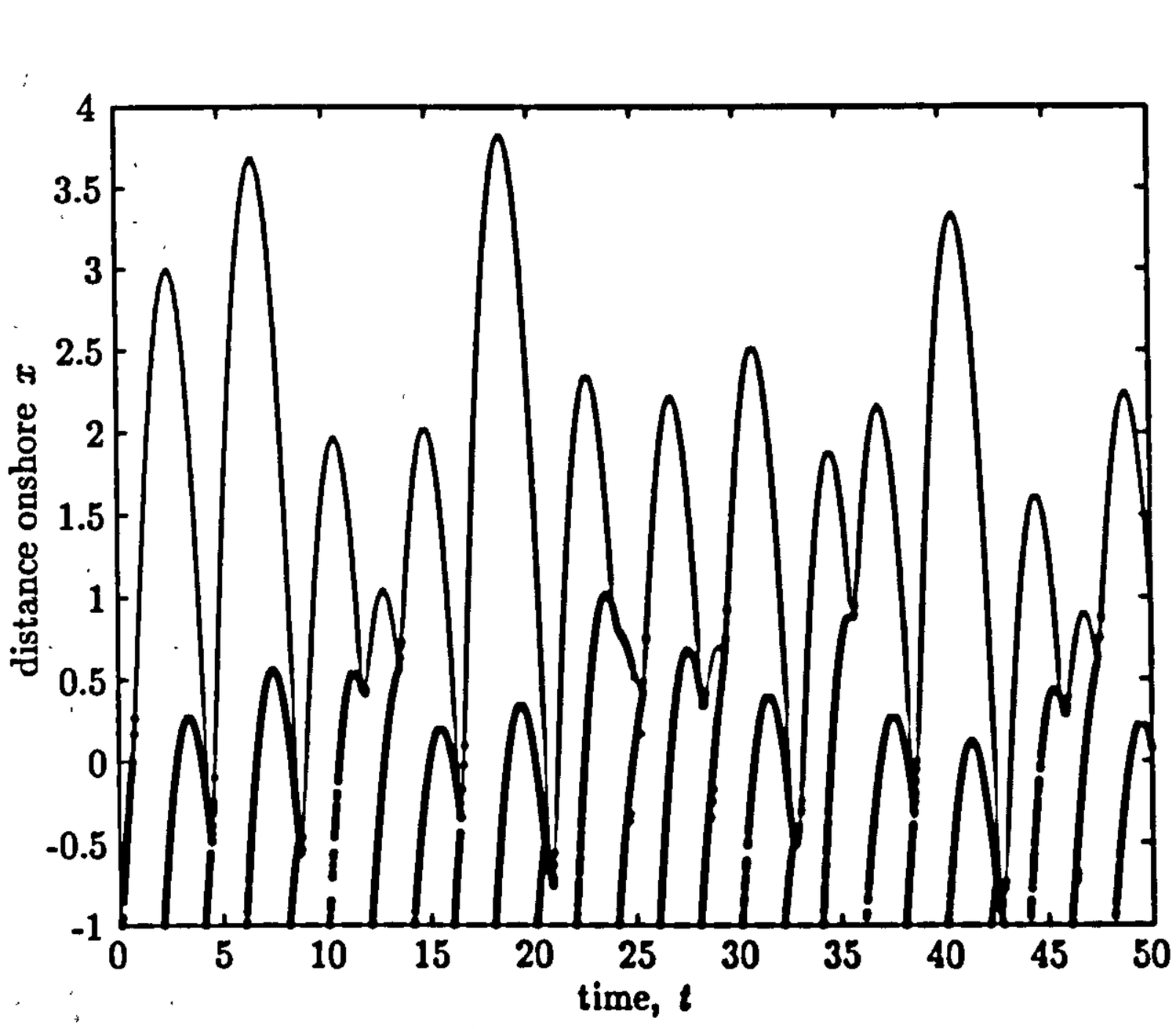

Figure 5.26: Shoreline position of random swash with forcing period 2.0. $\alpha_i = 3.3$.

to a different bore height. Measuring the lengths of these discontinuties and taking the average gives us the average wave height at the seaward boundary.

Comparing figure 5.26 with figure 5.24 we notice that there is significantly less waves to each swash event. In the case when $t_f = 1.0$, the average number of waves per swash is 3.2 and in the case of $t_f = 2.0$, the average number of waves per swash is 1.6. As the value of t_f increases the average number of waves per swash tends to one. We shall consider a case when this is true.

Our final example is forcing period $t_f = 4.0$. The shoreline motion for this case is shown in figure 5.28. We see in this case that there are relatively no interactions between swash events, and that every new bore to enter the surf zone, creates a new swash event i.e. one wave per swash. The height and velocity in this case aren't of any interset, since all events are practically independent. When this is true, we can say that the swash events can easily be modelled using the method of Shen & Meyer (1963) for motion of a single swash event up a plane beach (See also chapters 2 and 3 for details).

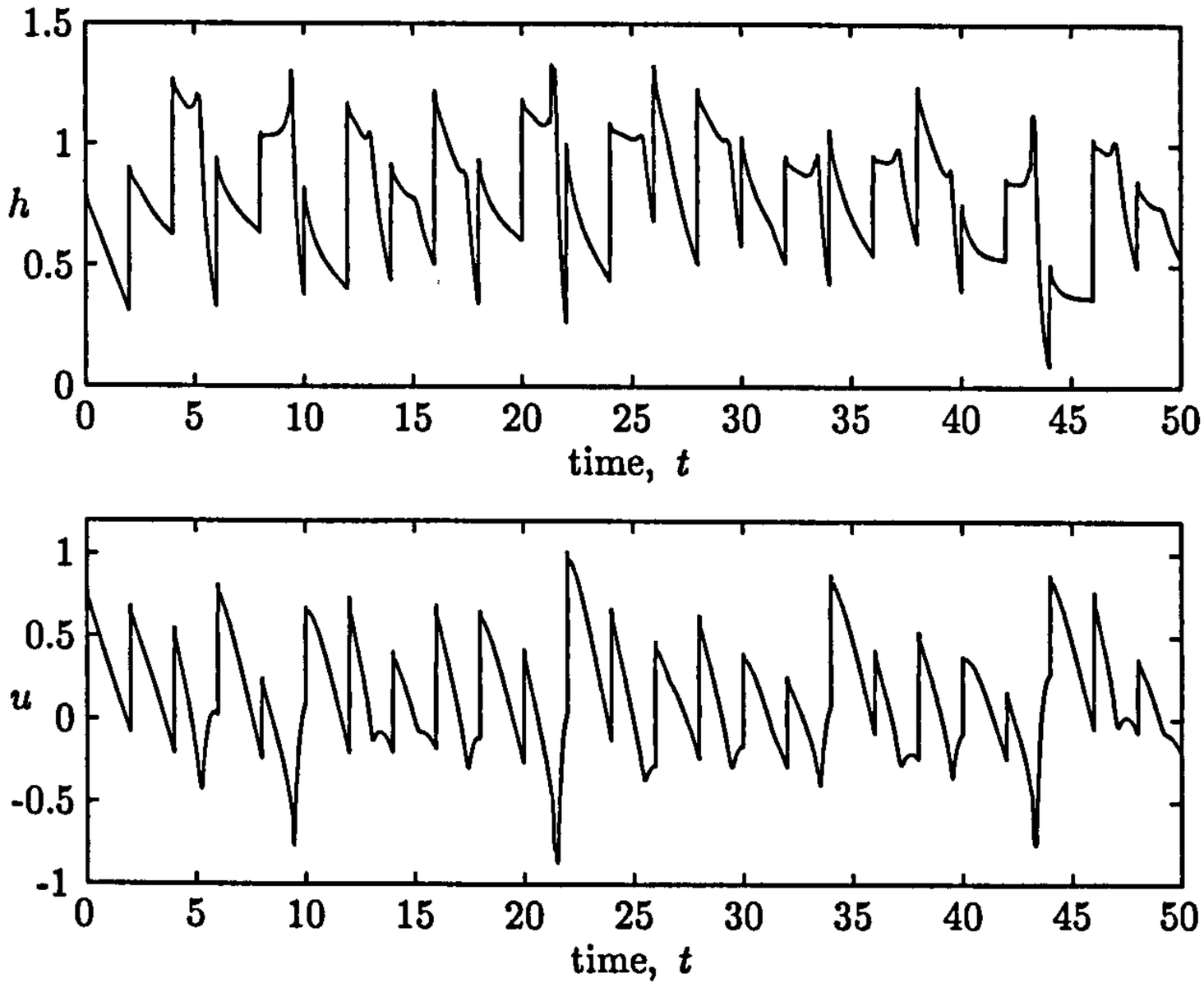

Figure 5.27: Height and velocity profiles at the seaward boundary as a function of time. Forcing period is 2.0 and $\alpha_i = 3.3$. Swash from bores of random amplitudes.

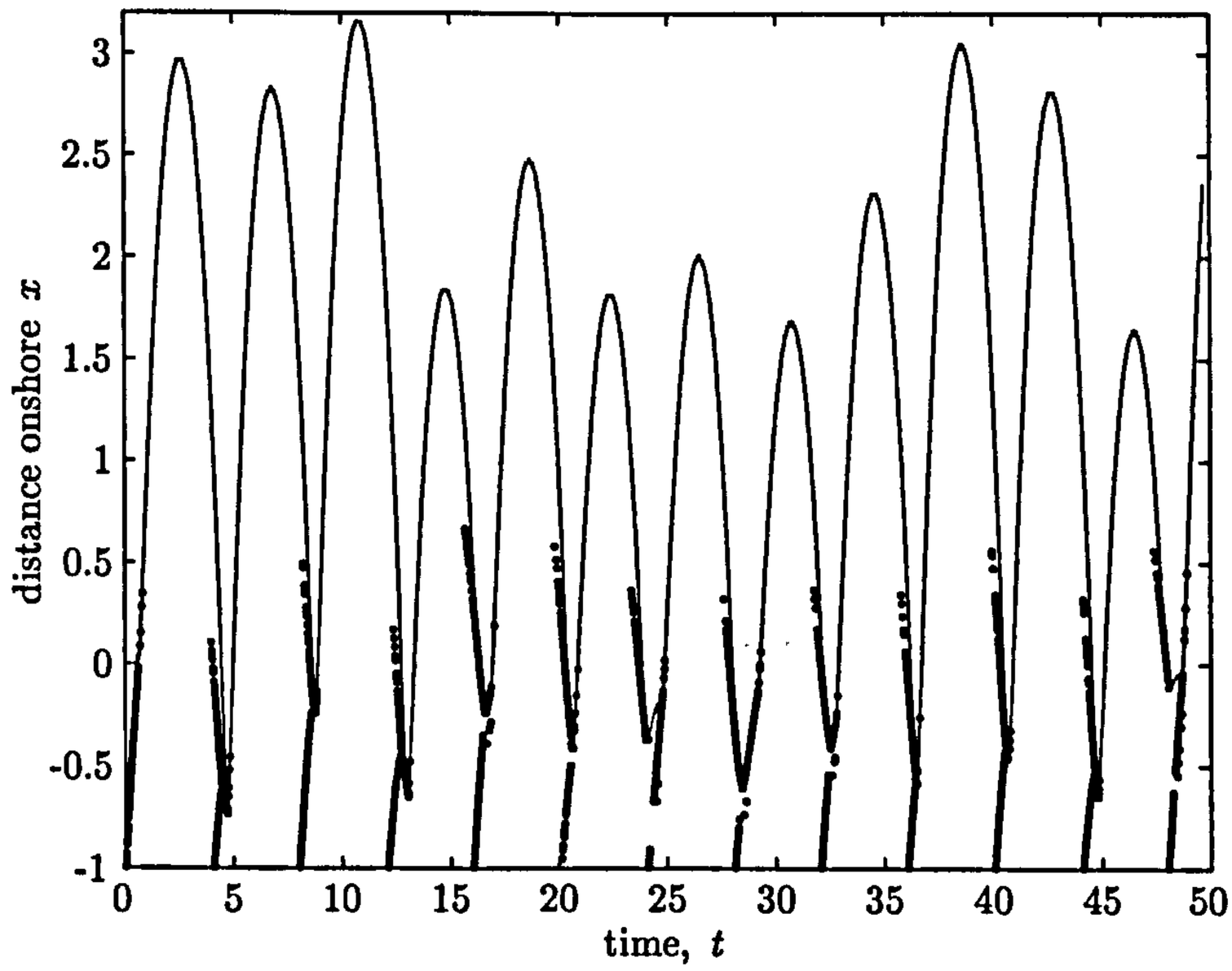

Figure 5.28: Shoreline position of random swash with forcing period 4.0. $\alpha_i = 3.3$.

As in the previous section we want to have a figure of relative wave height against the Iribarren number ξ. Computations were run for forcing period in the interval $[1.0, 4.0]$. The average run-up height was calculated in each case, along with the mean wave height at the seaward boundary. Using this information figure 5.29 was produced to see how the relative wave height relates to the Iribarren number. We have already seen that a linear relationship was found in the case of equal bore amplitudes, although there were two different linear relationships. The first was for when there were two waves per swash event, and the second relationship was for when there was one wave per swash event. Inbetween this criteria a different relationship was found. The first relationship corresponds to swash on small beach slopes. Whereas the second relationship corresponds to swash on steep slopes.

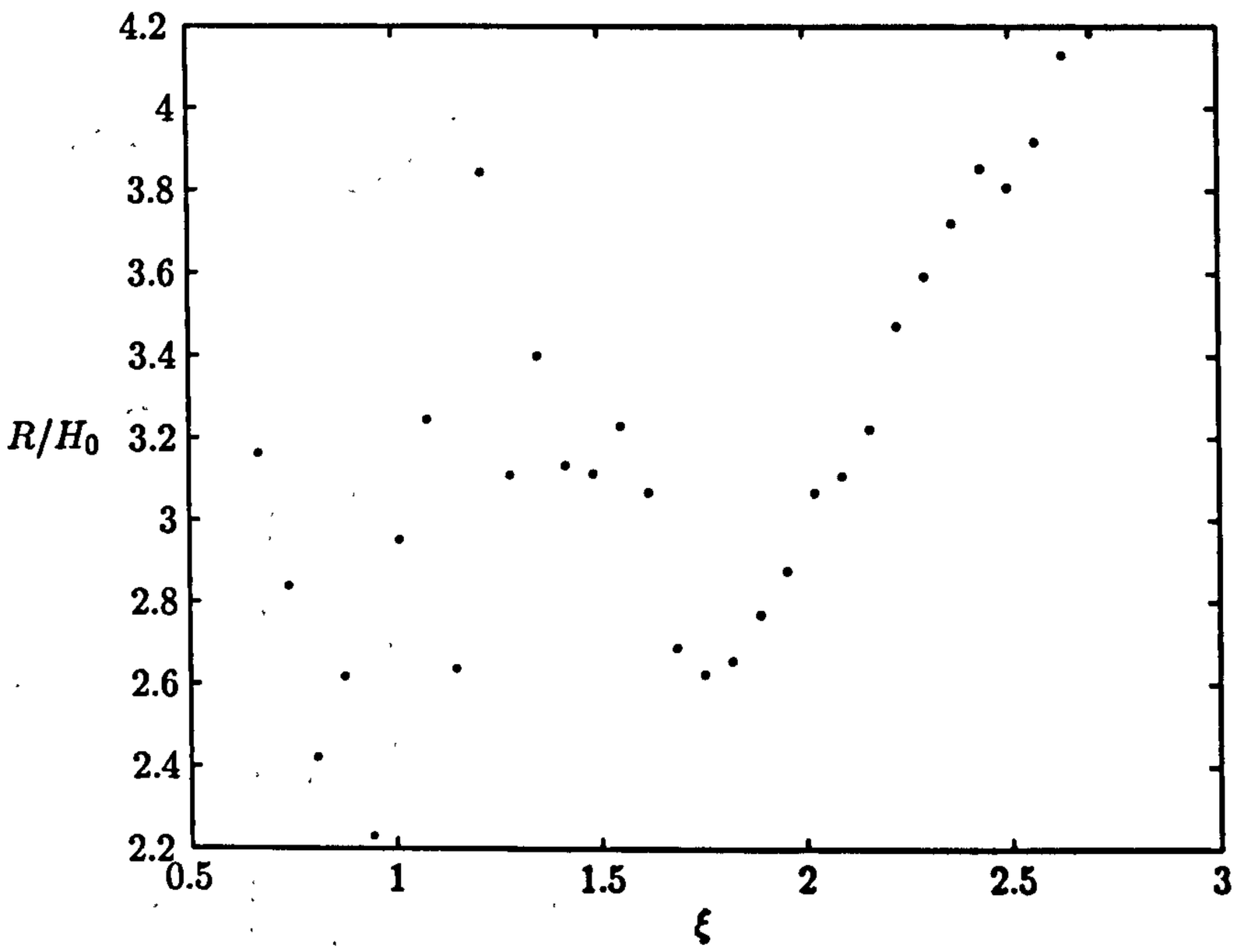

Figure 5.29: Relative wave height R/H_0 as a function of the Iribarren number ξ.

The case of random bore amplitudes is shown in figure 5.29. In this case we see that there exists a linear relationship between the two variables when $\xi > 1.75$. Using table 5.1 we can see that this corresponds to forcing period greater than $t_f = 2.6$. In all the cases when $t_f \geq 2.6$, it was found that there was only one wave

per swash event. For $t_f < 2.6$ the number of waves per swash event varied. This is unlike the case considered in section 5.3, in this case for smaller forcing periods the number of waves per swash was two. In each case here for $t_f < 2.6$ a different value was found for average number of waves per swash event. These values are shown in table 5.2. The entries $W/S|_1$ and $W/S|_2$ correspond to number of waves per swash event for equal and random bore amplitudes respectively.

t_f	$W/S\|_1$	$W/S\|_2$		t_f	$W/S\|_1$	$W/S\|_2$		t_f	$W/S\|_1$	$W/S\|_2$
1.0	2.11	3.25		2.0	1.27	1.64		3.0	1.00	1.00
1.1	2.25	2.71		2.1	1.37	1.75		3.1	1.00	1.00
1.2	2.25	2.36		2.2	1.22	1.60		3.2	1.00	1.00
1.3	2.20	2.20		2.3	1.11	1.38		3.3	1.00	1.00
1.4	2.06	2.00		2.4	1.11	1.22		3.4	1.00	1.00
1.5	2.25	1.83		2.5	1.00	1.09		3.5	1.00	1.00
1.6	2.00	2.00		2.6	1.00	1.00		3.6	1.00	1.00
1.7	2.00	1.79		2.7	1.00	1.00		3.7	1.00	1.00
1.8	2.00	2.00		2.8	1.00	1.00		3.8	1.00	1.00
1.9	2.00	1.67		2.9	1.00	1.00		3.9	1.00	1.00
								4.0	1.00	1.00

Table 5.2: Comparison of number of waves per swash event for equal and random bore amplitudes.

Next we plot the period of response as a function of the Iribarren number ξ. This is given in figure 5.30. As in figure 5.29, there is a linear relationship between the two variables for $\xi > 1.75$. As in the case of equal bore amplitudes the figures appear to be very similar and thus we would expect to find a linear relationship between the period of response t_r and the relative wave height R/H_0. A plot of these two quantities is shown in figure 5.31

As can be seen from this figure, there is in fact a linear relationship between the period of response t_r and the relative wave height R/H_0.

From the two types of waves considered in this section and in section 5.3 we have seen a linear relationship can be found between the Iribarren number and the relative wave height as well as the period of response. In both cases these relationships exist when the number of interactions in the swash zone is small, that is when the forcing wave period is relatively large. This usuallly corresponds to swash on steep beach

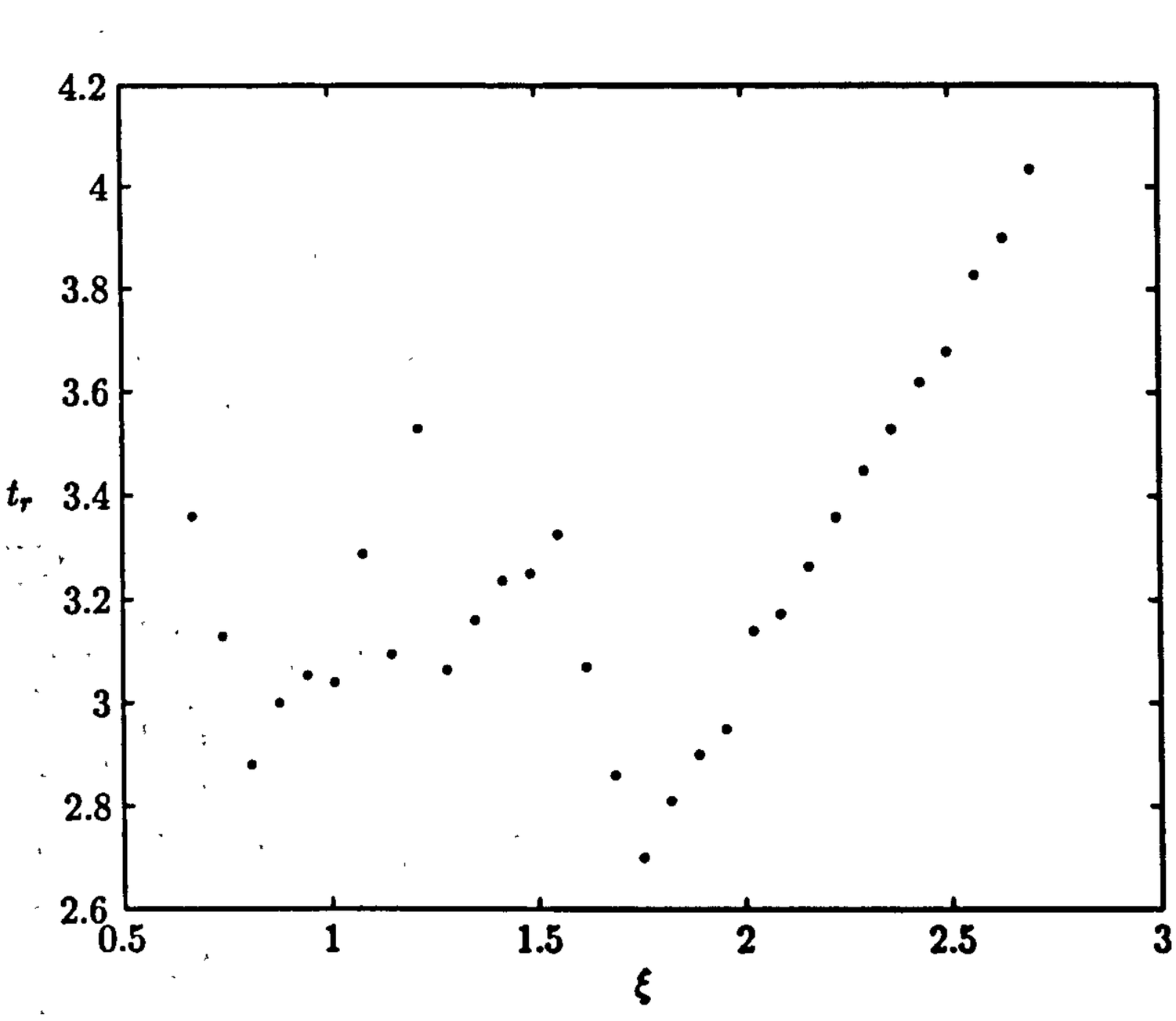

Figure 5.30: The period of response, t_r as a function of the Iribarren number, ξ.

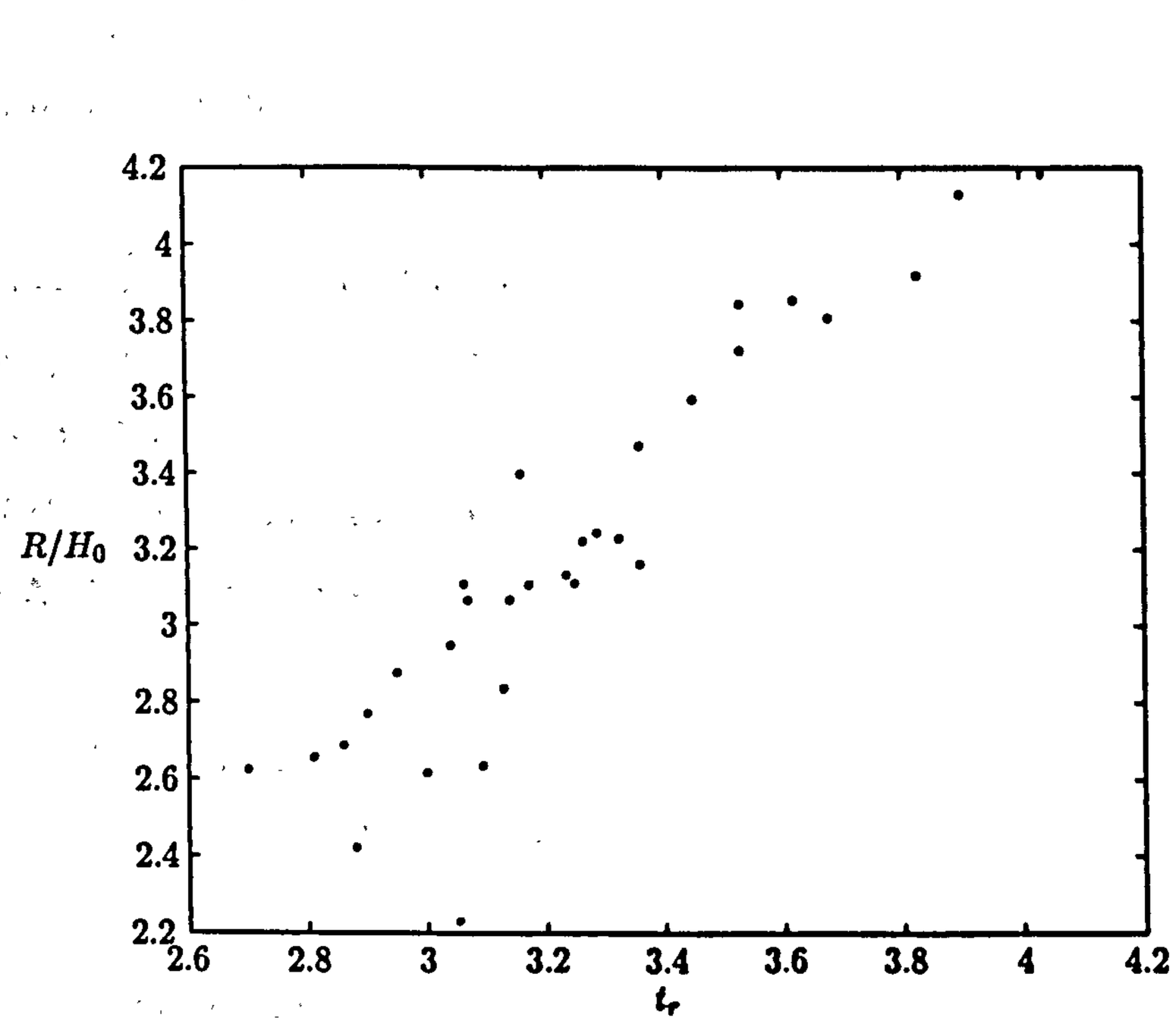

Figure 5.31: The relative wave height, R/H_0 as a function of the period of response, t_r.

slopes, which is when ξ is large.

In the case of equal bore amplitudes of section 5.3, a linear relationship was also found for swash on gentle beaches. This corresponds to smaller values of ξ and thus smaller wave forcing periods. In the case of random bore amplitudes there seems to exist no relationships between ξ and R/H_0 or t_r when ξ is small. This is possibly down to the fact that in this case there are many more interactions occuring in the swash zone and thus the flow is much harder to model.

In both cases though, a linear relationship was found between the period of response of the swash and the relative wave height. This is incouraging since one would expect swash of longer periods to create greater run-up heights up the beach.

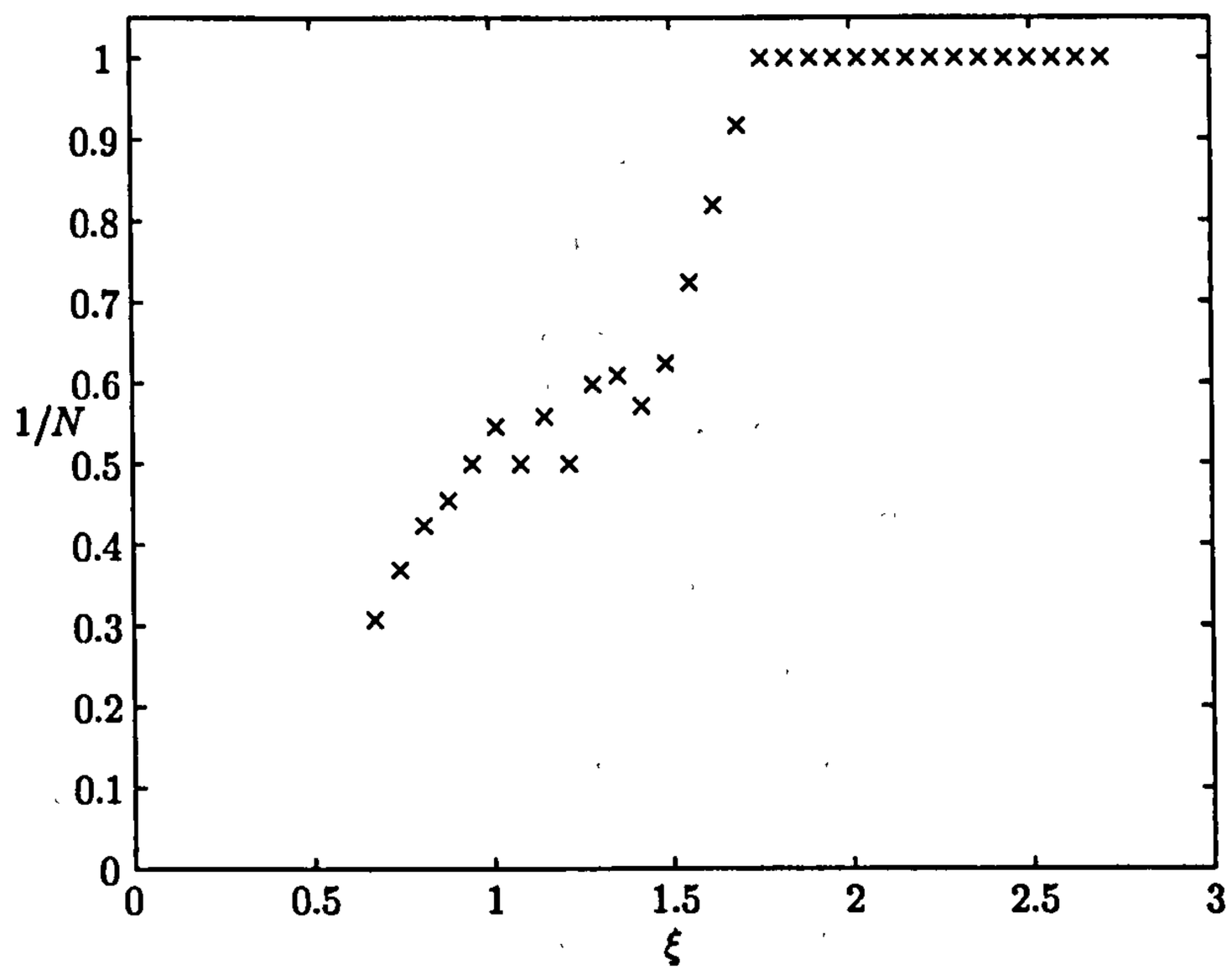

Figure 5.32: Ratio of incident waves to response waves as a function of ξ. N is defined to be the number of waves per swash event.

As in section 5.3 a figure of the ratio of incident waves to swash events as a function of the Iribarren number ξ, is plotted in figure 5.32. This time the relationship between the two parameters seems to compare better with the results of Mase

(1995). We see that as the Iribarren numer ξ increase, so does the ratio of incident waves to swash events. For low values of this ratio, interactions in the swash zone are dominant. When the value of the ratio is one, we have the situation of every incident wave creating a new swash event. Thus in this case, standing waves are dominant in the swash zone.

5.5 Results - Random, non-periodic bores

We have already considered swash from bores sent in at periodic intervals. We have also considered keeping the bore heights the same, and chosen a random distribution of heights. The other type of swash which is considered is that from bores sent into the computational domain at non-periodic intervals. Just as for the setup of the random bore heights, the non-periodic bore intervals are based on a random uniform distribution. We consider both random and exact bore heights in this case. Three cases are considered, the first is when the time between each new bore varies between 1 and 1.5, the second is for t in the interval $t = 1$ to $t = 2$ and finally we consider varying the time between each new bore between $t = 1$ and $t = 4$.

The computations are shown for different end times in each case. In the first two cases shown in figures 5.33 and 5.34, the results are shown in the time interval $[0, 18]$. In the case shown in figure 5.35, we show the results over a longer period of time, since the time intervals between bores can be up to 4 units apart. In this case we show the results in the time interval $[0, 44]$.

The case when the time interval between each new bore is between 1 and 1.5, is uninteresting, since we have events that look very similar to those shown in the previous section. The same goes for the case shown in figure 5.34, where the interval times are now between 1 and 2. The case when the time interval between each new bore lies between 1 and 4 still shows us nothing different to what we saw in section 5.4. From the seventeen bores that enter the computational domain in the time shown, sixteen swash events are created. So we see that in this case practically all new bores create swash events. This is what we expect, since averaging over the forcing period, we find that the average forcing period is 2.5. In section 5.4,

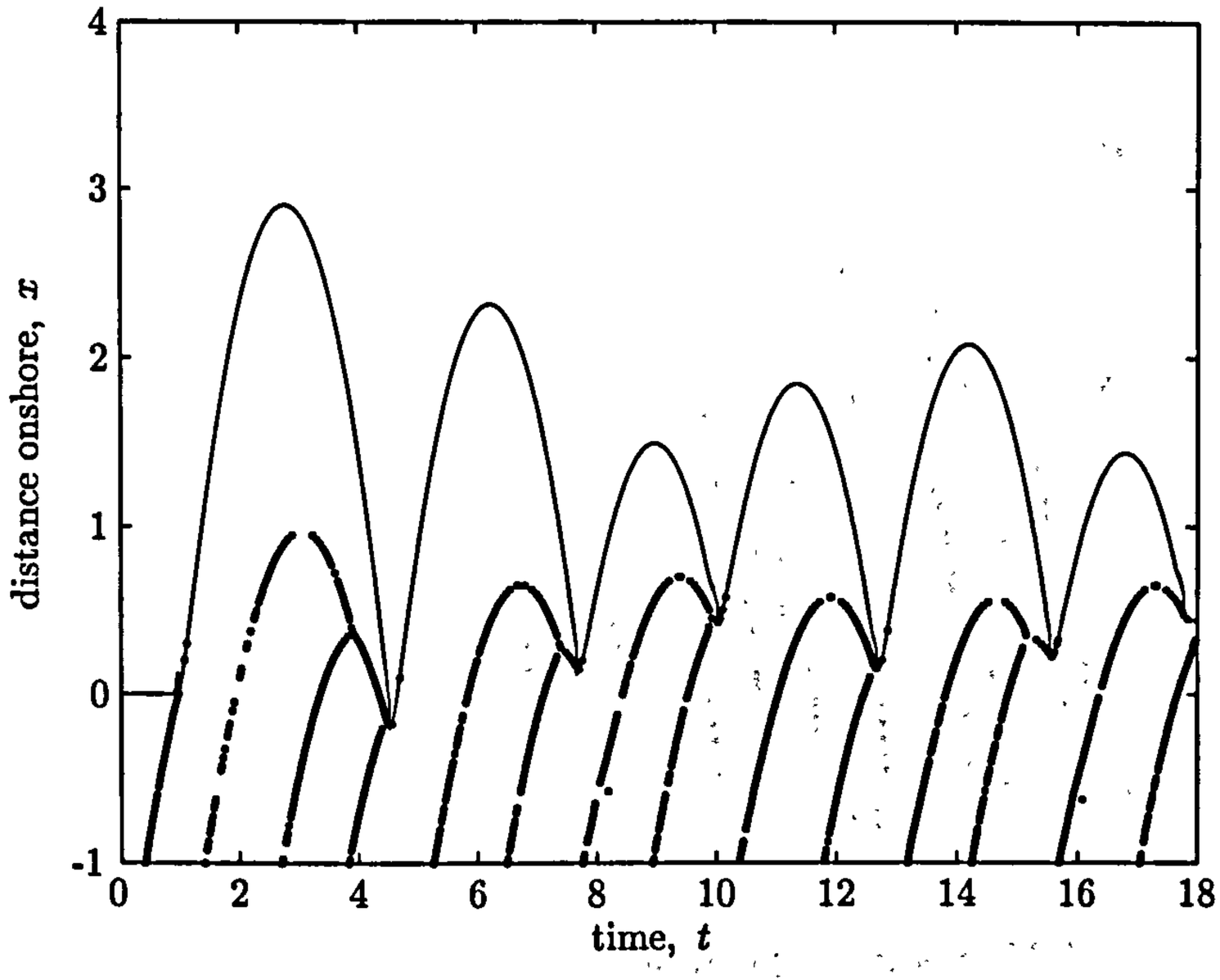

Figure 5.33: Shoreline position of swash with random period. Period is between $t = 1.0$ and $t = 1.5$. $\alpha_i = 3.3$.

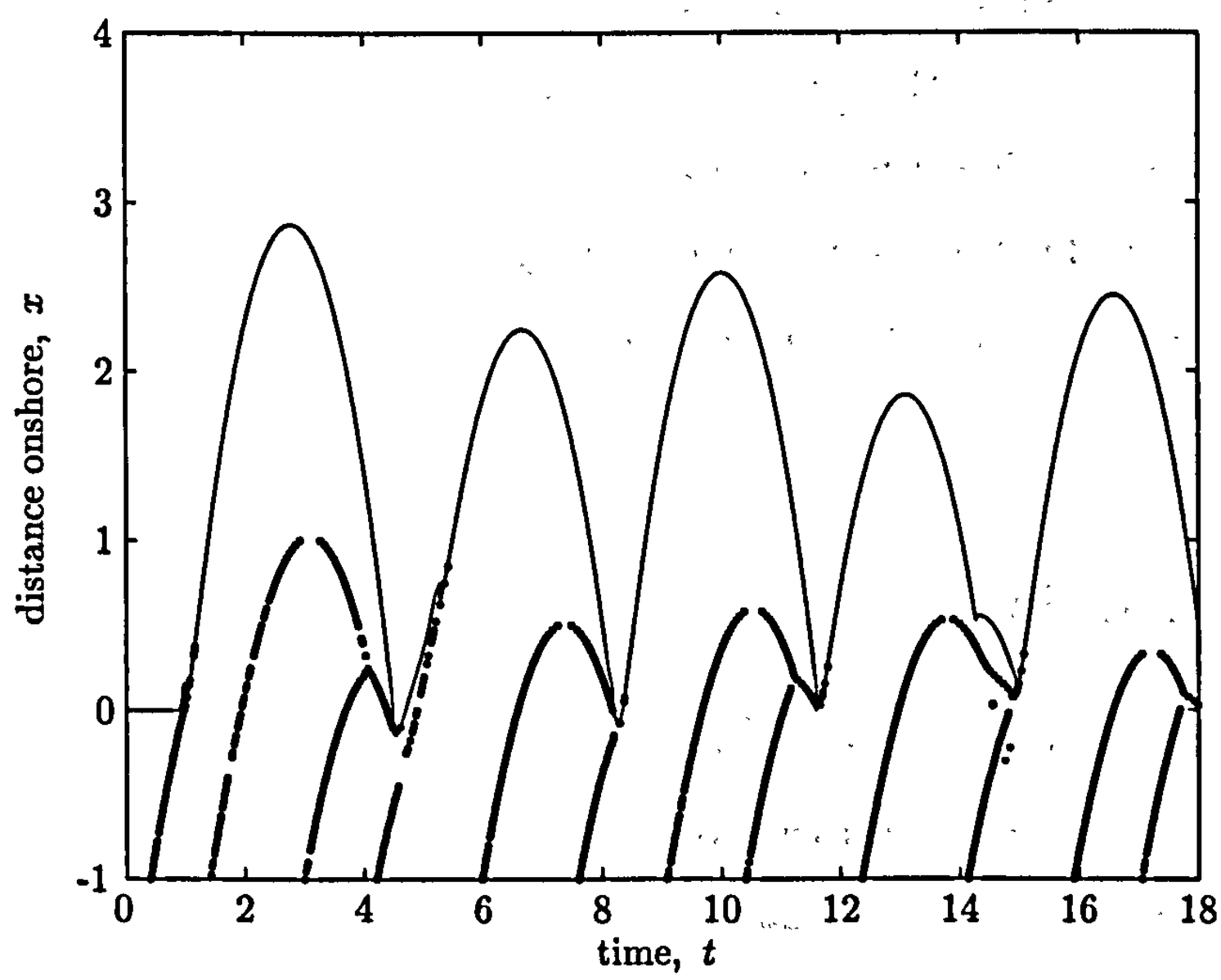

Figure 5.34: Shoreline position of swash with random period. Period is between $t = 1.0$ and $t = 2.0$. $\alpha_i = 3.3$.

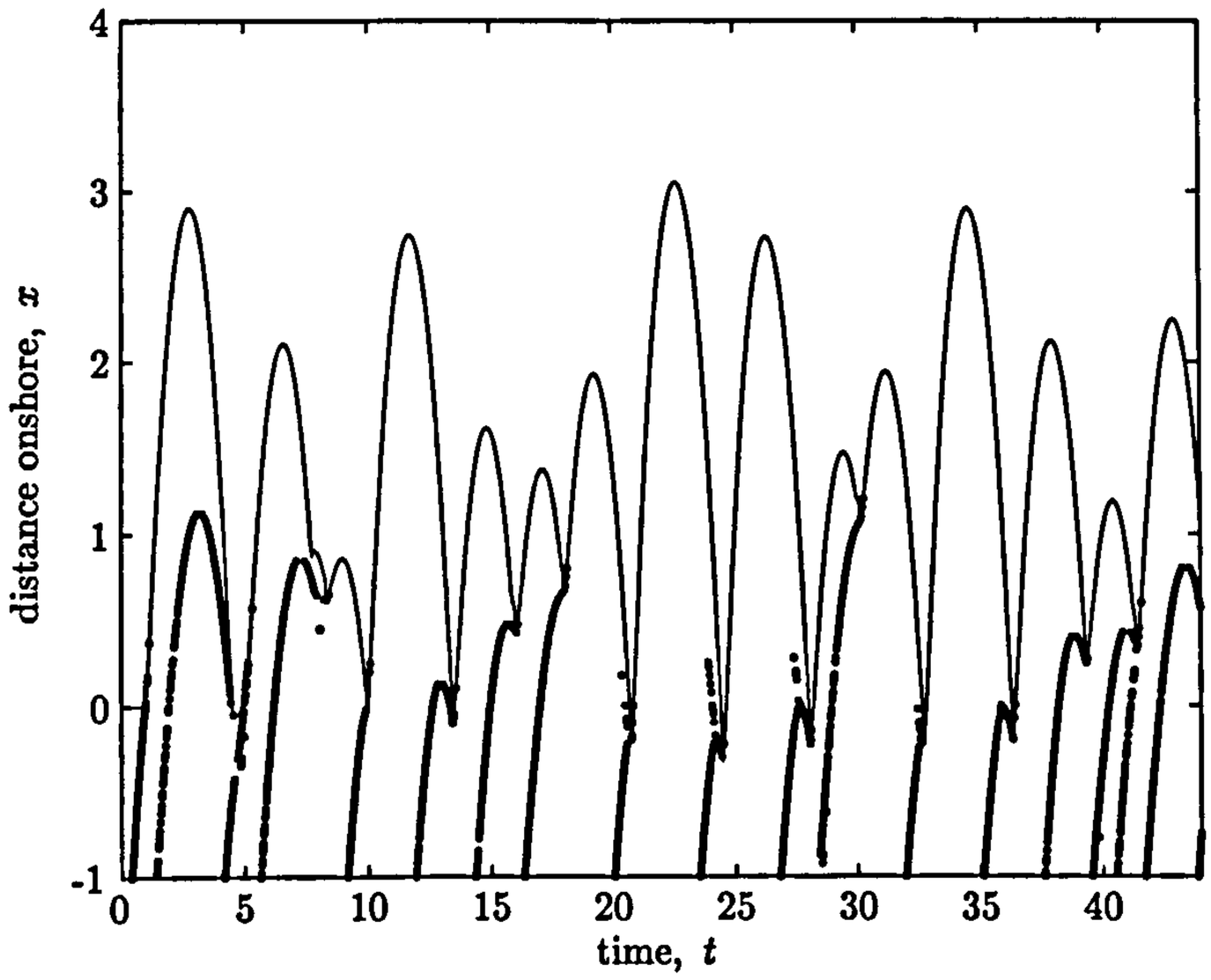

Figure 5.35: Shoreline position of swash with random period. Period is between $t = 1.0$ and $t = 4.0$. $\alpha_i = 3.3$.

swash created from bores with forcing period 2.5 had on average 1.09 waves per swash event (see table 5.2). In this case we have on average 1.08 waves per swash event. Thus we see that the two cases are comparable. From this we deduce that nothing especially different is found by considering non-time periodic bores. Thus we decide not to further our studies on this type of flow. When considering the effects of overtopping in chapter 6, we decide not to include the results for non-time periodic bores.

5.6 Conclusion

The run-up of multiple swash events has been considered numerically. This was achieved using the numerical scheme RUSH, which was presented in chapter 4. The swash events are created by sending into the computational domain, bores at specific time intervals. Information is sent into the computational domain through the seaward boundary, which is a boundary, far away from the still initial shoreline. The way information was introduced through the seaward boundary was by specifying

the form of the Riemann invariant $\alpha = u + 2c + t$, where u is the velocity at the seaward boundary, c is the local wave height at the seaward boundary and t is time. The form of α in the case of bores was found by using the bore conditions, which were introduced in chapter 2.

To send bores through the seaward boundary at specific times intervals, we chose α to be in the form of a saw-tooth. The saw-tooth profiles considered are shown in section 5.2. Three different kind of bores were considered. The first was the case of time-periodic bores of equal amplitudes. The second was the case of time-periodic bores of random amplitudes. Finally, the last case was when the bores are no longer time-periodic.

For three different periods in each case, the shoreline motion was plotted with the form of the height and velocity profiles at the seaward boundary being shown.

In the first two cases, shown in sections 5.3 and 5.4, the Iribarren number was calculated for various different values of the forcing period. The value of the Iribarren number in each case was plotted against the relative wave height. A linear relationship was found for two different ranges of Iribarren number in the first case shown in section 5.3. The first relationship corresponded to two waves to every swash event and the second relationshop corresponded to one wave per swash event. In the second case given in section 5.4, only one linear relationship is found. This relationship is for the case when there is one wave per swash event.

In the first two cases, a linear relationship was also found between the relative wave height and the average period of run-up.

With the model for the run-up of multiple swash events working well, we extended the solutions to include the effects of overtopping on the waves presented in this chapter. The effects of overtopping are now considered in chapter 6.

Chapter 6

The overtopping of multiple swash events

6.1 Introduction

The overtopping of waves on beaches is a very interesting and important situation to be able to model. When considering the effects of overtopping we are usually concerned with the overtopping of waves over shore structures such as seawalls and dykes. Here we are interested in introducing a simple model which could be applied to modelling the overtopping of such structures as these. We consider the motion of waves in the nearshore region i.e. the surf and swash zones. A simple overtopping model is used to consider what the effects maybe of introducing a truncation point along the beach.

In chapter 3 an analytical model and solution for the overtopping of a single swash event over a truncated plane beach was considered. In this chapter we extend the model of chapter 3 numerically to consider the effects of overtopping from multiple swash events. The run-up of multiple swash events was considered in chapter 5. The forms of the Riemann invariant α used to produce the swash events in chapter 5 are used in this chapter, so we can model the effects of overtopping.

The numerical model RUSH used in chapter 5 is extended to include the effects of overtopping. The only difference in the new model RUSH-OVER (**Run-Up**

of **SH**allow water with **OVER**topping) is that an overtopping boundary condition is introduced to include the effects of overtopping. This boundary condition is described in section 4.4.4. Different schemes are used at the truncation point dependent on whether the flow is supercritical or subcritical there. This boundary condition is determined from within the flow and is dependent on the velocity of the flow in the neighbourhood of the truncation point.

The seaward boundary condition is exactly the same as that used in chapter 5. This is because we are considering the same initial wave setup in this chapter as to that was produced in chapter 5. In all the numerical experiments described in this chapter the step size in space is $\Delta x = 0.0125$ and in the step size in time is $\Delta t = 0.00055$, which gives $\lambda = 0.044$.

In section 2 of this chapter the form of α from section 5.3 is used to produce swash events and then overtopping is introduced through the truncation of the beach at a given point. This swash is generated from time periodic bores of equal amplitude (see section 5.3 for further details). In section 3 of this chapter the effects of overtopping are included in the swash motion seen in section 5.4. This swash is generated from time periodic bores of random amplitudes (see section 5.4 for further details).

Peregrine & Williams (2001) showed that for a single wave overtopping a truncated plane beach, the backwash starts at an earlier time than in the non-overtopping case. Peregrine & Williams (2001) found that the overtopping solution differs to just considering the flow past a given point. Since the truncation point acts as a control point, different approaches must be made for subcritical and supercritical flow. This is what is done here. Some of the results given in section 6.3 can be found in Williams & Peregrine (2003)

When considering the volumes of overtopping in later sections, the contribution from the first swash event up the beach is not included.

6.2 Results - Periodic bores

In this section the Riemann invariant α of section 5.3 is used to create time periodic bores. The effects of overtopping on the waves produced from these bores is considered.

The three cases from section 5.3 are considered in this section. These are the cases of when the forcing periods at the seaward boundary are $t_f = 1.3$, 2.2 and 3.0. The swash events are created from time periodic bores of equal amplitudes. In each case we introduce a truncation point at a given point on the plane beach. At the place where overtopping takes place i.e. the truncation point, a boundary condition is imposed. The boundary condition is setup to allow water to freely overshoot the truncation point and be lost from the system. Different approaches are made numerically dependent on whether the flow approaching the truncation point is supercritical or subcritical. In the supercritical case the flow doesn't sense the edge ahead, whereas in the subcritical case the flow must accelerate smoothly to supercritical flow as it passes over the edge and into free-fall. Full details of this boundary condition are given in section 4.4.4. All figures shown are in the time interval $[0, 25]$, just as in the non-overtopping case.

In the numerical experiments presented here we decide to investigate the effects of overtopping for four different truncation points. The truncation points are chosen to be at $x = 1.1$, 1.4, 1.8 and 2.2, where x is the distance onshore. Firstly we consider the case when $t_f = 1.3$. The run-up of the swash created in the case of no overtopping can be seen in figure 5.9. The shoreline motion in this case is shown in figure 6.1. In this figure and in all subsequent shoreline figures, the bold lines represent the individual bore paths. The dashed lines are the position of the shoreline as a function of time. The horizontal line in each figure corresponds to the beach truncation point.

In the first case (top left) in figure 6.1 we can see that the truncation point is extreme, in the sense that all swash events overtop the edge. We immediately see that in this case there are exactly 2 waves per swash event, unlike the non-overtopping case shown in figure 5.9, where there are three waves in the first swash

event. In the first case of this figure we can see that the flow is very periodic, the individual bores all have the same run-up height and all events look like they might produce the same amount of overtopping. The flux past the truncation point and the volume of overtopping are discussed later in this section.

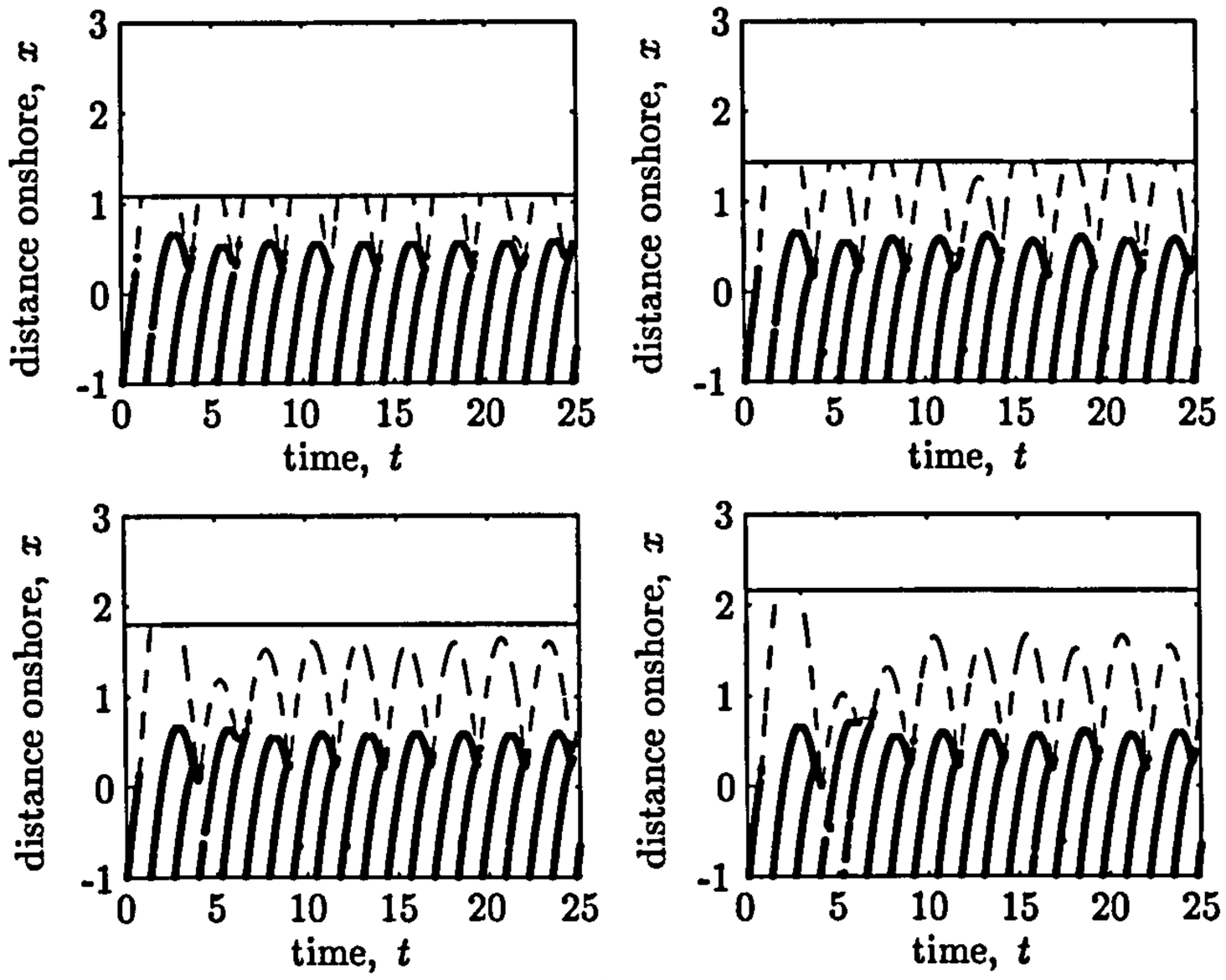

Figure 6.1: Overtopping of swash with forcing period 1.3. Truncation points at $x = 1.1$, 1.4, 1.8, 2.2. Swash from bores of equal amplitudes.

As we increase the value of the truncation point to 1.4, we notice the behaviour is the same as for truncation point 1.1. It is when we increase this point further that we start to see changes. In the third and fourth cases (bottom left and right) of figure 6.1 we notice that only the first event overtops. In the shoreline figures of sections 5.3, 5.4 and 5.5 we saw that the first event usually reaches a higher run-up level than the next few proceeding swash events. The overtopping of the first event changes the proceeding flow significantly from what we saw in chapter 5.

In figure 5.9 we saw that the first three bores to enter the computational domain are taken up by the first event. The second swash event to occur is a consequence of the fourth bore to enter the domain. In the overtopping case we see that the

second swash event to occur is actually created from the third event to enter the computational domain. Thus the proceeding flow is very different. We see that the events which do not overtop do settle to a fixed run-up level as in the non-overtopping case, so the flow doesn't differ too much from that given in the non-overtopping case. Different bores entering the domain create the new swash events, but since all bore amplitudes are equal in this case we don't expect anything unusual to happen. The main difference is a phase shift in the time that new events are created.

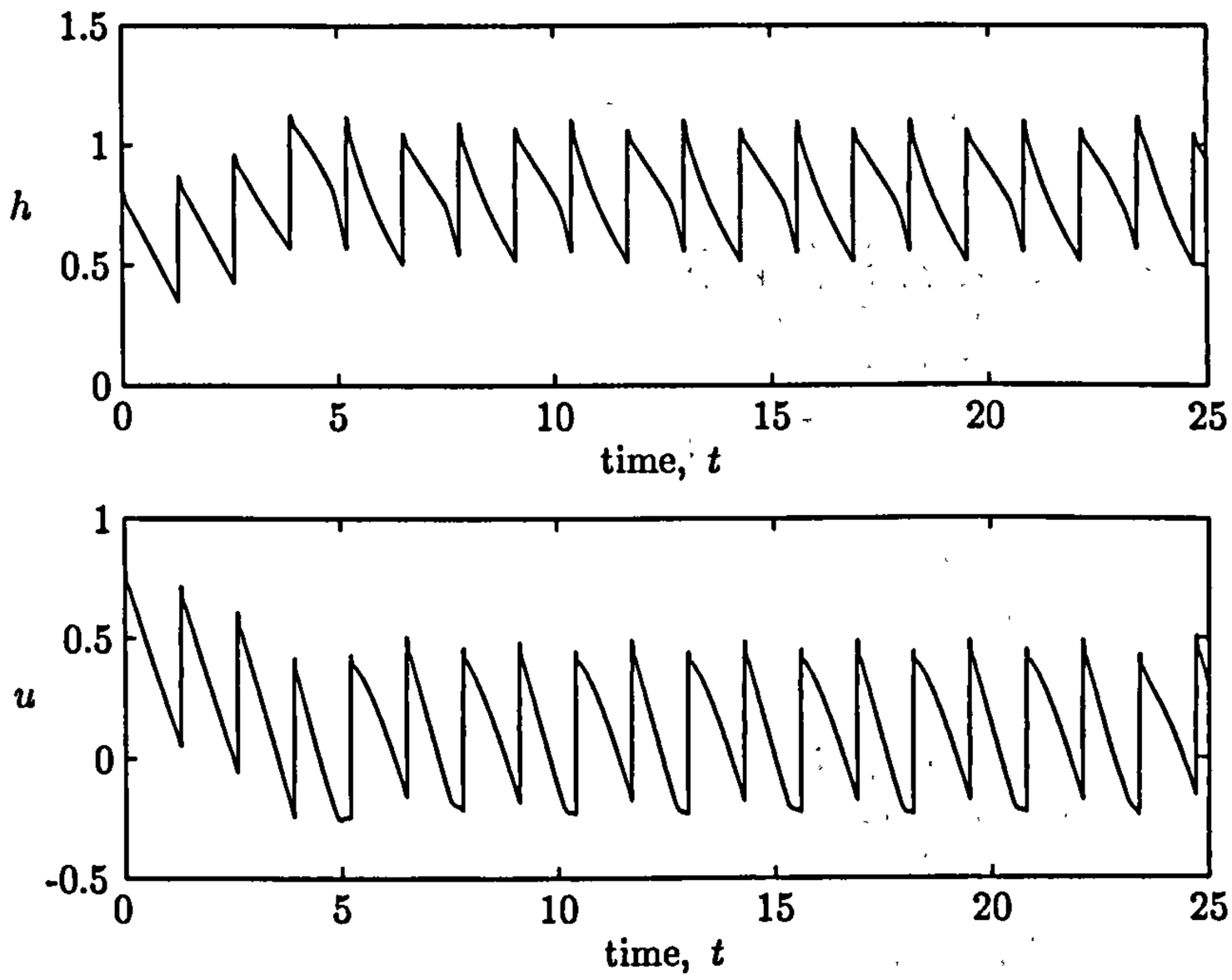

Figure 6.2: Height and velocity profiles at the seaward boundary as a function of time. Forcing is 1.3 and $\alpha_i = 3.3$. Overtopping case of swash from bores of equal amplitudes.

The form of the height and velocity at the seaward boundary is shown in figure 6.2. Comparing this with figure 5.10 we see the main difference is the discontinuity at $t = 5.2$. The fact that the first event overtops changes the form of the height and velocity profile at this time.

Just as in section 5.3 we next consider the case when $t_f = 3.0$. The run-up of these waves with no overtopping is shown in figure 5.11. The shoreline position of the swash generated with the effects of overtopping is shown in figure 6.3. In this

case we see that all events overtop for the first three truncation points. In the last case only the first event overtops and the remaining swash settles to a fixed run-up level, just as in the non-overtopping case. Just as in the non-overtopping case we have one wave per swash and the results are what we expect. Each separate swash event seen here could easily be modelled by the analytical solution of Peregrine & Williams (2001) for the overtopping of a single swash event.

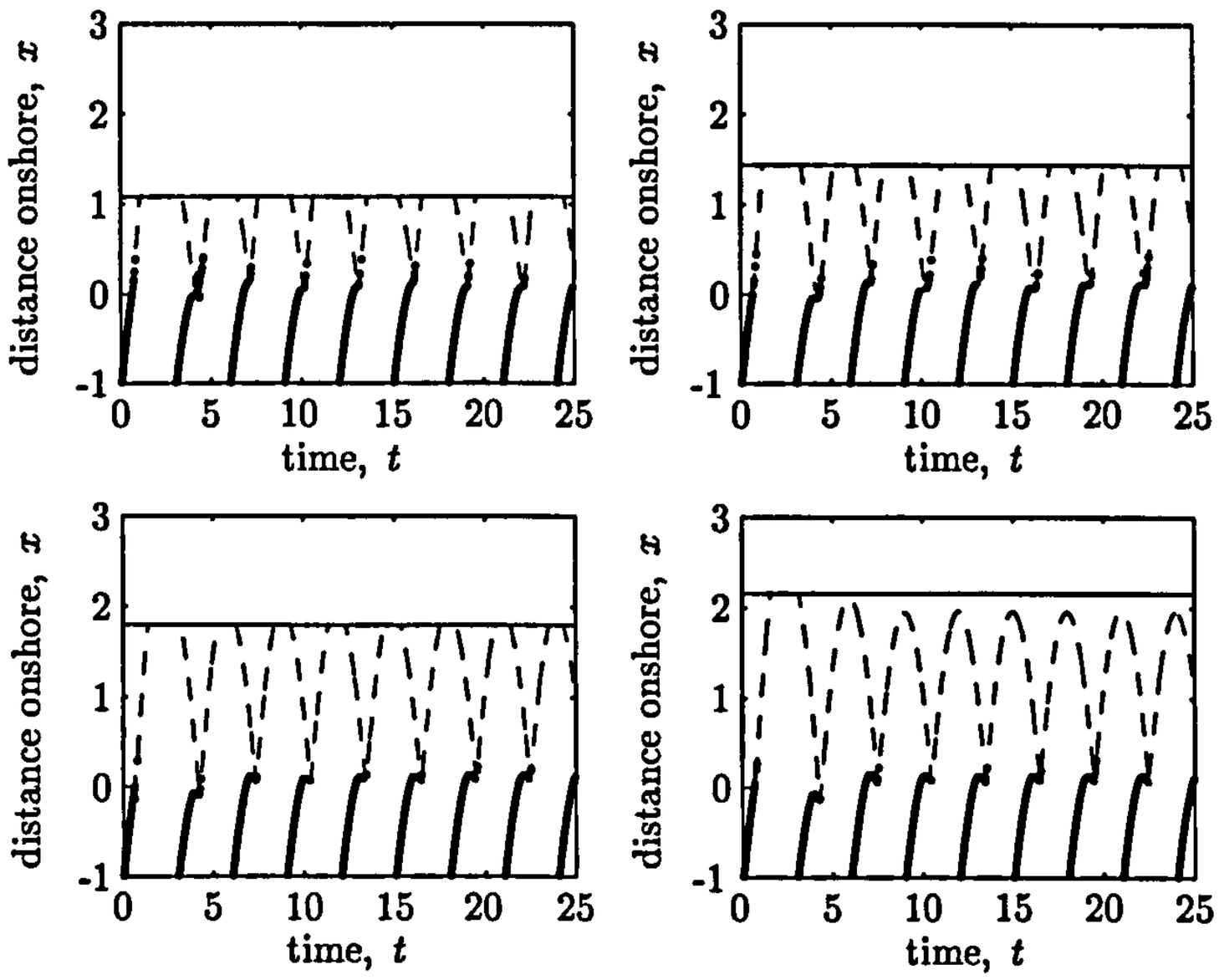

Figure 6.3: Overtopping of swash with forcing period 3.0. Truncation points at $x = 1.1,\ 1.4,\ 1.8,\ 2.2$. Swash from bores of equal amplitudes.

The height and velocity profiles of the flow at the seaward boundary are shown in figure 6.4. Comparing this figure to that in the non-overtopping case, shown in figure 5.12, we notice that the profiles are very similar, the main difference being a change in the appearance of the velocity profile in front of each discontinuity. Here we have a linear profile, whereas in figure 5.12, it is more quadratic.

Let us now consider the case when the forcing period $t_f = 2.2$. In section 5.3 we saw that in the non-overtopping case the run-up level of the swash events did not reach a fixed level like in the other two cases considered (see figure 5.15). This was

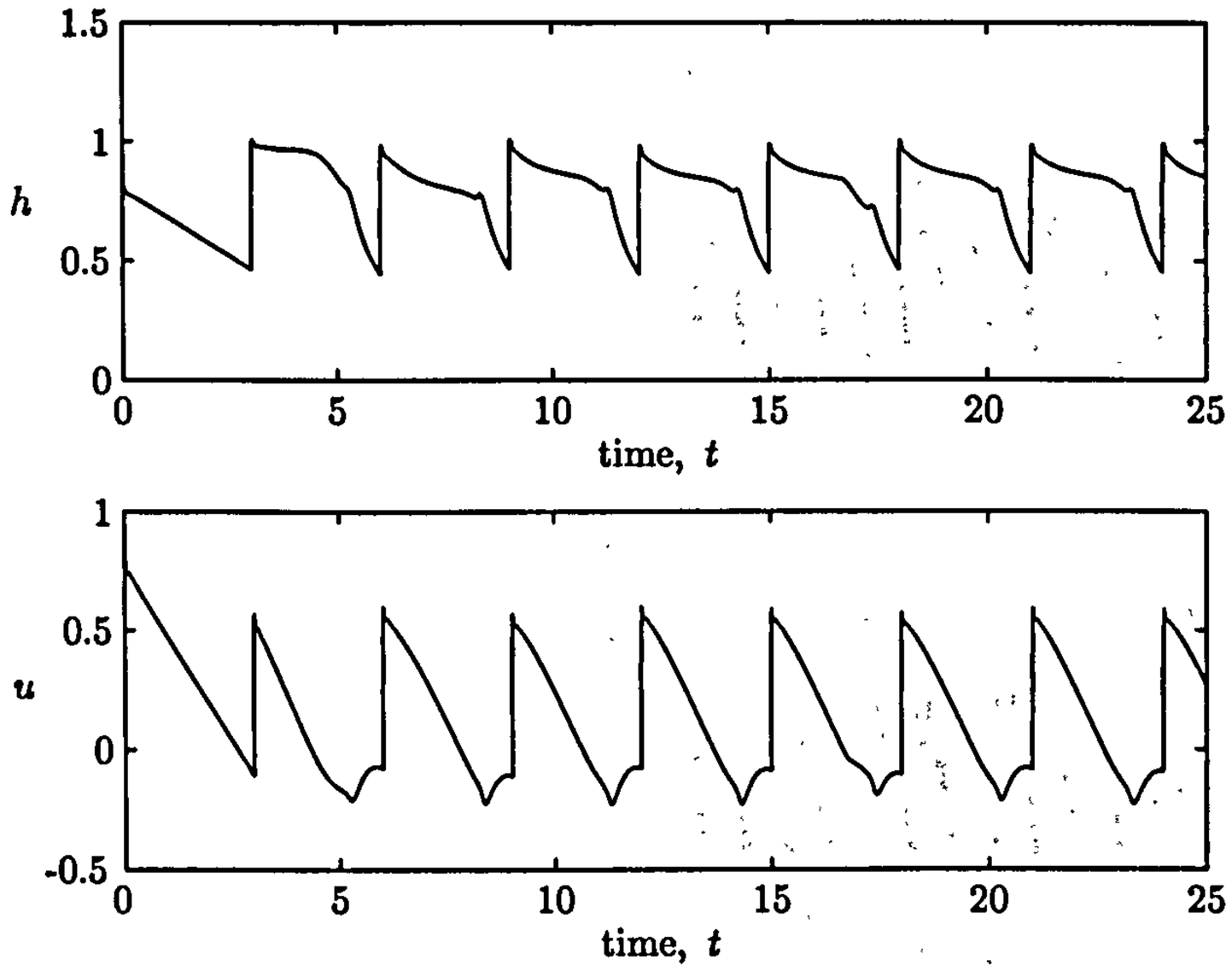

Figure 6.4: Height and velocity profiles at the seaward boundary as a function of time. Forcing is 3.0 and $\alpha_i = 3.3$. Overtopping case of swash from bores of equal amplitudes.

put down to the fact that on average there were between 1 and 2 waves per swash, as a consequence the shoreline position didn't reach a fixed level. In the overtopping case, shown here in figure 6.5 we see that we now have one wave per swash event and thus we would expect the run-up level to reach a fixed limit. This is indeed shown in the fourth plot (bottom right) in figure 6.5, where the swash does seem to settle to a fixed level.

When the truncation point is at $x = 1.1$ we notice that every swash event overtops, just as in the case when $t_f = 1.3$ and 3.0. Increasing the truncation point to 1.4, we notice that only the first two events now overtop the beach. When the truncation point is increased further we see, like in the other two cases, that only the first event overtops. As the truncation point increases from 1.8 to 2.2 we notice that the backwash from the first event must have a thicker depth and thus the run-up from the second event becomes smaller, to such an extent that when no overtopping exists, the second wave to enter the computational domain doesn't create a swash event at all.

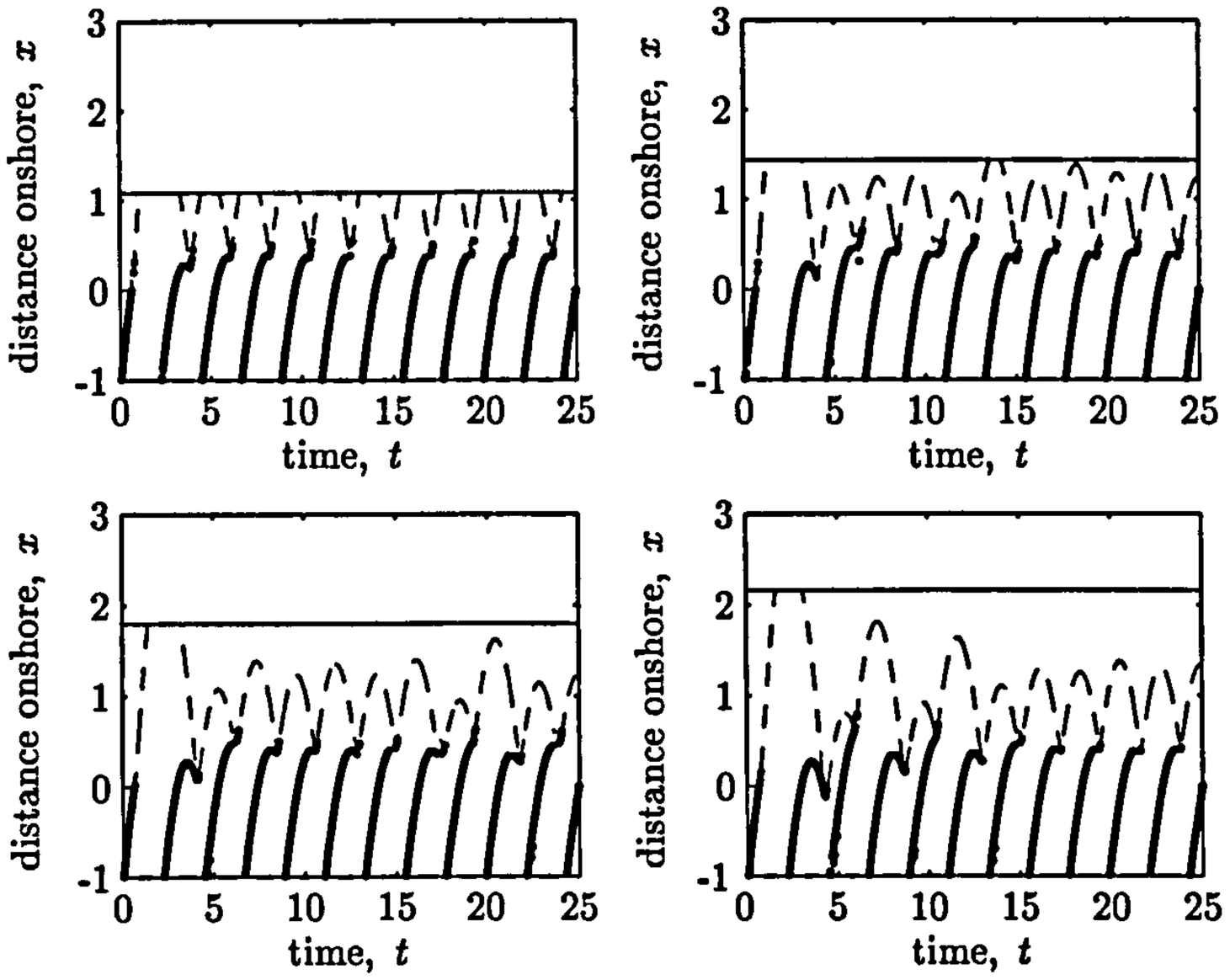

Figure 6.5: Overtopping of swash with forcing period 2.2. Truncation points at $x = 1.1$, 1.4, 1.8, 2.2. Swash from bores of equal amplitudes.

The height and velocity profiles at the seaward boundary as a function of time are shown in figure 6.6. We notice that the profiles settle to a periodic state very quickly, unlike in the non-overtopping case shown in figure 5.16.

In all the cases shown, we see that the first swash seems to dominate the overtopping flow. The form of the proceeding swash events is highly dependent on the amount of backwash from this first event. We saw in the case when $t_f = 2.2$ that the effects of overtopping change the form of the shoreline motion. In the non-overtopping case, our run-up didn't reach a fixed level, but in the overtopping case we found that the run-up did reach a fixed level. We also saw how overtopping can change the number of waves per event. For $t_f = 2.2$, in the case of no overtopping the average number of waves per event was 1.2, whereas in the case of overtopping the number of waves is reduced to one.

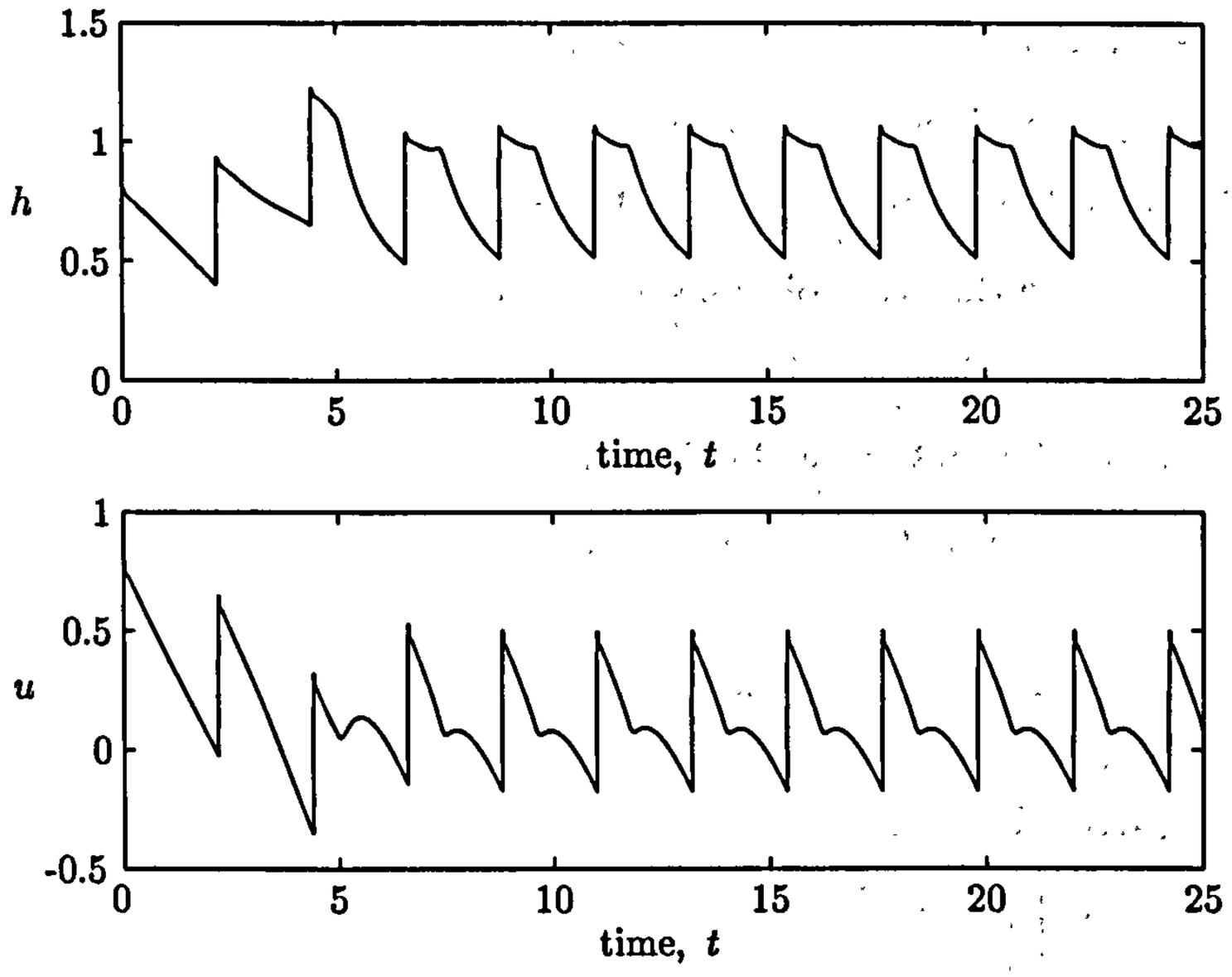

Figure 6.6: Height and velocity profiles at the seaward boundary as a function of time. Forcing is 2.2 and $\alpha_i = 3.3$. Overtopping case of swash from bores of equal amplitudes.

6.2.1 Flux comparison

To calculate the amount of water that overtops the edge of the beach, one must first investigate the flux of the flow at the truncation point. The flux is defined as $q = uh$, where u and h are the velocity and height of the flow at a given point in space. Here, we calculate the flux, q, at the truncation point $x = E$. The amount of overtopping in each case considered in section 6.2 is discussed later in section 6.2.2.

In all the flux figures in this section we compare the flux at the truncation point in the overtopping case with the flux passed the same point in the non-overtopping case. We do this to highlight the differences between the overtopping and non-overtopping cases.

Our first case was when $t_f = 1.3$, the flux q at the truncation point, is plotted as a function of time in figure 6.7. The overtopping flux is shown in the dotted

line and the non-overtopping flux is shown with a solid line. We see from the top plot in figure 6.7 that the only time the flux is the same for the overtopping and non-overtopping cases, is when considering the first swash event. In this plot, it is not possible to see both sets of lines for the first swash event. If we zoomed in on the first event, we see that the solutions are slightly different, this difference is seen in the solution of Peregrine & Williams (2001). In all the cases shown it can be seen that the flux from the first event dominates. In the second plot the flux from the first event is left out so that we can zoom in on the flux from other events.

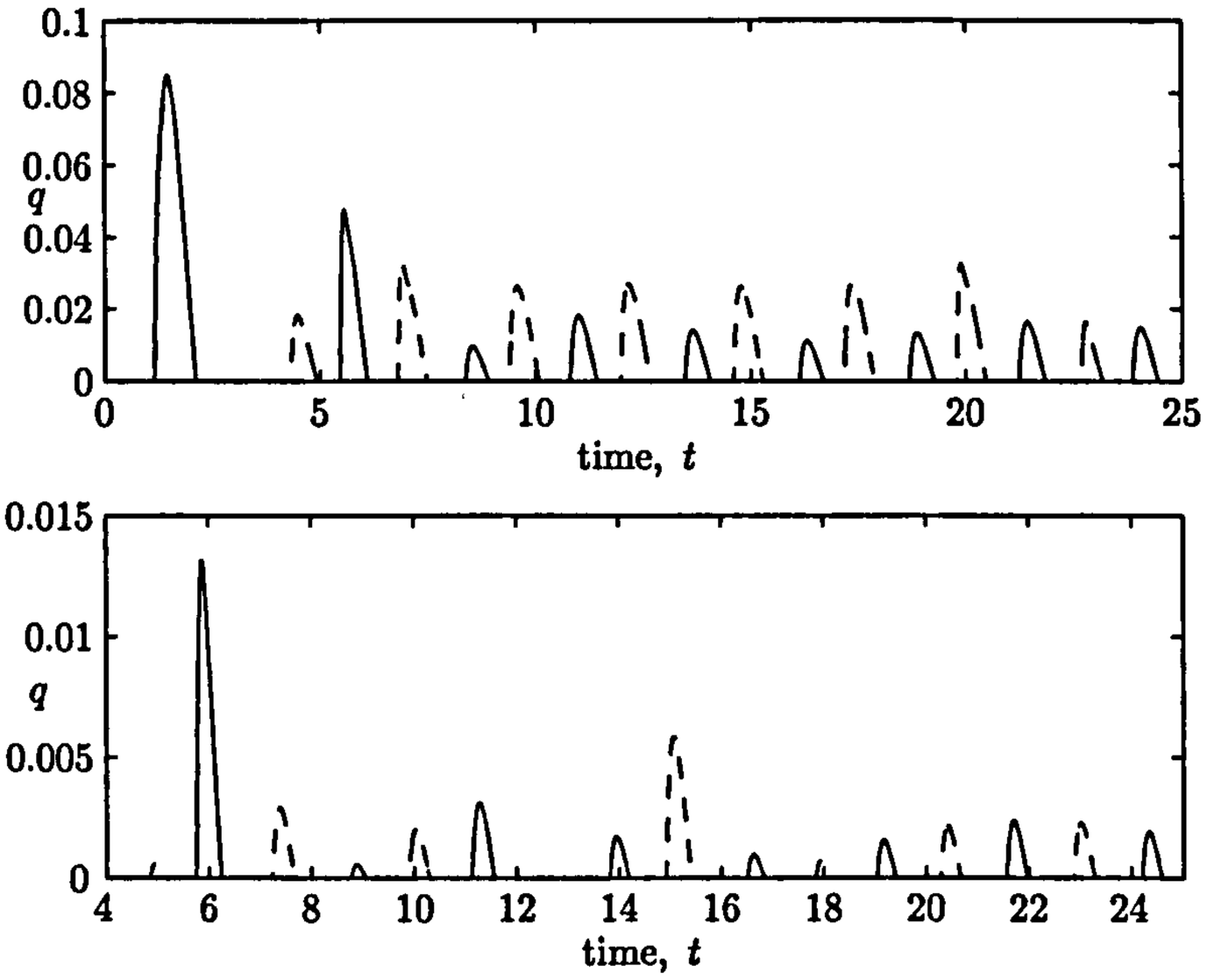

Figure 6.7: Flux comparison at cut-off point between overtopping and non-overtopping data. Cut-offs at $x = 1.1$, 1.4, 1.8 and 2.2. Forcing period is $t_f = 1.3$. Swash from bores of equal amplitudes. Overtopping data (- -), non-overtopping data (–).

The flux at the points $x = 1.8$ and 2.2 are left out of figure 6.7, since the only contribution in the case of overtopping and no overtopping is from the first swash event.

We notice from both plots in figure 6.7 that there seems to be a phase difference between the fluxes from the two cases. This comes from the fact that waves which were once taken with the backwash from the first swash event, now create new

events. This has the consequence of new swash being created at different times. We notice that the period of these new events seems to be the same in each case.

If the flux past the truncation point is different in each case, it doesn't necessarily mean that the amount of overtopping is different. As long as the same number of events are overtopping then the volumes could be the same. The problem arises in the fact that the run-up heights in the two cases will normally differ. This may not be true in the case of swash from bores of equal amplitudes.

The flux in the case $t_f = 2.2$ is shown in figure 6.8. Again we see that the flux from the first event is the same in the overtopping and non-overtopping cases. Looking at the first plot (top), we notice the phase difference again, as seen in figure 6.7. In the last case the flux comparisons were very similar apart from the phase shift. In this case though we see a big contribution from the second swash event in the non-overtopping case, which is not found in the overtopping case. The contribution from this second event in the non-overtopping case also seems to dominate the other plots in figure 6.8.

The flux in the case $t_f = 3.0$ is shown in figure 6.9. As in the last two cases the flux from the first swash event dominates. This time there doesn't seem to be a phase difference between the two flux solutions. In fact the data in the two cases are very similar. It seems that when the forcing period is such that every bore to enter the computational domain creates a swash event then the difference between the two examples is very slight.

In the third plot of figure 6.9, the contribution from the first event is not shown, so that we can zoom in on the contributions from other swash events.

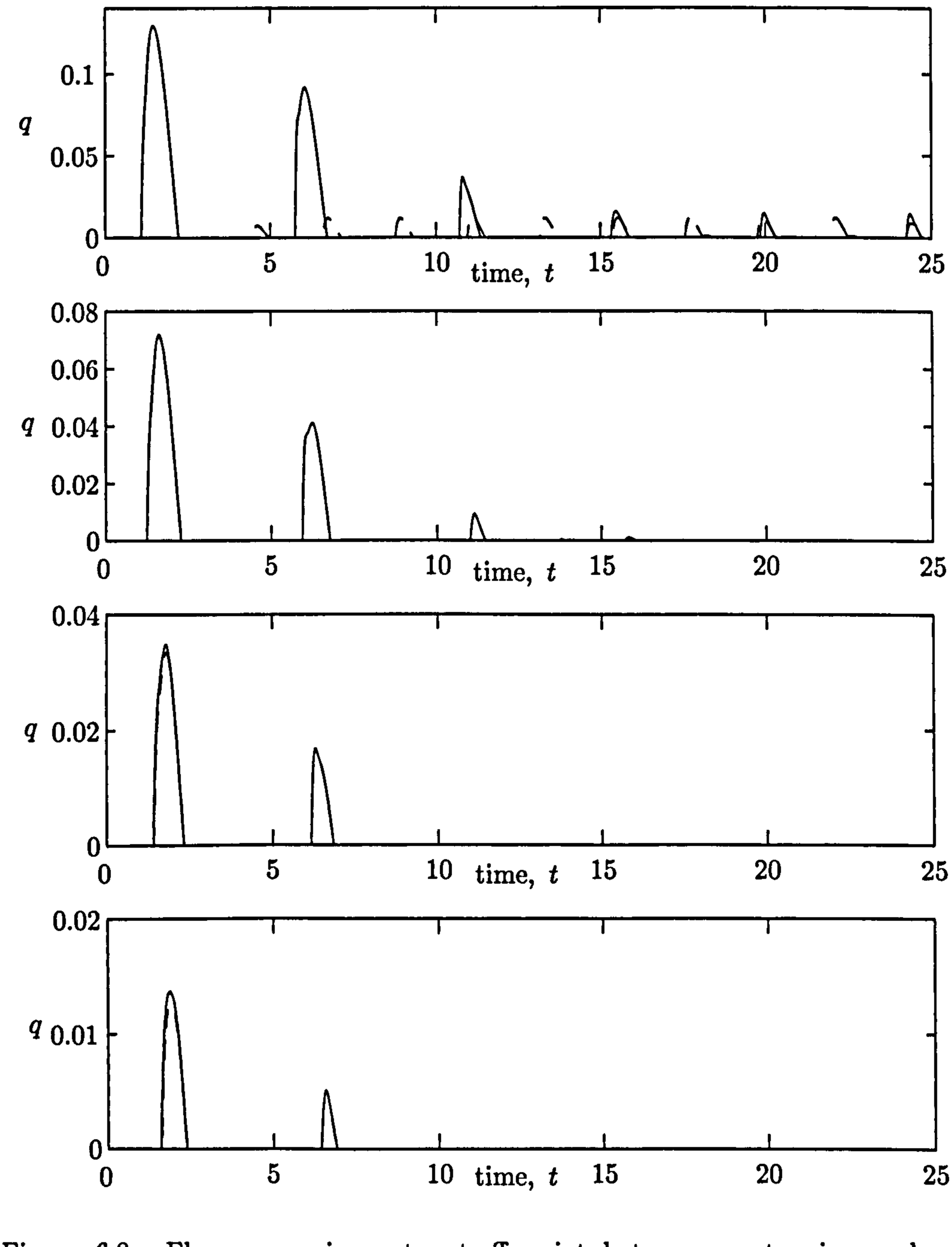

Figure 6.8: Flux comparison at cut-off point between overtopping and non-overtopping data. Cut-offs at $x = 1.1$, 1.4, 1.8 and 2.2. Forcing period is $t_f = 2.2$. Swash from bores of equal amplitudes. Overtopping data (- -), non-overtopping data (–).

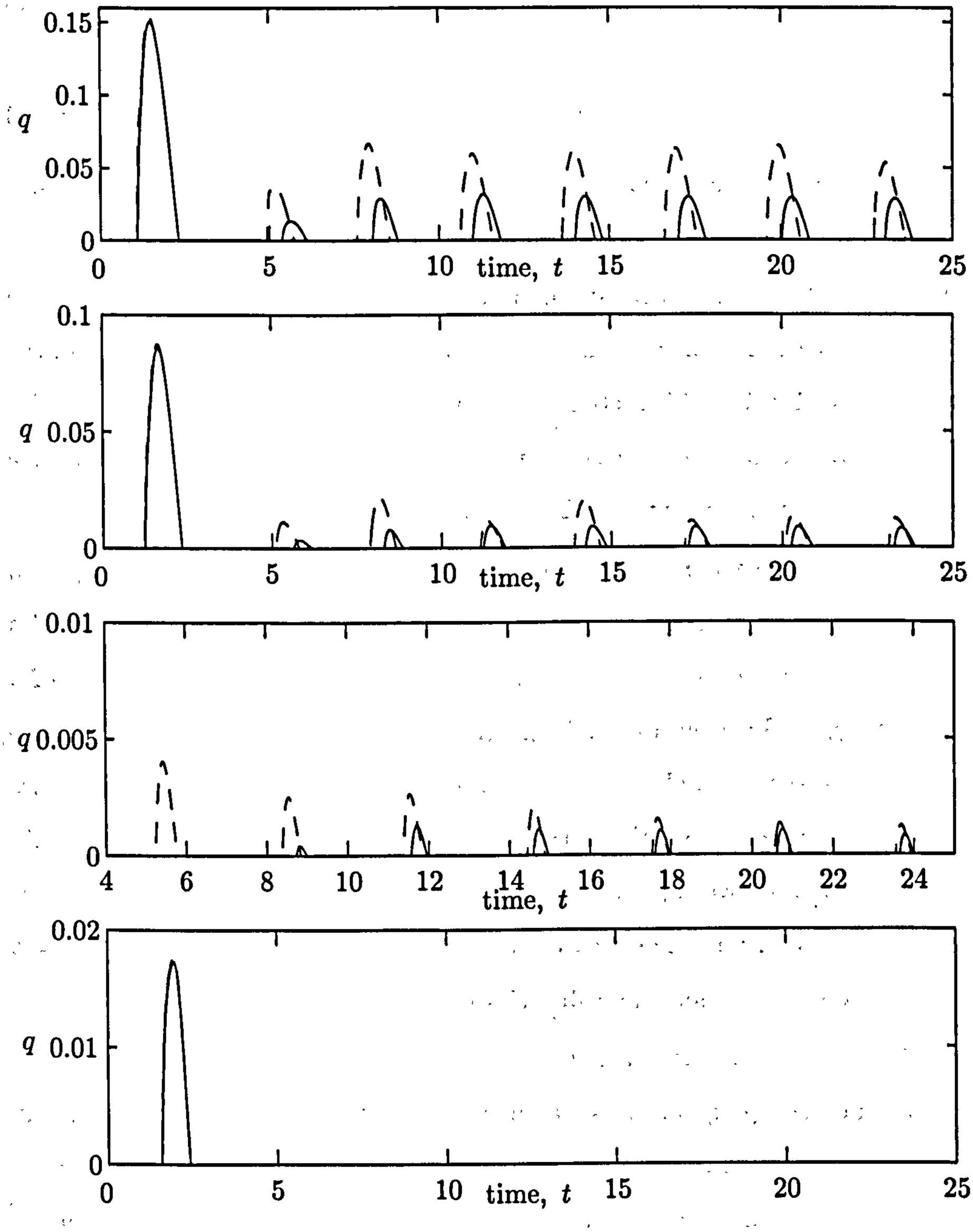

Figure 6.9: Flux comparison at cut-off point between overtopping and non-overtopping data. Cut-offs at $x = 1.1$, 1.4, 1.8 and 2.2. Forcing period is $t_f = 3.0$. Swash from bores of equal amplitudes. Overtopping data (- -), non-overtopping data (–).

6.2.2 Volumes of overtopping

With an expression found for the flux of the flow at the truncation point, we can now calculate the amount of water that overtops in a given time interval. The volume of overtopping is defined as

$$V = \int_{t_1}^{t_2} q \, \mathrm{d}t, \tag{6.2.1}$$

where q is the flux at the truncation point, t_1 and t_2 are the lower and upper time limits. The integral in (6.2.1) is integrated numerically using Simpson's rule.

The interval here is taken as $[0, 25]$, thus $t_1 = 0$ and $t_2 = 25$. The value of the flux at the truncation point as a function of time is already known. In each of the three cases considered in this section, we vary the position of the truncation point up the beach and then calculate the amount of water that overtops in the given time interval. The truncation point $x = E$ was considered in the interval $[1, 2.5]$.

In figure 6.10 the volumes of overtopping in the three different forcing period cases are plotted as a function of the truncation point $x = E$. We notice each plot in this figure is similar to figure (3.4) given in chapter 3 for the overtopping of a single swash event. Since even a small amount of overtopping may be of importance in some circumstances, we also show these volumes on a logarithmic scale in figure 6.11. Comparing this figure with figure 3.5 of chapter 3, we see that the relationship between the volume of overtopping and the cut-off point for multiple swash is similar to that in the case of a single swash event. We see from these figures, that as the value of t_f increases, so does the value of overtopping.

Models of overtopping are usually based on exponential relationships between the volume of overtopping and some quantity, usually the freeboard position. These relationships are seen in tables 1.1-1.3 of chapter 1, where details of some overtopping models are given. In all these cases it is assumed that overtopping always takes place.

In figures 6.10 and 6.11 we see that overtopping begins to cease at different cut-off points for different forcing periods t_f. Thus when the number of interactions in the swash zone is high the total volume of overtopping is less than in the case of few interactions.

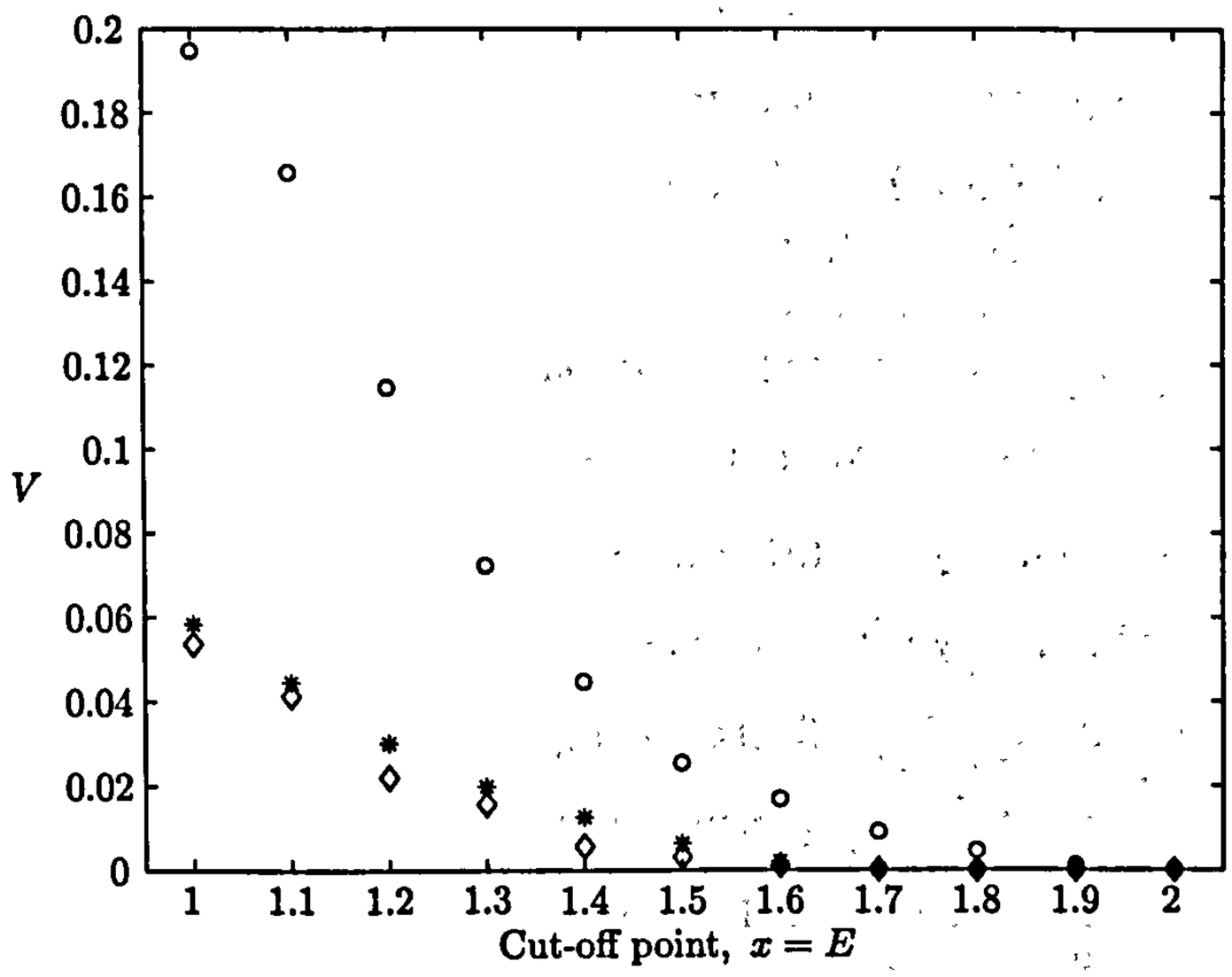

Figure 6.10: Volume of overtopping against cut-off position $x = E$. $\diamond$ is for $t_f = 1.3$. $*$ is for $t_f = 2.2$ and $\circ$ is for $t_f = 3.0$. Swash from bores of equal amplitudes.

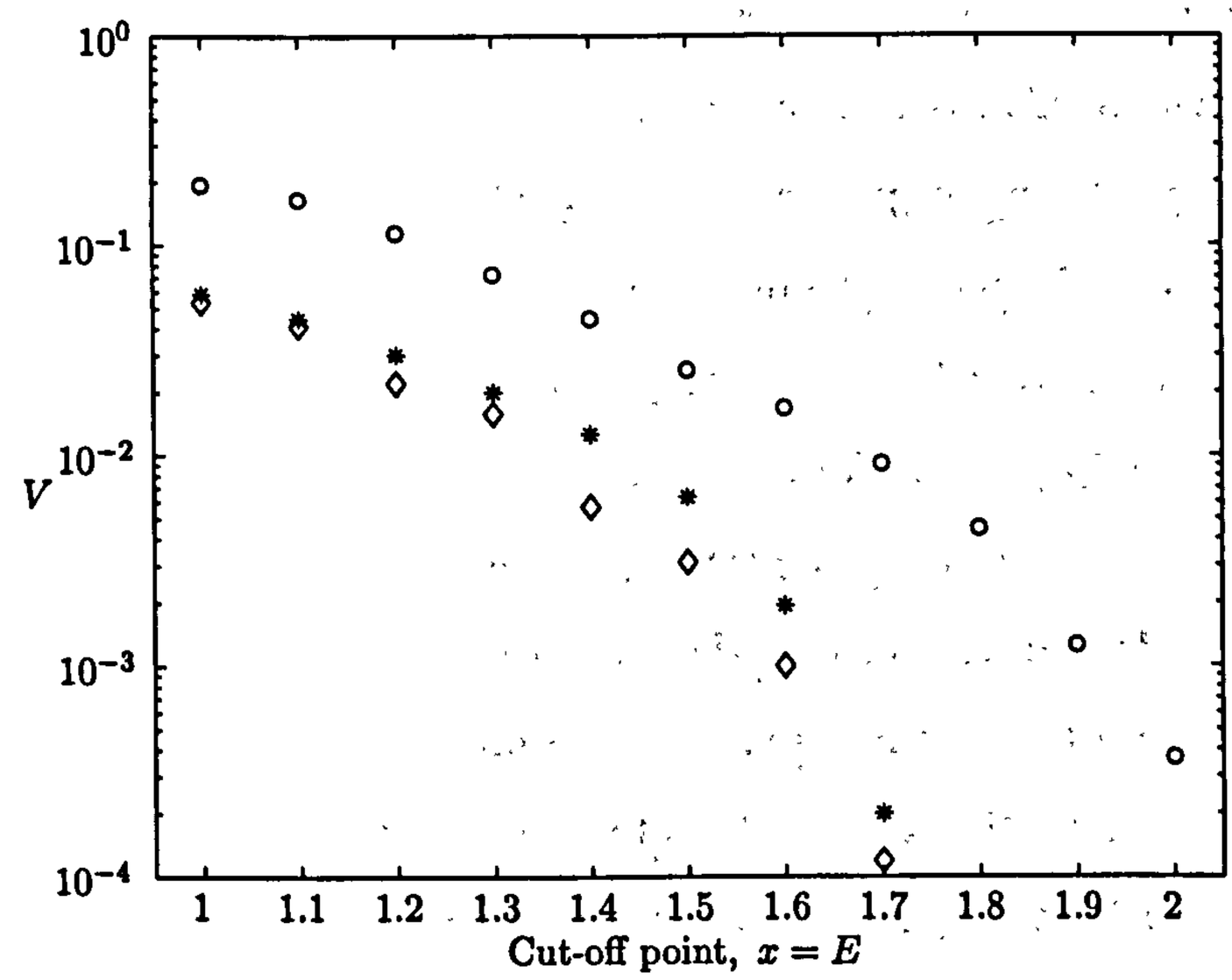

Figure 6.11: Volume of overtopping against the cut-off position $x = E$ on a logarithmic scale. $\diamond$ is for $t_f = 1.3$. $*$ is for $t_f = 2.2$ and $\circ$ is for $t_f = 3.0$. Swash is from bores of equal amplitudes.

6.3 Results - Random, periodic bores

The case of overtopping of swash from time periodic bores of equal amplitudes has been discussed in section 6.2. We now consider the overtopping of swash from time periodic bores of random amplitudes. The swash events we are interesting in, have already been shown and discussed in section 5.4. We use the form of α used in section 5.4 to see how the introduction of overtopping affects the shoreline motion.

The seaward boundary condition for this flow is given in detail in section 5.2. The overtopping boundary is the same as in section 6.2 and a description is given in section 4.4.4. Results for three different computations are presented in this section. The different cases are for non-dimensional forcing period $t_f = 1.0$, 2.0 and 4.0. The computional experiments are shown in the time interval $[0, 30]$.

Firstly, we consider the case when $t_f = 1.0$. The run-up of the swash created in this case is shown in figure 6.12. This case is different to that of swash from bores of equal amplitudes, in that now, not all swash events overtop in the case when the truncation point is at $x = 1.1$. This is down to the fact that each swash event now has a different maximum run-up height. In the case of no overtopping it was found that on average in this case, there were 3.2 waves per swash event. In this case we have on average 2.5 waves per swash event. The introduction of overtopping cuts down the number of interactions in the swash zone.

The first swash event in the non-overtopping case shown in figure 5.24 contains 4 waves, whereas in the first 3 cases shown in figure 6.12, there is only 2 waves in the first swash event. In the non-overtopping case, it is the fifth wave to enter the computational domain that creates the second swash event. In the first three cases here, it is the third wave that creates the second event. As the truncation point becomes larger we see that the number of waves per event increases also. When the truncation point is at $x = 2.2$, we notice that just as in the non-overtopping case, the fifth wave to enter the computational domain creates the second swash event.

This result is what we expect, since as we increase the truncation point, the overtopping solution should tend to the non-overtopping solution. In fact if we compare the last plot in figure 6.12, with figure 5.24, we can see similarities between

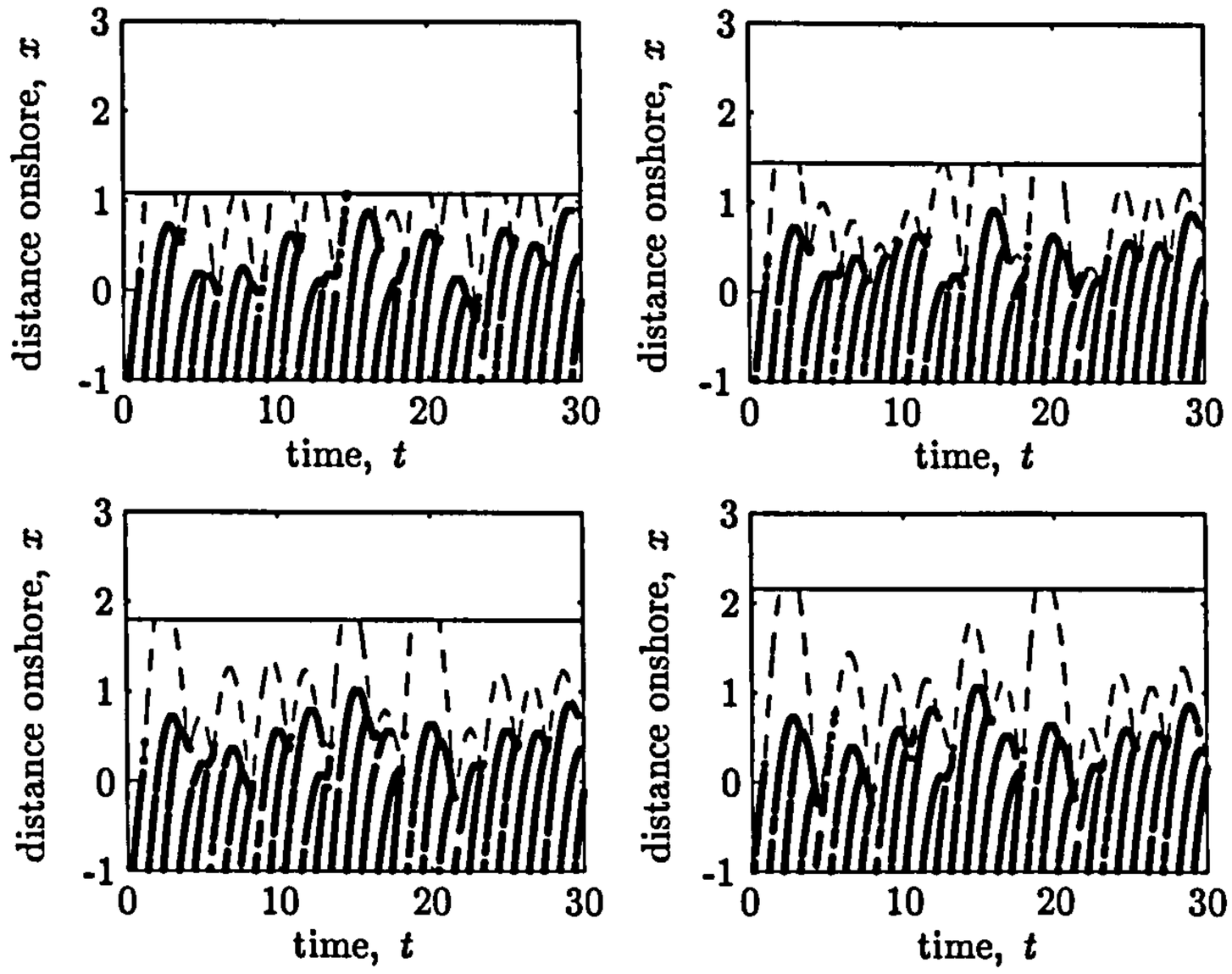

Figure 6.12: Overtopping of random swash with forcing period 1.0. Truncation points at $x = 1.1$, 1.4, 1.8, 2.2. Swash from bores of random amplitudes.

the shoreline motions.

Figure 6.13 shows the height and velocity profiles for the flow at the seaward boundary. Comparing with the no overtopping case shown in figure 5.25, we notice that there are time intervals where the profiles look the same. But there are some differences, which arise from the fact that the second swash event starts earlier.

The shoreline motion for the case of forcing period $t_f = 2.0$ is shown in figure 6.14. We see from the first plot in this figure that every wave to enter the computational domain creates a new swash event. The number of waves per swash increases as the truncation point is increased. In the second plot in figure 6.14, the number of waves per swash is 1.4. This number increases to 1.5 in the case when the truncation point is at 2.2. In the non-overtopping case, the average number of waves per swash event is 1.64. thus the number of interactions in the swash zone increases as the truncation point increases.

The height and velocity profiles at the seaward boundary are shown in figure 6.15.

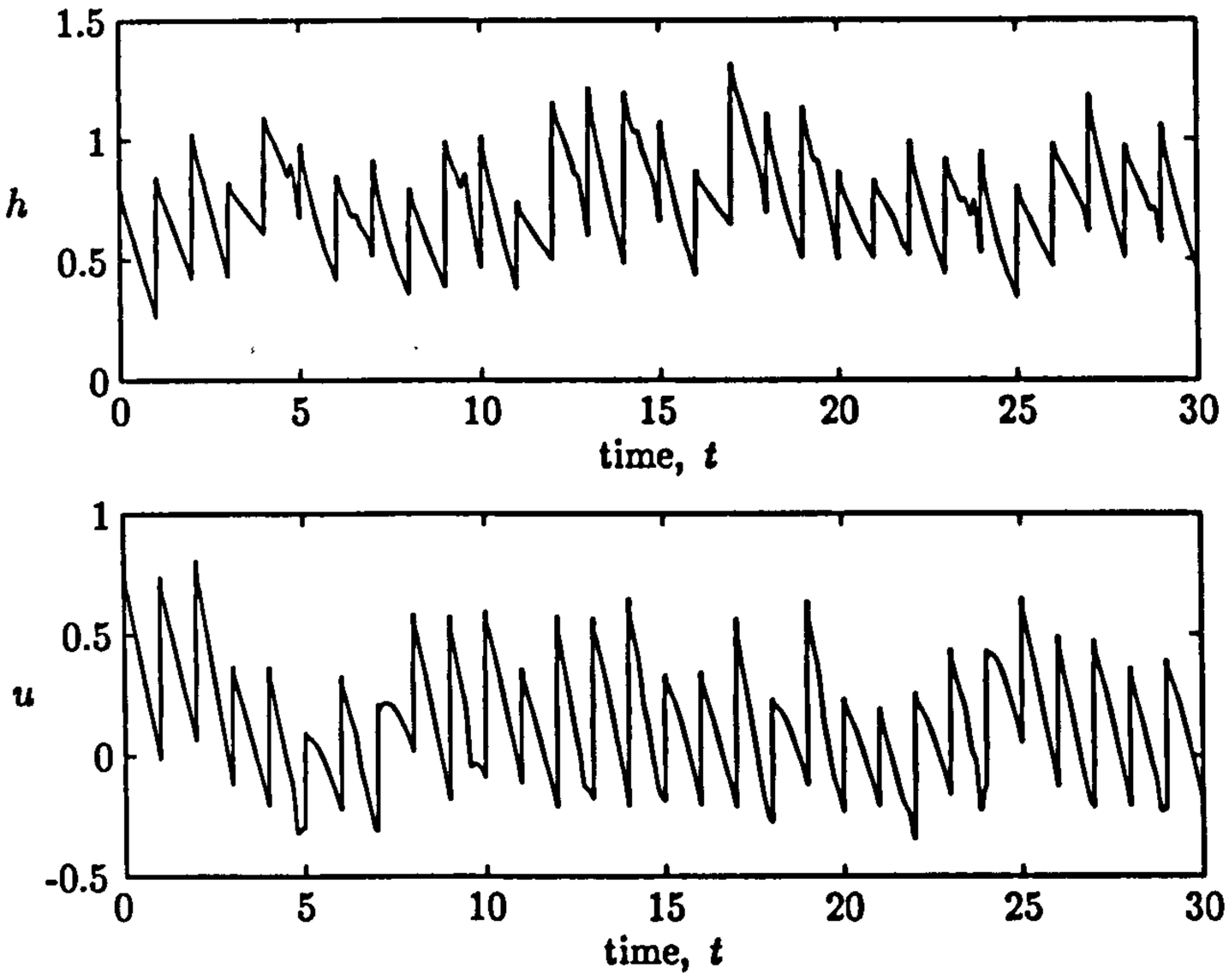

Figure 6.13: Height and velocity profiles at the seaward boundary as a function of time. Forcing is 1.0 and $\alpha_i = 3.3$. Overtopping case of swash from bores of random amplitudes.

There are differences between these profiles and the ones in the non-overtopping case, shown in figure 5.27. The main differences arise from the fact that there are less interactions in the swash zone due to the introduction of overtopping. As the truncation point is increased, the two profiles begin to become more similar.

The shoreline motion in the case $t_f = 4.0$ is shown in figure 6.16. We see that as in the non-overtopping case, there is one wave per swash event. As the truncation point increases the shoreline motion is tending to the shoreline motion shown in figure 5.28.

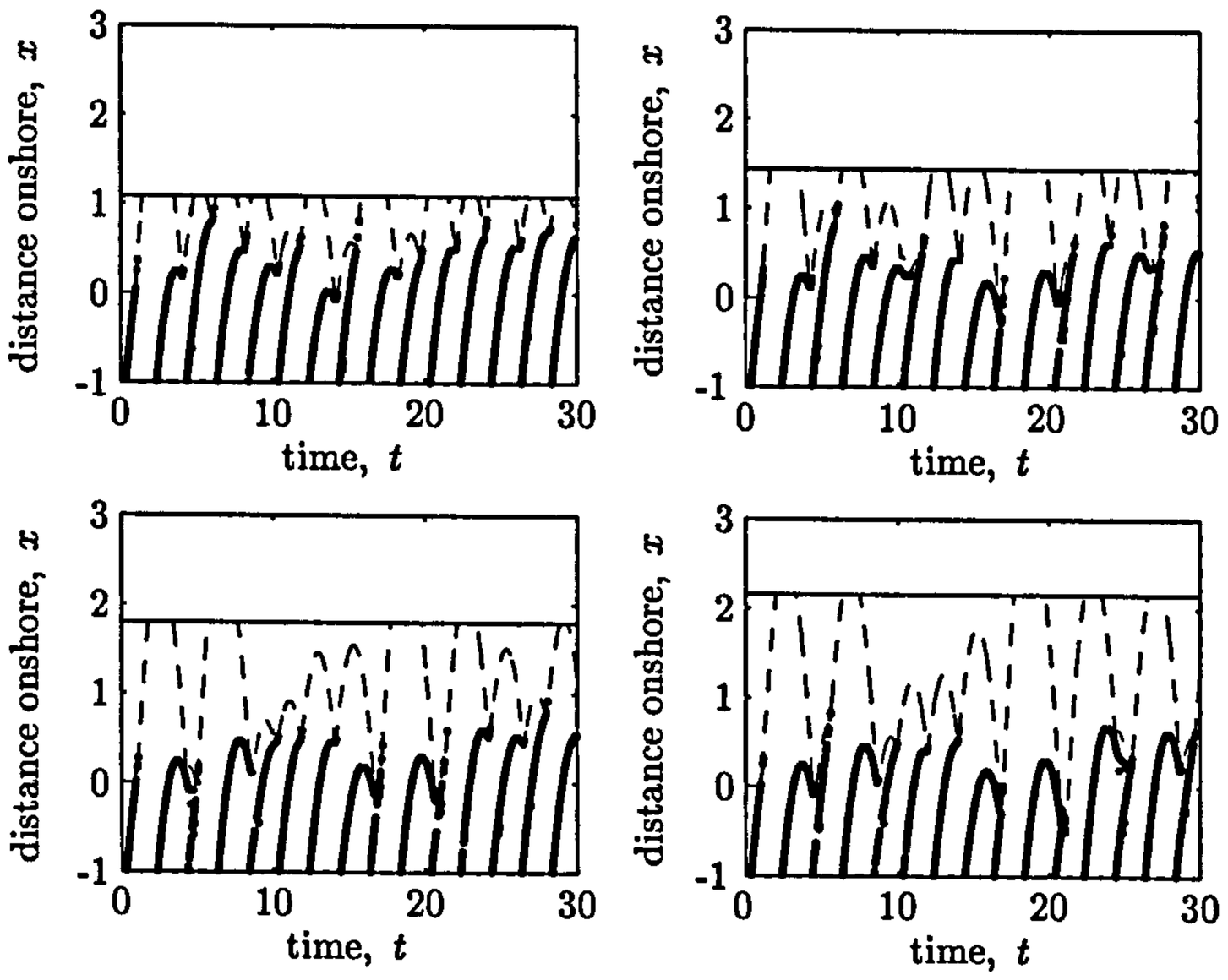

Figure 6.14: Overtopping of random swash with forcing period 2.0. Truncation points at $x = 1.1$, 1.4, 1.8, 2.2. Swash from bores of random amplitudes.

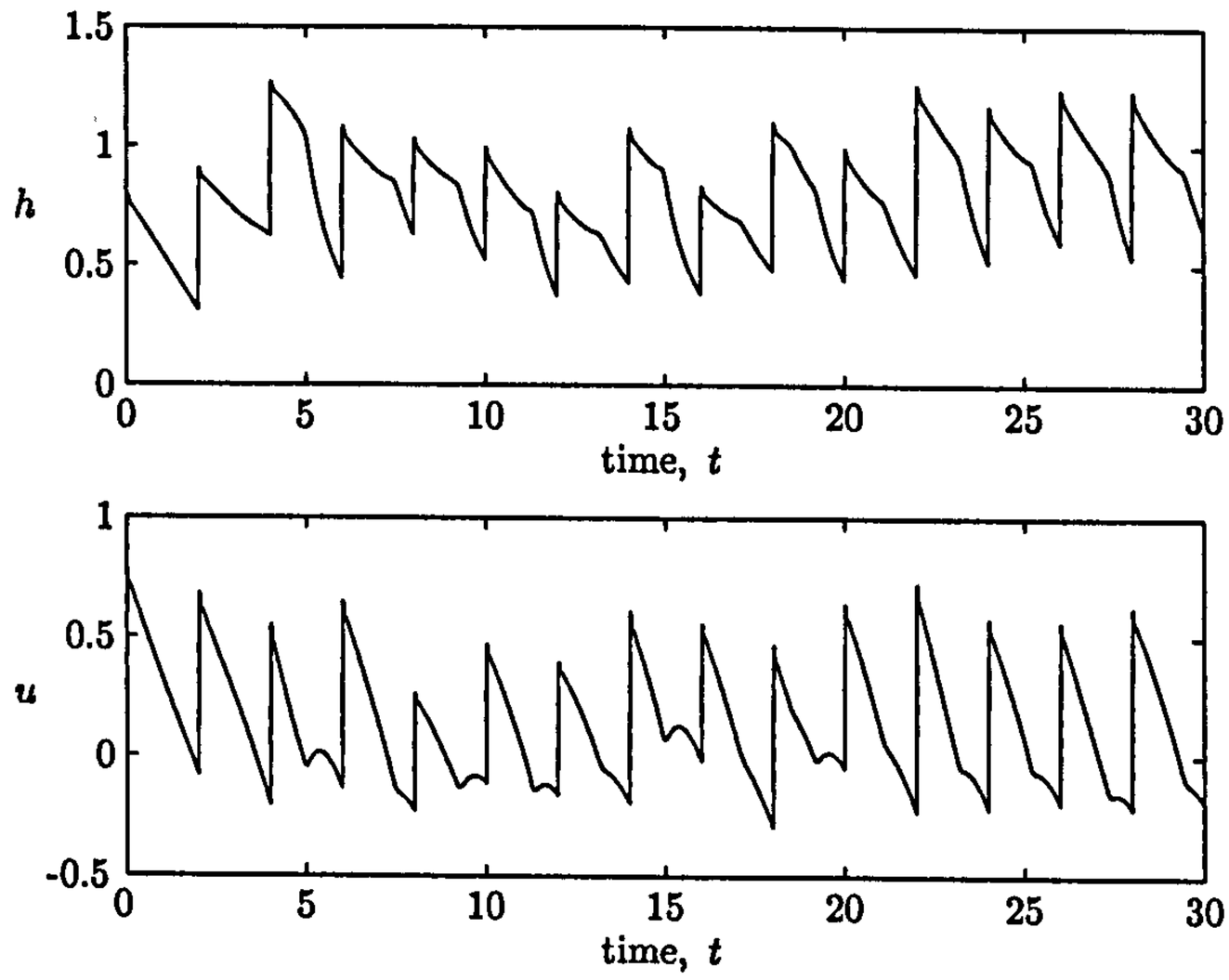

Figure 6.15: Height and velocity profiles at the seaward boundary as a function of time. Forcing is 2.0 and $\alpha_i = 3.3$. Overtopping case of swash from bores of random amplitudes.

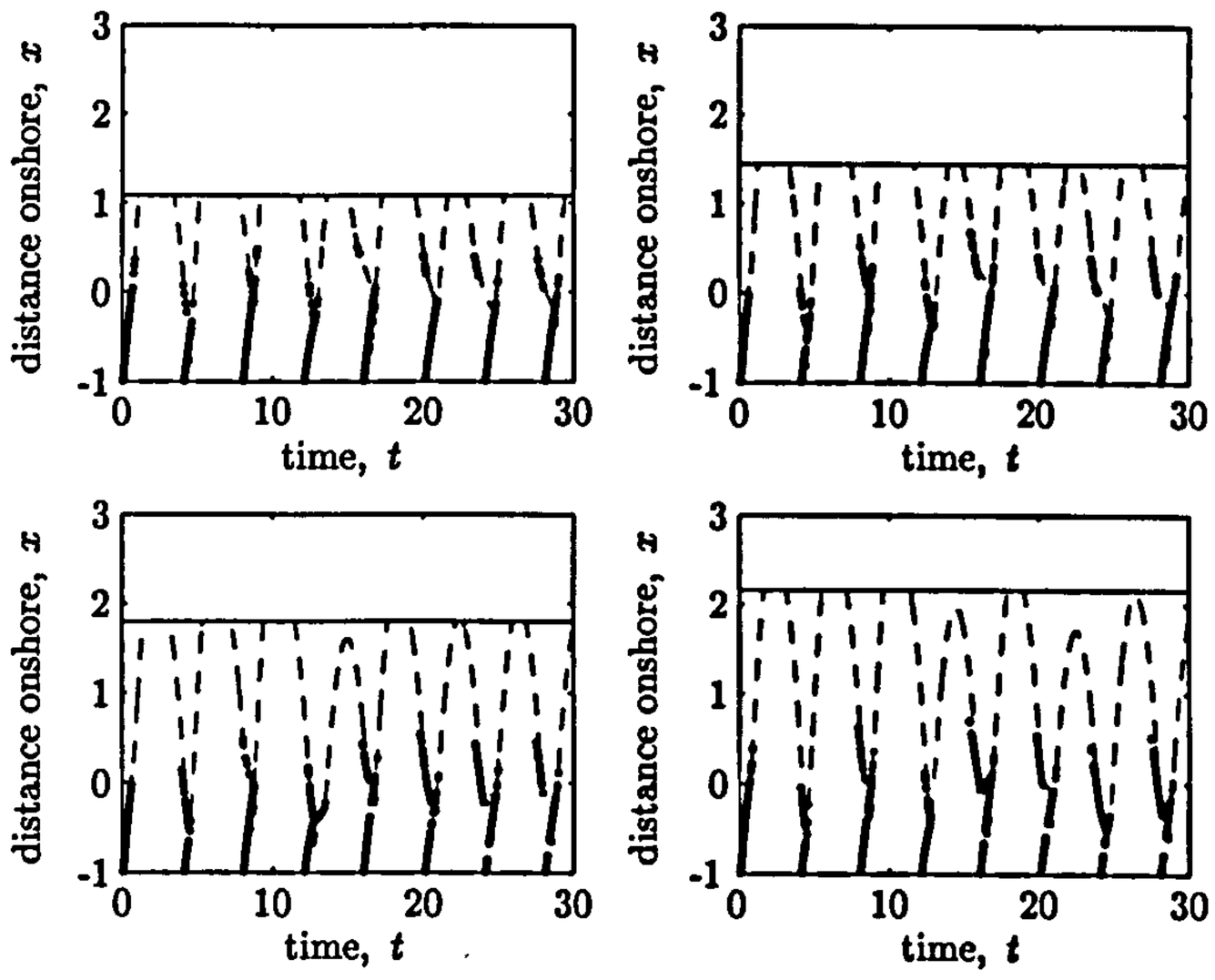

Figure 6.16: Overtopping of random swash with forcing period 4.0. Truncation points at $x = 1.1, 1.4, 1.8, 2.2$. Swash from bores of random amplitudes.

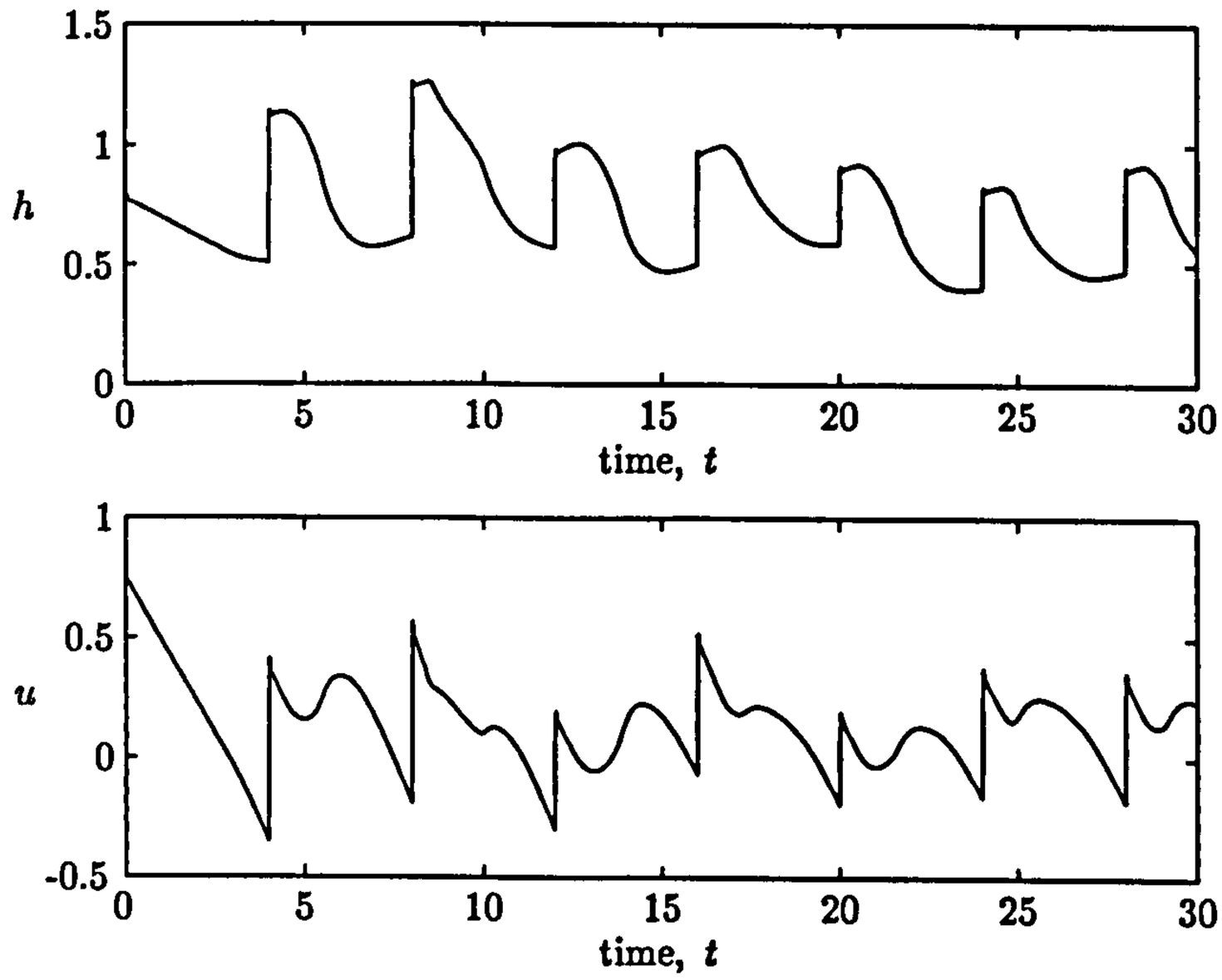

Figure 6.17: Height and velocity profiles at the seaward boundary as a function of time. Forcing is 4.0 and $\alpha_i = 3.3$. Overtopping case of swash from bores of random amplitudes.

6.3.1 Flux comparison

Now that the shoreline positions have been found as functions of time, the next step is to calculate the flux of the flow at each truncation point. As in the case of swash from bores of equal amplitudes, which is given in section 6.2.1, we plot a comparison with the flux past the same point when there is no overtopping.

The flux past the points $x = 1.1,\ 1.4,\ 1.8$ and 2.2 in the case $t_f = 1.0$ is shown in figure 6.18. We see from these plots that the flux from the first swash events compare well in both the overtopping and non-overtopping cases. We also notice that the flux is higher in the non-overtopping case. We see from figure 6.18 that the non-overtopping case is significantly different from the overtopping case.

The flux comparison in the case $t_f = 2.0$ is shown in figure 6.19. Again we see that the fluxes in the overtopping and non-overtopping cases are significantly different. As in all previous examples the flux from the first event compares well for overtopping and no overtopping.

We see in the second plot of figure 6.19 that the biggest flux profile, which occurs just before $t = 20$ is also the same in both the overtopping and non-overtopping cases. The first three flux profiles in the third plot also compare well between the two cases. As does the first and third profile in the fourth plot. This might suggest that as the forcing period is increased the better the comparison between the overtopping and non-overtopping is. To see if this is true we consider a higher value of t_f.

The case of $t_f = 4.0$ is shown in figure 6.20. We now see that in this case the fluxes from both the overtopping case and the no overtopping case compare very well. In fact when the truncation point is at $x = 1.1$, we see that all fluxes except the last compare very well. We also see from the other truncation points that the comparison between overtopping and no overtopping is very good.

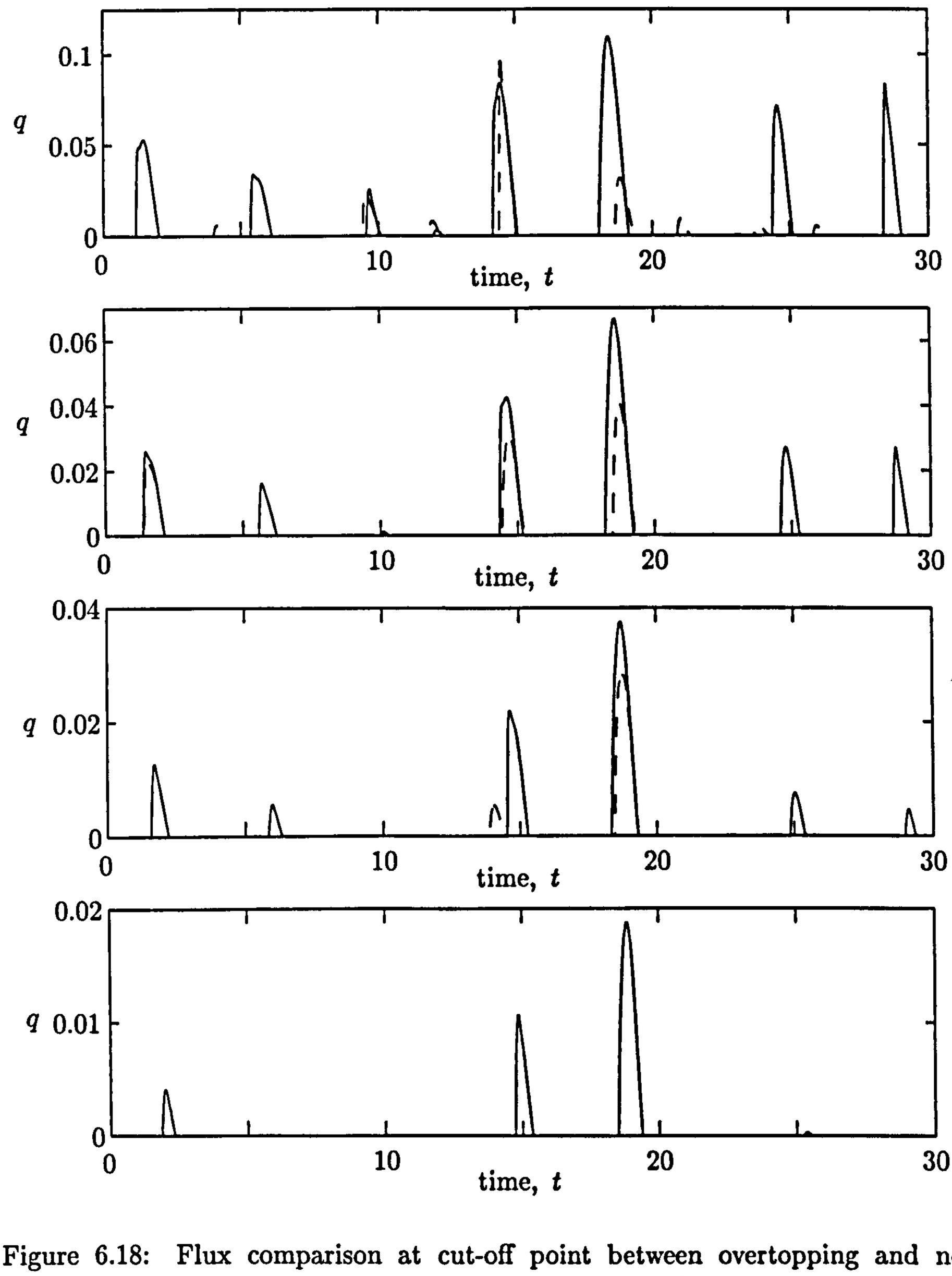

Figure 6.18: Flux comparison at cut-off point between overtopping and non-overtopping data. Cut-offs at $x = 1.1$, 1.4, 1.8 and 2.2. Forcing period is $t_f = 1.0$. Swash from bores of equal amplitudes. Overtopping data (- -), non-overtopping data (–).

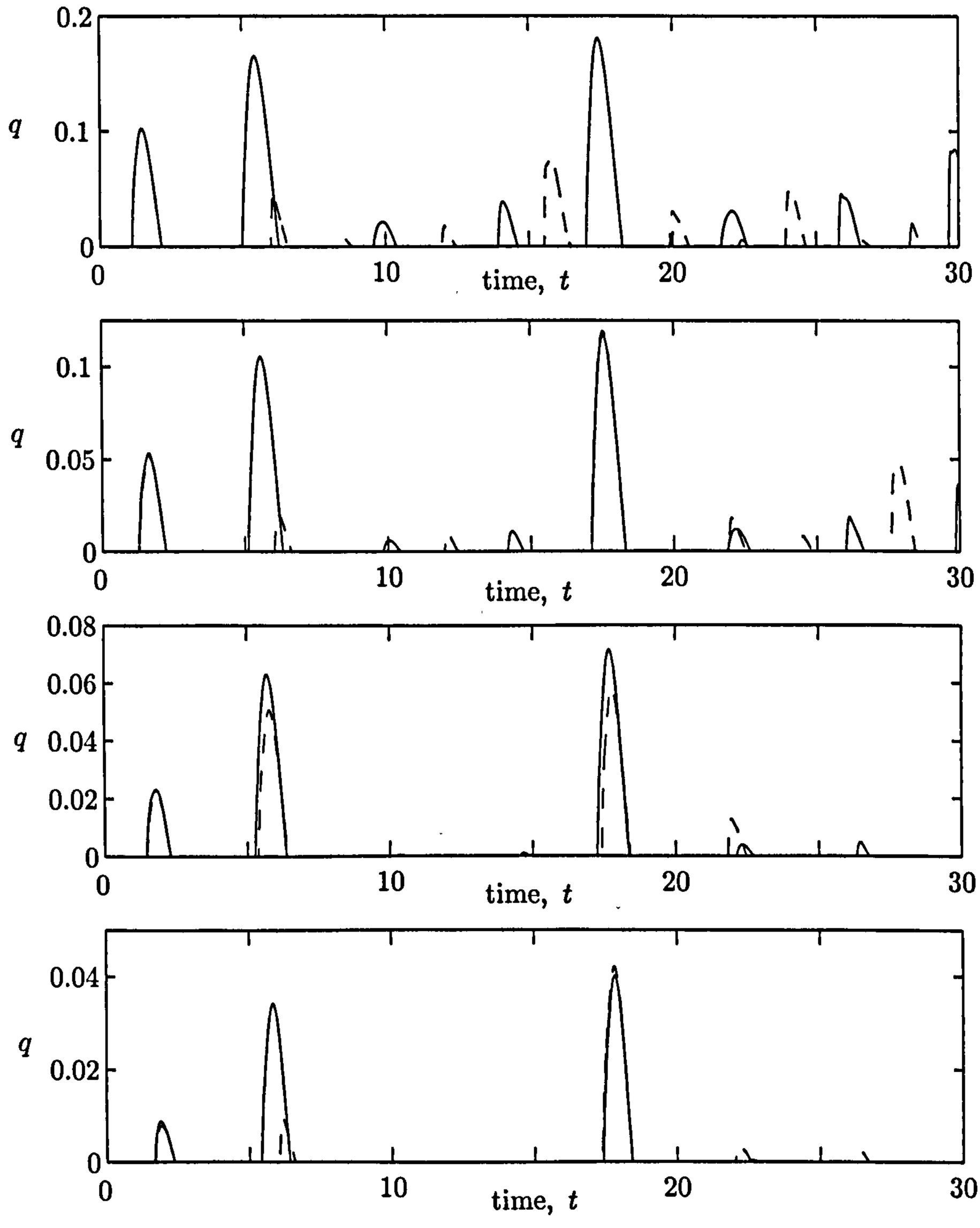

Figure 6.19: Flux comparison at cut-off point between overtopping and non-overtopping data. Cut-offs at $x = 1.1$, 1.4, 1.8 and 2.2. Forcing period is $t_f = 2.0$. Swash from bores of equal amplitudes. Overtopping data (- -), non-overtopping data (–).

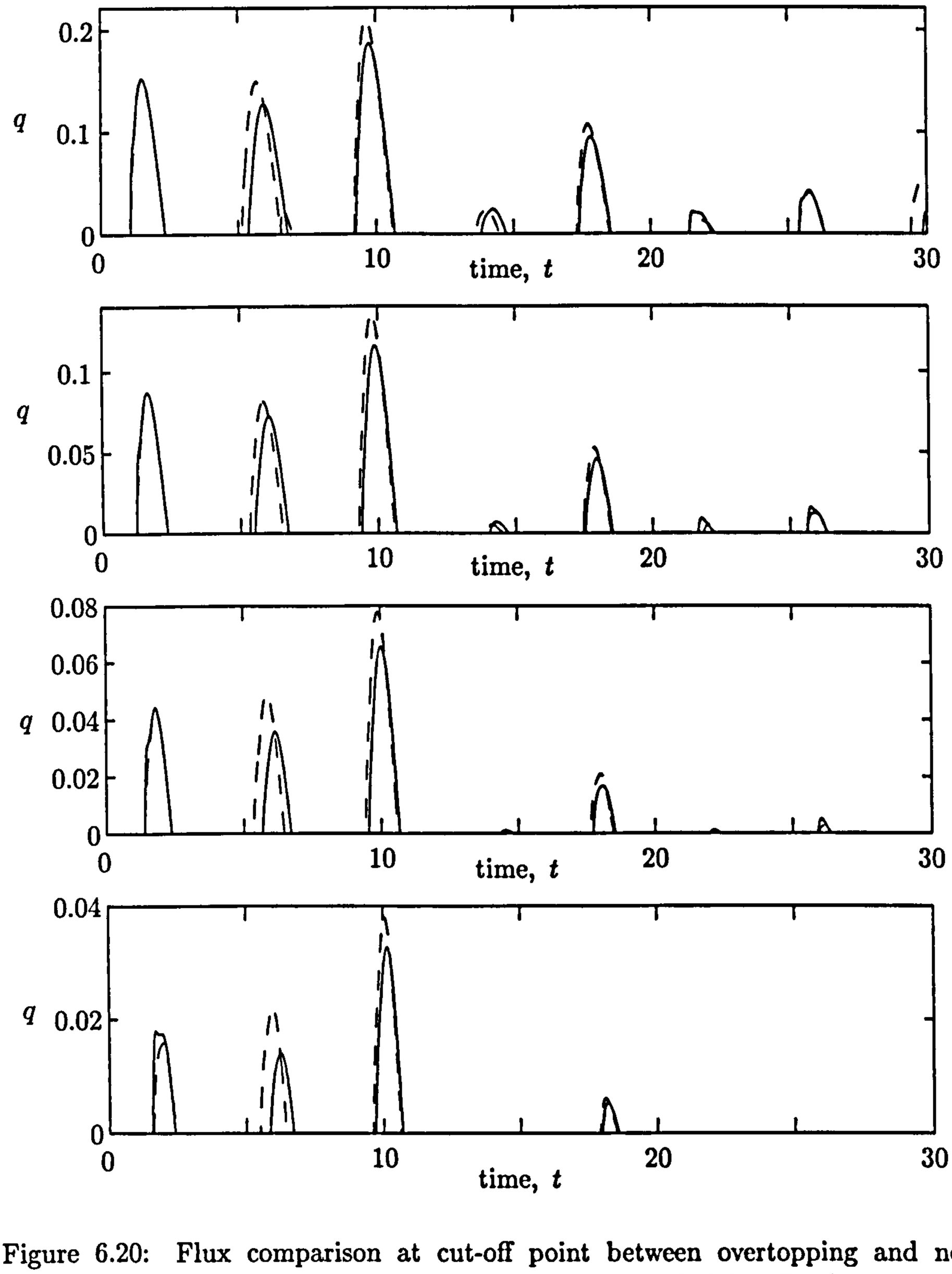

Figure 6.20: Flux comparison at cut-off point between overtopping and non-overtopping data. Cut-offs at $x = 1.1$, 1.4, 1.8 and 2.2. Forcing period is $t_f = 4.0$. Swash from bores of equal amplitudes. Overtopping data (- -), non-overtopping data (–).

6.3.2 Volumes of overtopping

With the form of the flux known at the truncation point we integrate the flux over a given time interval to find the volume of overtopping. The form of the integral is given by equation (6.2.1).

The volume of overtopping plotted against the cut-off point $x = E$ is given in figure 6.21. As in figure 6.10 we see that the form of each plot in figure 6.21 is similar to the case of overtopping from a single swash event.

As in the case of swash from bores of equal amplitudes, given in section 6.2.2, we also plot the total volume of overtopping on a logarithmic scale. This is because that in some circumstances even a small amount of overtopping may be important. This plot is given in figure 6.22. In these examples the time interval over which we integrate is $[0, 30]$, and the interval over which the truncation point is considered is $[1, 2.5]$.

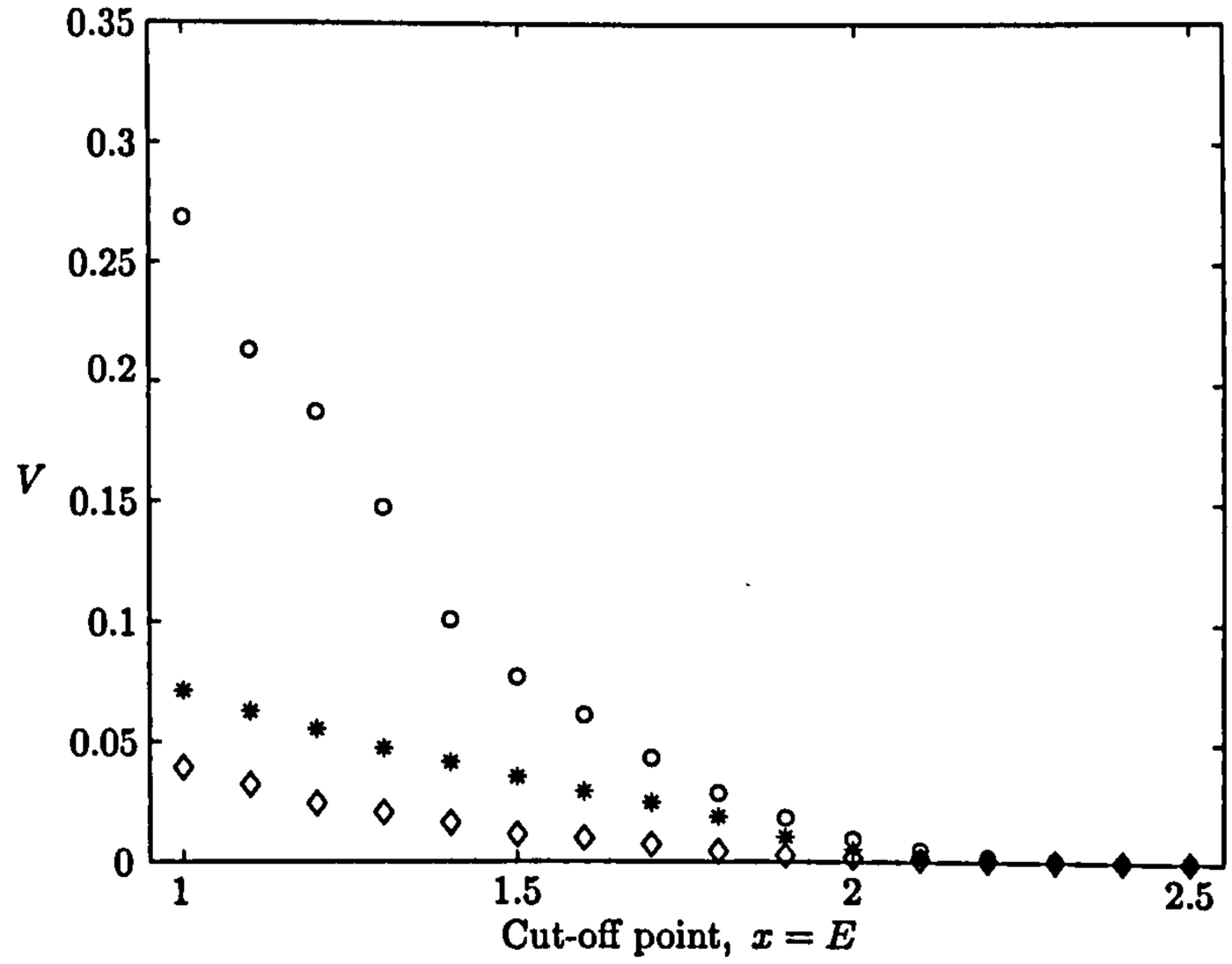

Figure 6.21: Volume of overtopping against cut-off position $x = E$. $\diamond$ is for $t_f = 1.0$. $*$ is for $t_f = 2.0$ and $\circ$ is for $t_f = 4.0$. Swash from bores of random amplitudes.

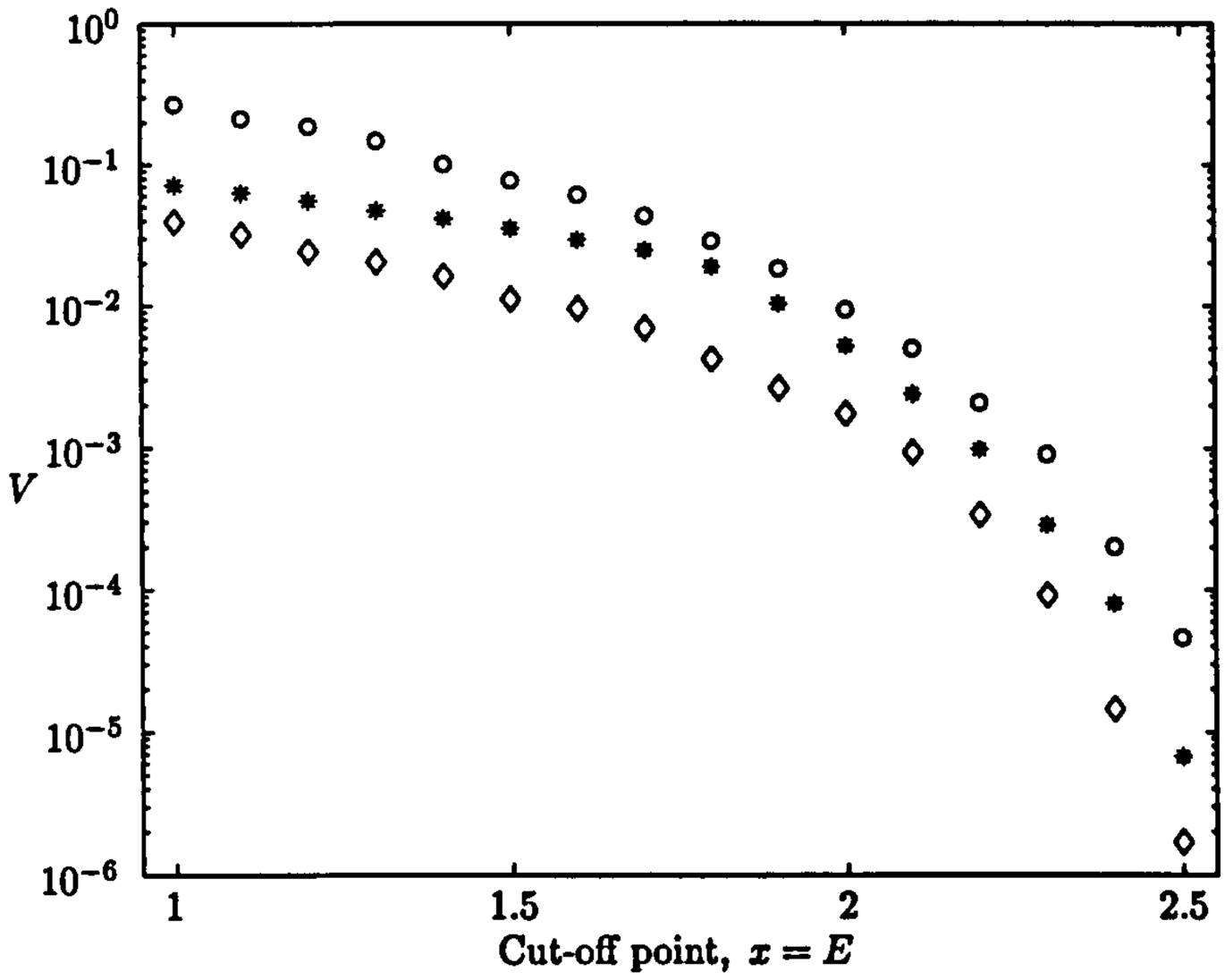

Figure 6.22: Volume of overtopping against the cut-off position $x = E$ on a logarithmic scale. $\diamond$ is for $t_f = 1.0$. $*$ is for $t_f = 2.0$ and $\circ$ is for $t_f = 4.0$. Swash is from bores of random amplitudes.

The three different forcing periods, which have already been considered above are used. The volume of overtopping as a function of the truncation point for the cases $t_f = 1.0$, 2.0 and 4.0 is shown in figures 6.21 and 6.22. As in the cases of section 6.2 we see that the results for multiple swash events are very similar as those given in chapter 3 for single swash events.logarithm of the volume and the position of the truncation point.

We see that as the value of t_f increases the total amount of overtopping also increases. This is exactly the same as what we found in section 6.2.2 for swash from bores of equal amplitudes.

For each considered truncation point we plot the total volume of overtopping as a function of the forcing period t_f, where t_f is allowed to vary between 1.0 and 4.0. The truncation points considered are as those shown in the diagrams in sections 6.2 and 6.3, these are $x = 1.1$, 1.4, 1.8 and 2.2. In all these cases the contribution from the first swash event to overtop the edge is ignored.

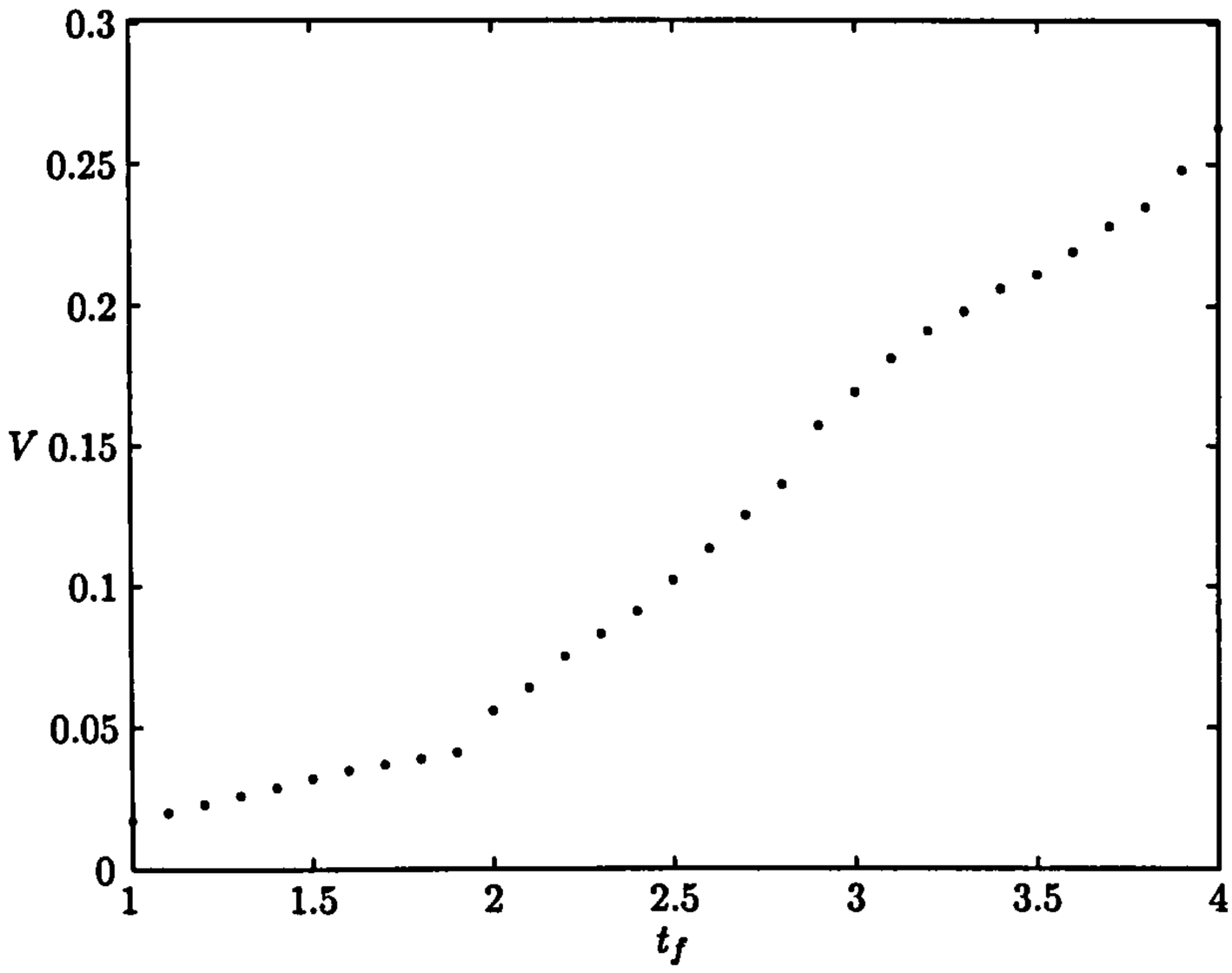

Figure 6.23: Volume of overtopping against the forcing period t_f. Cut-off is taken at $x = 1.1$. Swash is from bores of random amplitudes

The case when the truncation point is at $x = 1.1$ is shown in figure 6.23. We see that a linear relationship could possibly be used to describe the relationship between the volume of overtopping and the forcing period t_f. Looking closer at the figure we notice that there seems to be two linear relationships in the data, one for $1.0 < t_f < 2.0$ and one for $2.0 < t_f < 4.0$. This is realised further as we increase the value of the truncation point.

The case when the truncation point is at $x = 1.4$ is shown in figure 6.24. As stated in the case $x = 1.1$, there are two linear relationships between the two sets of data. The two relationships are in the same intervals of t_f as in the case when the truncation point is 1.1. In the case shown in figure 6.24 the jump in the volume between $t_f = 1.9$ and $t_f = 2.0$ is smaller than in the case shown in figure 6.23. This is down to the fact that as the truncation point increases, the volume of overtopping decreases.

It should be noted that the scales over which the four figures 6.23-6.26 are plotted are not the same. The jumps seen in these plots look like they are increasing but in

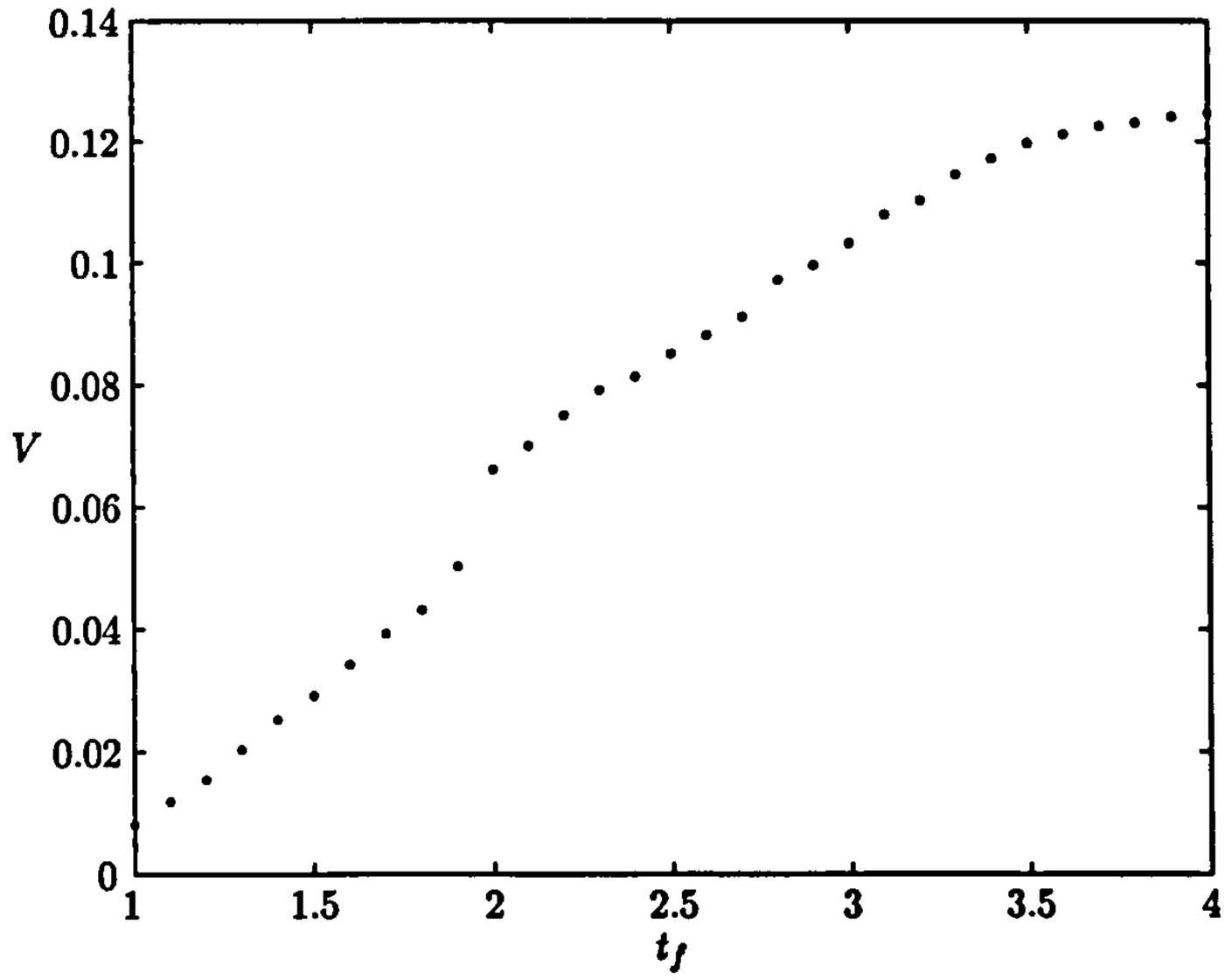

Figure 6.24: Volume of overtopping against the forcing period t_f. Cut-off is taken at $x = 1.4$. Swash is from bores of random amplitudes

fact this is just a consequence of the chosen scales. It could be argued that in fact there are three linear relationships seen in figures 6.23-6.26. There seems to exist another possible linear relationship for $t_f > 3.0$. A reason for this relationship is unclear but could be a consequence of the amount of waves which are present in each swash event. There seems to be one relationship for when there are on average two waves per swash event, one relationship for one wave per swash event, and one relationship for when the number of waves per swash event is between one and two.

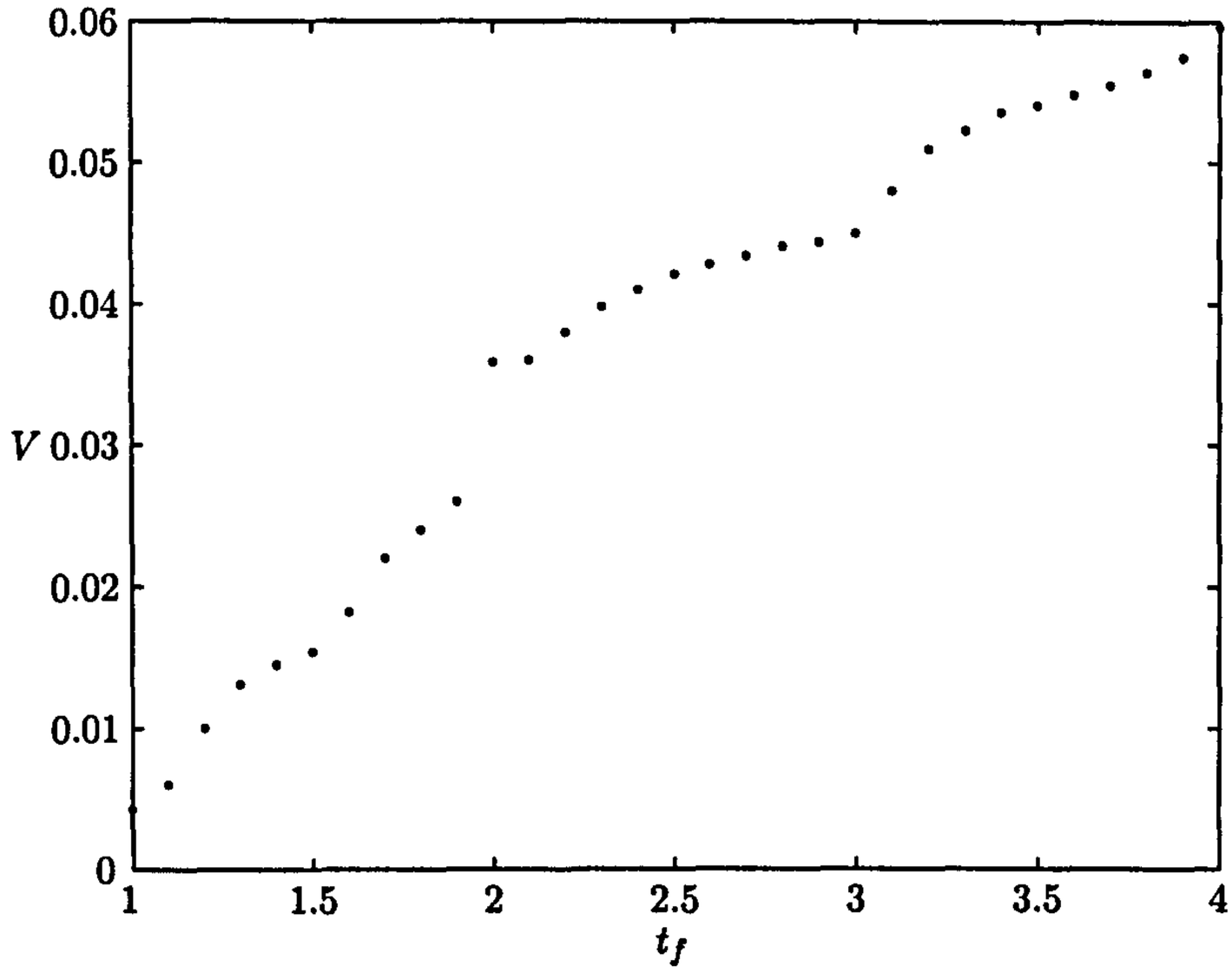

Figure 6.25: Volume of overtopping against the forcing period t_f. Cut-off is taken at $x = 1.8$. Swash is from bores of random amplitudes

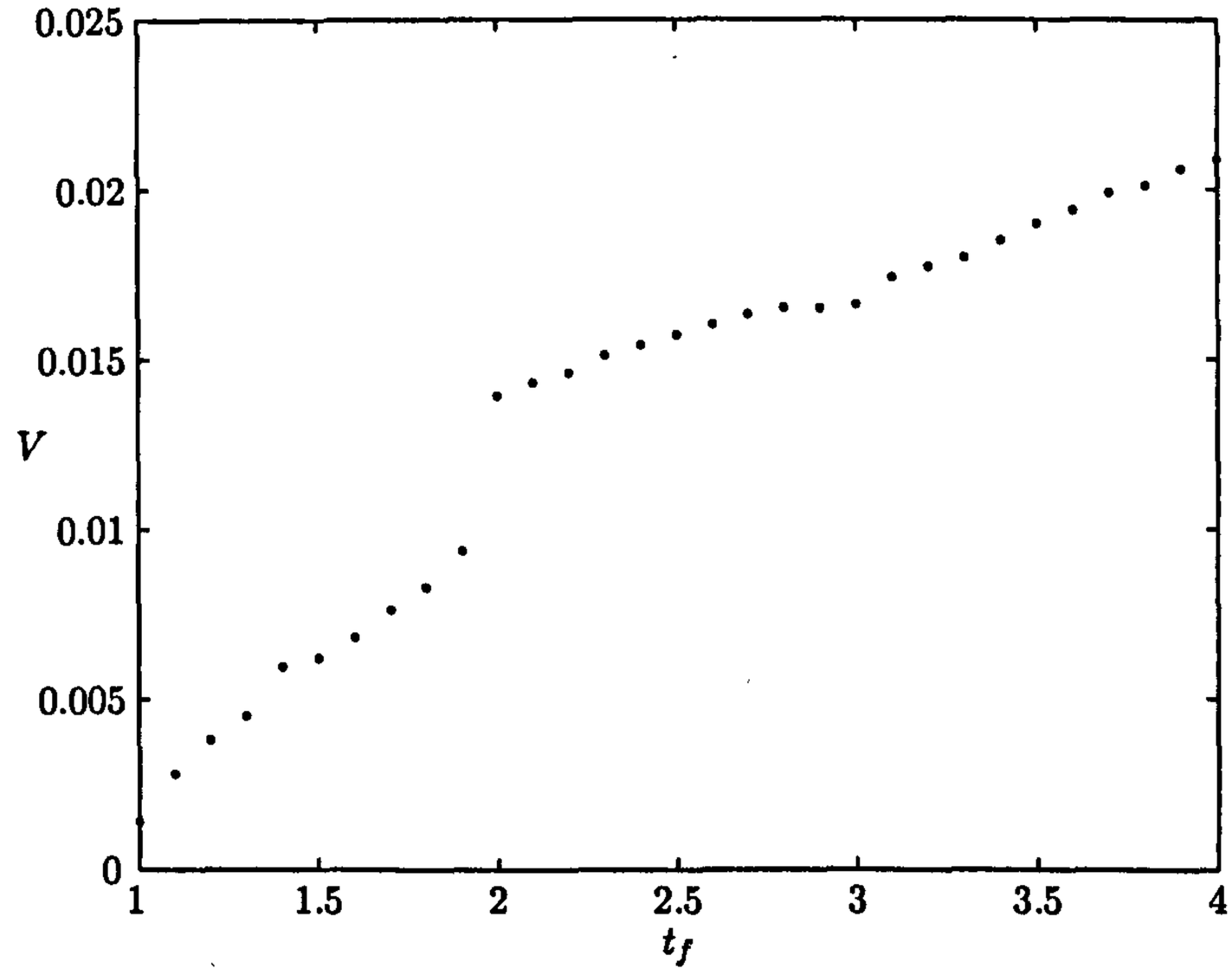

Figure 6.26: Volume of overtopping against the forcing period t_f. Cut-off is taken at $x = 2.2$. Swash is from bores of random amplitudes

6.4 Random, non-periodic bores

The results for non-periodic bores are very similar to the results for bores of random amplitudes. For example a set of results with random forcing period between 1.0 and 2.0 has an average forcing period of 1.5. Thus we could replace the varying time period with the fixed average amount. Doing this we find that the average run-up height period over the time interval considered are nearly exact. It is for this reason that the overtopping results for swash from non-periodic bores are not discussed any further.

6.5 Conclusion

The overtopping of the waves produced in chapter 5 was considered in this chapter. We saw how the shoreline motions in each considered case differed from what was seen in chapter 5. In each of the cases considered, the flux past the truncation point on the beach was found and plotted. A comparison between the flux in the overtopping case was compared with the flux past the same point on the beach with no overtopping. The plots were found to be comparable when the forcing period of the incoming waves was large. For small forcing periods though, the fluxes in the two cases are very different.

With the flux known, the volume of water to overtop the beach truncation point was calculated for a fixed time interval. For different values of the truncation point, the volume was calculated and plotted on a logarithmic scale. The figures produced, showed a linear relationship between the logarithm of the volume of overtopping and the truncation point $x = E$. Thus an exponential relationship is found between the volume and the truncation point. A relationship of this type was hoped to be found, since most overtopping models used by other authors are in an exponential form.

The volume of overtopping was also plotted as a function of t_f, the forcing period of the incoming waves. As the forcing period increased, the volume of overtopping was seen to increase. In these plots two linear relationships were found for different intervals of the forcing period. The first interval corresponds to two waves per swash

event and the second interval corresponds to one wave per swash event.

The relationships found are very promising, in that they seem to reflect the trends seen in existing overtopping models based on laboratory experiments.

Chapter 7

The overtopping of a vertical wall by a thin jet

7.1 Introduction

The motivation for this work comes from some experiments, which took place in Hannover between the 27th and 28th of February 2003 and between 30th June and 4th July 2003. The large wave flume was setup to consider the interaction of violent waves with a wall. As seen in figure 7.1, a thin sheet of water shoots into the air, very much like a jet flow. This sheet flow is very rapid and the pressures against the wall are very high, see Cooker & Peregrine (1990). In experiments of this type there is always an amount of water which overtops the wall rather than falling back into the flume. In this chapter we estimate the amount of water that overtops a vertical wall. In the example shown in figure 7.1, it should be noted that the velocity of the upward jet was so high that it in fact damaged the roof.

Previous studies of overtopping at vertical walls have been done in small scale experiments, see Franco et al. (1994) and Juhl & Sloth (1994). A theoretical and numerical approach has been made by Jervis & Peregrine (1996). In this work, the impact on a vertical wall is modelled by considering the symmetrical collision of two steep solitary waves. This flow is an appropriate model for a jet of water projected up the face of a vertical wall. This part of the flow is solved numerically using the

program of Cooker, Peregrine, Vidal & Dold (1990), which is based on the accurate flow solver of Dold & Peregrine (1986) for inviscid, irrotational and incompressible flow. To model flow after it passes the top of the wall, Jervis & Peregrine (1996) assumed that once a jet is formed, the motion of any fluid particle in the jet is governed by its initial momentum and gravity. Thus portions of fluid are modelled by considering their motion once above the crest of the wall as if they are a free particle moving under gravity.

To calculate the amount of overtopping, the method of Jervis & Peregrine (1996) was to take horizontal slices of water as they passed the top of the wall. They then proceed to calculate the horizontal momentum of each element. They treated each element as a particle moving freely under gravity, then they considered each element as it returned to the level of the top of the wall. The position of the centre of mass of each element was used to decide if any water passed horizontally over the wall. The total volume was calculated from adding the contribution from each element.

The situation to be considered is modelled in three parts. The first part examines how a thin jet travels up and along a vertical wall. This type of flow is known as a wall flow. Flows of this type have been considered in the past by Keller & Weitz (1952), Keller & Geer (1973) and Geer & Keller (1979). In these papers asymptotic methods are used to find a series expansion representation for the flow. A connection was also found for when a wall flow becomes a jet flow. It is this situation that we consider in the second part of the flow. Once the jet along the wall separates from the wall at the top, the flow becomes a jet flow. Keller & Geer (1973), Geer & Keller (1979), Geer & Strikwerda (1980) and Strikwerda & Geer (1980) consider flows of this kind, when wall flows become jet flows. Outer expansions are found for both flows away from the junction of the two flows. These solutions are then matched to the inner expansions for the flow near the junction between the flows.

In the second part of the model, we consider the shape that the flow takes after the wall flow reaches the top of the wall. Once solutions for this flow are found, we then consider the third part of the model. In this part the jet in free fall is considered, with a model of how the jet then interacts with the wall on its way

down. From this part of the solution an expression can be found for the amount of water that may overtop the wall.

Since we consider thin jets in which the distance that the water jet travels in the vertical direction is much larger than the jet width, we invoke shallow water theory to model the jet flow part of the model. If a solution is known for the wall flow it can be used as an initial condition for the jet flow.

In section 7.2 the jet flow part of the problem is solved for a general wall flow. It is assumed that the velocity and jet width of the wall flow is known at the top of the wall, so that the shallow water equations can be solved for the jet flow.

In section 7.3 a solution from Longuet-Higgins (1976) is introduced, which is based on a solution by John (1953). This solution is for a parabolic free surface contracting as it moves in the horizontal direction. The solution of Longuet-Higgins (1976) is modified in section 7.4 to model how the parabolic free surface solution changes when the flow is considered to be in free fall. The parabolic free surface will then move in the vertical direction under the influence of gravity. One half of this new parabolic free surface is taken to model the wall flow. This solution is chosen since the free surface contracts and becomes thinner as time increases and thus seems to give a good model of flow along a wall. The jet flow that emanates from this solution is also described in section 7.5, with solutions for the jet width, jet velocity and the horizontal distance covered by the jet given.

The final part of the model is solved in section 7.6. From the results of section 7.5, we can model the jet as its falling back down to the top of the wall. The width and the position of a jet element over the wall is found in section 7.5. With these solutions an expression is found for the amount of water that may overtop a wall of fixed height.

Finally in section 7.7, the results of the preceding sections are brought together in a discussion.

Figure 7.1: Violent wave impact against a wall. Taken from experiments in Hannover 27/2/03. (Picture courtesy of D.H. Peregrine)

7.2 General wall flow

In this section we consider how to find the jet flow that emanates from an analytic wall flow. A wall flow is considered to be the type of flow that arises when a jet is climbing a wall. We consider only analytical solutions here. A numerical approach has been considered previously by Jervis & Peregrine (1996) using the boundary integral method.

Consider a wall flow with free surface given analytically by $y = f(x,t)$, where y is in the vertical direction, x is in the horizontal direction and t is time. We assume here that $y = f(x,t)$ is a single valued function. For a given free surface y, one can find and expression for the jet width along the wall x, in terms of y and t i.e. $x = k(y,t)$.

Since we are interested in thin jet flows, we choose the height of our wall to be greater than the wave amplitude. So that we can invoke the shallow water equations, the length of the jet in the vertical direction must be much greater than the jet width along the wall. A depiction of the setup is given in figure 7.2.

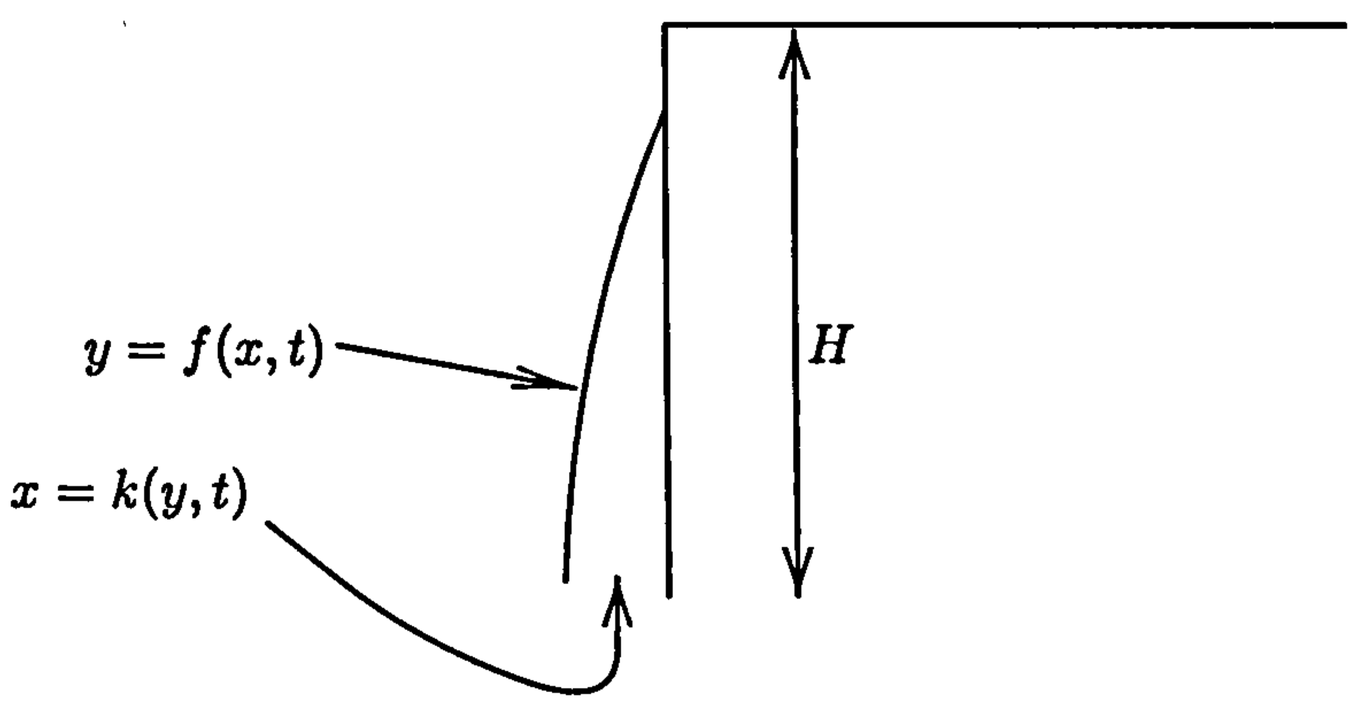

Figure 7.2: Setup of initial wall flow

Suppose the form of the wall flow is known. From this flow an expression for the jet width x along the wall can be found by rearranging the given wall flow for x. Consider a wall of height H, then we can say that at the top of the wall $y = H$, $t = \tau$ and $x = W$, where $W = k(H,\tau)$. τ is defined to be the time at which the

wall flow feeds the jet flow. For the jet flow past the top of the wall, each τ labels a point on the jet. These conditions act as a initial condition for the subsequent flow past the top of the wall. Before we invoke the shallow water approximations we must also specify the horizontal and vertical components of velocity, of the flow. If a velocity potential ϕ is known for the flow, then we simply have $u = \dfrac{\partial \phi}{\partial x}$ and $v = \dfrac{\partial \phi}{\partial y}$, where u and v are the horizontal and vertical components of velocity of the flow along the wall. If the velocity potential is unknown, then an expression for both velocities must be specified.

7.2.1 Jet flow above the wall

We now assume that an analytic expression for the wall flow $y(x,t)$, the jet width along the wall $x = k(y,t)$ and velocities $u(x,t)$ and $v(y,t)$ are known from the offset. We assume that the jet length is much greater than the jet width, thus the shallow water approximation is invoked, the shallow water equations in this case are:

$$\frac{\partial b}{\partial t} + \frac{\partial (vb)}{\partial y} = 0 \tag{7.2.1}$$

and

$$\frac{\partial v}{\partial t} + v\frac{\partial v}{\partial y} = -g, \tag{7.2.2}$$

where b is the jet width, v is the vertical jet velocity, y is the vertical direction and t is time. The momentum equation (7.2.2) can be solved directly using the method of characteristics. Doing so we find the characteristics are

$$\frac{\mathrm{d}y}{\mathrm{d}t} = v \qquad \text{on which} \qquad \frac{\mathrm{d}v}{\mathrm{d}t} = -g. \tag{7.2.3}$$

On each of these characteristics we have τ = constant. Thus each characteristic correponds to following an individual jet element.

For bounds on τ we need an expression for the time at which the jet is first at the top of the wall. This time is our lower bound on τ. Since τ is defined to be the time at which the wall flow influences the jet flow, an upper bound on τ is found when the vertical velocity of the wall flow reduces to zero at the top of the wall. At this time the wall flow no longer influences the jet flow and thus it is an upper

bound on τ. Each τ between these bounds corresponds to a slice or element of the jet.

The second expression in (7.2.3) implies that $v = -gt + \text{constant}$. Now when $t = \tau$, $v = v(\tau) = V(\tau)$ and $y = H$. Thus our expression for the vertical velocity above the wall is

$$v = V(\tau) - g(t - \tau). \tag{7.2.4}$$

The first equation in (7.2.3) can now be solved. We have $\frac{\mathrm{d}y}{\mathrm{d}t} = v$, which upon integration using $t = \tau$ when $y = H$ gives an expression for y, the vertical position of a jet element, as

$$y = (t - \tau)V(\tau) - \frac{g}{2}(t - \tau)^2 + H. \tag{7.2.5}$$

Each τ in the above expression gives the vertical position of the corresponding jet element as a function of time. When $V(\tau)$ is known, τ can be found in terms of y and t. Then one can find an expression for $v(y, t)$.

Now that an expression for v is known we can solve equation (7.2.1) also using the method of characteristics. It has the same characteristics

$$\frac{\mathrm{d}y}{\mathrm{d}t} = v \qquad \text{on which} \qquad \frac{\mathrm{d}b}{\mathrm{d}t} = -b\frac{\partial v}{\partial y}. \tag{7.2.6}$$

The first of these differential equations has already been solved, so we are left to consider $\frac{\mathrm{d}b}{\mathrm{d}t} = -b\frac{\partial v}{\partial y}$. Separating the variables and integrating we find

$$b = b_0 \exp\left(-\int_{t_w}^{t} \frac{\partial v}{\partial y}\,\mathrm{d}t\right), \tag{7.2.7}$$

where b_0 is a constant to be determined. Now letting $V_\tau = \frac{\mathrm{d}V}{\mathrm{d}\tau}$, we find

$$\frac{\partial v}{\partial y} = \frac{\partial v}{\partial \tau}\frac{\partial \tau}{\partial y} = \frac{V_\tau + g}{(V_\tau + g)(t - \tau) - V}. \tag{7.2.8}$$

Thus integrating the above with respect to t, we find

$$\int_{t_w}^{t} \frac{\partial v}{\partial y}\,\mathrm{d}t = \ln\left(\frac{(V_\tau + g)(t - \tau) - V}{(V_\tau + g)(t_w - \tau) - V}\right), \tag{7.2.9}$$

which finally gives us

$$b = b_0 \exp\left(-\int_{t_w}^{t} \frac{\partial v}{\partial y}\,\mathrm{d}t\right) = \frac{b_0[(V_\tau + g)(t_w - \tau) - V]}{(V_\tau + g)(t - \tau) - V}. \tag{7.2.10}$$

Now an expression for b_0 must be found. We know that when $t = \tau$, $y = H$ and $b = W(\tau)$. Thus we find

$$b_0 = \frac{-VW(\tau)}{(V_\tau + g)(t_w - \tau) - V}. \tag{7.2.11}$$

So our expression for the width of the jet in the subsequent motion above the wall is

$$b = \frac{W(\tau)V}{V - (V_\tau + g)(t - \tau)}. \tag{7.2.12}$$

7.2.2 Downward motion

We already know that the time at which the flow passes the top of the wall is given by $t = \tau$, we now need to find the time at which each jet element hits the top of the wall on it's way down. To find this time we rearrange and solve equation (7.2.5) for t in terms of τ. Doing so we find that $t = \tau$, which we already know and $t = \tau + \frac{2V}{g}$. This second time is now denoted by t_i and is known as the impact time.

To find the time at which the vertical position of each jet element is a maximum, we differentiate the expression for y given by equation (7.2.5) with respect to time, t, this gives v. Setting this equal to zero, we find an expression for the time at which each jet element reaches its maximum position. This time is $t_m = \tau + \frac{V}{g}$, at this time the maximum vertical position of each jet element is given by

$$y_m = \frac{V^2}{2g} + H. \tag{7.2.13}$$

The only thing left to find is the horizontal distance travelled by each jet element once it goes over the top of the wall. To find this distance we need to calculate the horizontal momentum of each element. If an expression is known for the horizontal velocity of the jet up the wall u, then one can find an expression for the average velocity of each jet element. The horizontal velocity of each jet element will vary across its width, thus if u is averaged across the total width, we will have a mean horizontal velocity for each element. The horizontal velocity of a jet element is given as

$$\bar{u}(\tau) = \frac{1}{W(\tau)} \int_0^{W(\tau)} |u(\tau)| \, \mathrm{d}t, \tag{7.2.14}$$

where $W(\tau)$ is the width of a jet element at the top of the wall. With an expression for the horizontal velocity of each jet element known, we find an expression for the horizontal distance d, travelled by each jet element as

$$d = \int_\tau^t \left(\frac{1}{W(\tau)} \int_0^{W(\tau)} |u(\tau)| \, \mathrm{d}x \right) \mathrm{d}t = \frac{t-\tau}{W(\tau)} \int_0^{W(\tau)} |u(\tau)| \, \mathrm{d}x. \qquad (7.2.15)$$

7.3 Parabolic free surface: Longuet-Higgins (1976) solution

In this section the solution due to Longuet-Higgins (1976) for fluid with a parabolic free surface is described. The parabolic free surface considered by Longuet-Higgins (1976) was first described by John (1953). It was shown that the flow decreased like t^{-3}, and the free surface contracts about a point which lies one-third of the way from the vertex of the parabola to the focus. The flow is an exact limiting form of either a Dirichlet ellipse or hyperbola, as the time t tends to infinity.

Among the simplest of non-trivial solutions to the time-dependent problem is the flow where the free surface takes the form of a parabola, whose linear dimensions vary as t^{-3} (where t denotes time) and which therefore reduces to a thin sheet as $t \to \infty$. This flow was discovered by John (1953), in whose treatment, however, the nature of the solution is somewhat hidden by the inclusion of gravity in a non-essential way. When viewed in the natural free fall frame of reference it is clear that the flow is self-similar, and that the parabolic surface contracts (or expands) about a fixed point one-third of the distance from the vertex to the focus.

The solution of Longuet-Higgins (1976) for a parabolic free surface is now derived: Consider the velocity potential

$$\phi = \frac{1}{2t}(x^2 - y^2) - \epsilon \frac{x}{t^\lambda}, \qquad (7.3.1)$$

where (x, y) are rectangular co-ordinates, t is the time and ϵ and λ are constants to be determined. Taking the density as unity, we find that the pressure p, from Bernoulli's equation, is given by

$$-p = \frac{y^2}{t^2} - (1-\lambda)\epsilon \frac{x}{t^{\lambda+1}} + \frac{\epsilon^2}{2t^{2\lambda}} + f, \qquad (7.3.2)$$

where f is a function of the time only. Hence the rate of change of p following the particle is given by

$$\frac{\mathrm{D}p}{\mathrm{D}t} = \frac{4y^2}{t^3} - \lambda(1-\lambda)\epsilon\frac{x}{t^{\lambda+2}} + (2\lambda-1)\frac{\epsilon^2}{t^{2\lambda+1}} - \frac{\mathrm{d}f}{\mathrm{d}t}. \tag{7.3.3}$$

At the free surface both p and $\frac{Dp}{Dt}$ must vanish. The vanishing of equations (7.3.2) and (7.3.3) represents the same surface provided the coefficients of corresponding forms are in proportion. Hence, either $\lambda = 1$ or $\lambda = 4$. If $\lambda = 1$ then from equation (7.3.1) we may, by choice of a different frame of reference, take $\epsilon = 0$, so

$$\frac{\mathrm{d}f}{\mathrm{d}t} = -\frac{4}{t}f, \qquad f = -\frac{Q}{t^4} \tag{7.3.4}$$

say. The free surface is then $y = \frac{Q}{t^2}$, which represents two planes parallel to the x axis. Leaving aside this flow, which is described and demonstrated experimentally in Longuet-Higgins (1972*a*), consider the case $\lambda = 4$. The terms in p and $\frac{\mathrm{D}p}{\mathrm{D}t}$ dependent on t alone will then be in proportion to the terms in x provided that

$$\frac{\mathrm{d}f}{\mathrm{d}t} + \frac{4}{t} = \frac{5\epsilon^2}{t^9}, \tag{7.3.5}$$

whence we have

$$f = -\frac{5\epsilon^2}{4t^8} - \frac{Q}{t^4}, \tag{7.3.6}$$

where Q is constant. The velocity potential is now

$$\phi = \frac{1}{2t}(x^2 - y^2) - \epsilon\frac{x}{t^4} \tag{7.3.7}$$

and the free surface is

$$y^2 = -3\epsilon\frac{x}{t^3} + \frac{3\epsilon^2}{4t^6} + \frac{Q}{t^2}, \tag{7.3.8}$$

where ϵ and Q are both constants. For our purposes, we interchange x and y in the above expression for the free surface. A plot of the type of free surface we are interested in is given in figure 7.4. It is this free surface that we decide to work with in the next section.

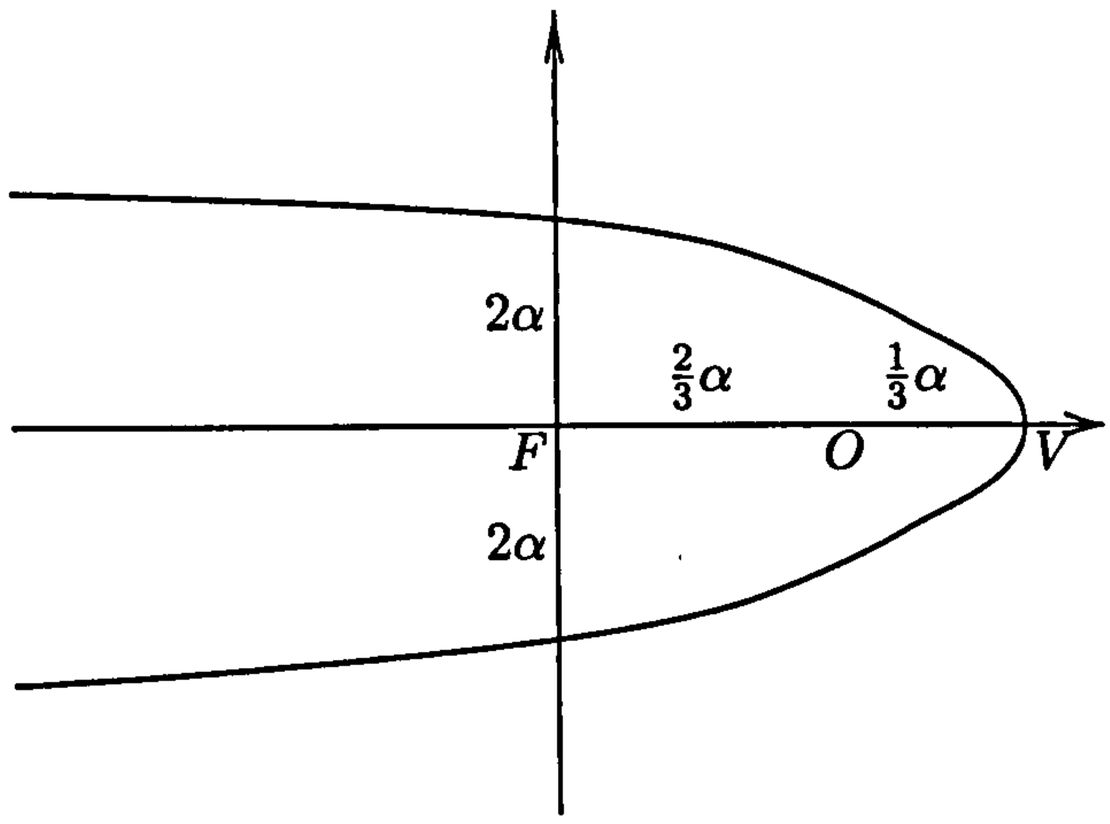

Figure 7.3: A cross-section of the free surface given by Longuet-Higgins (1976). The curve is a parabola which contracts about the point O, lying one-third of the way from V to F. The distance VF is proportional to t^{-3}.

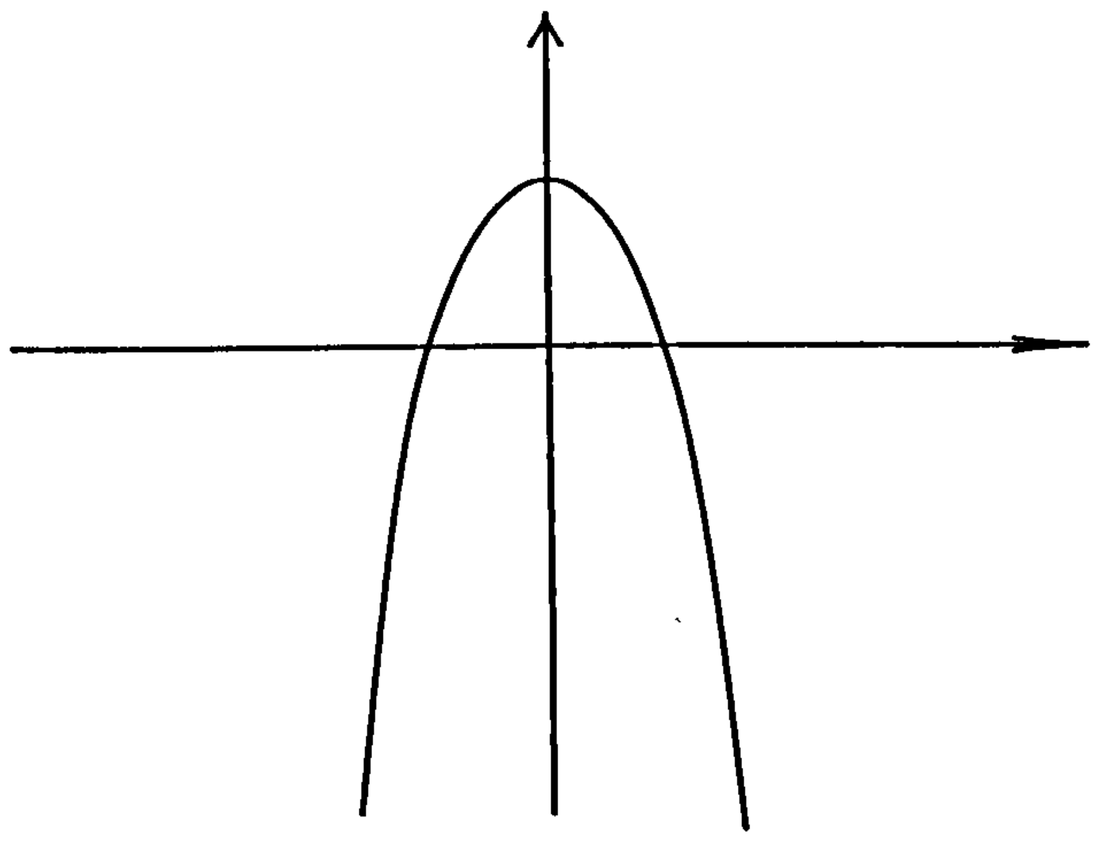

Figure 7.4: Cross section of the free surface given by the modified version of the Longuet-Higgins (1976) solution.

To fix ideas, suppose $\epsilon > 0$ and $t > 0$. Then setting

$$\alpha(t) = \frac{3\epsilon}{4t^3}, \qquad c = \frac{Q}{3\epsilon} \tag{7.3.9}$$

the equation of the free surface given by (7.3.8) becomes

$$y^2 = -4\alpha(t)(x - \frac{1}{3}\alpha(t) - ct). \tag{7.3.10}$$

This obviously represents a parabola, with vertex at the point $(\frac{1}{3}\alpha(t) + ct, 0)$ and distance $\alpha(t)$ between vertex and focus (see figure 7.3).

As t increases, so $\alpha(t)$, and all the dimensions of the parabola, vary as t^{-3}. The free surface contracts towards the origin O as the centre of similitude. This point lies inside the parabola, at one-third of the distance from the vertex to the focus.

When t is small, the free surface (for bounded values of y) is almost plane. When on the other hand as $t \to \infty$, the free surface becomes very elongated in the x-direction, producing a thin jet of fluid, ejected to the right with velocity

$$\phi_x = \frac{x}{t} - \frac{\epsilon}{t^4}. \tag{7.3.11}$$

The velocity normal to the median plane of the jet is

$$\phi_y = -\frac{y}{t}, \tag{7.3.12}$$

which is always independent of x. It follows that any line of particles parallel to the median plane always remains so, and that the flow may be realised by the ejection of fluid from between two approaching parallel plates. Longuet-Higgins (1976) pointed out that a more interesting realisation might be in the jet of water formed by a 'plunging breaker' during the short time that the jet is thin and almost horizontal (McIver & Peregrine 1981, Longuet-Higgins & Cokelet 1976).

The parabolic free surface described above, given by Longuet-Higgins (1976) is now modified to consider a parabolic free surface moving in the vertical direction freely under gravity.

To modify the flow from being in the horizontal direction to being in the vertical direction, we just interchange x and y. To consider the effects of gravity the vertical

frame of reference must also be changed to a frame accelerating with gravity. It is this that is now considered in section 7.4.

7.4 Parabolic free surface moving under gravity

The solution of Longuet-Higgins (1976) given in section 7.3 for a parabolic free surface profile is used to model a thin jet travelling up a wall. The solution of Longuet-Higgins (1976) is for a parabola moving in the horizontal direction. This solution is modified so as to consider the flow in the vertical direction. The solution of Longuet-Higgins (1976) becomes thin as time increases, therefore models a possible jet flow. We assume that there is a wall along the line of symmetry of the flow and thus consider only one half of the parabolic solution.

The modified version of the Longuet-Higgins (1976) solution is given by

$$y = \frac{1}{3}\alpha(t) + ct - \frac{x^2}{4\alpha(t)}, \tag{7.4.1}$$

where c and $\alpha(t)$ are both positive. This equation gives a contracting parabola moving in the vertical direction without the effects of gravity. Thus the parabola will 'shoot off' in the y-direction. Since we expect the parabola to fall back, we must include the effects of gravity. This is done by changing the frame of reference to one accelerating with acceleration g. To do this we introduce a new variable $y' = y - \frac{1}{2}gt^2$, where g is the acceleration due to gravity. Substitution of this into (7.4.1) gives

$$y = \frac{1}{3}\alpha(t) + ct - \frac{x^2}{4\alpha(t)} - \frac{1}{2}gt^2, \tag{7.4.2}$$

where we have dropped the $'$ notation. Now that we have a free surface profile the method of section 7.2, in which the jet flow was found for an arbitrary wall flow, can be adopted to find how this jet of water behaves after it passes the top of a wall. Before proceding further, we simplify the problem by introducing dimensionless quantities given by

$$y = y^* H_0, \qquad t = t^* \sqrt{\frac{H_0}{g}}, \qquad x = x^* H_0, \qquad \alpha(t) = \alpha^*(t^*) H_0, \tag{7.4.3}$$

where * denotes a dimensionless quantity and $H_0 = c^2/g$. Using the above transformation reduces equation (7.4.2) to

$$y = \frac{\alpha}{3} + t - \frac{x^2}{4\alpha} - \frac{t^2}{2}, \tag{7.4.4}$$

where we have dropped the * notation. All variables are now dimensionless. Remembering that $\alpha = \frac{\epsilon}{4t^3}$, the expression for y becomes

$$y = \frac{\epsilon}{4t^3} + t - \frac{x^2 t^3}{3\epsilon} - \frac{t^2}{2}, \tag{7.4.5}$$

where ϵ is a constant. Now we are interested in thin jets. For the fluid domain to be small in the x-direction and long in the y-direction, we must decide what values of ϵ are sensible for thin jets. On inspection of equation (7.4.2) we see that for the profile to be thin in the y-direction we must have ϵ small. ϵ is thus a measure of the jet thickness up the wall. If ϵ is not chosen to be small, then the shallow water approximation will breakdown.

7.5 Thin jets along a wall

The modified solution of section 7.4 for a parabolic free surface under gravity is now used to model the flow of a jet along a wall. This solution is used as an initial condition to find the jet flow produced when the wall flow reaches the top of the wall.

7.5.1 The wall flow

Consider $x < 0$, and let a wall height H be at $x = 0$. For fixed $y = y_w (\leq H)$, we find the width of the jet as

$$x(t) = \sqrt{\frac{3\epsilon^2}{4t^6} + \frac{3\epsilon}{t^2} - \frac{3\epsilon y_w}{t^3} - \frac{3\epsilon}{2t}}. \tag{7.5.1}$$

Now for this flow the velocity potential is

$$\phi = \frac{1}{2t}\left[\left(y - \frac{t^2}{2}\right)^2 - x^2\right] - \frac{\epsilon}{t^4}\left(y - \frac{1}{2}t^2\right). \tag{7.5.2}$$

Calculating the horizontal and vertical velocities from the above velocity potential gives

$$v = \phi_y = \frac{y}{t} - \frac{t}{2} - \frac{\epsilon}{t^4} \tag{7.5.3}$$

and

$$u = \phi_x = -\frac{x}{t}. \tag{7.5.4}$$

Now the tip of the jet reaches the top of the wall, height H after time, t_w, given by

$$H = \frac{\epsilon}{4t_w^3} + t_w - \frac{t_w^2}{2}, \tag{7.5.5}$$

which can be rearranged to give:

$$t_w^5 - 2t_w^4 + 2Ht_w^3 - \frac{\epsilon}{2} = 0. \tag{7.5.6}$$

We can find t_w numerically for given ϵ and H. Now since ϵ is small, we obtain

$$t_w \approx 1 - \sqrt{1-2H}. \tag{7.5.7}$$

We wish to model what happens in the subsequent motion when the tip of the jet passes over the top of the wall. The width of the jet at the top of wall is W and is given by

$$W = \sqrt{\frac{3\epsilon^2}{4\tau^6} + \frac{3\epsilon}{\tau^2} - \frac{3\epsilon H}{\tau^3} - \frac{3\epsilon}{2\tau}}, \tag{7.5.8}$$

where τ is the time when a jet element is at the top of the wall. The first time the jet reaches the top of the wall is t_w, therefore τ must be greater than this time. There exists an upper limit for τ, since at a given time the wall flow stops influencing the jet flow above the wall. To discover the upper limit on τ we consider when the forcing vertical velocity $v(\tau) = V$ is zero. From this we find that upper limit of τ satisifes

$$\tau^5 - 2H\tau^3 + 2\epsilon = 0, \tag{7.5.9}$$

which for small ϵ gives the solution $\tau = \sqrt{2H}$. Thus we know that for small ϵ, $1 - \sqrt{1-2H} \leq \tau \leq \sqrt{2H}$. When $\tau = t_w$, $W = 0$. A plot of the jet width at the top of the wall, W against τ is given in figure 7.5, various values of the wall height H are shown. From the expression for t_w, we see that the maximum height of wall

that can be chosen is $H = 0.5$. The smaller the height of the wall, the less accurate the solutions become for small ϵ. This is due to the fact that the shallow water approximation becomes less accurate as the ratio of the jet width to wall height decreases. A plot of the forcing vertical velocity V at the top of the wall is given in figure 7.6.

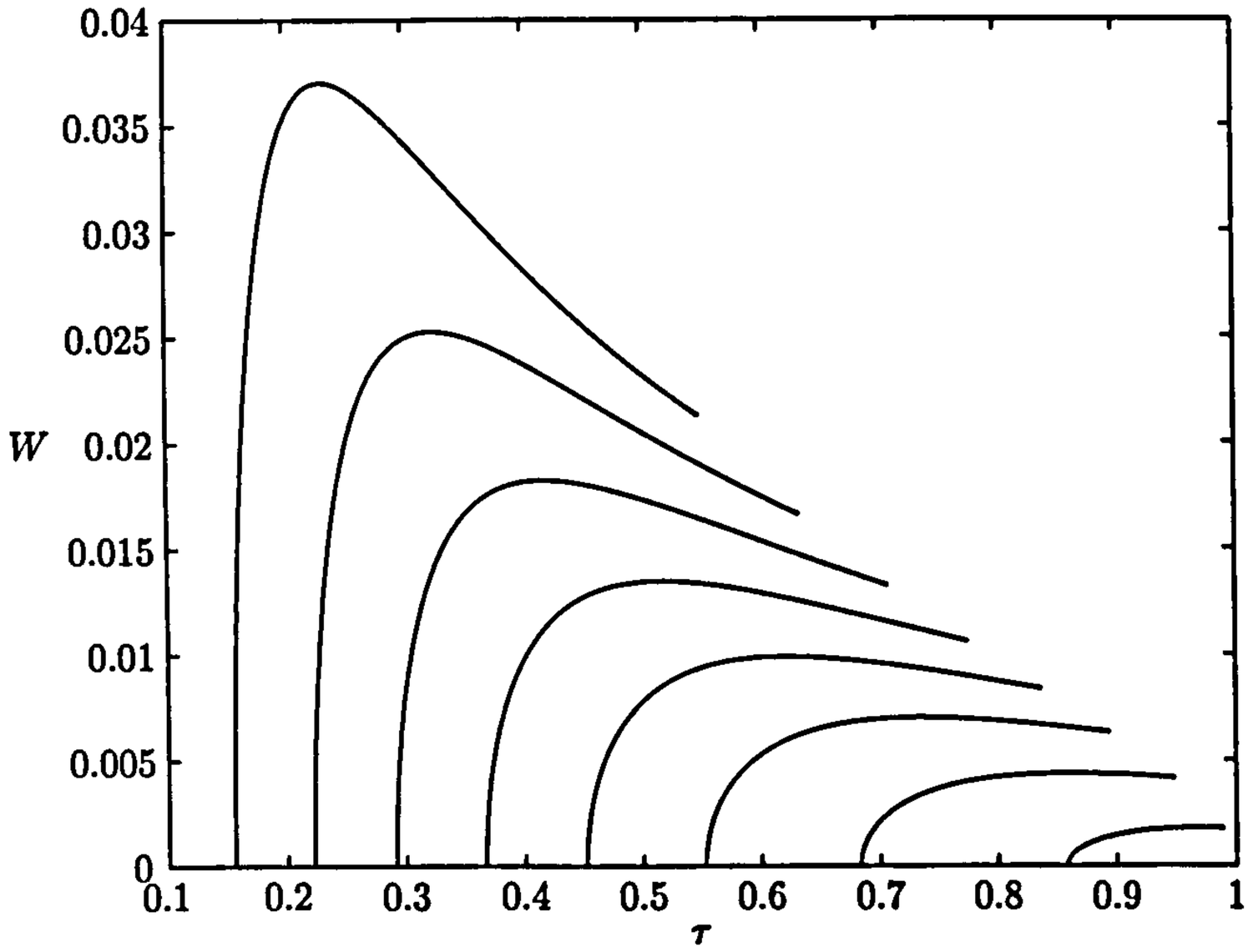

Figure 7.5: Jet width at top of wall as a function of τ. $H = 0.15, 0.2, 0.25, 0.3, 0.35, 0.4, 0.45, 0.49$. $\epsilon = 0.0001$.

Now that an expression is known for the vertical velocity at the top of the wall, the subsequent jet flow solutions are found from the shallow water equations.

7.5.2 The jet flow

For the jet flow above the top of the wall, we assume that the flow is thin enough so that the shallow water wave equations can be used. Let the jet width be defined by $b(y,t)$. Let $v(y,t)$ be the velocity of the jet in the y-direction. The dimensionless shallow water equations are given by

$$\frac{\partial b}{\partial t} + \frac{\partial (vb)}{\partial y} = 0 \tag{7.5.10}$$

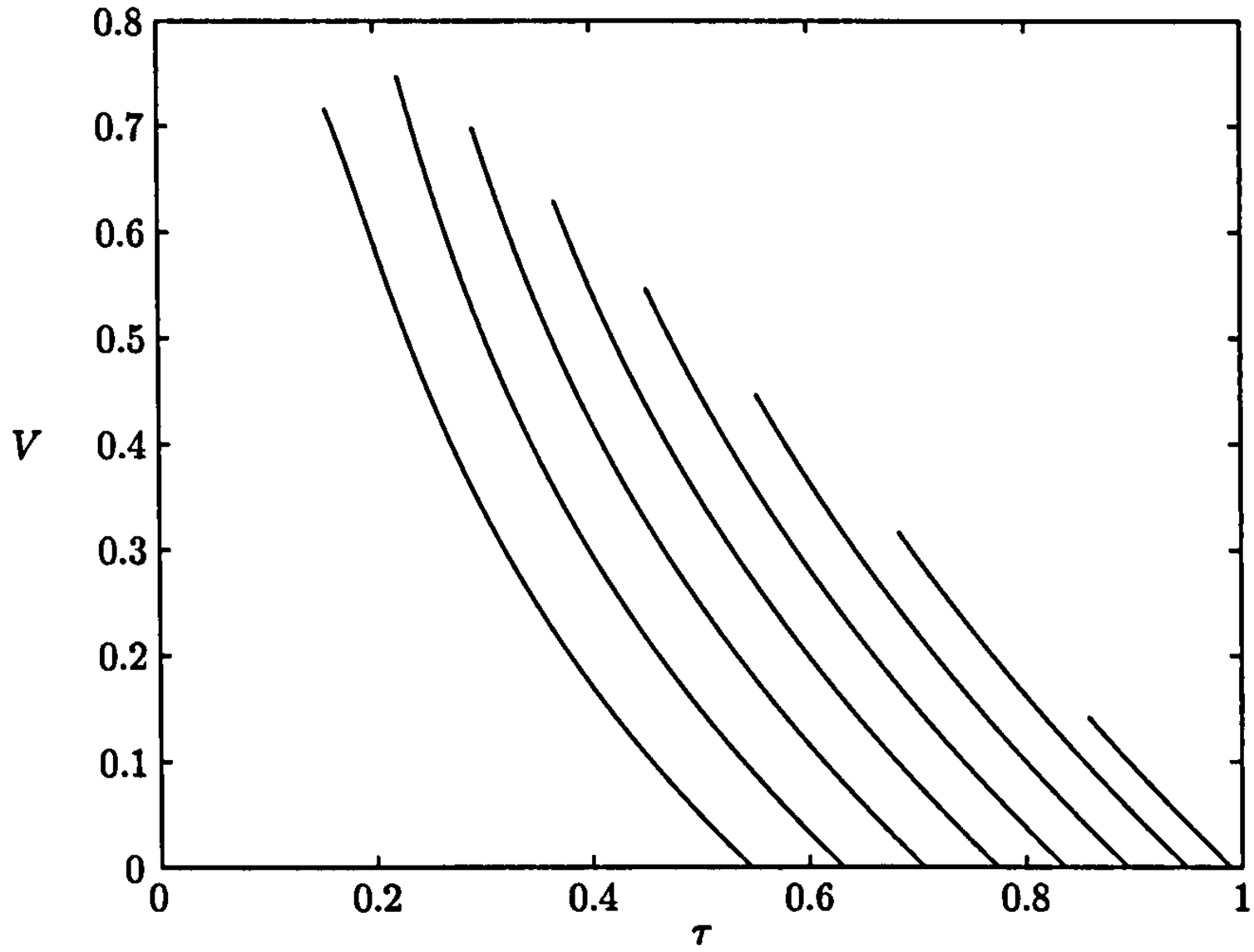

Figure 7.6: Vertical velocity at top of wall as a function of τ. $H = 0.15, 0.2, 0.25, 0.3, 0.35, 0.4, 0.45, 0.49$. $\epsilon = 0.0001$.

$$\frac{\partial v}{\partial t} + v\frac{\partial v}{\partial y} = -1. \tag{7.5.11}$$

We can solve the second equation with respect to the forcing velocity at the top of the wall. Using the method of characteristics, we have already found that the characteristics are given by $\frac{\mathrm{d}y}{\mathrm{d}t} = v$ and on these curves $\frac{\mathrm{d}v}{\mathrm{d}t} = -1$. The second of these implies that $v = -t + \text{constant}$. Now when $t = \tau$, $v = \frac{H}{\tau} - \frac{\tau}{2} - \frac{\epsilon}{\tau^4}$ at $y = H$. From this we find an expression for v on each characteristic as

$$v = \frac{H}{\tau} + \frac{\tau}{2} - \frac{\epsilon}{\tau^4} - t \tag{7.5.12}$$

Now $\frac{\mathrm{d}y}{\mathrm{d}t} = v$, implies

$$y = \frac{Ht}{\tau} + \frac{t\tau}{2} - \frac{\epsilon t}{\tau^4} - \frac{t^2}{2} + \text{constant} \tag{7.5.13}$$

when $t = \tau$, $y = H$, which implies constant $= \frac{\epsilon}{\tau^3}$. So our expression for y is

$$y = \frac{Ht}{\tau} + \frac{t\tau}{2} - \frac{\epsilon t}{\tau^4} - \frac{t^2}{2} + \frac{\epsilon}{\tau^3}. \tag{7.5.14}$$

A plot of y against t for different values of τ is given in figure 7.7. In this plot we take, $H = 0.3$ and $\epsilon = 0.0001$.

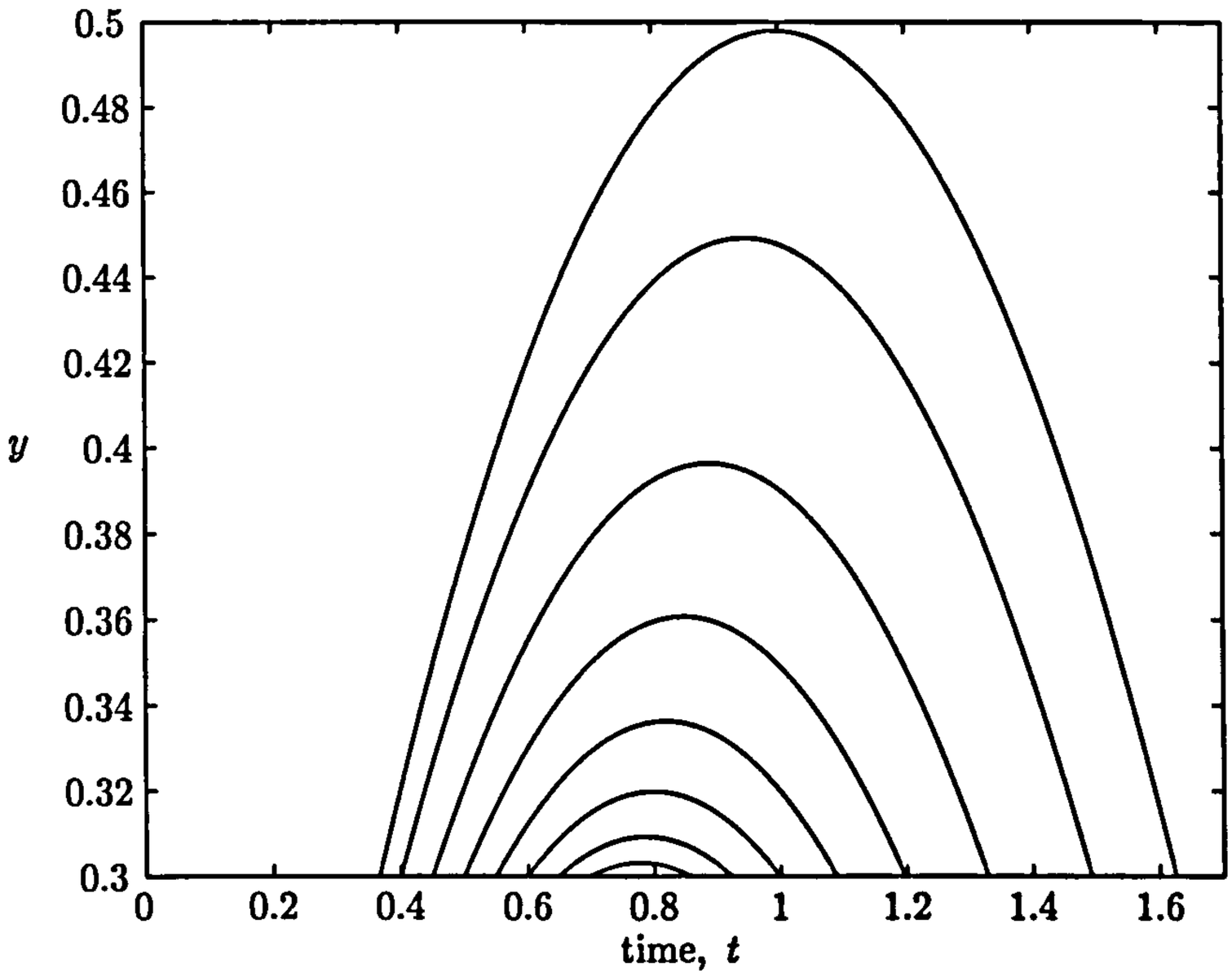

Figure 7.7: Vertical position of a jet element as a function of time. τ takes the values $0.36, 0.4, 0.45, 0.5, 0.55, 0.6, 0.65, 0.7$. Wall height, $H = 0.3$ and $\epsilon = 0.0001$.

From the above expression for y we can find an expression for τ in terms of y and t. Rearranging the above we find

$$\tau^5 - (\frac{2y}{t} + t)\tau^4 + 2H\tau^3 + \frac{2\epsilon}{t}\tau - 2\epsilon = 0. \qquad (7.5.15)$$

τ can be found numerically for given ϵ, H, and fixed y and t. Once τ is found as a function of y and t, v is found as a function of y and t only. Since ϵ is considered small, we find that

$$\tau \approx \frac{y}{t} + \frac{t}{2} - \sqrt{\frac{y^2}{t^2} + \frac{t^2}{4} + y - 2H}. \qquad (7.5.16)$$

Since an expression for τ has been found, we can find $v(y,t)$. A plot of $v(y,t)$ is given in figure 7.8 for different values of y above the wall.

Let us now look at the mass equation from the shallow water equations:

$$\frac{\partial b}{\partial t} + v\frac{\partial b}{\partial y} = -b\frac{\partial v}{\partial y}. \qquad (7.5.17)$$

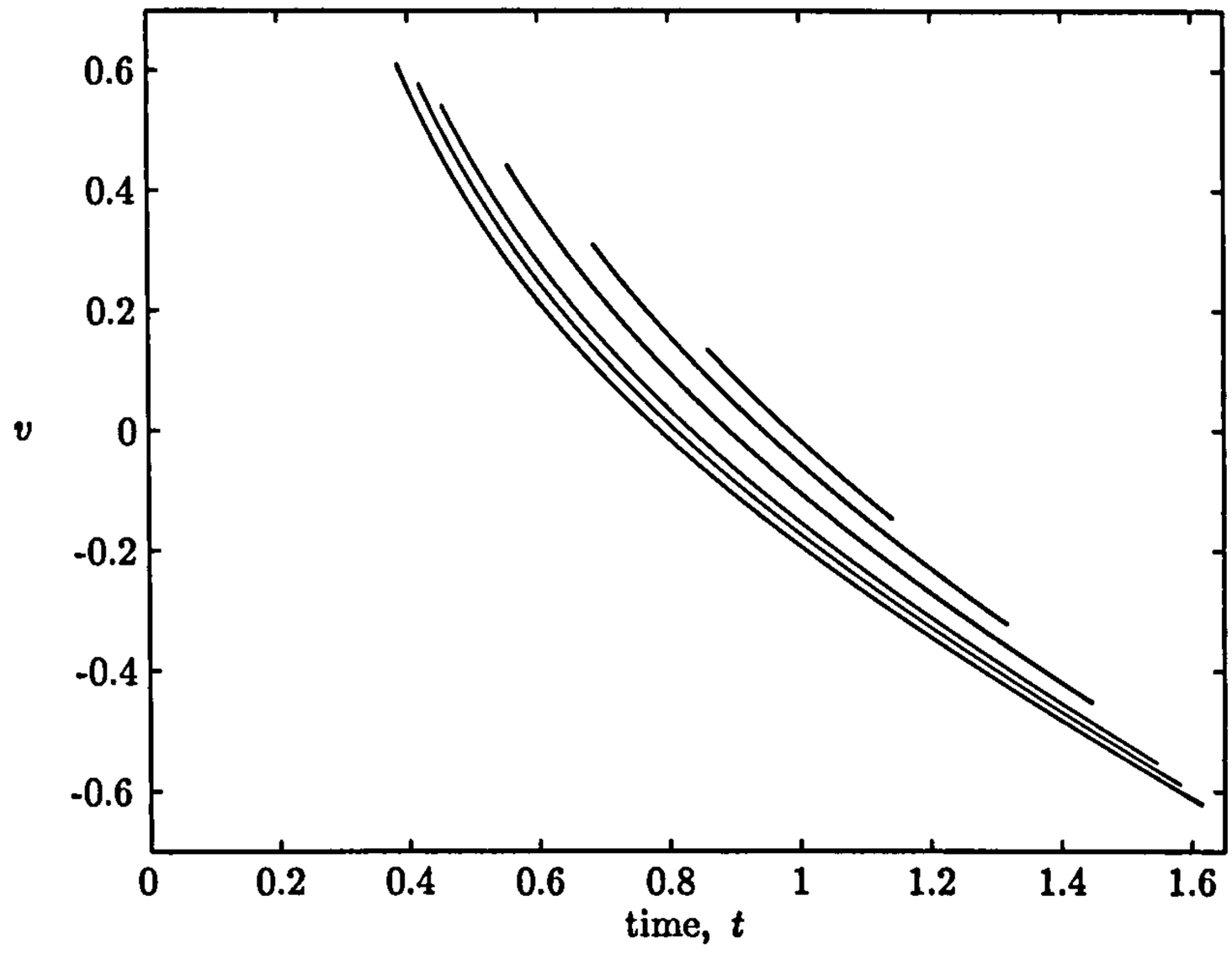

Figure 7.8: Vertical velocity above wall against time, t. Profiles are at $y = 0.31, 0.33, 0.35, 0.4, 0.45, 0.49$. $H = 0.3$ and $\epsilon = 0.0001$.

In section 7.2 we saw that the method of characteristics gives the characteristics as $\frac{\mathrm{d}y}{\mathrm{d}t} = v$, on which $\frac{\mathrm{d}b}{\mathrm{d}t} = -b\frac{\partial v}{\partial y}$ We have already considered $\frac{\mathrm{d}y}{\mathrm{d}t} = v$, above. So we now need to consider $\frac{\mathrm{d}b}{\mathrm{d}t} = -b\frac{\partial v}{\partial y}$. From these we found that

$$b = b_0 \exp\left(-\int_{t_w}^{t} \frac{\partial v}{\partial y}\,\mathrm{d}t\right). \tag{7.5.18}$$

Letting $I = \int_{t_w}^{t} \frac{\partial v}{\partial y}\,\mathrm{d}t$, we have $b = b_0\,\mathrm{e}^{-I}$. Now

$$\frac{\partial v}{\partial y} = \frac{\partial v}{\partial \tau}\frac{\partial \tau}{\partial y} = \frac{-2H\tau^3 + \tau^5 + 8\epsilon}{-2Ht\tau^3 + t\tau^5 + 8\epsilon t - 6\epsilon\tau} \approx \frac{1}{t}. \tag{7.5.19}$$

Using this expression with the fact that when $y = H$, $t = \tau$ and $x = W(\tau)$, we find

$$b = \frac{W(\tau^6 - 2H\tau^4 + 2\epsilon\tau)}{t\tau^5 - 2Ht\tau^3 + 8\epsilon t - 6\epsilon\tau} \approx \frac{W\tau}{t}. \tag{7.5.20}$$

Since τ is known as a function of y and t for small ϵ, an expression can be found for a jet element's width as a function of y and t. A plot of the jet width, b above the wall as a function of time, t for different values of y is shown in figure 7.9.

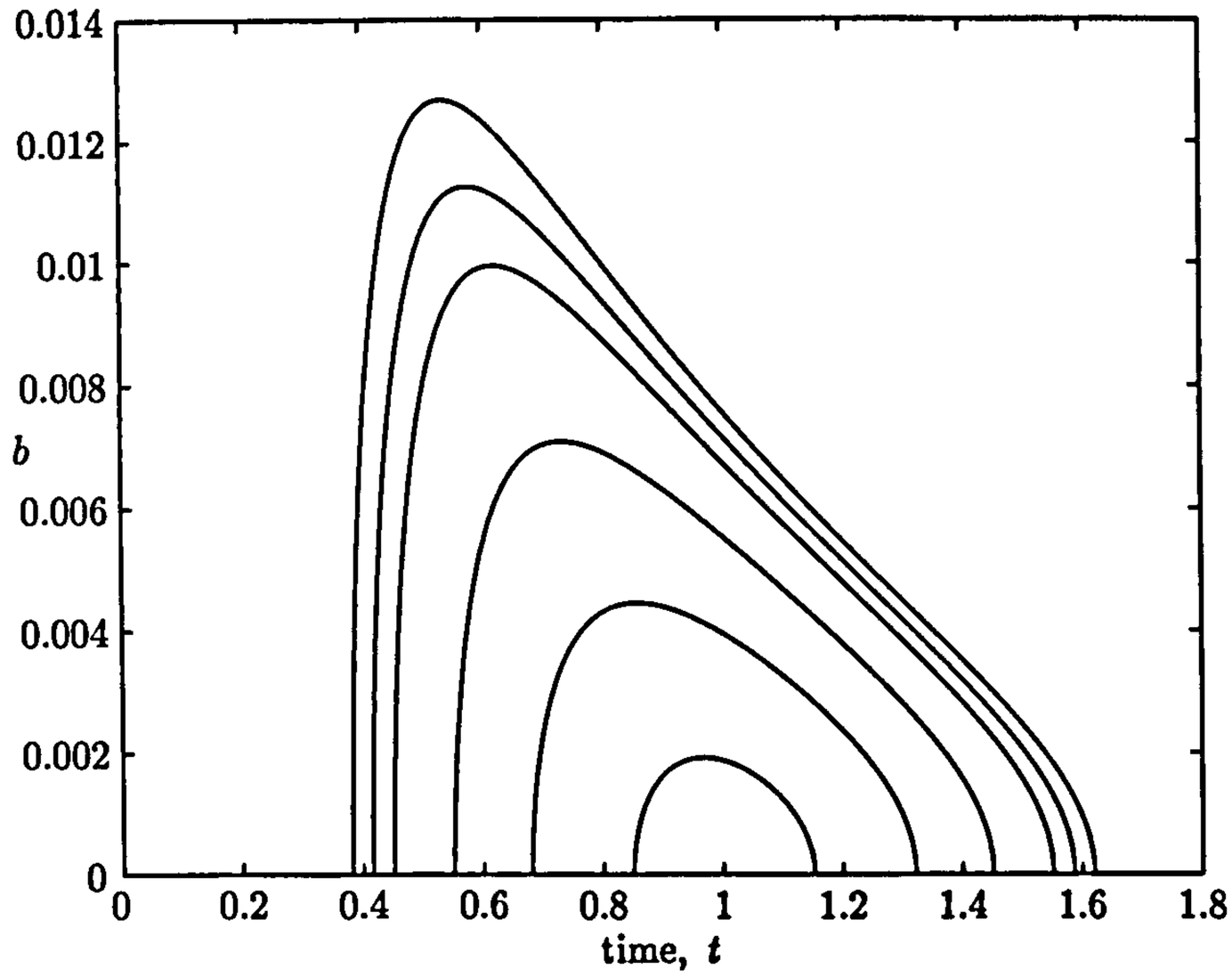

Figure 7.9: Jet width above wall, b against time, t. Profiles are at $y = 0.31, 0.33, 0.35, 0.4, 0.45, 0.49$. $H = 0.3$ and $\epsilon = 0.0001$.

7.5.3 Downward motion

To find the horizontal distance travelled by each jet element, we need an expression for the horizontal momentum of each jet element. Thus we need an expression for the horizontal velocity of each jet element at the top of the wall. From the velocity potential for the flow we know that $u(\tau) = \dfrac{x}{\tau}$ at the top of the wall. From this expression, we can see that the horizontal velocity varies across the width of each jet element. An easier way to use this velocity is to calculate the average horizontal velocity across the width of each jet element. The average horizontal velocity of each jet element is given by

$$\bar{u} = \bar{u}(\tau) = \frac{1}{W(\tau)} \int_0^{W(\tau)} \frac{x}{\tau} \, \mathrm{d}x = \frac{W(\tau)}{2\tau} = \frac{\text{horiz. mom.}}{\text{mass}}. \tag{7.5.21}$$

To find the horizontal distance covered by each jet element we integrate the above expression for the velocity between the times at which each element is at the top of the wall. Integration gives us the displacement of the jet in the x-direction

$$d(\tau) = \frac{W(\tau)(t_i - \tau)}{2\tau}, \tag{7.5.22}$$

where t_i is the time at which a jet element returns to the top of the wall. An expression for t_i is now needed. On each characteristic we know that the vertical position given by equation (7.5.14) is

$$y = \frac{Ht}{\tau} + \frac{t\tau}{2} - \frac{\epsilon t}{\tau^4} - \frac{t^2}{2} + \frac{\epsilon}{\tau^3}. \tag{7.5.23}$$

Setting $y = H$, in the above and solving for t, we find that $t = \tau$ and

$$t = t_i = \frac{2H}{\tau} - \frac{2\epsilon}{\tau^4}. \tag{7.5.24}$$

Since we are considering ϵ to be small, we can say that $t_i = \frac{2H}{\tau}$. Thus we have an expression for τ in terms of the impact time, t_i. Putting this expression into our expression for the horizontal displacement, gives us d as a function of t_i. This expression is given by

$$d = \sqrt{\frac{3\epsilon^2 t_i^6}{256H^6} + \frac{3\epsilon t_i^2}{4H^2} - \frac{3\epsilon t_i^3}{8H^2} - \frac{3\epsilon t_i}{4H}}\left(\frac{t_i^2 - 2H}{4H}\right). \tag{7.5.25}$$

A particular plot of d as a function of t_i in shown in figure 7.10.

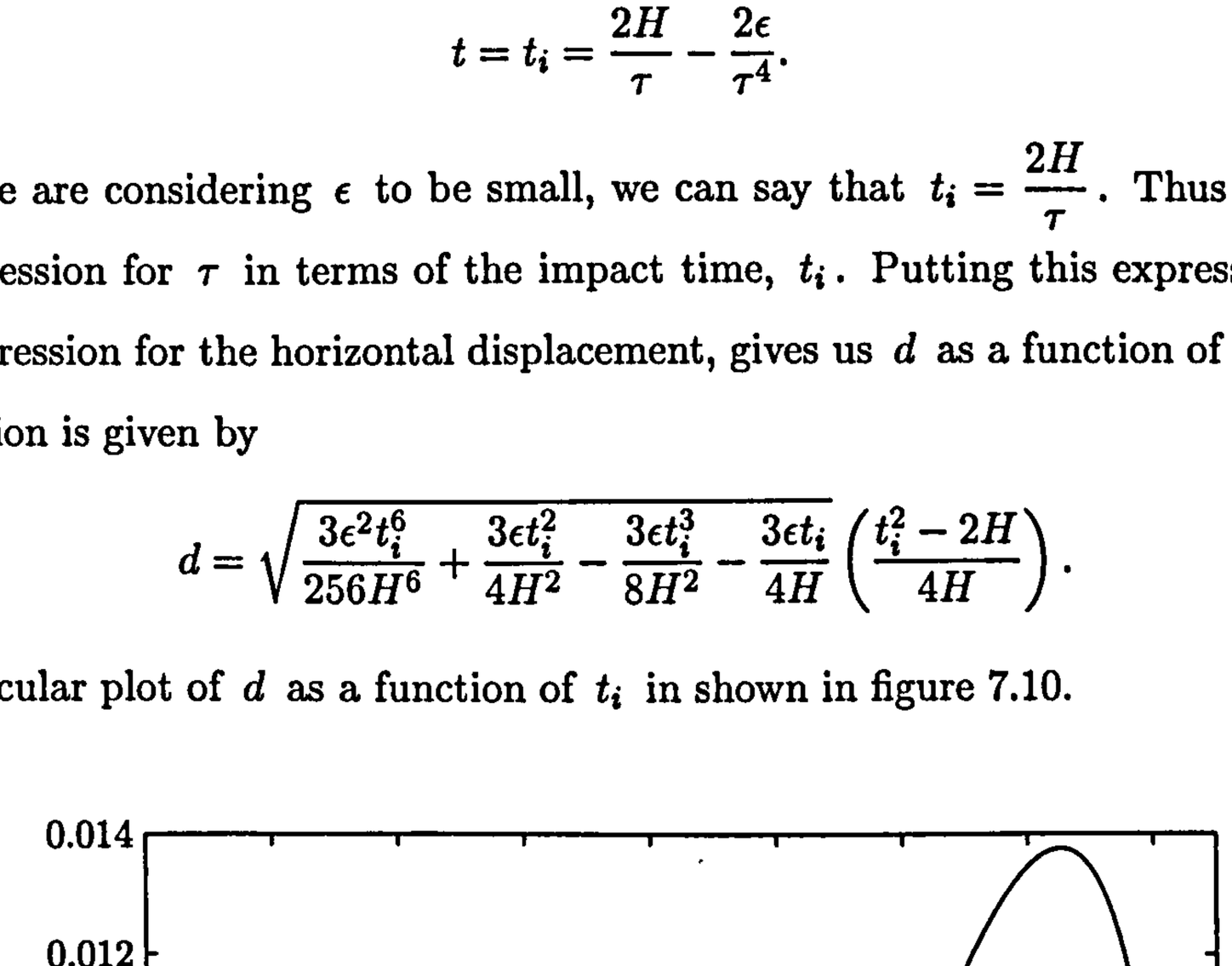

Figure 7.10: Horizontal displacement as a function of the impact time, t_i. The wall height is $H = 0.3$ and $\epsilon = 0.0001$.

With an expression for the horizontal displacement of the each jet element known, we can find, for a given impact time, the distance travelled by each jet element in the horizontal direction. With a value for the width and the horizontal distance travelled of each jet element, we can model the motion of a jet element falling on to the top of the wall. This is considered in section 7.6.

Since it is useful to calculate the amount of water that may overtop the wall, we find an expression here for the amount of water that may overtop the wall.

With v and b known at the top of the wall, we can find an expression for the volume that passes the top of the wall.

$$\text{Volume} = \int_{t_w}^{t_e} bv \, \mathrm{d}t. \tag{7.5.26}$$

For small ϵ, we find

$$\text{Volume} \approx \int_{1-\sqrt{1-2H}}^{\sqrt{2H}} \sqrt{\frac{3\epsilon}{t^2} - \frac{3\epsilon H}{t^3} - \frac{3\epsilon}{2t}} \left(\frac{H}{t} - \frac{t}{2}\right) \mathrm{d}t, \tag{7.5.27}$$

where both b and v have been approximated above to make the integration easier.

Evaluating the integral, we find

$$\text{Volume} \approx \frac{2\sqrt{3\epsilon}}{3}(1 - \sqrt{2H})^{\frac{3}{2}}. \tag{7.5.28}$$

When the wall height is chosen as $H = 0.3$ and $\epsilon = 0.0001$, we find that the total amount of water that passes the top of the wall is 0.0012357.

We next calculate in section 7.6 the amount of water that overtops the wall.

7.6 Jet flow hitting the top of a wall

We now model each jet element as it falls back onto the top of the wall. When an element hits the wall, some water goes back to where it started, to the left of the wall and the rest will go to the right and thus overtop the wall.

For each jet element, the results found in the previous section are used. With the width of each element and the horizontal distance travelled by each element known, we setup a model to estimate the amount of water that may overtop the wall.

Figure 7.11: Jet of water on its way down. Taken from experiments in Hannover 30/6/03. (Picture courtesy of D. H. Peregrine)

Figure 7.12: Jet of water on its way down. Taken from experiments in Hannover 30/6/03. (Picture courtesy of D. H. Peregrine)

We consider two-dimensional inviscid flow in a small region close to the top of the wall, thus we assume the effects of gravity are negligant.

The problem we are interested in solving is that of a jet element hitting the top of a wall. Two pictures of the type of flow we are interested in, are shown in figures 7.11 and 7.12. The pictures are taken from experiments which took place in Hannover on 30th June 2003. The first picture shown in figure 7.11 shows a jet of water on its way back down. We can see in this picture the start of the water overtopping which is taking place. We see that the amount of water that is beginning to overtop in this picture, seems to be uniform along the total length of the wall of water. Thus a model of a vertical cross-section through this wall is sufficient. This is what our model is set-up to solve.

The picture given in figure 7.12 shows the jet of water at a further point in time. We can now see that quite a lot of water seems to be overtopping. Both these pictures support the reason behind the modelling of this type of flow.

A depiction of the flow setup is given in figure 7.13. Since the time scales involved are so small, all sideways velocities can be ignored. This is why we choose to take a vertical cross-section through the flow.

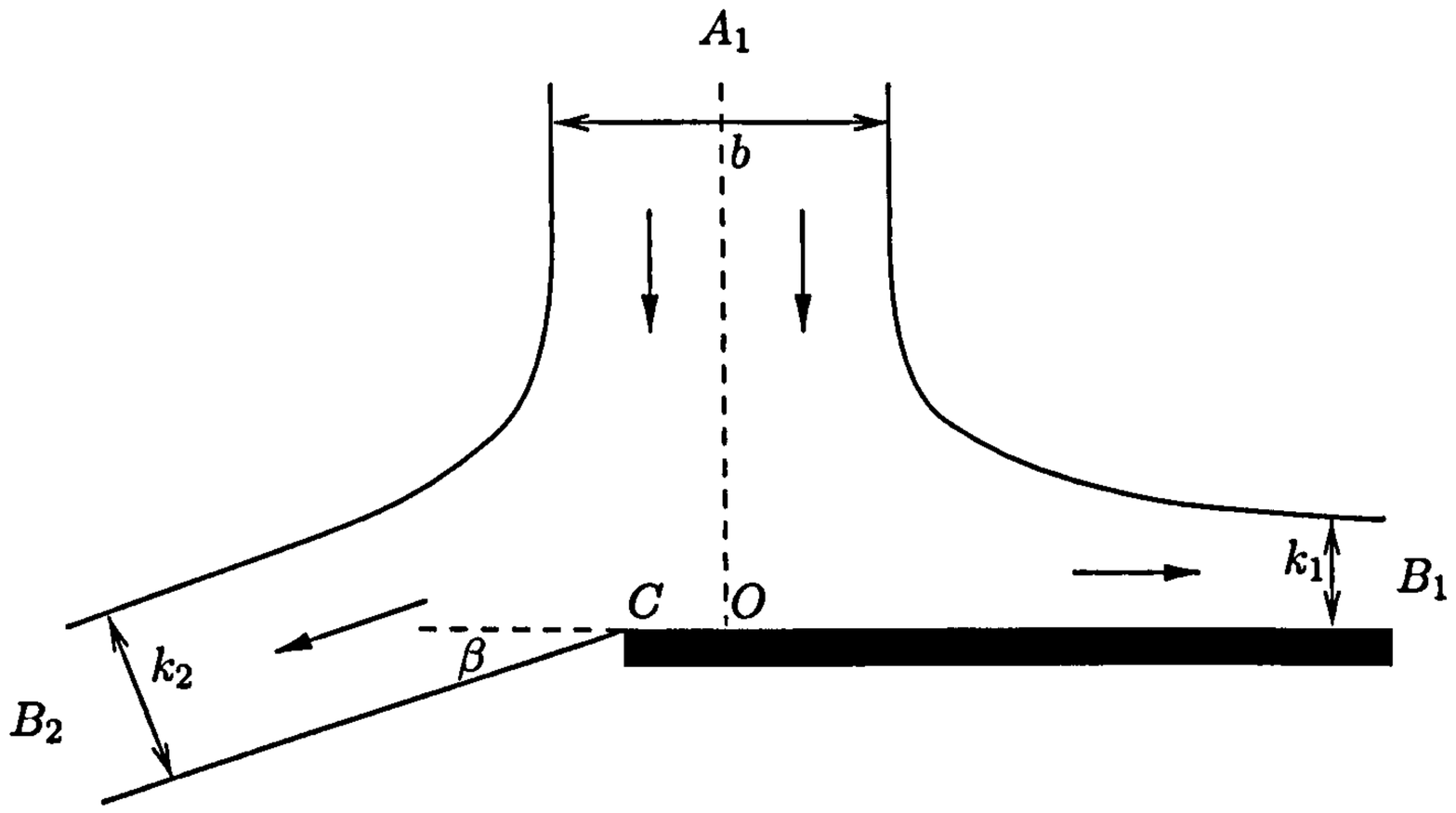

Figure 7.13: Flow setup for jet hitting the corner of the wall.

A problem of this type maybe solved using free surface flow techniques, see Milne-Thomson (1968). On a free streamline $\psi =$ constant (the streamfunction), speed and pressure are constants and also the density $\rho = 1$. Since we are considering flow in a small region at the top of the wall. We assume that the incoming jet element has speed U faraway from the corner. Then as the edges of the jets are free streamlines, and thus have a constant speed, all three jets must have speed U faraway from the corner of the wall. We can calculate the value of U for each jet element from equation (7.5.12) in the previous section. Since the velocity remains constant on the free surfaces it is easier to choose U to be 1. The origin of the flow is taken at the stagnation point. The incoming jet element has width b, and the two outgoing jets are of width k_1 and k_2. The jet formed of width k_2 is assumed to make an angle β with the horizontal. From equation (7.5.20) we have a value for b on each jet element.

Let us consider a jet of width h. In time δt, the mass of flow in from this jet is, $h\delta x\rho$, where δx is the distance a portion of fluid has travelled in δt. Therefore in unit time, the mass flowing in from this jet is $h(\delta x/\delta t)\rho = h\rho$ (as $\delta x/\delta t = U = 1$ at ∞). Thus mass of fluid entering the system must be the same as that leaving it, therefore, using the notation shown in figure 7.13 (and dividing by ρ):

$$b = k_1 + k_2. \tag{7.6.1}$$

The components of momentum are conserved in the x-direction. Momentum = mass $\times$ velocity. Mass flux = $h\rho$. Therefore flux of momentum = $h\rho$ in the direction of flow (velocity taken to be one). Conservation of momentum flux in the x-direction (after dividing by ρ) gives:

$$k_1 = k_2 \cos\beta. \tag{7.6.2}$$

From equations (7.6.1) and (7.6.2) we find expression for k_1 and k_2 in terms of our one known variable b and one unknown variable β. The expressions are:

$$k_1 = \frac{b\cos\beta}{1+\cos\beta} \qquad \text{and} \qquad k_2 = \frac{b}{1+\cos\beta}. \tag{7.6.3}$$

The way in which we solve the problem is to consider the complex velocity w, which is written as $w = qe^{-i\theta}$, where θ is the angle of the velocity to the positive

x-axis, and q is the speed. In the $w = u - iv$ plane the point B_1 corresponds to $\theta = 0$, the point A_1 corresponds to $\theta = -\pi/2$, the point B_2 corresponds to $\theta = -(\pi - \beta)$ and the point C corresponds to $\theta = -\pi$. The w-plane is shown in figure 7.14. On the free streamlines, q is constant, 1, so $w = \mathrm{e}^{-i\theta}$, where θ lies between 0 and $-\pi$.

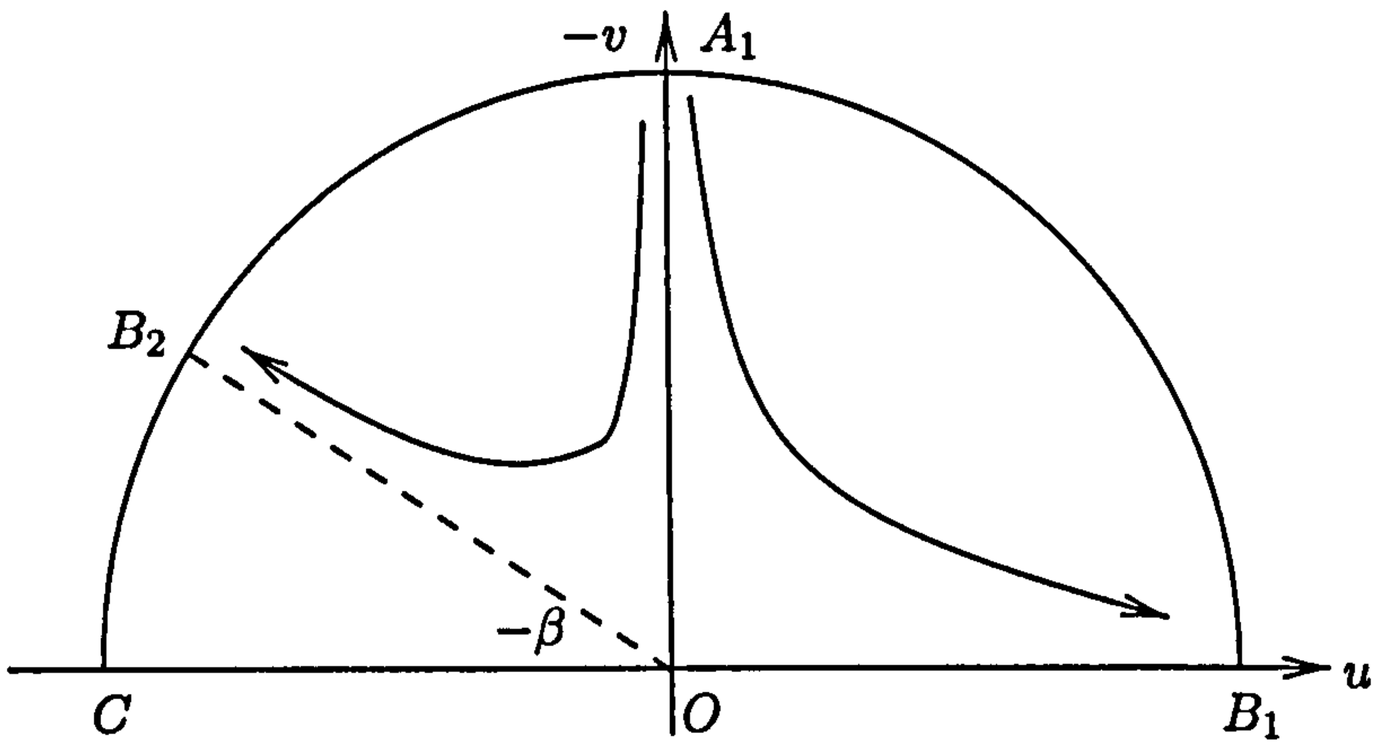

Figure 7.14: $w = u - \mathrm{i}v = \mathrm{e}^{-\mathrm{i}\theta}$ plane.

To proceed to find a solution for this flow we transform the semi-circle in the w-plane to a straight line in the t-plane. The transformation used is given by

$$t = \frac{1}{w - \mathrm{i}} + \frac{1}{w + \mathrm{i}} = \frac{2w}{w^2 + 1} = \frac{2}{\cos\theta}. \tag{7.6.4}$$

The setup in the t-plane is shown in figure 7.15.

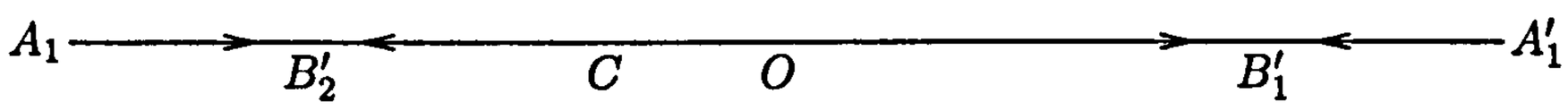

Figure 7.15: t-plane.

At the point A in the w-plane we have an incoming jet element, thus a source. At the two points B_1 and B_2 in the w-plane, there are outgoing jets, thus sinks. In the t-plane we add all the contributions from sources and sinks. In the case considered here we have two contributions from sinks at B_1' and B_2'. Considering the flux fluid volume across the outgoing jets we find the strengths of each sink.

Using the standard expressions for a sink, the complex potential for the flow is

$$f = -\frac{k_1}{\pi}\ln(t - B_1') - \frac{k_2}{\pi}\ln(t - B_2'). \tag{7.6.5}$$

We now substitute the expression for t in terms of w in the above. This gives

$$\pi f = -k_1 \ln\left(\frac{2w - B_1'(1+w^2)}{1+w^2}\right) - k_2 \ln\left(\frac{2w - B_2'(1+w^2)}{1+w^2}\right). \tag{7.6.6}$$

We now find expression for B_1' and B_2'. In the w-plane $B_1 = 1$ and $B_2 = -\mathrm{e}^{-\mathrm{i}\beta}$. Using the transformation from the w-plane to the t-plane, we find expressions for B_1' and B_2' as

$$B_1' = 1 \qquad \text{and} \qquad B_2' = -\frac{2\mathrm{e}^{-\mathrm{i}\beta}}{\mathrm{e}^{-2\mathrm{i}\beta} - 1} = -\frac{1}{\cos\beta}. \tag{7.6.7}$$

Thus using (7.6.1) and factorising, the complex potential becomes

$$\pi f = b\ln(1+w^2) - k_1[\mathrm{i}\pi + 2\ln(1-w)] + k_2[\ln(\cos\beta) - \ln(w+\mathrm{e}^{-\mathrm{i}\beta}) - \ln(w+\mathrm{e}^{\mathrm{i}\beta})]. \tag{7.6.8}$$

To find an expression for z, we use the fact that $w = \dfrac{\mathrm{d}f}{\mathrm{d}z}$ and $w\mathrm{d}z = \dfrac{\mathrm{d}f}{\mathrm{d}w}\mathrm{d}w$. Differentiating the complex potential f with respect to w, we find

$$\pi\frac{\mathrm{d}f}{\mathrm{d}w} = \frac{2bw}{1+w^2} + \frac{2k_1}{1-w} - \frac{k_2(2w + 2\cos\beta)}{w^2 + 2\cos\beta w + 1} \tag{7.6.9}$$

and thus

$$\pi\mathrm{d}z = \left(\frac{2b}{1+w^2} + \frac{2k_1}{w(1-w)} - \frac{k_2}{w}\frac{(2w+2\cos\beta)}{(w^2+2\cos\beta+1)}\right)\mathrm{d}w. \tag{7.6.10}$$

Integrating, using $z = 0$ when $w = 0$, we find

$$\begin{aligned}\pi z \;=\; & 2b\tan^{-1}w - \frac{b\cos\beta}{1+\cos\beta}\ln\left(\frac{(1-w)^2}{1+2\cos\beta w + w^2}\right) \\ & -\frac{2b\sin\beta}{1+\cos\beta}\tan^{-1}\left(\frac{w+\cos\beta}{\sin\beta}\right) + \frac{b\sin\beta}{1+\cos\beta}(\pi - 2\beta).\end{aligned} \tag{7.6.11}$$

Substituting $w = \mathrm{e}^{-\mathrm{i}\theta}$ into (7.6.11) and then taking the real and imaginary parts, we have explicit solutions for x and y as functions of θ. Since the logarithms take different values on different branches we find different values for x and y for

different values of θ. The expressions are given by:

$$x = \begin{cases} \dfrac{b}{2\pi(1+\cos\beta)}\left[(1+\cos\beta)\pi + 2\cos\beta\ln\left|\dfrac{\cos\theta+\cos\beta}{1-\cos\theta}\right| - 2\beta\sin\beta\right] \\ \qquad\qquad \text{for} \quad -\pi/2 < \theta < 0 \\ \dfrac{b}{2\pi(1+\cos\beta)}\left[-(1+\cos\beta)\pi + 2\cos\beta\ln\left|\dfrac{\cos\theta+\cos\beta}{1-\cos\theta}\right| - 2\beta\sin\beta\right] \\ \qquad\qquad \text{for} \quad -(\pi-\beta) < \theta < -\pi/2 \\ \dfrac{b}{2\pi(1+\cos\beta)}\left[-(1+\cos\beta)\pi + 2\cos\beta\ln\left|\dfrac{\cos\theta+\cos\beta}{1-\cos\theta}\right| + 2\sin\beta(\pi-\beta)\right] \\ \qquad\qquad \text{for} \quad -\pi < \theta < -(\pi-\beta) \end{cases} \tag{7.6.12}$$

$$y = \begin{cases} \dfrac{b}{2\pi(1+\cos\beta)}\left[(1+\cos\beta)\ln\left(\dfrac{1+\sin\theta}{1-\sin\theta}\right) + 2\pi\cos\beta + 2\sin\beta\ln\left|\dfrac{\cos\theta+\cos\beta}{1+\cos(\theta-\beta)}\right|\right] \\ \qquad\qquad \text{for} \quad -\pi/2 < \theta < 0 \quad \text{and} \quad -(\pi-\beta) < \theta < -\pi/2 \\ \dfrac{b}{2\pi(1+\cos\beta)}\left[(1+\cos\beta)\ln\left(\dfrac{1+\sin\theta}{1-\sin\theta}\right) + 2\sin\beta\ln\left|\dfrac{\cos\theta+\cos\beta}{1+\cos(\theta-\beta)}\right|\right] \\ \qquad\qquad \text{for} \quad -\pi < \theta < -(\pi-\beta) \end{cases} \tag{7.6.13}$$

The three regions above correspond to the free surfaces, A_1B_1, A_1B_2 and B_2C respectively. In the expressions for x and y, we still have one unknown β. To find β, we use a method introduced by Keller (1991). Taking the limit as $\theta \to -\pi/2$ on the free surface A_1B_1 takes us onto the right side of the incoming jet element. So the position of the right hand side of the jet is given by

$$x = \frac{b}{2\pi(1+\cos\beta)}\left[\pi(1+\cos\beta) + 2\cos\beta\ln(\cos\beta) - 2\beta\sin\beta\right]. \tag{7.6.14}$$

From the previous section we know the distance travelled by each jet element in the horizontal direction. So if we can find an expression for the distance from the corner of the wall to the right hand side of the jet element, then we can find a β corresponding to each impact time t_i.

Now to find the position of the corner of the wall as a function of β, we take the limit $\theta \to -\pi$ on the free surface B_2C. Doing this we find the position of the corner x_c as

$$x_c = \frac{b}{2\pi(1+\cos\beta)}\left[-\pi(1+\cos\beta)+2\cos\beta\ln\left(\frac{1-\cos\beta}{2}\right)+2\sin\beta(\pi-\beta)\right]. \tag{7.6.15}$$

Since we have an expression for the position of the corner and the jet element we can now find an expression for the distance from the right side of a jet element to the corner. The distance x_d is given by

$$x_d = \frac{b}{\pi(1+\cos\beta)}\left[\pi(1+\cos\beta)+\cos\beta\ln\left(\frac{2\cos\beta}{1-\cos\beta}\right)-\pi\sin\beta\right]. \tag{7.6.16}$$

From the previous section we know that

$$x_d = d = W\left(\frac{2H}{t_i}\right)\left(\frac{t_i^2-2H}{4H}\right). \tag{7.6.17}$$

Thus for each t_i we can find a corresponding β. A plot of β against t_i for $H = 0.3$ is given in figure 7.16. Also a plot of x_d against β for $H = 0.3$ is given in figure 7.17.

With values of β known, we can calculate the width of each jet element that will overtop the wall. From the conservation of mass and momentum we found that the jet width at B_1, the overtopping side, is given by

$$k_1 = \frac{b\cos\beta}{1+\cos\beta}, \tag{7.6.18}$$

where β and b change for each jet element that interacts with the wall. An expression for b at the top of the wall was found in the previous section as

$$b = W\left(\frac{2H}{t_i}\right)\frac{2H}{t_i^2}. \tag{7.6.19}$$

Thus for each jet element we can calculate the width of the flow that passes over the wall. To calculate the amount of water that overtops the wall, we need to find an expression for the height of each jet element. In the previous section and expression for a jet element height above the wall was found as

$$y = \frac{Ht}{\tau}+\frac{t\tau}{2}-\frac{\epsilon t}{\tau^4}-\frac{t^2}{2}+\frac{\epsilon}{\tau^3}. \tag{7.6.20}$$

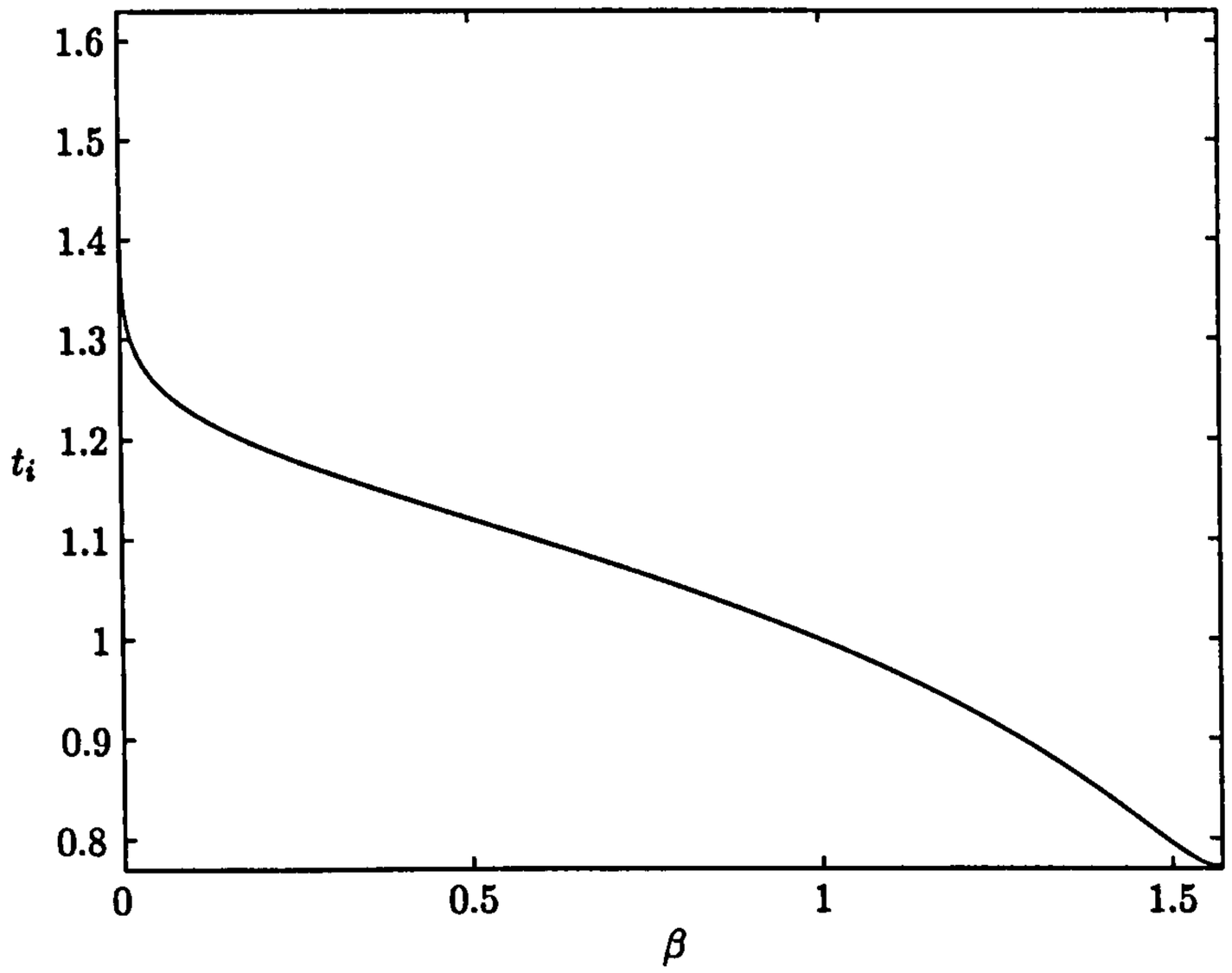

Figure 7.16: Angle of deflection β against impact time t_i. $H = 0.3$ and $\epsilon = 0.0001$.

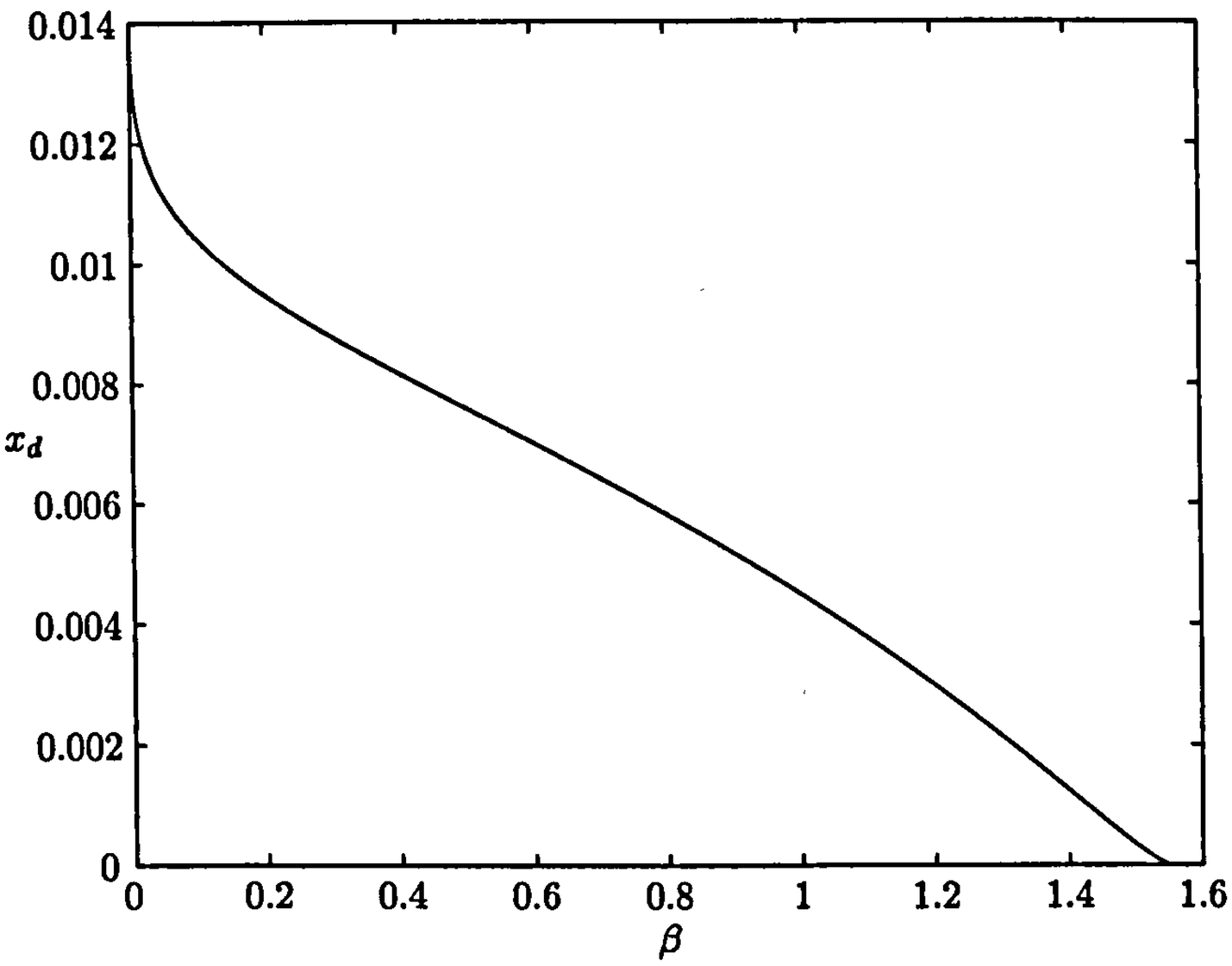

Figure 7.17: Distance from right side of jet to the corner of the wall, x_d as a function of the angle of deflection β. $H = 0.3$ and $\epsilon = 0.0001$.

Remembering that each τ labels a point on the jet. We find the height of a jet element between two points as

$$y_n = \frac{H\tau_{n+1}}{\tau_n} + \frac{\tau_{n+1}\tau_n}{2} - \frac{\epsilon\tau_{n+1}}{\tau_n^4} - \frac{\tau_{n+1}^2}{2} + \frac{\epsilon}{\tau_n^3}, \tag{7.6.21}$$

where τ_n and τ_{n+1} label succesive jet elements.

With an expression know for the height of each jet element that passes the top of the wall, we find that the total water that overtops the wall is given by

$$V_o = \sum_{n=0}^{N} \left(y_n \times \frac{\cos\beta_n}{1+\cos\beta_n} \times W(\tau_n)\frac{\tau_n}{\tau_{n+1}} \right), \tag{7.6.22}$$

where τ_0 is the first time that the wall flow reaches the top of the wall i.e. $\tau_0 = t_w = 1 - \sqrt{1-2H}$. τ_N is the time at which the wall flow no longer influences the jet flow i.e. $\tau_N = \sqrt{2H}$. y_n is given by (7.6.21), β_n is found from (7.6.16) and (7.6.17) for different values of τ and hence t_i, and $W(\tau_n)$ is given by (7.5.8). A table of the amount of water that overtops various wall heights is given in table 7.1.

Wall Height H	Total volume	V_o	percentage
0.2	0.002573	0.00035531	13.81
0.25	0.00183	0.000292	15.95
0.3	0.0012357	0.0002202	17.82
0.35	0.0007623	0.0001422	18.65
0.4	0.0003961	0.000074172	18.73
0.45	0.000134	0.000021465	15.99

Table 7.1: Volumes of overtopping for different wall heights

In table 7.1, the total volume represents the amount of water that actually passes the top of each wall height, whereas V_o is the total amount of water overtopped. The final column in the table is the percentage of water that overtops in each case. From the six cases considered we can see that the percentage of water that overtops in each case is very similar. A plot of the overtopping volume V_o as a function of the wall height is given in figure 7.18. The plot is shown for wall heights in the interval $[0.2, 0.5]$.

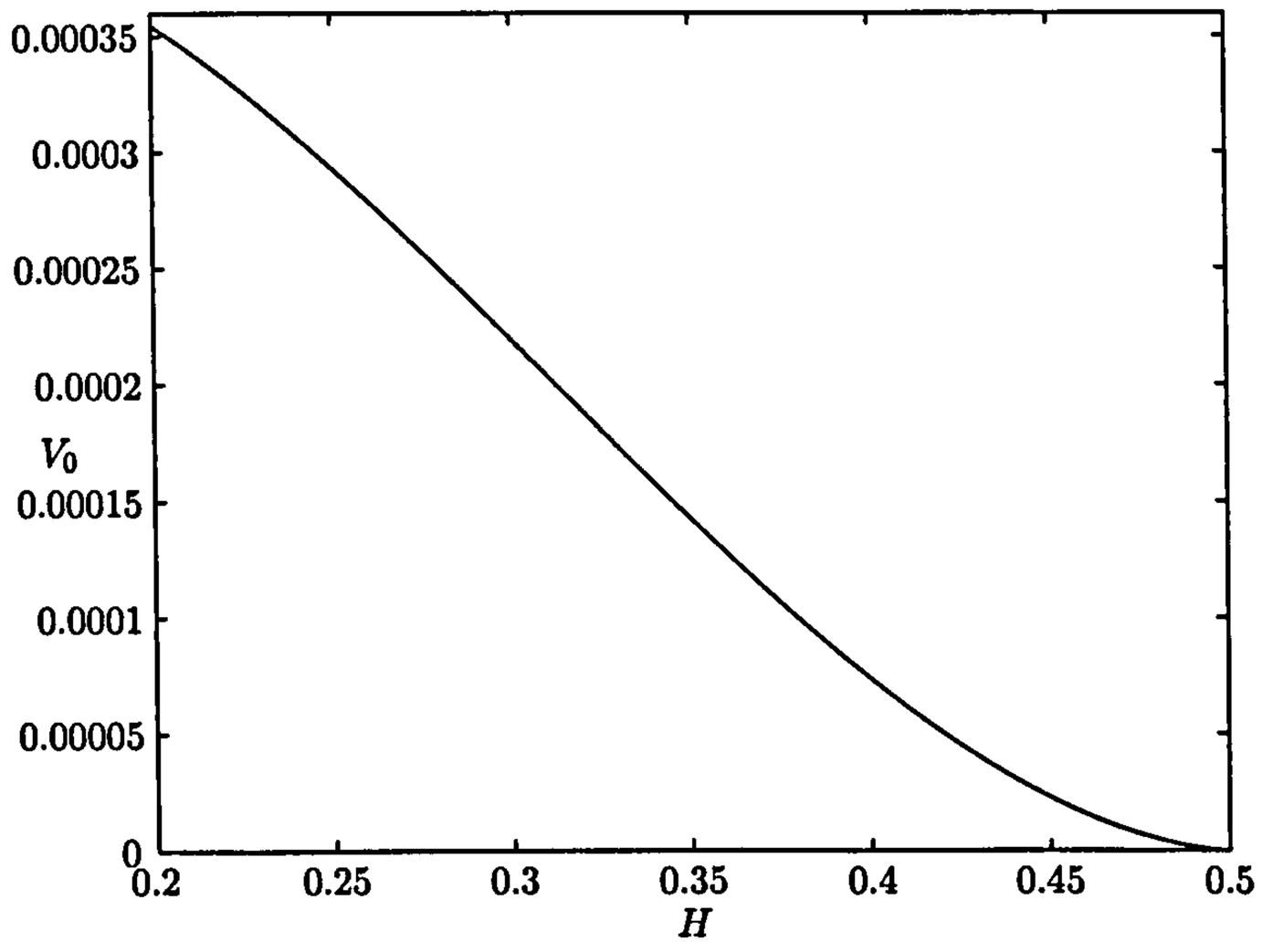

Figure 7.18: Overtopping volume, V_0 as a function of wall height H . $\epsilon = 0.0001$.

Some plots of jet elements for different values of t_i are given in figures 7.19 and 7.20. In all these figures the wall height is taken as $H = 0.3$ and the jet thickness parameter $\epsilon = 0.0001$. Information about each plot considered is given in table 7.2.

t_i	τ	β	jet width	x_d	x_c
0.8	0.75	1.491	0.01	0.000365	-0.0003318
0.9	0.67	1.2835	0.00896	0.002117	-0.00117
1.0	0.60	0.9943	0.00775	0.0043	-0.00229
1.1	0.55	0.591	0.00664	0.0068	-0.004042
1.2	0.50	0.1749	0.056	0.0094	-0.00665
1.3	0.46	0.015	0.0046	0.0118	-0.00947
1.4	0.43	0	0.0036	0.0135	-0.01153

Table 7.2: Properties of a jet element for varying t_i , with $H = 0.3$

For higher values of t_i upto $2H/(1-\sqrt{1-2H})$, the angle of deflection is $\beta = 0$. Plots of these are not shown since in these cases half of the water overtops and half doesn't. The jet widths in each plot may look large but referring to table 7.2 we see

that these widths are much smaller than the wall height considered. The figures are plotted locally to the top of the wall.

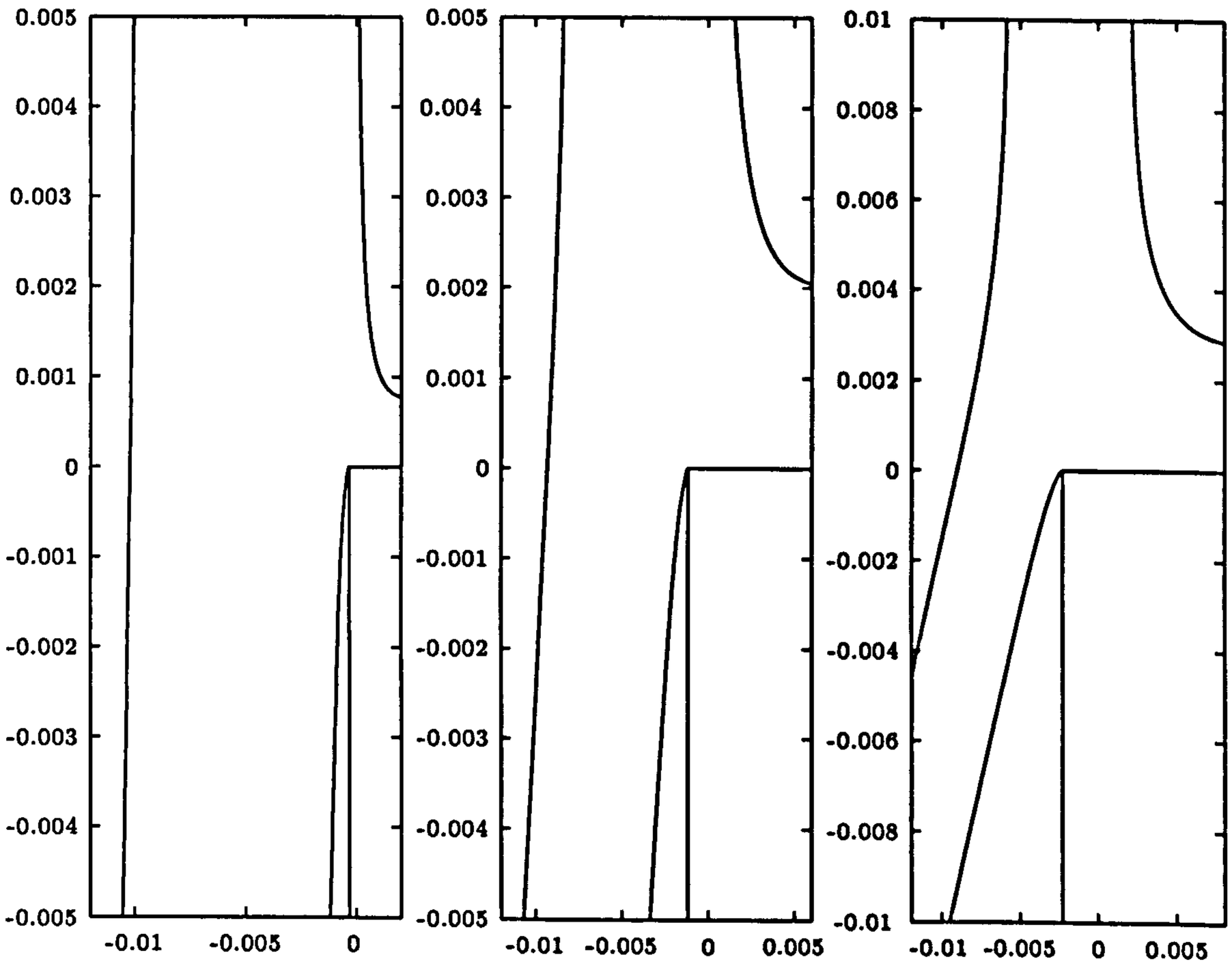

Figure 7.19: Impact of a jet element with top of wall of height 0.3. Plots are for $t_i = 0.8, 0.9$ and 1.0

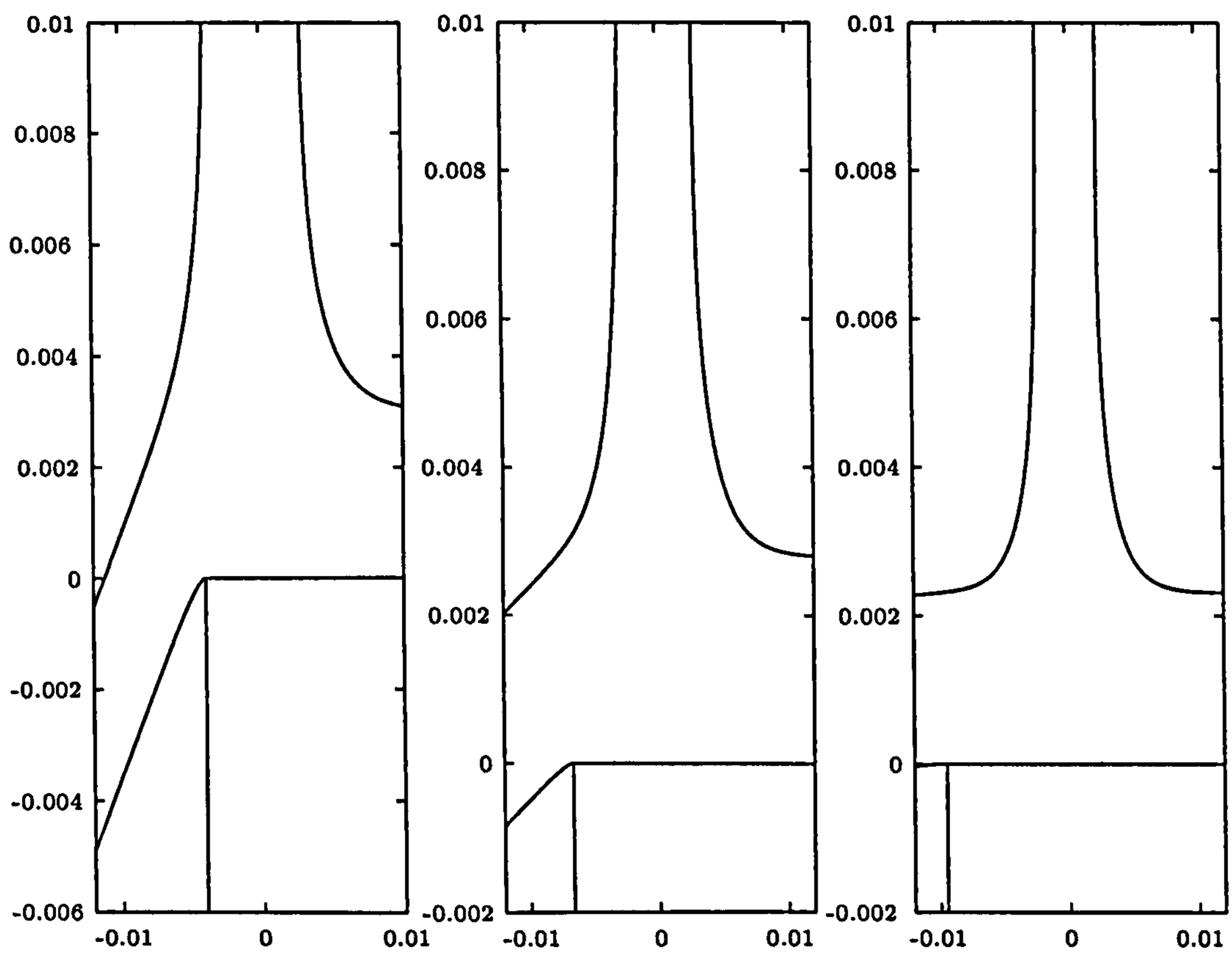

Figure 7.20: Impact of a jet element with top of wall of height 0.3. Plots are for $t_i = 1.1, 1.2$ and 1.3

7.7 Conclusion

We have seen how the parabolic free surface solution of Longuet-Higgins (1976) can be modified to model a jet climbing a vertical wall. The shallow water water equations were invoked to solve the flow above the wall. From this an expression was found for the velocity and position of the jet above the wall. An expression was also found for the amount of water that passes the top of a wall of fixed height. The horizontal displacement of the jet was also found in terms of the impact time, the time at which the jet returns to the top of the wall. From the results of this jet flow the incoming jet hitting the wall was considered, in the aim to find an expression for the amount of water that may overtop the wall. An expression for this volume was found, along with expressions for the free surfaces of the jets.

Chapter 8

Conclusions

8.1 Review of thesis

In this work we have used the shallow water wave equations to model water wave motion in the nearshore region. The run-up of waves from bores travelling through the surf and swash zones towards a still shoreline were considered. Once a model for the run-up is setup, the effects of introducing ovetopping are then examined.

Chapter 1 gave an insight into previous studies on the run-up of water waves on beaches. Various different cases of overtopping studies were also introduced.

In chapter 2, the equations of motion used in this work, the shallow water wave equations, were introduced and discussed. The work of Shen & Meyer (1963) and Ho & Meyer (1962), used in chapter 3 was also discussed in detail.

In chapter 3 the overtopping of a single swash event was considered. Analytical solutions were provided for the height and velocity of the flow in the neighbourhood of the overtopping point. An expression for the amount of water to overtop the beach was also given. The solution is found as an extension to the work of Shen & Meyer (1963) for the run-up of a single swash event on a plane beach. The work presented in this chapter can also be found in Peregrine & Williams (2001).

With an analytical model of the overtopping of a single swash event found, the next step was to investigate the run-up and overtopping from multiple swash events. This was done numerically, with the numerical method used being described in

chapter 4.

In chapter 4 a numerical solution was devised which is used to describe the behaviour of water waves approaching the shore. The numerical scheme is setup to include the presence of bores. The numerical program used, RUSH, uses a staggered scheme, based on the non-oscillatory scheme of Nessyahu & Tadmor (1990) for a system of hyperbolic equations. The numerical program RUSH was tested satisfactorily against known smooth solutions of the shallow water equations. These solutions included the dam-break problem, the non-breaking wave solution of Carrier & Greenspan (1958), the run-up of a single swash event solution of Shen & Meyer (1963) and also the overtopping solution of Peregrine & Williams (2001). With the tests proving succesful, RUSH was used to model the run-up of multiple swash events. This was done in chapter 5.

In chapter 5 the run-up of swash created from three different types of bores is considered. The first is the case of time periodic bores of equal amplitudes, given in section 5.3. The second case is the case of time periodic bores of random amplitudes, given in section 5.4. Finally in section 5.5 non-periodic bores were considered. In sections 5.3 and 5.4, three examples of different forcing periods were considered. In each case the shoreline motion was discussed, along with the form of the height and velocity profiles at the seaward boundary. Also the relationship between the relative wave height and the Iribarren number was discussed, along with a linear relationship between the relative wave height and the average period of swash run-up.

The effects of overtopping on the run-up of multiple swash events was considered in chapter 6. In this chapter the run-up results of chapter 5 are used with the introduction of overtopping. The overtopping of swash from time periodic bores of equal amplitudes is given in section 6.2. The overtopping of swash from time periodic bores of random amplitudes is given in section 6.3. In each of these sections we see how the introduction of overtopping drastically changes the shoreline motion. Also in this chapter, volumes of overtopping are calculated, with relationships between the volumes and other variables being setup.

In chapter 7, the overtopping of a vertical wall by a thin jet is considered. Mo-

tivation for this chapter comes from laboratory experiments in Hannover, in which the impact of violent water waves with walls was considered.

A simple analytical model of the type of thing seen in the Hannover experiments is setup. The initial jet motion along the wall is described using a solution due to Longuet-Higgins (1976). This solution is used along with the shallow water eqution to model the jet motion above the wall.

Once a solution for the motion of the jet above the wall is known, we analyse how the jet flow interacts with the top of the wall, on its way down. This is done using free surface flow techniques, see Milne-Thomson (1968). With this technique an expression can be found for the form of all the free surfaces connected with the flow. From these analytical solutions, the volume of water which overtops the wall is calculated.

8.2 Remarks

An analytical expression for the overtopping of a single swash event over a truncated plane beach has been found, which we believe is the first analytical overtopping solution of its type. The solution is not realistic in the sense that beaches aren't usually truncated at a given point along the beach. The more usual case of overtopping comes from water waves overtopping seawalls and dykes. The solution presented is very important though; it serves as a numerical test for numerical shallow water wave solvers, especially if the effects of overtopping want to be considered. As no other analytical solutions seem to exist for the overtopping at coastal structures, this solution is good enough.

In chapter 5, we saw how the run-up of swash on a beach can be modelled numerically. In all the numerical experiments presented, the beach slope was assumed to be planar and the effects of friction were ignored. During this study the effects of friction were considered, but are not presented here. Various studies of the effects of friction on the run-up of swash have been made previously by Archetti & Brocchini (2002), Puleo & Holland (2001), Kobayashi et al. (1987) and Packwood (1980), but for different input wave data. The results found for the run-up of periodic bores

and non-periodic bores compared well with the work of these authors and thus the reader is pointed in the direction of these papers.

The addition of friction into the model doesn't emit any surprises, the types of motion found are as those shown in sections 5.3, 5.4 and 5.5, but with the shoreline motion being damped by the effects of the friction. Even so, the effects of friction are very important, since on natural beaches friction is a very important quantity to be able to model.

In the overtopping case of chapter 6, the effects of friction were to decrease the volumes of overtopping. This decrease in volume is strictly down to how large we choose the friction parameter f_c to be.

Another analytical solution for overtopping is found in chapter 7. This time we considered the overtopping of a vertical wall by a thin jet. A numerical approach had previously been made by Jervis & Peregrine (1996), the theoretical approach used in this paper was extended analytically to find expressions for how the jet evolved as it passed the top of the wall. Expressions were also shown for the amount of water that may overtop the wall.

This research fulfills its purpose in obtaining a better theoretical understanding of the phenomena involved in run-up and overtopping of broken waves. It is hoped that this understanding of water motions may lead to improved descriptions in water wave overtopping.

8.3 Further work

In the future is it hoped that an analytical model might exist to model both the run-up and overtopping of multiple swash events. An attempt has been made by Baldock & Holmes (1999), this is only in the case when the forcing wave period is so large that no interactions exist in the swash zone and then the solution of Shen & Meyer (1963) can be fitted to each event.

If an analytical solution could be found then it would act as a good numerical test, to see whether the shoreline positions found in chapter 5 are indeed correct.

Results from other sets of wave data, using the same approach as described in chapter 5 would be good. The Iribarren plots found in sections 5.3 and 5.4 could then be questioned more. Would different data give rise to the same behaviours that were shown in sections 5.3 and 5.4?

Other extensions that could be considered are different beach profiles in chapters 5 and 6. How would the solutions change?

The last consideration could be the addition of the effects of sediment. It is well known that there is a lot of sediment activity in the swash zone. The effects of sediment transport in the dam-break problem have already been considered analytically by Pritchard & Hogg (2002*a*). Sediment transport has also been including analytically in the non-breaking wave solution of Carrier & Greenspan (1958), by Pritchard & Hogg (2003). The Shen & Meyer (1963) solution has also been modified to include the effects of sediment transport this is found in Pritchard & Hogg (2002*b*). As in the case of chapter 3, one could extend the Shen & Meyer (1963) solution with sediment to include the effects of overtopping.

References

Abramowitz, M. & Stegun, I. A. (1965), *Handbook of mathematical functions*, Dover.

Aminti, P. & Franco, L. (1988), 'Wave overtopping on rubble mound breakwaters', *Proc 21st Conf. Coastal Engng* **1**, 770–781. ASCE.

Archetti, R. & Brocchini, M. (2002), 'An integral swash zone model with friction: an experimental and numerical investigation', *Coastal Engng* **45**(2), 89–110.

Baldock, T. E. & Holmes, P. (1999), 'Simulation and prediction of swash oscillations on a steep beach', *Coastal Engng* **36**, 219–242.

Barnes, T. C. D. (1996), The Generation of Low-frequency Water Waves on Beaches, PhD thesis, University of Bristol.

Battjes, J. A. (1974), 'Surf similarity', *Proc. 14th Conf. Coastal Engng* pp. 466–480. ASCE.

Binnie, A. M. & Orkney, J. C. (1955), 'Flow of water from a reservoir II', *Proc Roy. Soc. A* **230**, 237–246.

Birkemeier, W. A., Hathaway, K. K., Smith, J. M., Baron, C. F. & Leffler, M. W. (1991), Delilah experiment: Investigator's summary report, Technical report, Vicksburg, Miss.

Bokhove, O., Patterson, M. D. & Peregrine, D. H. (2000), 'Breaking shallow-water wave simulations in the surf zone', *Proc. 27th Conf. Coastal Engng* **1**, 733–744. ASCE.

References

Bradbury, A. P. & Allsop, N. W. H. (1988), 'Hydraulic effects of breakwater crown walls', *Proc. Conf. on Design of Breakwaters* pp. 385–396. Institution of Civil Engngs, London.

Brennen, C. & Whitney, A. K. (1970), 'Unsteady free surface flows; solutions employing the lagrangian description of the motion', *Proceed. 8th Symp. Naval Hyd.* pp. 117–145.

Brocchini, M. & Peregrine, D. H. (1995), 'Flow properties of the swash zone', *Proc. Coastal Dynamics '95* pp. 221–232.

Brunn, P. & Günbak, A. R. (1976), 'New design principles for rubble mound structures', *Proc. 15th Coast. Conf. Engng* pp. 2429–2443.

Butt, T. & Russell, P. (2000), 'Hydrodynamics and cross-shore sediment transport in the swash zone of natural beaches: a review', *Journal of Coastal Research* **16**(2), 255–268.

Carrier, G. F. & Greenspan, H. P. (1958), 'Water waves of finite amplitude on a sloping beach', *J. Fluid Mech.* **4**, 97–109.

Carrier, G. F., Wu, T. T. & Yeh, H. (2003), 'Tsumani run-up and drawdown on a plane beach', *J. Fluid Mech.* **475**, 79–99.

Cartwright, D. E. & Longuet-Higgins, M. S. (1956), 'The statistical distribution of the maxima of a random function', *Proc. Royal Soc. London, A* **237**, 212–232.

Chanson, H., Aoki, S.-I. & Maruyama, M. (2003), 'An experimental study of tsumani run-up on dry and wet horizontal coastlines', *Science of Tsunami Hazards* **20**(5), 278–293.

Cooker, M. & Peregrine, D. H. (1990), 'Computations of violent motion due to waves breaking against a wall', *Proc 22nd Int. Conf. Coastal Engng* **1**, 164–176.

Cooker, M., Peregrine, D. H., Vidal, C. & Dold, J. W. (1990), 'The interaction between a solitary wave and a submerged semi-circular cylinder', *J. Fluid Mech.* **215**, 1–22.

Dodd, N. (1998), 'Numerical model of wave run-up, overtopping and regeneration', *J. Waterways, Port, Coast. and Ocean Engng.* **124**, 73–81.

Dold, J. W. & Peregrine, D. H. (1986), 'An efficient boundary integral method for steep unsteady surface waves', *Numerical methods for fluid dynamics II* pp. 671–679. Oxford Uni. Press.

Elfrink, B. & Baldock, T. (2002), 'Hydrodynamics and sediment transport in the swash zone: a review and perspectives', *Coastal Engng* **45**(3), 149–167.

Favre, H. (1935), *Etude theorique et experimentale des ondes de translation dans les canaux decouverts.*, Paris: Dunod.

Franco, C. & Franco, L. (1999), 'Overtopping formulas for caisson breakwaters with nonbreaking 3-d waves', *J. Waterway, Port, Coastal and Ocean Engng* **125**(2), 98–108.

Franco, L., De Gerloni, M. & van der Meer, J. W. (1994), 'Wave overtopping on vertical and composite breakwaters', *Proc. 24th Conf. Coast. Engng.* pp. 1030–1045. ASCE.

Freeman, J. C. & Mehaute, B. L. (1964), 'Wave breakers on a beach and surges on a dry bed', *Journal of Hyd. Engng* **90**(2), 187–216.

Galvin, C. J. (1968), 'Breaker type classification on three laboratory beaches.', *J. Geophys. Res.* **73**, 3651–3659.

Galvin, C. J. (1972), 'Wave breaking in shallow water', *Waves on Beaches and Resulting Sediment Transport* pp. 413–456. Academic, ed. R. E. Meyer.

Geer, J. & Keller, J. B. (1979), 'Slender streams', *J. Fluid Mech.* **93**, 97–115.

Geer, J. & Strikwerda, J. C. (1980), 'Vertical slender jets', *J. Fluid Mech.* **101**, 53–63.

Goda, Y. (1971), 'Expected rate of irregular wave overtopping of seawalls', *Coastal Engng in Japan* **14**, 45–51.

Goda, Y. (1985), *Random Seas and Design of Maritime Structures*, 3rd edn, Uni. Tokyo Press.

Gupta, N. (1993), 'An analytical solution describing the motion of a bore over a sloping beach', *J. Fluid Mech.* **253**, 167–172.

Hawkes, P. J. (1999), 'Mean overtopping rate in swell and bimodal seas', *Proc. Inst. Civil Engngs - Water Maritime and Energy* **136**(4), 235–238.

Hebsgaard, M., Sloth, P. & Juhl, J. (1998), 'Wave overtopping of rubble mound breakwaters', *Proc. Coastal Engng Conf. 2* pp. 2235–2248.

Hedges, T. S. & Reis, M. T. (1998), 'Random wave overtopping of simple sea walls: A new regression model', *Proc. Inst. Civil Engngs - Water Maritime and Energy* **130**(1), 1–10.

Hibberd, S. (1977), Surf and Run-up, PhD thesis, University of Bristol.

Hibberd, S. & Peregrine, D. H. (1979), 'Surf and run-up on a beach: a uniform bore', *J. Fluid Mech.* **95**, 323–345.

Hiraishi, T. & Maruyama, H. (1998), 'Directional wave overtopping estimation model and experimental verification', *Proc. Coastal Engng Conf. 2* pp. 2249–2261.

Ho, D. V. & Meyer, R. E. (1962), 'Climb of a bore on a beach. part 1. uniform beach slope', *J. Fluid Mech.* **14**, 305–318.

Holland, K. T. & Holman, R. A. (1993), 'The statistical distribution of swash maxima on natural beaches', *J. Geophys Res.* **98**(C6), 10271–10278.

Horikawa, K., ed. (1988), *Nearshore Dynamics and Coastal Processes - Theory, measurement and predictive models*, University of Tokyo Press.

Hu, K., Mingham, C. G. & Causon, D. M. (2000), 'Numerical simulation of wave overtopping coastal structures using the non-linear shallow water equations', *Coastal Engng.* **41**, 433–465.

Hu, S.-L. J. & McCauley, J. L. (1997), 'Estimation of wave overtopping rates for irregular waves', *J. Waterway, Port, Coastal and Ocean Engng* **123**(5), 266–273.

Hubbard, M. E. & Dodd, N. (2002), 'A 2-d numerical model of wave run-up and overtopping', *Coastal Engng* **47**, 1–26.

Hunt, I. A. (1959), 'Design of seawall and breakwaters', *J. Waterways and Harbours Div.* **85**(WW3), 123–152.

Jensen, A., Pedersen, G. K. & Wood, D. J. (2003), 'An experimental study of wave run-up at a steep beach', *J. Fluid Mech.* **486**, 161–188.

Jervis, M. & Peregrine, D. H. (1996), 'Overtopping of waves at a wall: A theoretical approach', *Proc. 25th Conf. Coastal Engng.* pp. 2192–2205. ASCE.

Jiang, G. S. & Tadmor, E. (1998), 'Non-oscillatory central schemes for multidimensional hyperbolic conservation laws', *SIAM J. Sci. Comp.* **19**(6), 1892–1917.

John, F. (1953), 'Two-dimensional potential flows with a free boundary', *Comm. Pure Appl. Math.* **6**, 497–503.

Juhl, J. & Sloth, P. (1994), 'Wave overtopping of breakwater under oblique waves', *Proc. 24th Conf. Coast. Engng.* pp. 1182–1196. ASCE.

Kanoglu, U. & Synolakis, C. E. (1998), 'Long wave run-up on piecewise linear topographies', *J. Fluid Mech.* **374**, 1–28.

Keller, H. B., Levine, D. A. & Whitham, G. B. (1960), 'Motion of a bore over a sloping beach', *J. Fluid Mech.* **7**, 302–316.

Keller, J. B. (1991), 'On unsymmetrically impinging jets', *J. Fluid Mech.* **211**, 653–655.

Keller, J. B. & Geer, J. (1973), 'Flows of thin streams with free boundaries', *J. Fluid Mech.* **59**, 417–432.

Keller, J. B. & Weitz, M. L. (1952), Thin unsteady heavy jets, Technical Report Report no. IMM-NYU 186, Inst. Math. Mech., New York Uni.

Kemp, P. H. & Plinston, D. T. (1974), 'Internal velocities in the uprush and backwash zone', *Proc. 14th Coast. Conf. Engng* pp. 575–585.

Kikkawa, H., Shi-Igai, H. & Kono, T. (1968), 'Fundamental study of wave overtopping on levees', *Coastal Engng in Japan* **11**, 107–115.

Kobayashi, N. & Wurjanto, A. (1989), 'Wave overtopping on coastal structures', *J. Waterways, Port, Coast. and Ocean Engng* **115**(2), 235–251.

Kobayashi, N., DeSilva, G. S. & Watson, K. D. (1988), 'Wave transformation and swash oscillations on gentle and steep slopes', *J. Geophys. Res.* **95**(C1), 951–966.

Kobayashi, N., Otta, A. K. & Roy, I. (1987), 'Wave reflection and run-up on rough slopes', *J. Waterways, Port, Coast. and Ocean Engng* **113**(3), 280–298.

Kofoed, J. P. (2002), Wave overtopping of marine structures - utilization of wave energy, PhD thesis, Aalborg University.

Lamb, H. (1932), *Hydrodynamics*, 6th edn, C.U.P.

Lax, P. & Wendroff, B. (1960), 'Systems of conservation laws', *Commun. Pure and Applied Maths* **13**, 217–237.

Li, Y. & Raichlen, F. (2002), 'Non-breaking and breaking solitary waves', *J. Fluid Mech.* **456**, 295–318.

Liu, P. L.-F., Lynett, P. & Synolakis, C. E. (2003), 'Analytical solutions for forced long waves on a sloping beach', *J. Fluid Mech.* **478**, 101–109.

Liu, X. & Tadmor, E. (1998), 'Third order non-oscillatory central scheme for hyperbolic conservation laws', *Numerische Mathematik* **79**, 397–425.

Longo, S., Petti, M. & Losada, I. J. (2002), 'Turbulence in the swash and surf zones: a review', *Coastal Engng* **45**(3), 129–147.

Longuet-Higgins, M. S. (1970*a*), 'Longshore currents generated by obliquely incident sea waves I', *J. Geophys. Res.* **75**, 6778–6789.

Longuet-Higgins, M. S. (1970*b*), 'Longshore currents generated by obliquely incident sea waves II', *J. Geophys. Res.* **75**, 6790–6801.

Longuet-Higgins, M. S. (1972*a*), 'A class of exact, time-dependent, free-surface flows', *J. Fluid Mech.* **55**, 529–543.

Longuet-Higgins, M. S. (1972*b*), 'Recent progress in the study of longshore currents', *Waves on Beaches and Resulting Sediment Transport* pp. 203–248. Academic, ed. R. E. Meyer.

Longuet-Higgins, M. S. (1976), 'Self-similiar, time-dependent flows with a free surface', *J. Fluid Mech* **73**, 603–620.

Longuet-Higgins, M. S. & Cokelet, E. D. (1976), 'The deformation of steep surface waves: I. a numerical method of computation', *Proc. Roy. Soc. A* **350**, 1–26.

Longuet-Higgins, M. S. & Stewart, R. W. (1962), 'Radiation stress and mass transport in gravity waves, with application to 'surf-beats'', *J. Fluid Mech.* **13**, 481–504.

Mase, H. (1989), 'Random wave run-up height on gentle slopes', *J. Waterway, Port, Coastal and Ocean Engng* **115**(5), 649–661.

Mase, H. (1995), 'Frequency down-shift of swash oscillations compared to incident waves', *J. Hyd. Res.* **33**(3), 397–411.

McCabe, V. A. (2003), The effect of entrained air on violent wave impacts, PhD thesis, University of Bristol.

McIver, P. & Peregrine, D. H. (1981), 'Comparison of numerical and analytical results for waves that are starting to break', *Proc. Conf. Hydrodynamics in Ocean Engng* pp. 203–215.

Mei, C. C. (1983), *The Applied Dynamics of Ocean Surface Waves*, Wiley Interscience.

Meyer, R. E. & Taylor, A. D. (1972), 'Run-up on beaches', *Waves on Beaches and Resulting Sediment Transport* pp. 357–411. Academic, ed. R. E. Meyer.

Miller, R. (1968), 'Experimental determination of run-up of undular and fully developed bores', *J. Geophys. Res.* **73**(14), 4497–4510.

Milne-Thomson, L. M. (1968), *Theoretical Hydrodynamics*, fifth edn, Macmillan.

Mizuguchi, M. (1993), 'Wave overtopping rate over a vertical wall and reflection coefficient', *Coastal Engng in Japan* **36**(1), 37–47.

Nessyahu, H. & Tadmor, E. (1990), 'Non-oscillatory central differencing for hyperbolic conservation laws', *J. Comp. Physics* **87**(2), 408–463.

Oezhan, E. & Yalciner, A. C. (1991), 'Overtopping of solitary waves at model sea dikes', *Proc. Coastal Engng Conf. 2* pp. 1487–1498.

Owen, M. W. (1980), Design of sea walls allowing for wave overtopping, Technical Report Rep. EX 924, HR Wallingford.

Owen, M. W. (1982), 'The hydraulic design of seawall profiles', *Proc. Conf. Shoreline Protection* pp. 185–192.

Packwood, A. R. (1980), Surf and Run-up on Beaches, PhD thesis, University of Bristol.

Packwood, A. R. (1983), 'The influence of beach porosity on wave uprush and backwash', *Coastal Engng* **7**, 29–40.

Packwood, A. R. & Peregrine, D. H. (1980), 'The propagation of solitary waves and bores over a porous bed', *Coastal Engng* **3**, 221–242.

Patterson, M. D. (2002), Shallow water modelling of nearshore processes, PhD thesis, University of Bristol.

Pedersen, J. (1996), Wave forces and overtopping on crown walls of rubble mound breakwaters, PhD thesis, Aalborg University.

Pedersen, J. & Burcharth, H. F. (1992), 'Wave forces on crown walls', *Proc. 23rd Conf. Coastal Engng* **2**, 1489–1502. ASCE.

Peregrine, D. H. (1966), 'Calculation of the development of an undular bore', *J. Fluid Mech.* **25**, 321–333.

Peregrine, D. H. (1972), 'Equations for water waves and the approximation behind them', *Waves on Beaches and Resulting Sediment Transport* pp. 95–121. Academic, ed. R. E. Meyer.

Peregrine, D. H. (1974), 'Surface shear waves', *J. Hyd. Div. Proc.* **100**(HY9), 1215–1227.

Peregrine, D. H. & Williams, S. M. (2001), 'Swash overtopping a truncated plane beach', *J, Fluid Mech.* **440**, 391–399.

Petti, M. & Longo, S. (2001*a*), 'Hydrodynamics in the swash zone', *Int. Jour. Offshore and Polar Engng* **11**(3), 202–210.

Petti, M. & Longo, S. (2001*b*), 'Turbulence experiments in the swash zone', *Coastal Engng* **43**(1), 1–24.

Press, W. H., Teukolsky, S. A., Vetterling, W. T. & Flannery, B. P. (1992), *Numerical Recipes in Fortran 77*, 2nd ed. edn, Cambridge University Press.

Pritchard, D. (2001), Some problems in two-phase flow: intertidal mudflats and low Reynolds number gravity currents, PhD thesis, University of Bristol.

Pritchard, D. & Hogg, A. J. (2002*a*), 'On sediment transport under dambreak flow', *J. Fluid Mech.* **473**, 265–274.

Pritchard, D. & Hogg, A. J. (2002*b*), Test-bed solutions for the transport of fine sediment in a shallow water model, unpublished.

Pritchard, D. & Hogg, A. J. (2003), 'On fine sediment transport by long waves in the swash zone of a plane beach', *J. Fluid Mech.* **493**, 255–285.

Puleo, J. A. & Holland, K. T. (2001), 'Estimating swash zone friction coefficients on a sandy beach', *Coastal Engng* **43**, 25–40.

Raubenheimer, B., Guza, R. T., Elgar, S. & Kobayashi, N. (1995), 'Swash on a gently sloping beach', *J. Geophys. Res.* **100**(C5), 8751–8760.

Riabouchinsky, D. (1932), 'Sur l'analogie hydraulique des mouvements d'un fluide compressible', *Institut de France, Académie des Sciences, Comptes Rendus* **195**, 998.

Ritter, A. (1892), 'Die fortpflanzung der wasserwellen', *Zeitschrift des Vereines Deutscher Ingenieure* **36**(33), 947–954.

Sachdev, P. L. & Seshadri, V. S. (1976), 'Motion of a bore over a sloping beach: an approximate analytical approach', *J. Fluid Mech* **78**, 481–487.

Sakakiyama, T. & Kajima, R. (1998), 'Wave overtopping and stability of armour units under multidirectional waves', *Proc. Coastal Engng Conf. 2* pp. 1336–1350.

Schüttrumpf, H., Möller, J., Oumeraci, H., Grüne, J. & Weissmann, R. (2001), 'Effects of natural sea states on wave overtopping of seadikes', *Proc. Fourth Int. Symp. on Ocean Wave Measurement and Analysis* pp. 1565–1574.

Shankar, N. J. & Jayaratne, M. P. R. (2003), 'Wave run-up and overtopping on smooth and rough slopes of coastal structures', *Ocean Engng* **30**, 221–238.

Shen, M. C. & Meyer, R. E. (1963), 'Climb of a bore on a beach: Part 3. run-up.', *J. Fluid Mech.* **16**, 113–125.

Spielvogel, L. Q. (1976), 'Single wave run-up on sloping beaches', *J. Fluid Mech.* **74**, 685–694.

Stansby, P. K., Chegini, A. & Barnes, T. C. D. (1998), 'The initial stages of dambreak flow', *J. Fluid Mech.* **370**, 203–220.

Stoker, J. J. (1957), *Water Waves: The Mathematical Theory with Applications*, Interscience.

Strikwerda, J. C. & Geer, J. (1980), A numerical method for computing the shape of a vertical slender jet, Technical Report Report No. 80-7, NASA Langley Research Center, Hampton, Virginia.

Svendsen, I. A. & Madsen, P. A. (1984), 'A turbulent bore on a beach', *J. Fluid Mech.* **148**, 73–96.

Synolakis, C. E. (1986), The run-up of long waves, PhD thesis, California Institute of Technology.

Synolakis, C. E. (1987), 'The run-up of solitary waves', *J. Fluid Mech.* **185**, 523–545.

Teles da Silva, A. F. & Peregrine, D. H. (1990), 'Nonsteady computations of undular and breaking bores', *Proc 22nd Conf. Coastal Engng* **1**, 1019–1032.

Titov, V. V. & Synolakis, C. E. (1995), 'Modelling of wave breaking and nonbreaking long-wave evolution and run-up using vtcs-2', *J. Waterways, Port, Coast. and Ocean Engng* **121**, 308–316.

Tuck, E. O. & Hwang, L.-S. (1972), 'Long wave generation on a sloping beach', *J. Fluid Mech.* **51**, 449–461.

Umeyama, M. (1993), 'Wave overtopping on vertical boundary and water surface displacement', *J. Waterway, Port Coastal and Ocean Engng* **119**(3), 243–260.

Ursell, F. (1953), 'The long wave paradox on the theory of gravity waves', *Proc. Camb. Phil. Soc.* **49**, 685–694.

U.S. Army Corps of Engineers, Coastal Engng Research Center (1984), *Shore Protection Manual.* U.S. Government Printing Office, Washington DC.

van der Meer, J. W. & Janssen, J. P. F. M. (1994), 'Wave run-up and wave overtopping at dikes', *Wave Forces on Inclined and Vertical Structures* pp. 1–27. ASCE, eds. N. Kobayashi and Z. Demirbilek.

van Dorn, W. G. (1976), 'Set-up and run-up in shoaling breakers', *Proc. 15th Coast. Conf. Engng* pp. 738–751.

van Gent, M. R. A. (1994), 'The modelling of wave action on and in coastal structures', *Coastal Engng* **22**(3-4), 311–339.

van Gent, M. R. A. (1995), Wave interaction with permeable coastal structures, PhD thesis, Delft University of Technology.

van Gent, M. R. A. (2001), 'Wave run-up on dikes with shallow foreshores', *J. Waterway, Port, Coastal and Ocean Engng* **127**(5), 254–262.

Varley, E., Ventakaraman, R. & Cumberbatch, E. (1971), 'The propagation of large amplitude tsunamis across a basin of changing depth. part 1. offshore behaviour', *J. Fluid Mech.* **49**, 775–801.

Ward, D. L. & Ahrens, J. P. (1992), 'Overtopping rates for seawalls', *CERC miscellaneous paper 92-3.* U.S. Army Engineer Waterways Experiment Station Vicksburg.

Weggel, J. R. (1976), 'Wave overtopping equation', *Proc 15th Conf Coastal Engng* **3**, 2737–2755.

Whitham, G. B. (1958), 'On the propagation of shock waves through regions of non-uniform are or flow', *J. Fluid Mech.* **4**, 337–360.

Whitham, G. B. (1974), *Linear and nonlinear waves*, Wiley.

Whitham, G. B. (1979), *Lectures on Wave Propagation*, Springer-Verlag for Tata Inst. Fund. Res.

Williams, S. M. & Peregrine, D. H. (2003), 'The overtopping of a plane slope by multiple swash events', *Proc 28th Conf. Coastal Engng* **1**, 929–941.

Yeh, H. H. (1991), 'Tsunami bore run-up', *Natural Hazards* **4**, 209–220.